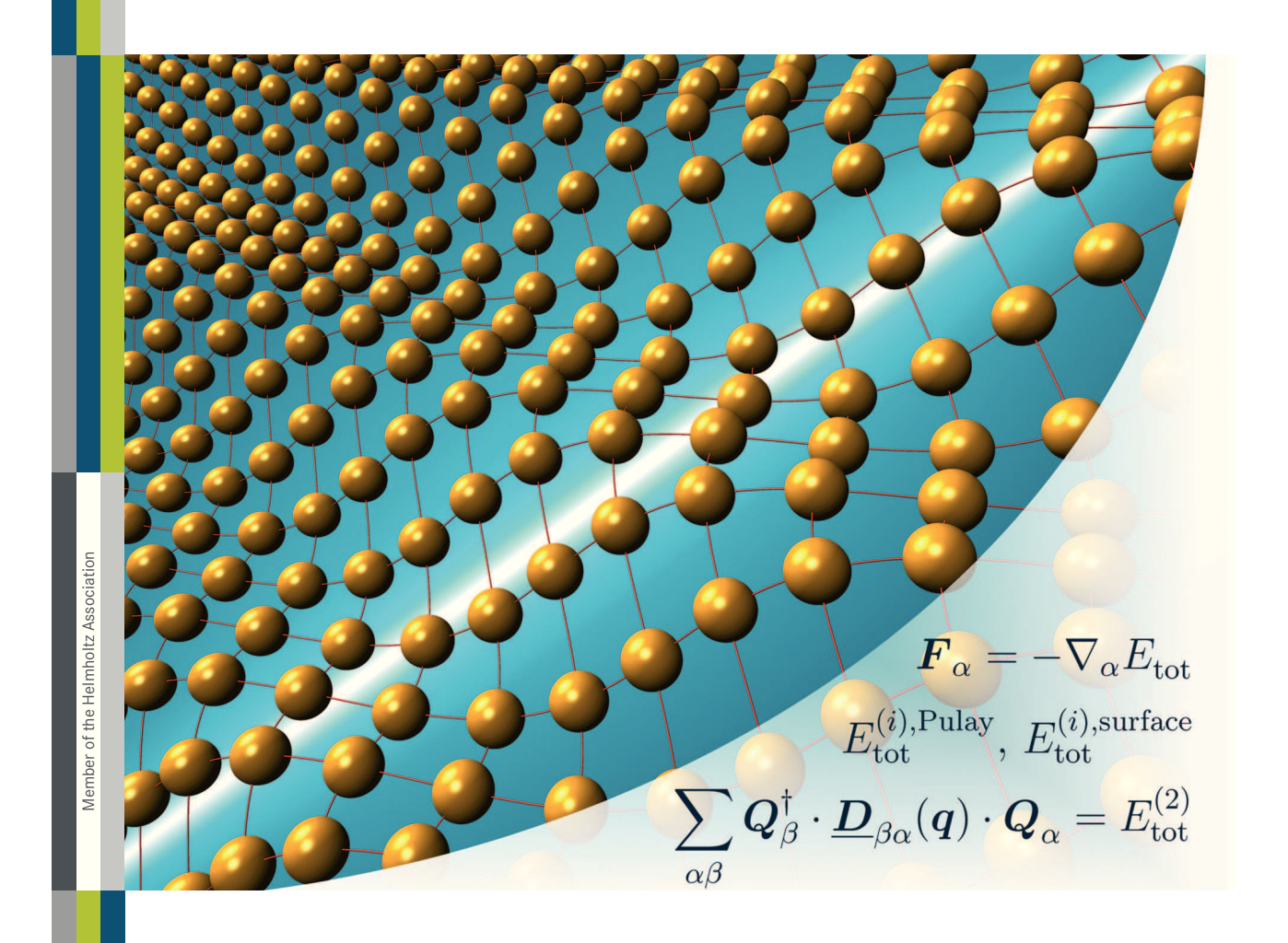
First-principle investigation of displacive response in complex solids

Daniel Aaron Klüppelberg



Schlüsseltechnologien/ Key Technologies Band/Volume 119 ISBN 978-3-95806-123-1



First-principle investigation of displacive response in complex solids

Von der Fakultät für Mathematik, Informatik und Naturwissenschaften der RWTH Aachen University zur Erlangung des akademischen Grades eines Doktors der Naturwissenschaften genehmigte Dissertation

vorgelegt von

Diplom-Physiker und Diplom-Mathematiker Daniel Aaron Klüppelberg

aus

Dormagen

Berichter: Univ.-Prof. Dr. rer. nat. Stefan Blügel

Univ.-Prof. Dr. rer. nat. Carsten Honerkamp

Tag der mündlichen Prüfung: 16.12.2015

Diese Dissertation ist auf den Internetseiten der Universitätsbibliothek online verfügbar.

Forschungszentrum Jülich GmbH Peter Grünberg Institute (PGI) Quantum Theory of Materials (PGI-1 / IAS-1)

First-principle investigation of displacive response in complex solids

Daniel Aaron Klüppelberg

Bibliographic information published by the Deutsche Nationalbibliothek. The Deutsche Nationalbibliothek lists this publication in the Deutsche Nationalbibliografie; detailed bibliographic data are available in the Internet at http://dnb.d-nb.de.

Publisher and Forschungszentrum Jülich GmbH

Distributor: Zentralbibliothek 52425 Jülich

Tel: +49 2461 61-5368 Fax: +49 2461 61-6103

Email: zb-publikation@fz-juelich.de www.fz-juelich.de/zb

Cover Design: Grafische Medien, Forschungszentrum Jülich GmbH

Printer: Grafische Medien, Forschungszentrum Jülich GmbH

Copyright: Forschungszentrum Jülich 2016

Schriften des Forschungszentrums Jülich Reihe Schlüsseltechnologien / Key Technologies, Band / Volume 119

D 82 (Diss. RWTH Aachen University, 2015)

ISSN 1866-1807 ISBN 978-3-95806-123-1

The complete volume is freely available on the Internet on the Jülicher Open Access Server (JuSER) at www.fz-juelich.de/zb/openaccess.

Neither this book nor any part of it may be reproduced or transmitted in any form or by any means, electronic or mechanical, including photocopying, microfilming, and recording, or by any information storage and retrieval system, without permission in writing from the publisher.

Abstract

In this work, we discuss two approaches to calculate phonon spectra of crystals within the all-electron full-potential linearized augmented-plane-wave (FLAPW) method. This method is one of the most precise implementations of Kohn-Sham (KS) density functional theory (DFT) due to the inclusion of all electrons into the calculation and the use of the full potential, *i.e.*, no shape approximations are applied to the potential.

The calculation of phonons requires the force-constant matrix (FCM). The FCM is the second-order derivative of the KS total energy with respect to two atomic displacements. Its Fourier transform yields the dynamical matrix (DM). The eigenvalues of the DM are the squares of the phonon frequencies. Its eigenvectors are the polarization vectors.

The first approach to calculate phonons is the finite-displacement (FD) method. In this method, the FCM is obtained from displacing one atom at a time from equilibrium, calculating the forces on all atoms, and dividing by the displacement amplitude. This is repeated for each atom and for each spatial direction. In practice, the number of calculations reduces significantly by exploiting the symmetry of the crystal lattice. The FCM is transformed to the DM and the phonon energies and polarization vectors are extracted. A drawback of this approach is given by the necessity to use supercells. The phonon frequencies are only correct for phonons whose wave vector \boldsymbol{q} is commensurable with the lattice. Hence, to correctly calculate phonon frequencies at small wave vectors, large supercells are needed, because the displacement pattern of such phonons repeats only after many instances of the primitive unit cell.

Since the FD procedure relies on an analytical derivation of the total energy followed by a numerical one, precise forces are necessary. Otherwise, the FCM is not symmetric, for example. We present a reformulation of the FLAPW force formalism which includes the whole unit cell into the calculation of the atomic force contribution from the core states and which incorporates additional terms to deal with the slight discontinuity of the LAPW basis functions and the quantities derived from them. The improvement of the force precision is demonstrated by the study of different criteria.

We then present phonon spectra for Al, MgO, GaAs, and $EuTiO_3$ obtained by the FD method from forces calculated in the FLAPW approach using our reformulation.

The second approach to calculate phonon spectra is density functional perturbation theory (DFPT). In DFPT, the second-order derivative of the KS total energy is directly calculated via perturbation theory. DFPT allows the determination of phonon frequencies at arbitrary wave vectors \boldsymbol{q} from calculations involving the primitive unit cell, only, by treating a phonon of this wave vector as the perturbation. The first-order changes of the basis functions, the electronic density, and the potential have to be obtained from the Sternheimer equation, which is the linearized Schrödinger equation. Additionally, the second-order changes of the external potential, the ion-ion energy, and the LAPW basis functions are required.

We provide formulas which explicitly include adjustments of the general DFPT approach when used in conjunction with the FLAPW method. These adjustments include Pulay terms, the correct treatment of the core state contribution, and surface terms which are analogous to those within the force formalism.

Zusammenfassung

In dieser Arbeit diskutieren wir zwei Varianten zur Bestimmung von Phononenspektren in Kristallen mit der all-electron full-potential linearized augmented-plane-wave (FLAPW) Methode. Diese ist eine der genauesten Realisierungen von Kohn-Sham (KS) Dichtefunktionaltheorie (DFT), denn sie behandelt alle Elektronen und verzichtet auf Näherungen, die die Form des Potentials betreffen.

Zur Bestimmung von Phononen ist die Kraftkonstantenmatrix (FCM) nötig. Die FCM ist die Ableitung zweiter Ordnung der totalen Energie des KS Systems bezüglich der Auslenkung zweier Atome. Ihre Fouriertransformierte stellt die dynamische Matrix (DM) dar. Die Eigenwerte der DM sind die Quadrate der Phononenenergien. Ihre Eigenvektoren sind die Polarisationsvektoren.

Die erste Variante zur Phononenberechnung ist die endliche-Verschiebungs-Methode (FD). In dieser Methode erhält man die FCM durch Verschiebung eines Atoms aus seiner Ruhelage, anschließende Berechnung der Kräfte auf alle Atome und schließlich durch die Division der Kräfte durch die Länge der Auslenkung. Dies wird für jedes Atom und für jede Raumrichtung wiederholt. Tatsächlich kann die Anzahl der Rechnungen durch das Ausnutzen von Symmetrien drastisch verringert werden. Die FCM wird zur DM transformiert und man erhält die Phononenenergien und die Polarisationsvektoren. Ein Nachteil dieser Methode ist die Notwendigkeit, Superzellen zur Berechnung zu benutzen. Nur diejenigen Phononen, deren Wellenvektor \boldsymbol{q} mit der Superzelle kommensurabel ist, können korrekt ermittelt werden. Daher müssen zur zuverlässigen Berechnung von Phononenfrequenzen bei kleinen \boldsymbol{q} große Superzellen herangezogen werden. Solche Phononen erzeugen Verschiebungsmuster, die sich erst nach vielen primitiven Einheitszellen wiederholen.

Da die FD Methode aus einer analytischen gefolgt von einer numerischen Ableitung der totalen Energie besteht, sind genaue Kräfte nötig. Andernfalls ist z.B. die FCM nicht symmetrisch. Wir präsentieren eine Erweiterung des Kraftformalismus der FLAPW Methode. Diese schließt die ganze Einheitszelle in die Berechnung des Kraftbeitrags der Kernelektronen ein und berücksichtigt darüberhinaus die Unstetigkeit der LAPW Basisfunktionen und ihrer abgeleiteten Größen durch Korrekturterme. Die Präzisionsverbesserung durch unseren Formalismus wird anhand verschiedener Beispiele demonstriert.

Wir zeigen die Phononenbandstrukturen von Al, MgO, GaAs und EuTiO₃, welche durch die FD Methode und FLAPW-Kräfte ermittelt wurden.

Der zweite Ansatz zur Bestimmung von Phononenbandstrukturen ist Dichtefunktional-Störungstheorie (DFPT). Die zweite Ableitung der KS totalen Energie wird in DFPT direkt durch Störungstheorie bestimmt. Dabei erlaubt DFPT, Phononenenergien beliebiger Wellenvektoren \boldsymbol{q} zu bestimmen und dabei nur die primitive Einheitszelle zur Berechnung heranzuziehen, indem das Phonon als Störung angesehen wird. Es ist nötig, die Änderungen erster Ordnung der Basisfunktionen, der Elektronendichte und des Potentials durch die Sternheimer Gleichung zu bestimmen. Die Sternheimergleichung ist die linearisierte Schrödingergleichung. Ausserdem muss die zweite Variation des externen Potentials, der Ionen-Ionen Energie und der LAPW Basisfunktionen berechnet werden.

Wir stellen Formeln zur Verfügung, die explizit die Anpassungen des DFPT Ansatzes an die FLAPW Methode berücksichtigen. Diese Anpassungen beinhalten Pulay-Terme, die korrekte Behandlung des Beitrags der Kernelektronen, sowie Oberflächenterme, die sich ähnlich wie bei den Kräften ergeben.

Contents

	Introduction	1
2.	2.4. The exchange-correlation functional	7 8 10 11 13
3.	3.1. The APW method 3.2. The LAPW method 3.3. The FLAPW method 3.4. Core states 3.5. Local orbitals 3.6. Evaluation of the exchange-correlation potential 3.7. Evaluation of the Coulomb potential 3.8. Constructing the Hamilton and overlap matrices 3.9. Relativism 3.9.1. The scalar-relativistic approximation 3.10. The origin of Pulay contributions	20 21 23 24 27 29 30 33 35 35 36
1.	4.1. Derivative of the total energy 4.2. Pulay force 4.2.1. Valence states 4.2.2. Core states 4.3. Surface force 4.4. Hellmann-Feynman force 4.5. Summary of differences to Yu, Singh, and Krakauer 4.6. Forces using DFT+U 4.7. Computational results 4.7.1. Analytic vs. numerical force 4.7.2. Drift force 4.7.3. Computation time	39 40 41 42 44 47 48 50 51 53 69 70
i.	Phonons in the finite-displacement approach 5.1. The force-constant matrix	

Contents

	5.3. 5.4. 5.5.	$ \begin{array}{llllllllllllllllllllllllllllllllllll$
		5.5.2. Phonon spectra
6.		sity functional perturbation theory and the FLAPW method 89
	6.1.	Density functional perturbation theory
		6.1.1. First-order changes
		6.1.2. Second-order changes
	6.2.	
	0.2.	6.2.1. Additional first-order changes
		6.2.2. Additional second-order changes
	6.3	Summary
	0.0.	Summary
7.	Pho	nons in FLAPW using DFPT 105
	7.1.	First-order changes
		7.1.1. Evaluation of $\phi_{KG}^{(1)}(r)$
		7.1.2. Evaluation of the core state change $\psi_{i\mathbf{k}}^{(1)}(\mathbf{r})$
		7.1.3. Evaluation of $\rho^{(1)}(r)$
		7.1.4. Evaluation of the first-order changes of the potential 116
		7.1.5. Solving the Sternheimer equation
	7.2.	Second-order changes
		7.2.1. Evaluation of $V_{\text{ext}}^{(2)}(\boldsymbol{r})$
		7.2.2. Evaluation of $E_{\rm ii}^{(2)}$
		7.2.3. Evaluation of $\phi_{\mathbf{k}\mathbf{C}}^{(2)}(\mathbf{r})$
		7.2.4. Evaluation of the core state change $\psi_{i\mathbf{k}}^{(2)}(r)$
	7.3.	The dynamical matrix
		The dynamical matrix
		7.3.2. Contribution from $E_{\text{tot,Pulay}}^{(2)}$
		7.3.3. Contribution from $E_{\text{tot,SF}}^{(c), \text{ ranky}}$
	7 4	Summary
	1.1.	Summary
8.	Sum	mary & Conclusions 143
Α.	Арр	endix 149
	A.1.	Implementation of core states
		A.1.1. $F_{\alpha}(G)$ inside the muffin-tin sphere of atom α
		A.1.2. $F_{\alpha}(G)$ outside of the muffin-tin sphere of atom α
	A.2.	Calculating $d\mu_{\rm xc}/d\rho$ for the VWN-LDA functional
	A.3.	Input file for VO_2
	A.4.	Nitty-gritties of $D^{\text{Pulay}}(q)$
		A.4.1. First bra-ket
		A.4.2. Second bra-ket
	۸ -	A.4.3. Third bra-ket
	A.5.	Nitty-gritties of $D^{\rm SF}(q)$

List of Figures

2.1.2.2.	Textbook physics follows the dotted path: From the external potential one obtains the wave functions, which give the density. DFT closes the loop, the external potential is uniquely defined by the ground state density Jacob's ladder of chemical accuracy, describing the quality of approximation of different approximations for the xc functional	9 12
3.1. 3.2. 3.3. 3.4.	Electronic structure methods. The figure is a modification of that shown in [107] and inspired by [108]	17 20 25 27
4.11	Leakage of core states of MgO. Numerical vs. analytical force for Al _I . Numerical vs. analytical force for Al _{II} . Numerical vs. analytical force for MgO. Numerical vs. analytical force for MgO. Numerical vs. analytical force for GaAs. Due to the large displacement, the quadratic fit is applied only to the seven inner point. Numerical vs. analytical force for EuTiO ₃ . $l_{\rm max} \ {\rm convergence} \ {\rm of} \ {\rm Al}_{\rm II}. \\ l_{\rm max} \ {\rm convergence} \ {\rm of} \ {\rm Al}_{\rm II}. \\ l_{\rm max} \ {\rm convergence} \ {\rm of} \ {\rm MgO}. \ {\rm Labeled} \ {\rm symbols}: \ {\rm LO} \ {\rm calculations}. \ {\rm Unlabeled} \ {\rm symbols}: \ {\rm Mg} \ 2s \ {\rm and} \ 2p \ {\rm states} \ {\rm are} \ {\rm core} \ {\rm states}. \\ l_{\rm max} \ {\rm convergence} \ {\rm of} \ {\rm GaAs}. \\ l_{\rm max} \ {\rm convergence} \ {\rm of} \ {\rm VO}_2. \ {\rm Labeled} \ {\rm symbols}: \ {\rm DFT+U} \ {\rm calculations}. \ {\rm Unlabeled} \ {\rm symbols}: \ {\rm Regular} \ {\rm LDA} \ {\rm calculations}. \ {\rm They} \ {\rm are} \ {\rm designated} \ {\rm as} \ {\rm in} \ {\rm Fig.} \ 4.8. \\ l_{\rm max} \ {\rm convergence} \ {\rm of} \ {\rm EuTiO}_3. \\ l_{\rm max} \ {\rm convergence} \ {\rm of} \ {\rm EuTiO}_3. \\ l_{\rm max} \ {\rm convergence} \ {\rm of} \ {\rm EuTiO}_3. \\ l_{\rm max} \ {\rm convergence} \ {\rm of} \ {\rm EuTiO}_3. \\ l_{\rm max} \ {\rm convergence} \ {\rm of} \ {\rm EuTiO}_3. \\ l_{\rm max} \ {\rm convergence} \ {\rm of} \ {\rm EuTiO}_3. \\ l_{\rm max} \ {\rm convergence} \ {\rm of} \ {\rm EuTiO}_3. \\ l_{\rm max} \ {\rm convergence} \ {\rm of} \ {\rm EuTiO}_3. \\ l_{\rm max} \ {\rm convergence} \ {\rm of} \ {\rm EuTiO}_3. \\ l_{\rm max} \ {\rm convergence} \ {\rm of} \ {\rm EuTiO}_3. \\ l_{\rm max} \ {\rm convergence} \ {\rm of} \ {\rm EuTiO}_3. \\ l_{\rm max} \ {\rm convergence} \ {\rm of} \ {\rm EuTiO}_3. \\ l_{\rm max} \ {\rm convergence} \ {\rm of} \ {\rm EuTiO}_3. \\ l_{\rm max} \ {\rm convergence} \ {\rm of} \ {\rm EuTiO}_3. \\ l_{\rm max} \ {\rm convergence} \ {\rm of} \ {\rm EuTiO}_3. \\ l_{\rm max} \ {\rm convergence} \ {\rm of} \ {\rm EuTiO}_3. \\ l_{\rm max} \ {\rm euti} \ {\rm eut} \ {\rm of} \ {\rm eut} \ {\rm eu$	46 54 55 56 57 58 62 64 65 65 66 68
5.1.5.2.	(a) 4×4 supercell and force decay radius with respect to the distance from the atom displaced. (b) 4×1 supercells with commensurable phonon modes. \times and \circ in the figures denote atomic positions of different atom types Phonon spectrum of Al obtained from a $2\times 2\times 2$ supercell at Level 3 of the force formalism (red solid line) and from a $4\times 4\times 4$ supercell at Level 3 (black dashed line). In both cases, Level 3 does not deviate from the other Levels. Blue asterisks mark experimental data	75 83

List of Figures

5.3.	Phonon spectrum of MgO obtained from a $2\times2\times2$ supercell at Level 0 (black solid line) and at Level 3 (red solid line). Respective data from a $4\times4\times4$ supercell calculation uses dashed lines. Blue asterisks mark experimental data. 84
5.4.	Phonon spectrum of GaAs obtained from a $2 \times 2 \times 2$ supercell at Level 0
	(black solid line) and at Level 3 (red solid line). Blue asterisks mark exper-
	imental data
5.5.	Phonon spectrum of EuTiO ₃ obtained from a $2 \times 2 \times 2$ supercell at Level 0
	(black solid line) and at Level 3 (red solid line). The Levels are nearly
	indistinguishable
7.1.	Flowchart depicting the algorithm to solve the Sternheimer equation, Eq. (7.24),
	self-consistently. Parallelization can be applied for every q and for every α .
	Within the Sternheimer loop (yellow box), k -point parallelization can be per-
	formed for fixed q and α

List of Tables

4.1.	Default setup parameters for the different systems considered. The number-	
	ing of the muffin-tin radii is according to their appearance in the structure formula F_{α} VO has $P_{\alpha} = P_{\alpha}$ $P_{\alpha} = P_{\alpha}$	5
1.2.	formula. E.g. VO ₂ has $R_1 = R_V$, $R_2 = R_O$	J
1.4.	Setup Al _I : A single fcc unit cell reconstructed in a sc unit cell. (b) Setup	
	A_{II} : A 2 × 2 × 2 grid of fcc unit cells. Only Levels 0 and 3 are shown,	
	since the differences between Level 3 and Levels 1 and 2 are negligible, as	
	suggested by the data in part (a). The angular-momentum cutoff is chosen as	
	$l_{\text{max}} = 10$ in both cases. The forces presented here are rounded to a precision	
	of $0.1 \mu \text{Htr}/a_B$. Therefore, the data does not add up exactly to a drift force	
	of zero	5
1.3.	Forces (in m Htr/ a _B) in MgO at the different Levels of implementation. (a)	
	Mg $2s$ and $2p$ states are treated as core states. (b) Mg $2s$ and $2p$ states are	
	treated using LOs. The angular-momentum cutoff is set to $l_{\text{max}} = 14$ for	
	both atoms	6
1.4.	Forces (in $mHtr/a_B$) in GaAs at the different Levels of implementation. The	
	angular-momentum cutoff is set to $l_{\text{max}} = 12$ for both atoms	6
4.5.	Forces (in $mHtr/a_B$) in EuTiO ₃ at the different Levels of implementation.	
	The titanium atom Ti has been displaced by 0.022 $a_{\rm B}$ in the [100] direction.	
	The angular momentum cutoff l_{max} is set to 10 in (a) and 12 in (b)	6
1.6.	Forces (in $mHtr/a_B$) in VO ₂ at the different Levels of implementation.	
	The atoms appear in the order specified in the input file presented in Ap-	
	pendix A.3. (a) Regular DFT calculation. (b) DFT+U calculation with	
	$U=4.0$ eV. The angular-momentum cutoff is set to $l_{\rm max}=12$ for all atoms.	6
1.7.	Computational overhead for computing the atomic force at the different force	
	LEVELS for all setups. The percentages are given with respect to the average	
	time of a single step of the self-consistency cycle listed in the column titled 'Comp. time'. The calculations were performed on a single Intel Year CPII	
	'Comp. time'. The calculations were performed on a single Intel Xeon CPU X5670 @ 2.93 Ghz	6
	A5070 @ 2.55 GHz	U
5.1.	x-component of the force matrix of EuTiO ₃ in μ Htr/ a_B . (a) corresponds to	
	forces obtained at Level 0. (b) corresponds to forces obtained at Level 3.	
	The first column of a row lists the atom which has been displaced by $0.02244~a_{\rm B}$	
	along x -direction. The component of the force along the same direction is	
	then shown for each atom in the unit cell. In the last column (row), the force	
	values of each row (column) are summed up	8

List of Abbreviations

AMF around mean-field APW augmented plane wave

BZ Brillouin zone

DFT density functional theory

DFPT density functional perturbation theory

DM dynamical matrix
EXX exact exchange
fcc face-centered cubic
FCM force-constant matrix
FD finite-displacement
FLL fully-localized limit

FLAPW full-potential linearized augmented plane wave

GGA generalized gradient approximation
HDLO higher derivative local orbital
HELO higher energy local orbital
HF Hellmann-Feynman
IR interstitial region
KKR Korringa-Kohn-Rostoker

KS Kohn-Sham l.h.s. left-hand side

LAPW linearized augmented plane wave LCAO linear combinatation of atomic orbitals

LDA local density approximation
LMTO linearized muffin-tin orbitals
LO local orbital / longitudinal optical
LSDA local spin density approximation

MT muffin-tin na non-analytical ni non-interacting

PAW projector augmented wave

PW plane wave r.h.s. right-hand side

RPA random phase approximation sc simple-cubic / supercell TO transverse optical

val valence

VASP vienna ab initio simulation package

 $\begin{array}{ll} {\rm VWN} & {\rm Vosko\text{-}Wilk\text{-}Nusair} \\ {\rm xc} & {\rm exchange\text{-}correlation} \end{array}$

1. Introduction

Most of the properties of a crystalline material arise from the collective behavior of the constituent particles, *i.e.*, the atomic nuclei and the surrounding electrons. Examples for these collective phenomena are plasmons, magnons, and phonons to name but a few. While plasmons correspond to a collective oscillation of the electron charge density, magnons describe the collective motion of the electron spins, and phonons the collective vibration of the atomic nuclei around their equilibrium position. In the course of this thesis, we focus on the latter.

Phonons are quasi particles of the crystal specified by their crystal momentum q and their energy in quantums of $\hbar\omega$. Each phonon corresponds to a displacement pattern of the atoms, along which the vibration of the atoms takes place. Phonons can be generated by external perturbations, e.q. by sound, by scattering of particles, e.q. electrons or neutrons, or by thermal agitation. Phonons are the main contributors to the specific heat of a material, starting with a T^3 -dependence at low temperatures and saturating at the Dulong-Petit result of classical mechanics for high temperatures, where each atom amounts for $3k_{\rm B}$ to the heat capacity of the material. Phonons are also a pivotal ingredient for explaining further material properties, like heat conductivity, which is the essential quantity for thermoelectrica; thermal expansion of a solid is governed by phonons under consideration of anharmonic effects; electrical conductivity is reduced by electron-phonon scattering, and the electron-phonon coupling is the driving mechanism for the BCS theory of superconductivity. Together with spin-orbit coupling, phonons lead to spin relaxation of a spin-polarized current passing through a crystal and provide a channel for the relaxation of angular momentum from the spin-degree of freedom into the lattice. All these items show that the investigation and understanding of phonons is a central theme of solid state research.

Several experimental techniques are available to measure the phonon dispersion relation. Common are inelastic neutron scattering [1–3], Raman spectroscopy [4–6], infrared absorption [7–9], or x-ray diffraction [10–12]. Surface phonons are measured with high-resolution electron energy loss spectroscopy [13–15]. For crystals with one atom in the unit cell, the resulting phonon dispersion exhibits one acoustic branch per spatial dimension, which goes to zero linearly for vanishing crystal momentum. The slope of the acoustic branches defines the speed of sound in a material. At zero crystal momentum, an acoustic phonon corresponds to a translation of the whole lattice, which does not require energy, as the atoms of the crystal move rigidly in phase. If more atoms (say $N_{\rm at}$) are contained in the primitive unit cell of the lattice, $3N_{\rm at}-3$ optical phonons occur and manifest in the phonon band structure as modes with a finite energy also for vanishing crystal momentum. In contrast to the acoustic modes, the optical modes represent a vibrational pattern in which the atoms move against each other.

From a theoretical point of view phonons are oscillatory eigenmodes of the atomic nuclei in the potential landscape generated by electrons. The eigenmodes and energies of the phonons are connected to the force-constant matrix, which is the Hesse matrix, *i.e.*, the

1. Introduction

second-order derivative of the total energy $E_{\rm tot}$ of a solid in the Taylor expansion of $E_{\rm tot}$ with respect to small atomic displacements. The symmetry of second derivatives (Young's theorem) holds for the force-constant matrix, defining it as a symmetric matrix. A Fourier transformation of the force-constant matrix from real space to momentum space yields the Hermitian dynamical matrix $\underline{\mathcal{D}}(q)$, whose eigenvalues are the squares of the phonon energies and whose eigenvectors are the polarization vectors specifying the atomic vibration patterns. In general, there is a relation between the phonon band structure and the symmetry of a crystal: If a lattice is subject to stress (or other environmental conditions), the phonon band structure changes and can become 'soft' for certain phonon modes, meaning that the energy necessary to excite this phonon decreases with increasing stress. Once the excitation energy is critically low, the material gains energy from undergoing a phase transition into a geometry in which no critically soft mode exists anymore. A more elaborate introduction into the theoretical description of phonons is given by Born and Huang [16].

Considering the importance of phonons in solids there is a strong motivation to simulate phonon spectra from first principles, that means the interaction between the atomic nuclei is determined directly from the laws of quantum mechanics of the interacting electrons. These calculations do not involve model parameters. In principle, one just has to specify what kind of atom is placed at which location in the lattice. Basically, the physical properties of the desired system are accessed by solving the Schrödinger equation describing this system. The Born-Oppenheimer approximation [17] is commonly employed to separate the solution of the Schrödinger equation into an electronic part, where the atomic charges and positions enter as external parameters, and an ionic part, where the atomic nuclei move in the energy landscape provided by the electronic solution. In many cases this approximation is appropriate since the mass difference between the nuclei and the electrons allows to separate the time scales on which both constituents move. The light and fast electrons instantaneously adjust to an atomic movement and thus see the atoms as static objects. The direct approach to generate the electronic solution of the Schrödinger equation is the representation of the many-electron wave function, which can be expressed for weakly correlated electron systems in terms of products of non-interacting single-particle wave functions in the Hartree- and Hartree-Fock methods and their descendants [18–20].

An alternative and highly successful approach is density functional theory [21, 22], which in the spirit of the Thomas-Fermi model [23, 24] replaces the complex many-electron wave function as the central quantity of interest by the simple electronic density. Hohenberg and Kohn showed that the electronic density contains in principle all information to describe the system. Today, density functional theory is the workhorse for solid state physics, quantum chemistry, materials and nanosciences. With the availability of increasingly more powerful computers, its importance will continue to rise. An indication for the popularity of density functional theory is the total number of publications concerning this topic, which exceeds 250.000 as of July 2015, with over 29.000 publications in 2014.

The strong interest in density functional theory manifests itself in the various realizations and in the development of different schemes to calculate phonon spectra.

One of the earliest schemes to determine phonon spectra from first principles is the frozenphonon method [25–27]. The frozen-phonon approach enables to compute phonon frequencies at a crystal momentum q, but requires the polarization vector of the corresponding

¹Search performed with the phrase "density functional theory" in the title, the abstract, and the keywords of publications on Web of Science, http://wokinfo.com/.

phonon as input before one can start the simulation. For simple systems and if high symmetry is present, the polarization vector can be deduced from group theoretical considerations. The crystal is then subjected to the phononic displacement and one calculates the total energy for different displacement amplitudes. The curvature of the resulting energy versus displacement-amplitude curve corresponds to the phonon energy. For systems with many atoms per unit cell and patterns belonging to arbitrary wave vectors \boldsymbol{q} , this approach becomes unfeasible for two reasons: (a) the determination of a polarization vector becomes drastically more involved and (b) the \boldsymbol{q} -vector defines the size of a supercell required to realize the displacement pattern. A $2\times2\times2$ supercell, *i.e.*, the repetition of the primitive unit cell in each direction by one, is needed so a high-symmetry \boldsymbol{q} displacement pattern can be hosted by the larger unit cell while keeping its translational symmetry. A phonon of such a \boldsymbol{q} -vector is called commensurable with the underlying supercell. The calculation of phonon energies at small \boldsymbol{q} -vectors, *i.e.*, with a long wavelength, requires very large supercells.

The tedious precalculation of a displacement pattern is avoided in the finite-displacement method [28–31], in which the force-constant matrix is approximated using atomic forces. Starting from the equilibrium configuration of the lattice, each atom is displaced in each spatial direction in a separate calculation. The forces on all atoms are calculated and subsequently divided by the amplitude of the displacement to obtain the force-constant matrix. The force-constant matrix is then Fourier transformed to get the dynamical matrix and the phonon energies and polarization vectors are extracted. This approach yields exact energies for phonons of a q-vector that is commensurable with the unit cell. Thus, a setup of large supercells is still required if more than just high-symmetry q phonons need to be determined exactly.

The need for supercells is omitted applying density functional perturbation theory [32–36], which is used to directly calculate the second-order derivative of the total energy in linear response. This approach enables to calculate exact phonon energies at arbitrary crystal momenta q. Starting from an electronic structure calculation, the underlying system is perturbed by a phonon of wave vector q. This results in a change of the external potential. The corresponding first-order responses of the wave functions and the density are constructed by solving the Sternheimer equation [37–40], which is the linearized Schrödinger equation. The solution has to be found self-consistently, since the change in the electronic density implies also a change in the Hartree and the exchange-correlation potential. The underlying self-consistent-field procedure is in analogy to the construction of the unperturbed density in a regular electronic structure calculation. From the first-order change in the wave functions and density, the dynamical matrix D(q) can be constructed almost immediately, giving rise to the phonon energies and polarization vectors. The computation of the necessary second-order changes is less involved, since no self-consistency has to be achieved. The calculation of a phonon band structure along a given path can be performed by repeating this procedure for every q-point of this path. This can become easily very time consuming. Alternatively, the construction of the dynamical matrix can be performed for some q only, and the force-constant matrix is approximated from a backtransformation from reciprocal space to real space.

In all cases above, the force-constant matrix is then used to Fourier interpolate the phonon band structure at the remaining q-points of the Brillouin zone.

By far, most of the phonon calculations are carried out using pseudopotential methods [41] and the projector augmented plane wave method [32].

In this thesis, we focus on phonon calculations employing the finite-displacement and density-

1. Introduction

functional-perturbation-theory schemes with the all-electron full-potential linearized augmented-plane-wave (FLAPW) method [42–45]. This method treats the tightly bound core states and the valence states on the same footing and without approximating the shape of the potential. Hence, it is widely considered to be the gold standard of electronic structure methods and often serves as a benchmark method to which other electronic structure methods and realizations of Kohn-Sham density functional theory are compared. The ability of the FLAPW method to treat the Schrödinger equation accurately stems from the choice of basis functions: plane waves are used in the interstitial region separating the atoms and numerical radial functions are used in the non-overlapping muffin-tin spheres around the atoms. The radial functions are solutions to the spherical potential for a given energy parameter. Quantities like the density or the potential are also represented piecewise in the muffin-tin spheres and the interstitial region.

Although the FLAPW method is highly accurate, the efficient and intricate basis set is technically and numerically very challenging if response quantities are required. Quantities like the force exerted on the atom - this involves the derivative of the wave function - are nontrivial quantities in the context of this method, because the derivative of the wave function might not be completely part of the Hilbert space spanned by the basis functions. Therefore, phonon calculations based on density functional perturbation theory with the FLAPW method are rare. They are limited to publications of Wang, Yu, and Krakauer [46–49] who however replace the all-electron aspect by integrating a pseudopotential into the method, and Kouba et al. [50] as well as Lee [51], who have presented a linear response formalism for the FLAPW method, whose applicability to real systems is still open at this point.

The interest in merging the calculation of phonon band structures with the FLAPW method comes from the fact that the FLAPW method is not only accurate, but it is also applicable to a wide variety of systems. Especially complex magnetic systems or low-symmetry systems containing many atoms are accurately described. In principle, the FLAPW method is able to treat solids which contain any element of the periodic table, be it light atoms or d and f atoms. Therefore, phonon calculations in the context of the FLAPW method will lead to the availability of reliable phonon band structures of complex materials.

In the finite-displacement method, the construction of the force-constant matrix corresponds to an analytical derivation of the total energy in terms of a force formalism followed by a numerical derivation of the obtained forces in the finite-displacement method. For the FLAPW method, a force formalism was introduced in the seminal works of Soler and Williams [52, 53], and Yu et al. [54] around 1990, approximately ten years after the advent of the FLAPW method. Both groups report the appearance of Pulay forces [55] in addition to the Hellmann-Feynman force. The additional Pulav terms arise due to the incompleteness of the LAPW basis set, which renders the wave functions to be variational and not pointwise solutions of the Schrödinger equation, and its dependence on the atomic positions. Further discussions of the atomic forces within the FLAPW method are given by Kohler et al. [56]. Despite this important correction, we have observed that the atomic forces of a practical calculation can add up to a net drift force in the order of magnitude of $mHtr/a_B$, which is a contradiction to the fact that the sum of the forces on all atoms of the unit cell must vanish. Obviously, conjugate entries of the force-constant matrix deviate from each other in the order of magnitude of mHtr/a_B (when the division by the displacement amplitude is not yet applied), making the force-constant matrix much too unreliable to calculate a phonon dispersion.

In this thesis, we present a refined force formalism based on the original work of Yu et~al., which includes the whole unit cell into the calculation of the force contribution from the core states. This contribution would otherwisely be calculated using only the muffin-tin sphere from which the core state originates. Furthermore, our formalism rigorously accounts for the discontinuity of the LAPW basis function, the density, and the potential at the muffin-tin sphere boundary. The latter arises from the fact that the muffin-tin representation is limited to a maximal angular-momentum cutoff $l_{\rm max}$ in practical calculations, while the interstitial representation contains all angular-momentum channels, as can be seen from a Rayleigh expansion of the plane waves. We demonstrate that the drift force is reduced by three orders of magnitude from $m{\rm Htr}/a_{\rm B}$ to $\mu{\rm Htr}/a_{\rm B}$ and that the symmetry of the force-constant matrix is improved to the same order of magnitude. This makes finally reliable phonon calculations possible.

The improvement of the forces is demonstrated for the prototype systems Al, MgO, GaAs, EuTiO₃, and VO₂. For the former four systems, we also provide phonon band structures calculated in the finite-displacement approach by using forces obtained with the FLEUR code [57] in conjunction with the finite-displacement code PHON by Alfè [58].

In the final part of this thesis, we derive DFPT in the context of the FLAPW method starting from the method-unspecific introduction to DFPT by Savrasov in [34], who eventually provided in this paper the DFPT scheme for the linearized muffin-tin orbital approach, which is a different all-electron method [59–61]. In our derivation, we draw from the experience obtained from the force formalism: The dependence of the LAPW basis on the atomic position leads to Pulay corrections. The discontinuity of the basis functions, the density, and the potential leads to surface corrections, and we include the whole unit cell into the calculation of the core-state contribution. These adjustments are included both in the derivation of the first-order quantities within the Sternheimer equation and in the derivation of the dynamical matrix.

Since the FLAPW wave functions are described in terms of a basis with corresponding expansion coefficients, the variation of a wave function results in separate variations of the basis functions and of the expansion coefficients. In this case, the Sternheimer equation transforms into a matrix equation defining the variation of the expansion coefficients, while the variation of the basis functions is calculated directly from the perturbation. In this matrix equation, we observe that the rigid part of the perturbed density and potential cancels before it has to be evaluated for the Sternheimer equation.

Although our derivation is independent of the FLAPW DFPT derivation of Kouba $et\ al.\ [50]$, we naturally arrive at a Sternheimer matrix equation similar to that in [50]. The difference between their equation and the one we present in this thesis manifests in the surface terms. We include also the zeroth and first order discontinuities of the basis functions into our considerations. Kouba $et\ al.$ on the other hand assume that the basis functions are completely continuous up to first order. Hence, our Sternheimer matrix equations deviate in the kind of representation that is to use to evaluate the surface integrals. While we consider the basis functions to be given in interstitial representation, for example, their Sternheimer matrix equation uses the muffin-tin representation in the surface integrals. However, in contrast to their theoretical derivation, Kouba $et\ al.$ also use the interstitial representation of the basis functions in practical calculations, since they assume that the basis functions are continuous and they claim that using the interstitial representation eases the evaluation of the surface terms. Therefore, our DFPT formalism for calculating phonons within the FLAPW method validates their implementation.

1. Introduction

We do not only present the first-order variations obtained from the self-consistent solution of the Sternheimer equation, but also the second-order variations in the wave functions, in the external potential and in the ion-ion energy. For all variations of the electrostatic potential terms it holds that the direct evaluation poses a challenge in the FLAPW method due to the distinction of the unit cell into muffin-tin spheres and the interstitial region. Instead, we use a procedure developed by Weinert [62] to calculate the first- and secondorder variations of the electrostatic potential. In this procedure, the potential of a charge density contained in a distant volume is computed purely from the multipole moments in this volume. Since the relation between charge distribution and multipole moments is not unique, the original density in the volume can be replaced by a smooth pseudo charge density that has the same multipole moments. Then, the electrostatic potential outside of the volume can be expressed by Poisson's equation in reciprocal space. The potential within the volume is constructed from a Dirichlet boundary-value problem afterwards, using the outside potential for the boundary values. In the FLAPW method, the volume is given by the muffin-tin spheres and the outside region is the interstitial. For the regular electronic structure calculation, the electrostatic density is used as the charge density in the procedure of Weinert. For expressing the first- and second-order variations in the Coulomb potential, the charge density is replaced by the first- and second-order variations of the electrostatic density.

The manuscript is organized as follows: In chapter 2, a brief introduction to density functional theory and the Kohn-Sham formalism is presented. This introduction includes the basic equations and quantities. The FLAPW method is discussed with its predecessors in chapter 3. Also the local orbital extension is introduced, as well as a detailed mathematical view on the Pulay terms. Chapter 4 introduces the FLAPW force formalism of Yu et al. and our refinements to yield more precise forces. This refinement is demonstrated for the prototype systems Al, MgO, GaAs, EuTiO₃, and VO₂. The construction of the dynamical matrix from the atomic forces is presented in chapter 5. Phonon spectra for the subset Al, MgO, GaAs, and EuTiO₃ are given. A general introduction to density functional perturbation theory is provided in chapter 6, where it also is applied to the FLAPW method. In chapter 7, the results from the previous chapter are used to derive the formulas necessary to treat phonons with density functional perturbation theory in the FLAPW method. Chapter 8 concludes this thesis.

Parts and results presented in chapters 4 and 5 have been published in *Physical Review* $\bf B$ [63].

2. Density functional theory

A molecule or a solid state body consists of a conglomerate system of many atoms, which in turn consist of the atomic nucleus and one or more electrons. The interplay between all these particles poses a many-body problem in which the current state and the evolution of a particular particle are dependent on state and evolution of all the other particles as well. A solution of this many-body problem provides knowledge on the properties of the system. These properties include, among others, the stable assembly of the participants into a molecule or solid in the first place, as well as the formation of electronic bands, conductance, and magnetism, most of which would not occur or not bear meaning if only single atoms were considered. Unfortunately, the complexity inherent to a full description of all particles involved and their dependencies on each other deny an analytic treatment of the problem in all but the simplest cases. Also, a direct numerical approach is unfeasible: To represent a function dependent on a sole iron atom and its twenty-six electrons on a coarse mesh of eight mesh points in each spatial direction would require to store the functions value for $(8^3)^{27}$ configurations of the particles. If the function would be stored with double precision, i.e., with eight bytes of storage per entry, this would amount to 8^{62} exabyte of memory space, which is an impossible amount of data to store, let alone to operate with or on it.

Indeed, already in 1929 Paul Dirac foreshadowed that even though "the underlying physical laws necessary for [...] a large part of physics and the whole of chemistry are thus completely known, [...] the difficulty is only that the exact application of these laws leads to equations which are too complicated to be soluble. It therefore becomes desirable that approximate practical methods of applying quantum mechanics should be developed, which can lead to an explanation of the main features of complex atomic systems without too much computation." [64]

After a more formal introduction to the many-body problem, this chapter will provide one such method in the form of density functional theory (DFT) [21], which has its foundation in the theorem of Hohenberg and Kohn. Furthermore, the Kohn-Sham formalism [22] is introduced that puts DFT into a practical method and different approximations are discussed for the exchange-correlation (xc) functional that includes the many-body interactions into Kohn-Sham DFT. We finalize this chapter by presenting spin-DFT.

2.1. The many-body Hamiltonian

We consider a system of $N_{\rm at}$ atomic nuclei of charges Z_{α} located at τ_{α} , $\alpha = 1...N_{\rm at}$. Furthermore, for each atomic nucleus, there be Z_{α} electrons, $N_{\rm el}$ in total. Their locations are denoted by \mathbf{r}_i , $i = 1...N_{\rm el}$. This system is governed by the many-body Schrödinger equation

$$\hat{\mathcal{H}} |\psi\rangle = i\partial_t |\psi\rangle$$
, with (2.1)

$$\hat{\mathcal{H}} = T_{\rm el} + T_{\rm ion} + U_{\rm el-el} + U_{\rm ion-ion} + U_{\rm ion-el}, \tag{2.2}$$

2. Density functional theory

where the Hamiltonian $\hat{\mathcal{H}}$ consists of the kinetic energy as well as the electrostatic attraction or repulsion between the particles

$$\begin{split} T_{\rm el} &= -\frac{1}{2} \sum_{i}^{N_{\rm el}} \nabla_{\rm i}^2, \qquad T_{\rm ion} = -\frac{1}{2 \tilde{M}_{\alpha}} \sum_{\alpha}^{N_{\rm at}} \nabla_{\alpha}^2, \\ U_{\rm el\text{-}el} &= \frac{1}{2} \sum_{\substack{i,j \\ i \neq j}} \frac{1}{|\boldsymbol{r}_i - \boldsymbol{r}_j|}, \qquad U_{\rm ion\text{-}ion} = \frac{1}{2} \sum_{\substack{\alpha,\beta \\ \alpha \neq \beta}} \frac{Z_{\alpha} Z_{\beta}}{|\boldsymbol{\tau}_{\alpha} - \boldsymbol{\tau}_{\beta}|}, \qquad U_{\rm ion\text{-}el} = -\sum_{i,\alpha} \frac{Z_{\alpha}}{|\boldsymbol{r}_i - \boldsymbol{\tau}_{\alpha}|}. \end{split}$$

 \tilde{M}_{α} denotes the relative mass of the nuclei with respect to a single electron. We employ Hartree units¹ here and in the following if not stated otherwise. The wave functions that are solutions to this Hamiltonian depend on the coordinates of each nucleus and each electron. The problem is cast to that of only the electronic system by the Born-Oppenheimer approximation [17]: The large relative mass of the nuclei as compared to the electrons suggests that the motion of the nuclei and the motion of the electrons appear on a different time scale. In the Born-Oppenheimer approximation the atomic positions are hence considered to be external parameters. Any configuration of nuclei provides an external potential for the electronic system, to which it adapts instantaneously.

Still, the electronic problem remains to be solved. In the quantum chemistry school of thought, this is attempted by searching for the many-body wave function. The difficulty to do so is due to the electron-electron term $U_{\rm el-el}$. Without it, the Hamiltonian would be the sum of single particle Hamiltonians and a product ansatz for the many-body wave function in terms of single particles would work perfectly fine. Each component of the product could be handled separately then. However, with the electron-electron interaction in place, such a product ansatz becomes an approximation and also lacks the antisymmetry which the many-body wave function has to possess. The easiest way to include this requirement is by the Hartree-Fock method [18], in which the product of the single particle wave functions is replaced by a single Slater determinant. Minimization of the total energy then determines the orbitals. Further refinements are linear combinations of Slater determinants in the configuration-interaction [19] and coupled-cluster methods [20]. The drawback of these methods is the increasingly bad scaling with system size. Therefore, they are not well suited to be used on solid state bodies.

In this work, we use a different approach in the form of density functional theory. In it, the electron density replaces the many-body wave function as the central quantity.

2.2. The theorem of Hohenberg and Kohn

In 1964, Hohenberg and Kohn published the foundation of density functional theory by two fundamental statements [21]:

1. The external potential $V_{\rm ext}(r)$ specifying the atomic configuration of a system is a unique functional of the electronic ground state density $\rho_0(r)$ of this system, apart from a constant shift in the potential. The same is true for the ground-state energy $E[\rho_0]$ and all other ground-state properties.

 $^{^1 \}text{In}$ Hartree units, the electron charge e and mass $m_{\rm e}$, the reduced Planck's constant $\hbar = h/2\pi,$ and Coulomb's constant $k_{\rm e} = 1/4\pi\varepsilon_0$ are the reference quantities, therefore $e=m_{\rm e}=\hbar=k_{\rm e}=1$ and every quantity is expressed with respect to these units.

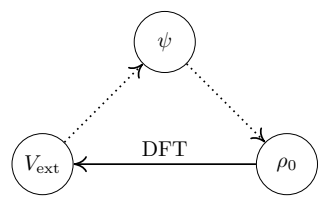


Figure 2.1.: Textbook physics follows the dotted path: From the external potential one obtains the wave functions, which give the density. DFT closes the loop, the external potential is uniquely defined by the ground state density.

2. The ground-state density minimizes the total-energy functional among all densities that reproduce the same number of electrons $N_{\rm el}$, i.e.,

$$E[\rho] > E[\rho_0] \tag{2.3}$$

for all $\rho(\mathbf{r}) \neq \rho_0(\mathbf{r})$, $\int \rho(\mathbf{r}) d^3 r = N_{\rm el} = \int \rho_0(\mathbf{r}) d^3 r$.

These statements allow to replace the many-body wave function as the central quantity of interest by the electronic ground-state density: The content of the first statement is basically that not only the complicated many-body wave function, but also the electronic ground-state density contains every information on the system; from it, the external potential can be reconstructed which in turn leads to the wave functions again. At the position of a positively charged nucleus, the electronic density is higher, and by Kato's theorem [65], the atom type of the nucleus can be extracted from the shape of the density. Therefore, any observable O can be expressed as a functional of the density, $O[\rho_0]$. The second statement means that the total energy of a system is variational with respect to the ground-state density. Any density from the same number of electrons that deviates from the ground-state density will result in a higher total energy of the system. Hence, the density can be made subject to a minimization procedure.

The advantage of the electronic density over the many-body wave function as the central quantity from which the properties of a system are determined is that the electronic density is a scalar, real-valued function of space, i.e., only dependent on one three-dimensional spatial coordinate r. As such, it is readily manageable in terms of computer storage and memory.

A comparison between textbook physics and DFT is sketched in Fig. 2.1: Usually, one starts from the Hamiltonian to find the wave functions. These in turn can be condensed to the electronic density. With the theorem of Hohenberg an Kohn, the external potential, being the degree of freedom in the Hamiltonian, can be extracted from the ground state density again, along with any other observable of interest, either explicitly or implicitly.

While density functional theory is a promising prospect up to this point, the theorem of Hohenberg and Kohn does not yet lead to a practicable scheme to find the ground-state density. There exist different approaches to make DFT a working scheme, like the one by Korringer, Kohn, and Rostoker [66–68], which is a Green function method. We use

2. Density functional theory

the Kohn-Sham formalism instead, where the electronic density is constructed from wave functions, not from the imaginary part of the Green function.

2.3. The Kohn-Sham formalism

The importance of the Hohenberg-Kohn theorem does not only arise from a convenience argument concerning the memory necessary to transfer the task to solve the Schrödinger equation onto a computing machine, but also from the implication that any way to obtain the correct ground-state density in principle suffices to find the ground-state properties of the system at hand. In 1965, Kohn and Sham [22] published a way to exploit this freedom in obtaining the ground-state density by suggesting an auxiliary set of non-interacting states ψ_1^{KS} , which solve a single-particle Schrödinger equation of the form

$$\left(-\frac{1}{2}\nabla^2 + V_{\text{eff}}(\mathbf{r})\right)\psi_i^{\text{KS}}(\mathbf{r}) = \epsilon_i^{\text{KS}}\psi_i^{\text{KS}}(\mathbf{r}), \tag{2.4}$$

where the effective, local potential $V_{\rm eff}(r)$ is such that the Kohn-Sham states filled according to the occupation number f_i of the electronic band i reproduce the same density as in the fully-interacting system,

$$\rho(\mathbf{r}) = \sum_{i} f_{i} \psi_{i}^{\text{KS}*}(\mathbf{r}) \psi_{i}^{\text{KS}}(\mathbf{r}). \tag{2.5}$$

The motivation behind this equation is the following: The total energy of the electron system is given by the sum of the kinetic energy $T_{\rm el}[\rho]$ and the Coulomb terms between the electrons $U_{\rm el-el}[\rho]$ and between the electrons and nuclei $U_{\rm ion-el}$,

$$E_{\rm el}[\rho] = T_{\rm el}[\rho] + U_{\rm el-el}[\rho] + U_{\rm ion-el}[\rho]$$
(2.6)

This energy can be rewritten in terms of the auxiliary, non-interacting (ni) system as

$$E_{\rm el}[\rho] = T_{\rm ni}[\rho] + \frac{1}{2} \int \int \frac{\rho(\boldsymbol{r})\rho(\boldsymbol{r}')}{|\boldsymbol{r} - \boldsymbol{r}'|} d^3r' d^3r - \sum_{\alpha}^{N_{\alpha}} \int \frac{Z_{\alpha}\rho(\boldsymbol{r})}{|\boldsymbol{r} - \boldsymbol{\tau}_{\alpha}|} d^3r + E_{\rm xc}[\rho]. \tag{2.7}$$

The first three terms are directly obtainable from the non-interacting Kohn-Sham system. The so-called exchange-correlation energy $E_{\rm xc}[\rho]$ is defined by the difference in energy between the interacting and the non-interacting system:

$$E_{\rm xc}[\rho] = (T_{\rm el}[\rho] - T_{\rm ni}[\rho]) + (U_{\rm el-el}[\rho] - \frac{1}{2} \int \int \frac{\rho(\mathbf{r})\rho(\mathbf{r}')}{|\mathbf{r} - \mathbf{r}'|} d^3 r' d^3 r)$$

$$+ (U_{\rm ion-el}[\rho] + \sum_{\alpha}^{N_{\alpha}} \int \frac{Z_{\alpha}\rho(\mathbf{r})}{|\mathbf{r} - \mathbf{\tau}_{\alpha}|} d^3 r)$$

$$(2.8)$$

$$= \int \rho(\mathbf{r})\epsilon_{\rm xc}[\rho](\mathbf{r})d^3r \tag{2.9}$$

We will discuss the exchange-correlation energy in more detail in the next section. For now it suffices to know that all effects related to the exchange of electrons and the correlations between them, which compose the many-body character of the fully-interacting system,

are hidden in the exchange-correlation terms. $\epsilon_{\rm xc}[\rho](\boldsymbol{r})$ is the exchange-correlation energy density. Variation of the electronic energy with respect to a Kohn-Sham state $\psi_i^{\rm KS*}(\boldsymbol{r})$ under the constraint that the KS states are normalized yields the Kohn-Sham equations from above, Eq. (2.4), with

$$V_{\text{eff}}(\mathbf{r}) = V_{\text{H}}(\mathbf{r}) + V_{\text{ext}}(\mathbf{r}) + \mu_{\text{xc}}[\rho](\mathbf{r}), \text{ and}$$
 (2.10)

$$V_{\rm H}(\mathbf{r}) = \int \frac{\rho(\mathbf{r}')}{|\mathbf{r} - \mathbf{r}'|} d^3 r', \tag{2.11}$$

$$V_{\text{ext}}(\mathbf{r}) = -\sum_{\alpha}^{N_{\text{at}}} \frac{Z_{\alpha}}{|\mathbf{r} - \boldsymbol{\tau}_{\alpha}|},$$
(2.12)

and the exchange-correlation potential

$$\mu_{\rm xc}[\rho](\mathbf{r}) = \frac{\delta E_{\rm xc}[\rho]}{\delta \rho(\mathbf{r})} = \frac{\delta(\rho(\mathbf{r})\epsilon_{\rm xc}[\rho](\mathbf{r}))}{\delta \rho(\mathbf{r})}.$$
 (2.13)

Equations (2.4), (2.5), and (2.10) form a set of self-consistent equations because $V_{\rm H}$ and $\mu_{\rm xc}[\rho]$ are dependent on the electronic density.

The total energy as given from the iteratively determined, self-consistent Kohn-Sham states, including the ion-ion interaction is given by

$$E_{\text{tot}} = \sum_{i} f_{i} \epsilon_{i}^{\text{KS}} - \int \rho_{0}(\boldsymbol{r}) V_{\text{eff}}(\boldsymbol{r}) d^{3}r + \frac{1}{2} \iint \frac{\rho_{0}(\boldsymbol{r}) \rho_{0}(\boldsymbol{r}')}{|\boldsymbol{r} - \boldsymbol{r}'|} d^{3}r' d^{3}r$$
$$- \sum_{\alpha}^{N_{\text{at}}} \int \frac{Z_{\alpha} \rho_{0}(\boldsymbol{r}')}{|\boldsymbol{\tau}_{\alpha} - \boldsymbol{r}'|} d^{3}r' + \frac{1}{2} \sum_{\alpha \neq \beta}^{N_{\text{at}}} \frac{Z_{\alpha} Z_{\beta}}{|\boldsymbol{\tau}_{\alpha} - \boldsymbol{\tau}_{\beta}|} + \int \rho_{0}(\boldsymbol{r}) \varepsilon_{\text{xc}}[\rho_{0}](\boldsymbol{r}) d^{3}r, \qquad (2.14)$$

where the contribution from the non-interacting kinetic energy was rewritten using the Kohn-Sham equations, Eq. (2.4).

It is important to stress that the Kohn-Sham states and energies are in principle nothing more than an auxiliary construct to obtain the true electronic density and that they do not represent any true physical quantity. That said, $E_{\rm xc}[\rho]$ more often than not seems to provide only a small part to the total energy so that large pieces of the big picture are already governed by the non-xc part of the energy decomposition. Therefore, by experience, having the band structure of the Kohn-Sham system can be meaningful and provides an understanding of certain mechanics such as for example the mechanism behind topological insulators [69, 70]. We will omit the label KS in the remaining parts of this thesis.

2.4. The exchange-correlation functional

Up to this point, KS DFT is exact. With the correct exchange-correlation functional, the representation of the electronic density in terms of the auxiliary non-interacting Kohn-Sham states using a local effective potential is just a valid algebraic transformation. However, while the xc energy is formally defined in Eq. (2.8), its exact form is unknown. Hence, approximations are needed.

2. Density functional theory

The simplest one is the local density approximation (LDA). In it, one assumes that the xc energy density at a point r is given by the xc energy density of the homogeneous electron gas of density $\rho(r)$, *i.e.*, that the energy density functional is a mere function of the electronic density,

$$\epsilon_{\rm xc}[\rho](\mathbf{r}) = \epsilon_{\rm xc}(\rho(\mathbf{r})).$$
 (2.15)

The same holds for the xc potential $\mu_{\rm xc}(\rho(r))$. Since the functional is local and hence the changes of the electronic density in the vicinity of a point r are not accounted for at that point, one might doubt the usefulness of the LDA, because near the atomic nuclei, the density will vary strongly. However, this approximation yields surprisingly good results. The LDA functional is manufactured with a real physical system in mind, the homogeneous electron gas in its high and low density limits. It is believed that thereby it automatically fulfills certain conditions that the correct exchange-correlation functional needs to comply with [71]. There are several approximations on the LDA level, which deviate in the correlation part of the functional [72–77]. The LDA represents the first rung in Jacob's ladder of chemical accuracy, a metaphor to describe increasing accuracy in the xc approximations coined by John Perdew [78]. Fig. 2.2 illustrates the concept.

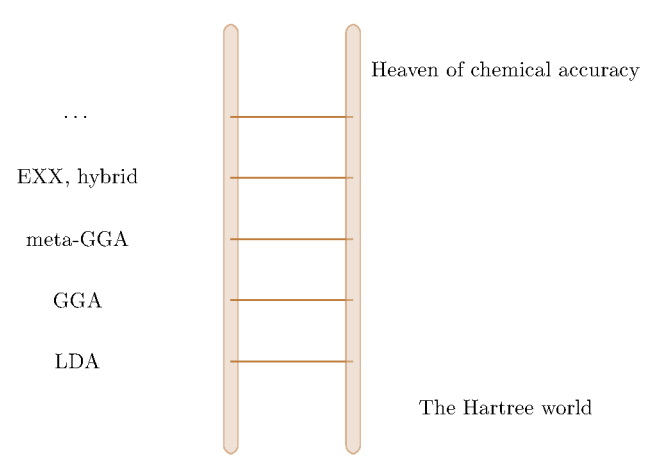


Figure 2.2.: Jacob's ladder of chemical accuracy, describing the quality of approximation of different approximations for the xc functional.

The next rung in this ladder is the generalized gradient approximation (GGA). It adds the gradient of the density as an argument to the xc energy density, but only in a local fashion:

$$\epsilon_{\rm xc}[\rho](\mathbf{r}) = \epsilon_{\rm xc}(\rho(\mathbf{r}), \nabla \rho(\mathbf{r}))$$
 (2.16)

Thereby, the xc functional is sensitive to the density in the vicinity of a point. Since this sensitivity also is of only local nature, the different GGA functionals [79–81] are often called semilocal.

A step further on Jacob's ladder includes meta-GGAs [82–84], where the kinetic energy density $\tau(r)$ defined by $T_{\rm ni} = \int \rho(r) \tau(r) d^3 r$ is taken into account in the exchange-correlation terms, and which is the last of the local approximations of the xc functional. The nonlocal approximations on the higher rungs include hybrid functionals [85–87] and exact exchange approaches [88–90], where different amounts of exact exchange energies are mixed to results from a local approximation and which are orbital dependent in order to construct this exact exchange.

In this work, however, we will restrict ourselves to the LDA, especially the formulation of the correlation energy density by Vosko, Wilk, and Nusair [74], whose parametrization we give in Appendix A.2, and only allow for the exception of LDA+U.

2.4.1. DFT + U

For historical reasons, the method we present in this chapter is also often called 'LDA+U', since first LDA calculations were augmented by it [91–93]. In fact, it has also been applied to GGA calculations [94] and can also have beneficial effects on other choices of the exchange-correlation functional, which do not properly take into account the self-interaction of the electrons.

By virtue of the Hartree energy $\frac{1}{2} \iint \rho(r) \rho(r')/|r-r'| d^3r' d^3r$ a Kohn-Sham state unphysically interacts with itself, because both electron densities contain a contribution from it. This effect has to be compensated for by the exchange-correlation energy $E_{\rm xc}$. However, since we need to employ approximations to the exchange-correlation terms, this compensation is imperfect for many choices of the exchange-correlation functional. Without a proper compensation for the self-interaction of the electronic state, the repulsion of this state is excessive compared to a compensated case. Thus, the state will be overly delocalized.

This effect becomes most prominent in systems with strongly localized electrons like transition metal oxides or systems where d and f electrons play an important role. The erroneous delocalization of these states leads to a larger overlap with other electronic states and thus to an artificial broadening of the electronic bands. Systems that should be insulating thus are often calculated as being metals due to this broadening of the bands.

To obtain more reliable results, in the DFT+U method the Kohn-Sham states $\psi_{ik}(r)$ required to be strongly localized are projected onto localized orbitals $\varphi_{lm}^{\alpha}(r)$ of atom α and of certain orbital character lm, which are then treated by a Hubbard model using a nonnegative parameter U_l^{α} to adjust the repulsion of the state from itself. The total energy then takes the form

$$E_{\text{DFT+U}}[\rho] = E_{\text{DFT}}[\rho] + E_{\text{Hub}}[\rho] - E_{\text{dc}}[\rho]$$

$$= E_{\text{DFT}}[\rho] + \sum_{\alpha} \left[\frac{U_l^{\alpha}}{2} \sum_{m \neq m'} n_{mm}^{\alpha l} n_{m'm'}^{\alpha l} - \frac{U_l^{\alpha}}{2} n^{\alpha l} (n^{\alpha l} - 1) \right]$$
(2.17)

with the double-counting term $E_{\text{dc}}[\rho]$ which subtracts the energy contribution from the states included in both the regular DFT total energy $E_{\text{DFT}}[\rho]$ and the Hubbard addendum $E_{\text{Hub}}[\rho]$, such that they are included only once. The $n_{mm}^{\alpha l}$ are the occupation numbers of the localized orbitals characterized by the atom index α where they are localized and the angular and magnetic momentum indices l and m:

$$n_{mm'}^{\alpha l} = \sum_{i\mathbf{k}} f_{i\mathbf{k}} \langle \psi_{i\mathbf{k}} | \varphi_{lm'}^{\alpha} \rangle \langle \varphi_{lm}^{\alpha} | \psi_{i\mathbf{k}} \rangle$$
 (2.18)

2. Density functional theory

$$n^{\alpha l} = \sum_{m} n_{mm}^{\alpha l} \tag{2.19}$$

We introduced here the bra-ket notation $\langle f|g\rangle$ as the scalar product between the functions f and g:

$$\langle f|g\rangle = \int f^*(\mathbf{r})g(\mathbf{r})d^3r$$
 (2.20)

The additional potential obtained from Eq. (2.17) can be calculated by variation with respect to ψ_{ik}^* to yield

$$V_{\rm U} = \sum_{\alpha} U_l^{\alpha} \left[\frac{1}{2} - n_{mm}^{\alpha l} \right] |\varphi_{lm}^{\alpha}\rangle \langle \varphi_{lm}^{\alpha}|. \tag{2.21}$$

Since U_l^{α} is positive, this additional potential penalizes less-than-half occupancies of the localized orbitals $\varphi_{lm}^{\alpha l}, n_{mm}^{\alpha l} < 1/2$, while it advocates a high occupancy of them, $n_{mm}^{\alpha l} > 1/2$. In total, fractional occupations of the localized states are suppressed, leading to a Mott localization of one state $n_{mm}^{\alpha l} \to 1$ at the cost of another state $n_{m'm'}^{\alpha l} \to 0$.

The choice of an appropriate value for U_l^{α} is a point of debate. Adjusting it to reproduce experimental results introduces the Hubbard interaction as an empirical parameter, thus leaving the realm of *ab-initio* electronic structure calculations. Two other approaches are to extract the parameter from constrained DFT calculations or from constrained random phase approximation (cRPA) calculations [95–100].

Another degree of freedom when using DFT+U is the exact form of the double-counting term. We introduced here the fully localized limit (FLL), which is appropriate for systems where the electrons are localized on specific orbitals. There exist other approaches like the around mean-field (AMF) formulation, which is more suited for systems that feature a quasi-homogeneous distribution of electrons but fluctuate slightly. We refer the interested reader to discussions on the choice of the double-counting term to [91, 101, 102].

Finally, the exact form of the orbitals φ^{α}_{lm} can be chosen among localized functions, such as Wannier functions [103, 104] or atomic orbitals [105].

2.5. Spin-density functional theory

While presenting the many-body Hamiltonian, Eq. (2.2), we pointed out that it naturally includes magnetism by the necessity to comply to the Pauli principle. This is also true for DFT and the single-particle Kohn-Sham system as introduced in the previous sections 2.2 and 2.3, since every observable is accessible as a functional dependent on the electronic density. However, the connection between the electronic density $\rho(r)$ and the magnetic density m(r) is not known explicitly. Instead, in spin-DFT [106]

$$\boldsymbol{m}(\boldsymbol{r}) = \sum_{i=1}^{N_{\rm el}} \boldsymbol{\psi}_i^*(\boldsymbol{r}) \cdot \underline{\boldsymbol{\sigma}} \cdot \boldsymbol{\psi}_i(\boldsymbol{r})$$
 (2.22)

is incorporated into the variational principle of the Hohenberg-Kohn theorem

$$E[\rho(\mathbf{r}), \mathbf{m}(\mathbf{r})] \ge E[\rho_0(\mathbf{r}), \mathbf{m}_0(\mathbf{r})]$$
(2.23)

and by distinguishing between majority and minority spin channels

$$\psi_i(\mathbf{r}) = \begin{pmatrix} \psi_{i\uparrow}(\mathbf{r}) \\ \psi_{i\downarrow}(\mathbf{r}) \end{pmatrix}, \tag{2.24}$$

$$\rho(\mathbf{r}) = \rho_{\uparrow}(\mathbf{r}) + \rho_{\downarrow}(\mathbf{r}). \tag{2.25}$$

 $\underline{\boldsymbol{\sigma}}$ is the vector of Pauli matrices

$$\underline{\boldsymbol{\sigma}} = (\underline{\boldsymbol{\sigma}}_x, \underline{\boldsymbol{\sigma}}_y, \underline{\boldsymbol{\sigma}}_z), \tag{2.26}$$

$$\underline{\boldsymbol{\sigma}}_{x} = \begin{pmatrix} 0 & 1 \\ 1 & 0 \end{pmatrix}, \underline{\boldsymbol{\sigma}}_{y} = \begin{pmatrix} 0 & -i \\ i & 0 \end{pmatrix}, \underline{\boldsymbol{\sigma}}_{z} = \begin{pmatrix} 1 & 0 \\ 0 & -1 \end{pmatrix}, \tag{2.27}$$

The magnetization density is also included in the exchange-correlation energy $E_{\rm xc}[\rho, m]$, while the Hartree and external potential are unaffected. Thus, variation of the Kohn-Sham equations with respect to $\psi_i^*(r)$ yields

$$\left(-\frac{1}{2}\nabla^2 + V_{\text{eff}}(\mathbf{r}) + \mu_{\text{B}}g_{\text{el}}\underline{\boldsymbol{\sigma}} \cdot \boldsymbol{B}_{\text{eff}}(\mathbf{r})\right)\boldsymbol{\psi}_i(\mathbf{r}) = \epsilon_i \boldsymbol{\psi}_i(\mathbf{r})$$
(2.28)

with the Bohr magneton $\mu_{\rm B}=1/2$ in Hartree units and the gyromagnetic ratio of the electron $g_{\rm el}$. The effective magnetic field subsumes a possible external magnetic field $\boldsymbol{B}_{\rm ext}(\boldsymbol{r})$ as well as the variation of the exchange-correlation energy with respect to the magnetization density $\boldsymbol{B}_{\rm xc}(\boldsymbol{r})$:

$$\boldsymbol{B}_{\text{eff}}(\boldsymbol{r}) = \boldsymbol{B}_{\text{ext}}(\boldsymbol{r}) + \boldsymbol{B}_{\text{xc}}(\boldsymbol{r}) \tag{2.29}$$

$$\boldsymbol{B}_{xc}(\boldsymbol{r}) = \frac{\delta E_{xc}[\rho, \boldsymbol{m}]}{\delta \boldsymbol{m}(\boldsymbol{r})}$$
(2.30)

The total energy is directly affected by the magnetization density in the exchange-correlation energy density yielding the contribution $E_{\rm xc}$ to it. However, if we apply analogous steps as for finding the total energy in the spinless case, Eq. (2.14), by replacing the kinetic energy contribution with the magnetic Kohn-Sham equation, Eq. (2.28), projected onto ψ_i and summed over all states i, we obtain another explicit contribution:

$$E_{\text{tot}} = \sum_{i} f_{i} \varepsilon_{i} - \int \rho_{0}(\mathbf{r}) V_{\text{eff}}(\mathbf{r}) d^{3}r - \mu_{\text{B}} g_{\text{el}} \int \mathbf{m}_{0}(\mathbf{r}) \cdot \mathbf{B}_{\text{eff}}(\mathbf{r}) d^{3}r$$

$$+ \frac{1}{2} \iint \frac{\rho_{0}(\mathbf{r}) \rho_{0}(\mathbf{r}')}{|\mathbf{r} - \mathbf{r}'|} d^{3}r' d^{3}r - \sum_{\alpha}^{N_{\text{at}}} \int \frac{Z_{\alpha} \rho_{0}(\mathbf{r}')}{|\mathbf{\tau}_{\alpha} - \mathbf{r}'|} d^{3}r' + \frac{1}{2} \sum_{\alpha \neq \beta}^{N_{\text{at}}} \frac{Z_{\alpha} Z_{\beta}}{|\mathbf{\tau}_{\alpha} - \mathbf{\tau}_{\beta}|}$$

$$+ \int \rho_{0}(\mathbf{r}) \varepsilon_{\text{xc}} [\rho_{0}, \mathbf{m}_{0}](\mathbf{r}) d^{3}r$$

$$(2.31)$$

Much insight already can be gained from the studies of ferromagnetic and antiferromagnetic systems or other configurations where the magnetic moments are aligned collinearily. In these important cases, an additional simplification can be applied. If the z-axis is set to point along the direction of the magnetic field, only $\underline{\sigma}_z$ contributes to the Kohn-Sham equation, decoupling the differential equations for spin-up and spin-down components of the wave function ψ_i . Then the total energy and all quantities derived from it are dependent only from the absolute value of the magnetization density m(r) = |m(r)|. In this case,

2. Density functional theory

the constituents of the second and third term of Eq. (2.31) are combined to yield the total effective potential $V_{\rm eff\sigma}$ per spin

$$V_{\text{eff}\sigma}(\mathbf{r}) = V_{\text{H}}(\mathbf{r}) + V_{\text{ext}}(\mathbf{r}) + \mu_{\text{xc}}[\rho_0, m_0](\mathbf{r}) - \sigma \mu_{\text{B}} g_{\text{el}} B_{\text{eff}\sigma}(\mathbf{r})$$
(2.32)

and σ corresponds to '+' in the spin up case and '-' in the spin-down case. The dependence of the total energy and the exchange-correlation quantities on $\rho(\mathbf{r})$ and $m(\mathbf{r})$ is sometimes expressed equivalently in terms of the spin-resolved densities $\rho_{\uparrow}(\mathbf{r})$ and $\rho_{\downarrow}(\mathbf{r})$ in collinear spin-density functional theory. Another representation uses the Seitz radius $r_s = r_s(\rho)$ and the spin polarization $\zeta = \zeta(\rho, m) = m/\rho$.

In this work, we will only consider collinear cases. As stated above, both spin channels can then be treated separately. Thus, we omit a distinction between spins except when explicitly stated.

3. Electronic structure methods

With density functional theory and the Kohn-Sham scheme as presented up until now, in principle any arrangement of atoms can be treated, be it a single atom, a molecule, a cluster, a slab, a semi-infinite volume with a single surface, or solid state bulk materials. Though, the different setups all come with particular properties. For example, isolated configurations like atoms or clusters impose that the wave functions decay far away from the configuration. On the other hand, a crystal features periodic boundary conditions in any direction. Due to this variety, many different electronic structure methods have been developed, as sketched in Fig. 3.1.

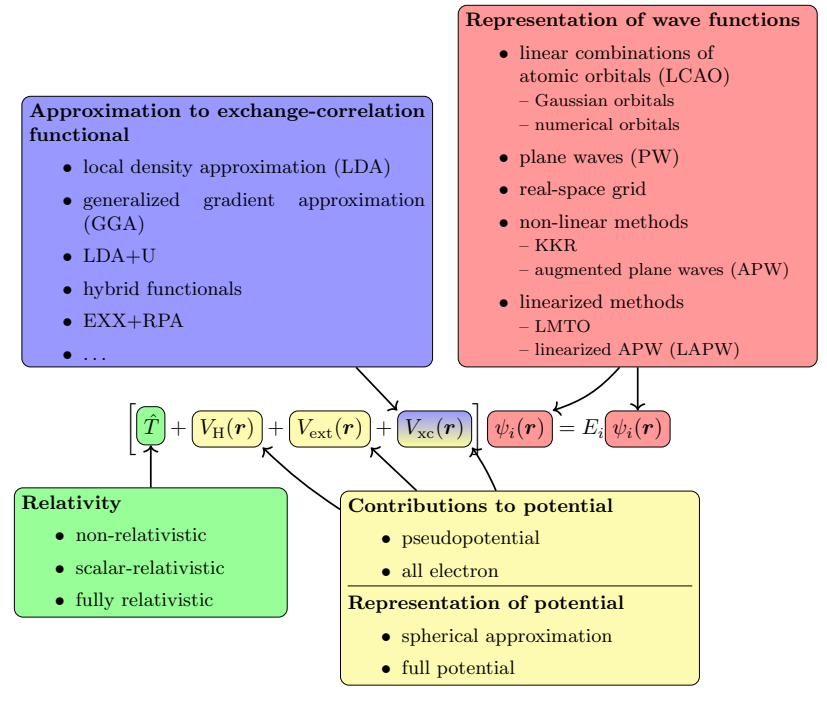


Figure 3.1.: Electronic structure methods. The figure is a modification of that shown in [107] and inspired by [108].

3. Electronic structure methods

The various electronic structure methods differ in a couple of aspects:

- The treatment of the kinetic energy can range from a non-relativistic approach to a fully-relativistic one, where the former is suited for calculations involving light atoms while the latter is appropriate if heavy atoms are considered. A scalar relativistic treatment poses a compromise between both ends of the scale. In it, relativistic effects are taken into account with the exclusion of spin-orbit coupling, such that different spin channels of the electron states do not couple [109].
- How the potential is handled is dependent on two choices:
- a) Does one wish to find solutions for any state or only for the states that contribute to chemical bonding? In the latter case, states that are low in energy and have little overlap with states from neighboring sites are merged with the external potential to pseudopotentials. Thereby, the states higher in energy are less complex. The price to pay is that the low energy states are not available and therefore effects that depend on them are excluded from the calculation. In the former case, all states are calculated and contribute to the total energy with how they perceive the effective potential.
- b) What approximations are done to the representation of the potential? If the physics one is interested in is governed by the spherical part of the potential near the atomic nuclei, it is sufficient to only consider it, at least to obtain a qualitative picture. The inclusion of the full potential leads to a description that is more accurate.
- We addressed already in chapter 2.4 the different approximations available to treat the exchange-correlation part of the potential.
- Finally, the choice of representing the wave functions depends on the system one
 is interested in. Atomic orbitals can be used in the context of isolated structures,
 while periodic systems allow for a plane-wave based approach. Furthermore, a Green
 function approach can be used instead of wave functions, as is done in the KKR [66–68]
 method.

For this thesis, we are interested particularly in bulk materials, which are periodic arrangements of atoms in a crystal structure. For such a setup, the all-electron full-potential linearized augmented plane-wave (FLAPW) method has proven to be the benchmark choice of electronic structure methods. We present in the following the historical evolution towards this methods starting from a plane-wave approach.

For the periodic systems we are interested in, we know by Bloch's theorem [110] that the solutions of the Kohn-Sham equations $\psi_{ik}(r)$ can be decomposed into a part $u_{ik}(r)$ periodic to the crystal and a phase factor containing the Bloch character k of the solution, which is a reciprocal vector within the first Brillouin zone:

$$\psi_{i\mathbf{k}}(\mathbf{r}) = e^{i\mathbf{k}\cdot\mathbf{r}} u_{i\mathbf{k}}(\mathbf{r}) \tag{3.1}$$

The periodicity of the u_{ik} enables us to apply a Fourier transform to it,

$$u_{i\mathbf{k}}(\mathbf{r}) = \sum_{\mathbf{G}} \hat{u}_{i\mathbf{k}}(\mathbf{G})e^{i\mathbf{G}\cdot\mathbf{r}},$$
 (3.2)

and thus to expand the wave function into plane waves,

$$\psi_{i\mathbf{k}}(\mathbf{r}) = \sum_{\mathbf{G}} z_{i\mathbf{k}\mathbf{G}} \phi_{\mathbf{k}\mathbf{G}}(\mathbf{r}). \tag{3.3}$$

These plane waves can be used as a basis set

$$\phi_{kG}(r) = \frac{1}{\sqrt{\Omega}} e^{i(k+G)\cdot r} \qquad (3.4)$$

with the expansion coefficients

$$z_{i\mathbf{k}\mathbf{G}} = \sqrt{\Omega}\hat{u}_{i\mathbf{k}}(\mathbf{G}),\tag{3.5}$$

where G are reciprocal lattice vectors and Ω is the volume of the unit cell, to which we can restrict ourselves due to periodicity. Using this representation in the Kohn-Sham equations (2.4) and projecting it onto $\phi_{kG'}$,

$$\sum_{\mathbf{G}} H_{\mathbf{G}'\mathbf{G}}(\mathbf{k}) z_{i\mathbf{k}\mathbf{G}} = \varepsilon_{i\mathbf{k}} \sum_{\mathbf{G}} S_{\mathbf{G}'\mathbf{G}}(\mathbf{k}) z_{i\mathbf{k}\mathbf{G}}, \text{ with}$$
(3.6)

$$H_{G'G}(\mathbf{k}) = \left\langle \phi_{\mathbf{k}G'} \middle| -\frac{1}{2} \nabla^2 + V_{\text{eff}} \middle| \phi_{\mathbf{k}G} \right\rangle_{\Omega}, \tag{3.7}$$

$$S_{\mathbf{G}'\mathbf{G}}(\mathbf{k}) = \langle \phi_{\mathbf{k}\mathbf{G}'} | \phi_{\mathbf{k}\mathbf{G}} \rangle_{\Omega},$$
 (3.8)

recasts the original differential equation into an algebraic one, where the expansion coefficients $z_{i\mathbf{k}\mathbf{G}}$ are the solutions of a (generalized) eigenvalue problem. The plane waves defined in (3.4) are orthogonal and normalized, meaning that the overlap matrix $S_{\mathbf{G}'\mathbf{G}}(\mathbf{k})$ is $\delta_{\mathbf{G}'\mathbf{G}}$, while the matrix $H_{\mathbf{G}'\mathbf{G}}(\mathbf{k})$ decomposes into $|\mathbf{k}+\mathbf{G}|^2/2 \cdot \delta_{\mathbf{G}'\mathbf{G}}$ and $\hat{V}_{\text{eff}}(\mathbf{G}'-\mathbf{G})$ since plane waves are eigenfunctions of the Laplacian and Fourier transform real space quantities.

While these properties advocate the use of plane waves as a basis set to represent the wave functions, there is a drawback: The 1-over-r character of the external potential produces wave functions that are heavily oscillating near the atomic nuclei. The reason for this is the necessity of the wave functions to be orthogonal to each other, thereby the wave functions higher in energy have to have more nodes than those lower in energy. To describe these oscillations using plane waves, these also need to be oscillating with a high frequency, resulting in contributions to the Fourier expansion with large reciprocal vectors G. Also, by Kato's theorem [65]

$$Z_{\alpha} = -\lim_{\mathbf{r} \to \tau_{\alpha}} \frac{1}{2} \frac{n'(\mathbf{r})}{n(\mathbf{r})},\tag{3.9}$$

the electronic density features cusps at the atomic positions, stemming from a discontinuous first derivative of the wave functions at τ_{α} .

Then, the second derivative which is generated from the Laplacian in the Hamilton operator produces a Dirac- δ which compensates the 1-over-r potential at the nucleus. Of course, also discontinuities in any order of a quantity to be Fourier transformed impede that a low reciprocal cutoff for the Fourier transform suffices.

The computational effort to handle such a large expansion is infeasible, which is why different methods were developed to reduce the amount of plane waves necessary to describe the wave functions. One way to deal with this problem is to exclude the low lying states from the description in terms of plane waves, as it is done in the pseudopotential [111] and projector augmented plane wave methods [112], reducing the amount of states to which the remaining states need to be orthogonal to. This procedure is justified by the assumption that only the valence states contribute to chemical bonding and determine the physical properties of

3. Electronic structure methods

a solid. Another way to reduce the number of plane waves is to change the description of the wave functions near the atomic nuclei from plane waves to a representation which more naturally includes the oscillations of the high lying states. This leads to the augmented plane wave (APW) type of approaches. The full-potential linearized-augmented plane-wave (FLAPW) method is an all-electron approach. It is implemented in the FLEUR-code [57], which has been used to produce the results of this thesis. In this chapter, we present the historical transition from the APW to the FLAPW method and elaborate on the treatment of core states and the local orbital extension. Furthermore, we showcase the Weinert approach to calculate the Coulomb potential. Lastly, we comment on the inclusion of relativism into an electronic structure calculation, explain Pulay contributions that can appear when for example a position dependent basis set such as the one used in the FLAPW method is differentiated with respect to the atomic positions, and present an extension of the KS formalism by Weinert and Davenport [113], which restores the variational property of the energy functional in case of metals.

3.1. The APW method

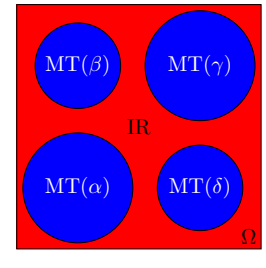
In the APW approach suggested by Slater [114], the unit cell Ω is partitioned into non-overlapping spheres $B_{R_{\alpha}}(\tau_{\alpha})$ of radius R_{α} around the atomic nuclei α at τ_{α} , so called muffintin (MT) spheres, and the interstitial region (IR) between these spheres. This partitioning is sketched in Fig. 3.2. According to the partitioning, the basis functions are defined piecewise

$$\phi_{kG}(\mathbf{r}) = \begin{cases} \frac{1}{\sqrt{\Omega}} e^{i(\mathbf{k}+\mathbf{G})\cdot\mathbf{r}} &, \mathbf{r} \in \mathbb{R} \\ \sum_{lm} a_{lm0}^{\alpha kG}(E_l^{\alpha}) u_l^{\alpha}(r_{\alpha}, E_l^{\alpha}) Y_{lm}(\hat{\mathbf{r}}_{\alpha}) &, \mathbf{r} \in \mathbf{MT}(\alpha) \end{cases}$$
(3.10)

Thus, plane waves are still used in the interstitial region, while sums of radial functions $u_l^{\alpha}(r_{\alpha}, E_l^{\alpha})$ times spherical harmonics $Y_{lm}(\hat{r}_{\alpha})$ are employed in the local coordinate frames $r_{\alpha} = r - \tau_{\alpha}$ of the muffin-tin spheres up to an atom dependent angular-momentum cutoff l_{\max}^{α} . The coefficients $a_{lm0}^{\alpha kG}(E_l^{\alpha})$ are determined by matching the muffin-tin representation of the basis function to the Rayleigh-expansion of its interstitial representation, yielding

$$a_{lm0}^{\alpha \mathbf{k} \mathbf{G}}(E_l^{\alpha}) = \frac{4\pi i^l}{\sqrt{\Omega}} e^{i(\mathbf{k} + \mathbf{G}) \cdot \boldsymbol{\tau}_{\alpha}} Y_{lm}^* (\widehat{\mathbf{k} + \mathbf{G}}) \frac{j_l(|\mathbf{k} + \mathbf{G}| R_{\alpha})}{u_l^{\alpha}(R_{\alpha}, E_l^{\alpha})}$$
(3.11)

Figure 3.2.: Division of space into muffin-tin spheres and the interstitial region.



with the spherical Bessel function $j_l(r)$. The index 0 denotes the affiliation of the matching coefficient to the radial function u_l^{α} in anticipation of the extention by the LAPW method, which we introduce in the next section. The functions u_l^{α} are solutions of

$$\left\{ -\frac{1}{2} \frac{d^2}{dr_{\alpha}^2} + \frac{l(l+1)}{2r_{\alpha}} + V_{\text{eff},00}^{\alpha}(r_{\alpha}) - E_l^{\alpha} \right\} r_{\alpha} u_l^{\alpha}(r_{\alpha}, E_l^{\alpha}) = 0$$
(3.12)

with the spherical (l=0, m=0) MT potential $V_{\text{eff},00}^{\alpha}$ of atom α (i.e., for $r_{\alpha} \leq R_{\alpha}$). E_{l}^{α} is a predefined energy parameter.

Furthermore, the potential is assumed to be constant in the IR and spherical in the MT spheres. It turns out that the wave function ψ_{ik} is only represented well by the APW basis functions for such a shape approximation to the potential, because only then the radial functions u_l^{α} constructed from energy parameters E_l^{α} set to the band energy ϵ_{ik} can be combined linearly to form an appropriate wave function; the APW basis is not flexible enough to provide a good description of ψ_{ik} when constructed from different energy parameters. However, the band energies are the quantities which one wants to determine with the electronic structure calculation. Therefore, starting from the lowest state, Hamilton and overlap matrices constructed from basis functions with an initial guess $E_l^{\alpha} = E$ for the band energy lead to the secular equation

$$\sum_{G} [H_{G'G}(\mathbf{k}, E) - \epsilon_{i\mathbf{k}} S_{G'G}(\mathbf{k}, E)] z_{i\mathbf{k}G} = 0.$$
(3.13)

From this equation, a refined guess can be extracted which serves as a foundation for the next iteration to find ϵ_{ik} , making the construction of the wave functions a non-linear procedure. Only if E and ϵ_{ik} coincide, selfconsistency is achieved, but only to represent the state ψ_{ik} . The whole procedure has to be repeated for each state.

Also, a bad choice of the muffin-tin radius R_{α} and the energy parameter E_l^{α} can result in a radial function u_l^{α} that is zero at the muffin-tin boundary. Then the matching coefficient $a_{lm0}^{\alpha kG}(E_l^{\alpha})$ is not well defined any more and the muffin-tin representation of the basis function decouples from its interstitial representation. This shortcoming of the APW method is called the asymptote problem.

Both the problem of lacking flexibility and the asymptote problem are avoided by introducing a linearization in energy of the basis functions, leading to the LAPW method.

3.2. The LAPW method

In the previous section, we discussed how a plane wave basis set could be augmented by replacing the description of the basis functions in the atom centered muffin-tin spheres by radial solutions to the Schrödinger equation. We also pointed out the asymptote problem and the issue of non-linearity when using the APW method, which makes it a computational demanding scheme. To circumvent these drawbacks, Andersen proposed to further augment the radial basis functions [59]. This is done in the spirit of a Taylor expansion around the energy parameter E_I^{α}

$$u_l^{\alpha}(r_{\alpha},\varepsilon) = u_l^{\alpha}(r_{\alpha}, E_l^{\alpha}) + (\varepsilon - E_l^{\alpha})\dot{u}_l^{\alpha}(r_{\alpha}, E_l^{\alpha}) + \mathcal{O}\left((\varepsilon - E_l^{\alpha})^2\right), \tag{3.14}$$

where an unknown radial function to an energy of ε can be approximated by a sum of the radial function u_l^{α} and its energy derivative \dot{u}_l^{α} evaluated at E_l^{α} . \dot{u}_l^{α} is obtainable by differentiating Eq. (3.12) with respect to the energy parameter:

$$\left\{ -\frac{1}{2} \frac{d^2}{dr_{\alpha}^2} + \frac{l(l+1)}{2r_{\alpha}} + V_{\text{eff},00}^{\alpha}(r_{\alpha}) - E_l^{\alpha} \right\} r_{\alpha} \dot{u}_l^{\alpha}(r_{\alpha}, E_l^{\alpha}) = r_{\alpha} u_l^{\alpha}(r_{\alpha}, E_l^{\alpha})$$
(3.15)

By adding a multiple of the homogeneous Eq. (3.12), \dot{u}_l^{α} is usually made orthogonal to u_l^{α} , as such a procedure eases further operation when a scalar product of both radial functions is formed. It is not mandatory, though. Using the local coordinate $\mathbf{r}_{\alpha} = \mathbf{r} - \mathbf{\tau}_{\alpha}$, the basis of the linearized-augmented plane-wave (LAPW) approach is given by

$$\phi_{kG}(\mathbf{r}) = \begin{cases} \frac{1}{\sqrt{\Omega}} e^{i(\mathbf{k} + \mathbf{G}) \cdot \mathbf{r}} &, \mathbf{r} \in \mathbf{IR} \\ \sum_{lm} \left[a_{lm0}^{\alpha \mathbf{k} \mathbf{G}} u_l^{\alpha}(r_{\alpha}, E_l^{\alpha}) + a_{lm1}^{\alpha \mathbf{k} \mathbf{G}} \dot{u}_l^{\alpha}(r_{\alpha}, E_l^{\alpha}) \right] Y_{lm}(\hat{\mathbf{r}}_{\alpha}) &, \mathbf{r} \in \mathbf{MT}(\alpha) \end{cases}$$
(3.16)

with the additional matching coefficient $a_{lm}^{\alpha kG}$ affiliated to the energy derivative \dot{u}_l^{α} of the radial basis function. The matching between the plane-wave and spherical-harmonic representation up to the angular-momentum cutoff l_{\max}^{α} now includes the first spatial derivative at the muffin-tin sphere boundary, leading to the equation

$$\begin{pmatrix} a_{lm0}^{\alpha\mathbf{k}\mathbf{G}} \\ a_{lm1}^{\alpha\mathbf{k}\mathbf{G}} \end{pmatrix} = \frac{4\pi i^{l}}{\sqrt{\Omega}} e^{i(\mathbf{k}+\mathbf{G})\cdot\boldsymbol{\tau}_{\alpha}} Y_{lm}^{*} \widehat{(\mathbf{k}+\mathbf{G})} \underline{\boldsymbol{U}}^{-1} \begin{pmatrix} j_{l}(|\mathbf{k}+\mathbf{G}|R_{\alpha}) \\ |\mathbf{k}+\mathbf{G}|j_{l}^{\prime}(|\mathbf{k}+\mathbf{G}|R_{\alpha}) \end{pmatrix}$$
(3.17)

with

$$\underline{\underline{U}}^{-1} = \frac{1}{W_l^{\alpha}(R_{\alpha}, E_l^{\alpha})} \begin{pmatrix} \dot{u}_l^{\alpha\prime}(R_{\alpha}, E_l^{\alpha}) & -\dot{u}_l^{\alpha}(R_{\alpha}, E_l^{\alpha}) \\ -u_l^{\alpha\prime}(R_{\alpha}, E_l^{\alpha}) & u_l^{\alpha}(R_{\alpha}, E_l^{\alpha}) \end{pmatrix}, \tag{3.18}$$

$$W_l^{\alpha}(R_{\alpha}, E_l^{\alpha}) = u_l^{\alpha}(R_{\alpha}, E_l^{\alpha})\dot{u}_l^{\alpha\prime}(R_{\alpha}, E_l^{\alpha}) - \dot{u}_l^{\alpha}(R_{\alpha}, E_l^{\alpha})u_l^{\alpha\prime}(R_{\alpha}, E_l^{\alpha}). \tag{3.19}$$

The LAPW method is not subject to the asymptote problem, because in place of the sole radial function u_l^{α} evaluated at R_{α} as in the APW method, now the Wronskian W_l^{α} appears in the denominator of the definition of the a_{lm0} and a_{lm1} coefficients. We show that the Wronskian does not vanish at the muffin-tin boundary. To see this, multiply Eq. (3.12) with r_{α} times \dot{u}_l^{α} and Eq. (3.15) with r_{α} times u_l^{α} , subtract both equations from each other and integrate to the muffin-tin boundary. The left hand side yields:

$$\frac{1}{2} \int_{0}^{R_{\alpha}} \left[r_{\alpha} \dot{u}_{l}^{\alpha} \frac{d^{2}}{dr_{\alpha}^{2}} r_{\alpha} u_{l}^{\alpha} - r_{\alpha} u_{l}^{\alpha} \frac{d^{2}}{dr_{\alpha}^{2}} r_{\alpha} \dot{u}_{l}^{\alpha} \right] dr_{\alpha} = \frac{1}{2} \left[r_{\alpha} \dot{u}_{l}^{\alpha} (r_{\alpha} u_{l}^{\alpha})' - r_{\alpha} u_{l}^{\alpha} (r_{\alpha} \dot{u}_{l}^{\alpha})' \right]_{0}^{R_{\alpha}}$$

$$= \frac{R_{\alpha}^{2}}{2} \left[\dot{u}_{l}^{\alpha} u_{l}^{\alpha'} - u_{l}^{\alpha} \dot{u}_{l}^{\alpha'} \right] \tag{3.20}$$

On the other hand, the right hand side is just

$$\int_0^{R_\alpha} r_\alpha^2 (u_l^\alpha)^2 dr_\alpha = 1. \tag{3.21}$$

Solved for the Wronskian, we see

$$W_l^{\alpha}(R_{\alpha}, E_l^{\alpha}) = -\frac{2}{R_{\alpha}^2} \neq 0. \tag{3.22}$$

Furthermore, the Taylor-like expansion of the radial function around E_{i}^{α} provides enough variational freedom to use this quantity as a parameter that does not need to be set to the exact band energy, since radial functions with an energy in the vicinity of this parameter are well approximated by u_i^{α} and \dot{u}_i^{α} . This allows for the determination of the band energies and wave functions by a single diagonalization of the Hamilton matrix (3.7). It also gives enough variational freedom to release the shape approximations to the potential employed within the APW scheme.

We will denote the zeroth-order energy derivative of the radial function $u_I^{\alpha}(r_{\alpha}, E_I^{\alpha})$ by $u_{10}^{\alpha}(r_{\alpha})$ and the first-order energy derivative as $u_{11}^{\alpha}(r_{\alpha})$, complying with the enumeration of the matching coefficients $a_{lm0/1}$ and suppressing the energy parameter. Since it is the matching coefficients that contain the G-dependence of the muffin-tin representation, we introduce a similar set of coefficients $A_{lm\lambda}$, $\lambda \in \{0,1\}$, which belong to the wave functions:

$$A_{lm\lambda}^{\alpha ik} = \sum_{G} z_{ikG} a_{lm\lambda}^{\alpha kG}$$
 (3.23)

$$A_{lm\lambda}^{\alpha i \mathbf{k}} = \sum_{\mathbf{G}} z_{i\mathbf{k}\mathbf{G}} a_{lm\lambda}^{\alpha \mathbf{k}\mathbf{G}}$$

$$\psi_{i\mathbf{k}}(\mathbf{r}_{\alpha}) = \sum_{\mathbf{G}} z_{i\mathbf{k}\mathbf{G}} \phi_{\mathbf{k}\mathbf{G}}(\mathbf{r}_{\alpha}) = \begin{cases} \sum_{\mathbf{G}} \frac{z_{i\mathbf{k}\mathbf{G}}}{\sqrt{\Omega}} e^{i(\mathbf{k}+\mathbf{G})\cdot\mathbf{r}} &, \mathbf{r} \in \mathbf{IR} \\ \sum_{lm\lambda} A_{lm\lambda}^{\alpha i \mathbf{k}} u_{l\lambda}^{\alpha}(r_{\alpha}) Y_{lm}(\hat{\mathbf{r}}_{\alpha}) &, \mathbf{r} \in \mathbf{MT}(\alpha) \end{cases}$$

$$(3.23)$$

The inclusion of \dot{u}_{r}^{α} to the basis set dealt with the asymptote problem and the non-linearity of the APW method. It is tempting to think that the systematic inclusion of \ddot{u}_i^{α} or even higher energy-derivatives of the solution of the radial Schrödinger equation are even more beneficial. However, these benefits are dampened by the price to pay for them: Two cutoff parameters define a practical calculation: G_{max} , which defines the number of IR plane waves included in the calculation and l_{\max}^{α} , which limits the spherical harmonics expansion of the MT basis functions. G_{max} sets for the interstitial region that all plane waves are included into the basis that fulfill $|\mathbf{k} + \mathbf{G}| \leq G_{\text{max}}$, or that have a kinetic energy less than $G_{\text{max}}^2/2$. The total radial functions of the muffin-tin spheres are constructed to be continuous to the plane waves up to first order in the l_{\max}^{α} angular-momentum channels, or up to higher order if the Taylor expansion would be continued. Therefore, the variational freedom the $u_{i\lambda}^{\alpha}$ provide is directly limited by the matching to and thus the number of the plane waves. To reap additional benefits from systematically adding higher energy-derivatives of the radial functions to the basis, also the number of plane waves would have to be increased. It is true that also the step from the APW method to its linearized counterpart already increases the number of plane waves required, but the omission of the asymptote problem, the possibility to use the E_r^{α} as parameters without worrying about non-linearity and the prospect of including the full potential into the description of the Hamiltonian outweights the additional cost in this case. The latter will be subject of the next chapter.

3.3. The FLAPW method

In the original APW scheme, the potential is usually set to a constant in the interstitial region and is assumed to be spherical within the muffin-tin spheres. The latter assumption is important in view of the choice of the energy parameters E_i^{α} , which need to be equal to the band energy corresponding to the spherical potential to give good results. A nonspherical potential on the other hand could be described by radial basis functions u_{α}^{α} .

dependent also on the magnetic moment m and for an appropriate energy. This is difficult to achieve in the APW formalism. However, the LAPW method is designed with the inherent flexibility to cope with an energy region close to the energy parameter. This opens the possibility to include the full potential into the electronic structure calculation by also implicitly approximating such u_{lm}^{α} by u_{l}^{α} and \dot{u}_{l}^{α} . This leads to the FLAPW method [42–44]. To that end, we first expand the electronic density ρ and the effective potential $V_{\rm eff}$ similar to the LAPW basis functions:

$$\rho(\boldsymbol{r}) = \begin{cases} \sum_{\boldsymbol{G}} \hat{\rho}(\boldsymbol{G}) e^{i\boldsymbol{G}\cdot\boldsymbol{r}} &, \ \boldsymbol{r} \in IR \\ \sum_{lm} \rho_{lm}^{\alpha}(r_{\alpha}) Y_{lm}(\hat{\boldsymbol{r}}_{\alpha}) &, \ \boldsymbol{r} \in MT(\alpha) \end{cases}$$
(3.25)

$$\rho(\mathbf{r}) = \begin{cases}
\sum_{lm} \hat{\rho}(\mathbf{G})e^{i\mathbf{G}\cdot\mathbf{r}} &, \mathbf{r} \in \mathbb{R} \\
\sum_{lm} \rho_{lm}^{\alpha}(r_{\alpha})Y_{lm}(\hat{\mathbf{r}}_{\alpha}) &, \mathbf{r} \in MT(\alpha)
\end{cases}$$

$$V_{\text{eff}}(\mathbf{r}) = \begin{cases}
\sum_{lm} \hat{V}_{\text{eff}}(\mathbf{G})e^{i\mathbf{G}\cdot\mathbf{r}} &, \mathbf{r} \in \mathbb{R} \\
\sum_{lm} V_{\text{eff},lm}^{\alpha}(r_{\alpha})Y_{lm}(\hat{\mathbf{r}}_{\alpha}) &, \mathbf{r} \in MT(\alpha)
\end{cases}$$
(3.25)

The density components can be easily obtained using the expansion of the wave functions $\psi_{i\mathbf{k}}$ in the LAPW basis:

$$\rho(\mathbf{r}) = \sum_{i\mathbf{k}} f_{i\mathbf{k}} \psi_{i\mathbf{k}}^*(\mathbf{r}) \psi_{i\mathbf{k}}(\mathbf{r})$$
(3.27)

$$\hat{\rho}(\mathbf{G}) = \sum_{i\mathbf{k}} \frac{f_{i\mathbf{k}}}{\Omega} \sum_{\mathbf{G}'} z_{i\mathbf{k}\mathbf{G}'}^* z_{i\mathbf{k}(\mathbf{G}+\mathbf{G}')}$$
(3.28)

$$\rho_{lm}^{\alpha}(r_{\alpha}) = \sum_{i\mathbf{k}}^{i\mathbf{k}} f_{i\mathbf{k}} \sum_{l'm'\lambda'} \sum_{l'm''\lambda'} A_{l'm''\lambda'}^{\alpha i\mathbf{k}*} A_{l'm''\lambda''}^{\alpha i\mathbf{k}} u_{l'\lambda'}^{\alpha}(r_{\alpha}, E_{l'}^{\alpha}) u_{l''\lambda''}^{\alpha}(r_{\alpha}, E_{l''}^{\alpha}) G_{l''ll'}^{m''mm'}$$
(3.29)

The product of the three spherical harmonics that appears in the last equation is denoted by the Gaunt coefficient

$$G_{l''ll'}^{m''mm'} = \oint Y_{l''m''}(\hat{r})Y_{lm}^*(\hat{r})Y_{l'm'}^*(\hat{r})dS = \oint Y_{l''m''}^*(\hat{r})Y_{lm}(\hat{r})Y_{l'm'}(\hat{r})dS, \qquad (3.30)$$

which is a real quantity and is used when expressing the product of two spherical harmonics as a sum over single spherical harmonics. It is non-vanishing only under the condition that $|l-l'| \le l'' \le l+l'$, l+l'+l'' even, and m'' = m+m' are fulfilled.

Because the LAPW basis functions are slightly discontinuous at the muffin-tin sphere boundary, so can be the wave functions, the density, and other quantities derived from it.

3.4. Core states

Chemical bonding is contributed to the valence states, which are delocalized and overlap with the states of neighboring atoms. The so-called 'core states' are solutions of the Schrödinger equation which are localized at an atomic nucleus because they are low in energy and cannot overcome the potential well from which they originate. This is sketched in Fig. 3.3. Other states of a similar energy with which they could hybridize are localized in other muffin-tin spheres, therefore, they take no part in chemical bonding.

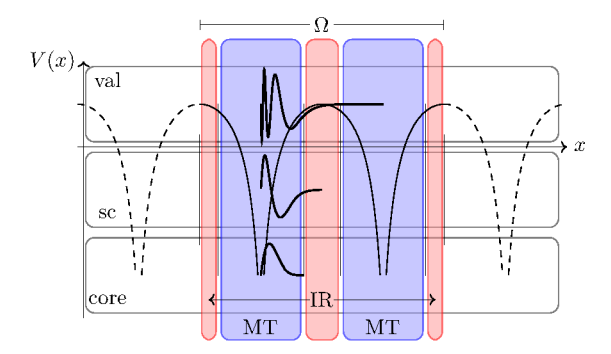


Figure 3.3.: Sketch of different states: The energetically high-lying valence states (val) overlap with those of neighboring atoms. The low-lying core states (core) are confined within their muffin-tin sphere. The semicore states (sc) slightly leak out of their muffin-tin sphere and are poorly described by the LAPW basis.

Ideally, the muffin-tin radius of an atom is chosen such that all its core states are confined within its MT sphere. If so, the core states cannot be described by the ϕ_{kG} of Eq. (3.10) because they cannot couple to the plane waves of the interstitial. Therefore, the muffin-tin radius affects the result of the electronic structure calculation threefold: First, it defines the region where the different representations of the potential are used to construct the LAPW basis functions. Second, the expansion of the basis in the muffin-tin spheres is only up to an angular-momentum cutoff $l_{\rm max}$, while the plane waves contain every l-channel due to the Rayleigh-expansion. Therefore, the muffin-tin radius defines the location of an area of discontinuity of the basis functions and possibly every quantity derived from it. Third, it defines to which functions the u_l^{α} are orthogonal.

We show now that the solutions of the homogeneous and inhomogeneous Schrödinger equation, Eqs. (3.12) and (3.15), are orthogonal to any solution \tilde{u}_l^{α} of Eq. (3.12) that is already decayed at the muffin-tin sphere boundary, such as an ideal core state. By 'decayed' we mean that \tilde{u}_l^{α} itself and every derivative is zero at $r_{\alpha} = R_{\alpha}$. Multiplying Eq. (3.12) to determine \tilde{u}_l^{α} by r_{α} times $u_{l\lambda}^{\alpha}$ and either Eq. (3.12) or Eq. (3.15) to determine $u_{l\lambda}^{\alpha}$ by r_{α} times \tilde{u}_l yields in the difference

$$2\left(E_l^{\alpha} - \tilde{E}_l^{\alpha}\right)r_{\alpha}^2 u_{l\lambda}^{\alpha} \tilde{u}_l^{\alpha} + 2\delta_{\lambda 1} u_{l0}^{\alpha} \tilde{u}_l^{\alpha} = r_{\alpha} \tilde{u}_l^{\alpha} \frac{d^2}{dr_{\alpha}^2} r_{\alpha} u_{l\lambda}^{\alpha} - r_{\alpha} u_{l\lambda}^{\alpha} \frac{d^2}{dr_{\alpha}^2} r_{\alpha} \tilde{u}_l^{\alpha}.$$
(3.31)

Integration up to the muffin-tin radius produces for $\lambda = 0$ the scalar product between u_{10}^{α} and \tilde{u}_{l}^{α} on the left hand side and the orthogonality of both functions on the right hand side of the equation after an integration by parts:

$$2\left(E_l^{\alpha} - \tilde{E}_l^{\alpha}\right)\left(u_{l0}^{\alpha}, \tilde{u}_l^{\alpha}\right) = \left[r_{\alpha}\tilde{u}_l^{\alpha}(r_{\alpha}u_{l0}^{\alpha})' - r_{\alpha}u_{l0}^{\alpha}(r_{\alpha}\tilde{u}_l^{\alpha})'\right]_0^{R_{\alpha}}$$
$$-\int_0^{R_{\alpha}} \left[(r_{\alpha}\tilde{u}_l^{\alpha})'(r_{\alpha}u_{l0}^{\alpha})'\right] - \left[(r_{\alpha}u_{l0}^{\alpha})'(r_{\alpha}\tilde{u}_l^{\alpha})'\right]dr_{\alpha} = 0$$
(3.32)

This is true since either r_{α} vanishes at the origin or $\tilde{u}_{l}^{\alpha(l)}$ vanishes at the muffin-tin sphere boundary. Since $(u_{l0}^{\alpha}, \tilde{u}_{l}^{\alpha})$ is zero, the same procedure yields in the case $\lambda = 1$ the orthogonality between \tilde{u}_{l}^{α} and u_{l1}^{α} .

Since the regular basis functions of the LAPW method are incapable of describing the core states, they are constructed as solutions of Eq. (3.12) on a radial mesh extended beyond the muffin-tin radius R_{α} instead. In FLEUR, the spherical lattice potential is replaced by an asymptotically decaying potential $V_{\rm asympt}^{\alpha}(r_{\alpha})$ outside of the muffin-tin sphere. No energy parameter E_l^{α} is used, because in this case, the boundary conditions only allow solutions at certain energies, the eigenenergies ϵ_{ik} . The core states are continuously differentiable to any order. Since they are considered non-overlapping, the energy bands of the core states show no dispersion over the Brillouin zone. A formal dependence on k is introduced by including a factor $\exp(ik \cdot R)$ to the description of the core state if it arises in a unit cell R other than the representative unit cell. The band index i comprises a superindex $i = (\beta plm_l)$ consisting of the atom index β from which the core state stems, the principal quantum number p, the angular momentum l, and the corresponding magnetic quantum number m_l . If the core states are constructed from a fully relativistic variant of Eq. (3.12), the Dirac equation, l and m_l have to be replaced by the quantum numbers j and m_j , which are the total angular momentum and its projection.

Since the muffin-tin radius is an artificial quantity, it is possible that there are states which physically behave like core states but which are not completely confined in their native muffin-tin sphere. Such states are called semicore states and the part of them outside of their muffin-tin sphere is called their coretail.

Once all (semi)core states are determined, the spherical local core density of atom α is constructed from the $\psi_{ik}(r)$ according to

$$\rho_{\text{core}}^{\alpha}(\mathbf{r}_{\alpha}) = \sum_{i\mathbf{k}}^{\text{core}} \delta_{\alpha\beta} f_{i\mathbf{k}} |\psi_{i\mathbf{k}}(\mathbf{r}_{\alpha})|^{2}.$$
 (3.33)

The total core density then is the sum over all local core densities at their corresponding locations,

$$\rho_{\text{core}}^{\text{tot}}(\mathbf{r}) = \sum_{\alpha} \rho_{\text{core}}^{\alpha}(\mathbf{r} - \boldsymbol{\tau}_{\alpha}). \tag{3.34}$$

It can be added to the valence density in Eq. (3.25) by expressing it similarly as

$$\rho_{\text{core}}^{\text{tot}}(\boldsymbol{r}) = \begin{cases} \sum_{\boldsymbol{G}} \hat{\rho}_{\text{core}}^{\text{tot}}(\boldsymbol{G}) e^{i\boldsymbol{G}\cdot\boldsymbol{r}} &, \boldsymbol{r} \in \text{IR} \\ \sum_{lm} \rho_{\text{core},lm}^{\text{tot},\alpha}(r_{\alpha}) Y_{lm}(\hat{\boldsymbol{r}}_{\alpha}) &, \boldsymbol{r} \in \text{MT}(\alpha) \end{cases}$$
(3.35)

The interstitial and nonspherical representations are important in the case of semicore states. They are found by replacing the spherical muffin-tin charge density of the local core density by a Gaussian curve which is matched to the resulting coretail density at the muffin-tin sphere boundary,

$$\tilde{\rho}_{\text{core}}^{\alpha}(\mathbf{r}_{\alpha}) = \begin{cases} A_{\alpha}e^{-a_{\alpha}r_{\alpha}^{2}} &, r_{\alpha} \leq R_{\alpha} \\ \rho_{\text{core}}^{\alpha}(r_{\alpha}) &, r_{\alpha} > R_{\alpha} \end{cases}$$
(3.36)

where A_{α} and a_{α} are degrees of freedom for the matching. They are determined by demanding for continuity up to first order and are given by

$$A_{\alpha} = \rho_{\text{core}}^{\alpha}(R_{\alpha})e^{a_{\alpha}R_{\alpha}^{2}} \text{ and}$$
 (3.37)

$$a_{\alpha} = -\frac{1}{2R_{\alpha}} \frac{\rho_{\text{core}}^{\alpha\prime}(R_{\alpha})}{\rho_{\text{core}}^{\alpha}(R_{\alpha})},\tag{3.38}$$

as a simple substitution shows. The sum of the pseudodensities of this type is then easily Fourier transformed and provides the coefficients for the total core density. For details regarding the implementation in FLEUR, we refer to Appendix A.1.

3.5. Local orbitals

In contrast to the APW basis, its linearized realization is fit to describe valence states in an energy region around the parameter E_l^{α} . It is still possible though that certain states are just at the border of this energy region and thus fail to be described accurately with the LAPW basis. These states could for example be semicore states that are not totally confined to the muffin-tin sphere due to the choice of the muffin-tin radius. Such core states would not be strictly orthogonal to the basis functions and the part of them that lies within the space of the LAPW functions could manifest in the band structure, leading to so-called ghost states. Another possibility are unoccupied states which are energetically far away from the occupied states, and are thus not the states for whose description the LAPW basis is optimized. Exemplified by the black solid line in Fig. 3.4 is the ability of a radial LAPW basis function to fill in for the solution of the radial Schrödinger Eq. (3.12) at a different energy by means of the linearization error

$$\Delta_l^{\text{lin}}(E) = \int_0^{R_\alpha} r_\alpha^2 |u_l^\alpha(r_\alpha, E) - \sum_{\lambda} c_\lambda u_{l\lambda}^\alpha(r_\alpha)|^2 dr_\alpha / ||u_l^\alpha(E)||^2.$$
 (3.39)

For convenience, we omitted the energy argument of the LAPW radial functions $u_{i\lambda}^{\alpha}$.

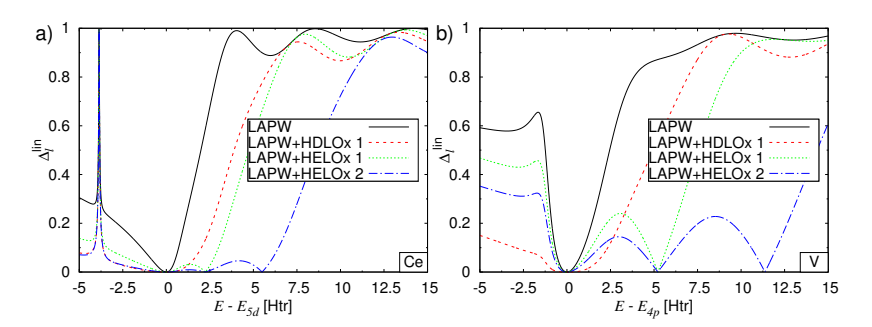


Figure 3.4.: Linearization error $\Delta_l^{\rm lin}(E)$ employing different kinds of local orbitals (a) of the Cerium 5d states and (b) of the Vanadium 4p states. (Recreated from data published in Ref. [115], with permission from Elsevier.)

Small values indicate that $u_l^{\alpha}(r_{\alpha}, E)$ can be represented well by the LAPW basis functions, while values close to 1 show near orthogonality of $u_l^{\alpha}(r_{\alpha}, E)$ to the LAPW basis functions. The black lines in the graphs have in common that the representation is good near the energy parameter E_l^{α} , while the representation gets worse the further away from E_l^{α} the function $u_l^{\alpha}(r_{\alpha}, E)$ is sampled. Notable are the core state in the Cerium graph at -3.8 Htr and the semicore state in the Vanadium graph at -1.4 Htr.

In order to increase the flexibility of the LAPW method to better include the states into the valence band description which are poorly described by the LAPW basis, further basis functions can be added locally at an atom α and with a specific angular-momentum l. Hence, they are called local orbitals (LOs). The radial part $R_l^{\alpha, \text{LO}}(r_\alpha, E_l^\alpha, E_l^{\alpha, \text{LO}})$ of these additional basis functions is constructed by adding a third radial function $u_l^{\alpha, \text{LO}}(r_\alpha, E_l^{\alpha, \text{LO}})$ to the existing u_Ω^α of a certain energy E_l^α .

$$R_l^{\alpha, \text{LO}}(r_{\alpha}, E_l^{\alpha}, E_l^{\alpha, \text{LO}}) = \sum_{\lambda=0}^{1} a_{l\lambda}^{\alpha, \text{LO}} u_{l\lambda}^{\alpha}(r_{\alpha}, E_l^{\alpha}) + a_l^{\alpha, \text{LO}} u_l^{\alpha, \text{LO}}(r_{\alpha}, E_l^{\alpha, \text{LO}}), \tag{3.40}$$

such that it vanishes up to first order at the muffin-tin sphere boundary and is normalized. These radial functions are multiplied by the 2l+1 spherical harmonics belonging to the appropriate l-channel; thus by adding a local orbital one adds a set of 2l+1 functions to the basis. There are conceptually two promising approaches to chose the energy parameter of $u_l^{\alpha,\text{LO}}$:

- a) Following the spirit of the Taylor expansion of the true radial function around the energy parameter E_l^{α} that led to the LAPW method in the first place, one increases the order of derivation of u_l^{α} , thus broadening the width of the energy region that is described accurately. In contrast to the discussion at the end of chapter 3.2, doing so conserves the flexibility of the LAPW basis without needing more interstitial basis functions. This is true since the LOs are not matched to the plane waves at the MT sphere boundary. Such LOs are called higher-derivative LOs (HDLO).
- b) One introduces a new energy around which the states can be well approximated by the augmented LAPW basis by including radial functions at a different energy parameter \tilde{E}^{α}_{l} closer to the state that is not well described. If this kind of LO is used to include high energies into the LAPW description, it is called an higher-energy LO (HELO). Both approaches can be subsumed as:

$$u_l^{\alpha, \text{LO}}(r_{\alpha}, E_l^{\alpha, \text{LO}}) = \begin{cases} \ddot{u}_l^{\alpha}(r_{\alpha}, E_l^{\alpha}) \\ u_l^{\alpha}(r_{\alpha}, \tilde{E}_l^{\alpha}) \end{cases}$$
(3.41)

The latter choice can be obtained from solving Eq. (3.12) at the new energy parameter, while the former choice (exemplified by the second order derivative of the radial function, higher orders are possible) needs to be constructed analogous to Eq. (3.15) for higher derivatives. It is possible to combine the two approaches and to include for example two sets of local orbitals, one that features $u_l^{\alpha}(r_{\alpha}, \tilde{E}_l^{\alpha})$ and one that adds its first energy derivative $\dot{u}_l^{\alpha}(r_{\alpha}, \tilde{E}_l^{\alpha})$, thus simulating the radial part of an LAPW basis function at \tilde{E}_l^{α} . However, the local orbitals vanish at the muffin-tin boundary. Thereby, they lack a matching to a plane wave in the interstitial and do not automatically inherit the symmetry that the LAPW functions show. To include it, the coefficients $a_{lm(\lambda)}^{\alpha,LO}$ are multiplied by $-4\pi i^l e^{i(k+G)\cdot\tau_{\alpha}}Y_{lm}^*(\widehat{k+G})/W(R_l^{\alpha}, E_l^{\alpha})$, which imitates the matching coefficients of a regular basis functions. In contrast to what

has been proved with Eq. (3.32), the local orbitals are not necessarily orthogonal to the LAPW basis functions, because the total radial part of the local orbital does not fulfill the radial Schrödinger equation (3.12) and the radial functions $u_{l\lambda}^{\alpha}$ and $u_{l}^{\alpha,\text{LO}}$ do not vanish at the MT sphere boundary themselves.

Coming back to Fig. 3.4, the effect of HDLOs and HELOs is demonstrated there. Notably, in both cases of (a) Cerium and (b) Vanadium, the inclusion of the HDLO best reduces the linearization error in the vicinity of the LAPW energy parameter, while the inclusion of one or two HELOs results at their additional energy parameters in new spots where the linearization error vanishes, which also affects the representability of $u_l^{\alpha}(E)$ in between those energy parameters. In the Cerium graph, $\Delta_l^{\rm lin}$ is nearly 1 at around -3.8 Htr for any LO setup presented here, meaning that the solution of Eq. (3.12) at this energy is a core state confined to the muffin-tin sphere of the Cerium atom. At around -1.4 Htr, the linearization error peaks in the Vanadium graph, because there, a semi-core state is present. When using an HDLO for the Vanadium 4p state, there is still some structure at -1.4 Htr, but the small value of $\Delta_l^{\rm lin}$ suggests the appearance of a ghost band in the band structure, since this local orbital is sensitive enough to describe the semicore state.

A more detailed analysis of different types of local orbitals can be found in the references [115-120].

Now that we have provided the electronic states from which the density $\rho(r)$ is constructed by Eq. (3.27), we continue with the construction of the xc and Hartree potential.

3.6. Evaluation of the exchange-correlation potential

As we have pointed out in chapter 2.4, we will limit ourselves to the local density approximation. Specifically the formulation of Vosko, Wilk, and Nusair for the exchange-correlation potential $\mu_{\rm xc}[\rho](r)$ and energy-density $\epsilon_{\rm xc}[\rho](r)$ will be used. In this case, potential and energy-density are functions of the electronic density ρ , which also dictates how to obtain them:

The interstitial representation of the electronic density given as plane-wave coefficients is put on a real space mesh by a fast Fourier transform, $\mu_{xc}(\rho(r))$ and $\epsilon_{xc}(\rho(r))$ are applied to it at each mesh point and the result is transformed back to reciprocal space by another fast Fourier transform.

To obtain μ_{xc} and ϵ_{xc} in the muffin-tin spheres, the fast Fourier transform is replaced by a method more suited for expanding and recollecting quantities from a mesh designed for a spherical harmonic representation in real space, which for example transfers their orthogonality properties to the mesh point set. Other than that, the procedure is analogous to that of the interstitial region.

Since the exchange-correlation potential and energy-density are non-linear functions of the electronic density, see Appendix A.2, the G components of the density will provide contributions to all other G coefficients of μ_{xc} and ϵ_{xc} . Therefore, the exchange-correlation quantities need a larger G_{max} -cutoff than the density.

3.7. Evaluation of the Coulomb potential

The calculation method by Weinert [62] to obtain the electrostatic potential that acts on a Kohn-Sham electron draws from the fact that to compute the potential from a charge distribution contained in a volume away from that volume requires knowledge only of the multipole moments within said volume. Thus, the Coulomb potential in the interstitial region of the unit cell, which is represented in a plane-wave expansion, can be calculated from a pseudodensity replacing the muffin-tin electronic density and reproducing the same multipoles. The interstitial potential will later be used as boundary values to find the true Coulomb potential within the muffin-tin spheres. In contrast to the original pointcharge density of the nuclei and the cusping electronic density, this pseudodensity can be constructed to be more easily Fourier expandable. We will proceed in introducing this method with an arbitrary charge density n(r), which in the case of the FLAPW method is the sum of the electronic density of Eq. (3.29) and the atomic pointcharge density $\rho_i(r) = -\sum_{\alpha} Z_{\alpha} \delta(r - \tau_{\alpha})$. Such a charge density produces the multipole moments

$$q_{lm}^{\alpha} = \int_{\mathrm{MT}(\alpha)} Y_{lm}^{*}(\widehat{\boldsymbol{r} - \boldsymbol{\tau}_{\alpha}}) |\boldsymbol{r} - \boldsymbol{\tau}_{\alpha}|^{l} n(\boldsymbol{r}) d^{3}r = \int_{0}^{R_{\alpha}} r_{\alpha}^{l+2} n_{lm}^{\alpha}(r_{\alpha}) dr_{\alpha}$$
(3.42)

with the local expansion $n_{lm}^{\alpha}(r_{\alpha})$ of the density into spherical harmonics. The total pseudodensity $n_{\rm ps}(\boldsymbol{r})$ is constructed from the local components $\bar{n}_{\rm ps}^{\alpha}(\boldsymbol{r}_{\alpha})$ as

$$n_{\rm ps}(\mathbf{r}) = n_{\rm PW}(\mathbf{r})[1 - \sum_{\alpha} \Theta(R_{\alpha} - |\mathbf{r} - \boldsymbol{\tau}_{\alpha}|)] + \sum_{\alpha} \bar{n}_{\rm ps}^{\alpha}(\mathbf{r}_{\alpha})\Theta(R_{\alpha} - |\mathbf{r} - \boldsymbol{\tau}_{\alpha}|)$$

$$= n_{\rm PW}(\mathbf{r}) + \sum_{\alpha} [\bar{n}_{\rm ps}^{\alpha}(\mathbf{r}_{\alpha}) - n_{\rm PW}(\mathbf{r}_{\alpha} + \boldsymbol{\tau}_{\alpha})]\Theta(R_{\alpha} - |\mathbf{r} - \boldsymbol{\tau}_{\alpha}|), \qquad (3.43)$$

where the plane-wave part of the original density is expanded over the whole unit cell and subtracted again in the muffin-tin spheres. Therefore, using the Rayleigh-expansion for the plane waves, the total second term of the last equation has the form

$$q_{lm}^{\alpha, \text{ps}} = q_{lm}^{\alpha} - q_{lm}^{\alpha, \text{PW}}, \tag{3.44}$$

$$q_{lm}^{\alpha,\text{PW}} = 4\pi i^l \sum_{\boldsymbol{G} \neq \boldsymbol{0}}^{2G_{\text{max}}} \hat{n}_{\text{PW}}(\boldsymbol{G}) e^{i\boldsymbol{G} \cdot \boldsymbol{\tau}_{\alpha}} Y_{lm}^*(\hat{\boldsymbol{G}}) \frac{R_{\alpha}^{l+3} j_{l+1}(GR_{\alpha})}{GR_{\alpha}} + \frac{\sqrt{4\pi}}{3} \hat{n}_{\text{PW}}(\boldsymbol{0}) R_{\alpha}^3 \delta_{l0}$$
(3.45)

for $l \leq 2l_{\max}^{\alpha}$ and only $-q_{lm}^{\alpha,\text{PW}}$ for larger l. The contribution from $R_{\alpha}^{l+3}j_{l+1}(GR_{\alpha})/GR_{\alpha}$ becomes negligible for larger l, though, by the choice $l_{\max}^{\alpha} \gtrsim G_{\max}R_{\alpha}$ and the property of the spherical Bessel functions to have their first maximum after the value of their argument passes their index.

In order to obtain a pseudodensity that is easily Fourier transformable, Weinert et~al. suggested the radial part of it to be a power series in r_{α} up to a power of l+2N with the parameter N specified after the construction of the pseudodensity. In the muffin-tin sphere of atom α , it then has the form

$$n_{\rm ps}^{\alpha}(\mathbf{r}_{\alpha}) = \sum_{l_m}^{2l_{\rm max}^{\alpha}} Q_{lm}^{\alpha} Y_{lm}(\hat{\mathbf{r}}_{\alpha}) \sum_{n=0}^{N} a_{\eta}^{\alpha} r_{\alpha}^{l+2\eta}. \tag{3.46}$$

Using formula (3.42) on this equation yields for the multipole moments of this part of the pseudodensity

$$Q_{lm}^{\alpha} \sum_{\eta=0}^{N} a_{\eta}^{\alpha} \frac{R_{\alpha}^{2l+2\eta+3}}{2l+2\eta+3} \stackrel{!}{=} q_{lm}^{\alpha, \text{ps}}, \tag{3.47}$$

thus defining Q_{lm}^{α} in dependence of the a_{η}^{α} . We will see that we can chose the latter in a way that they disappear from the equations when the pseudodensity is finally constructed. The Fourier transform of the pseudodensity, which is the expression we aim for to be described by a convenient number of expansion coefficients, is

$$\hat{n}_{ps}(\boldsymbol{G}) = \hat{n}_{PW}(\boldsymbol{G}) + \frac{1}{\Omega} \sum_{\alpha} \int_{MT(\alpha)} e^{-i\boldsymbol{G}\cdot\boldsymbol{r}} n_{ps}^{\alpha}(\boldsymbol{r} - \boldsymbol{\tau}_{\alpha}) d^{3}\boldsymbol{r}$$

$$= \hat{n}_{PW}(\boldsymbol{G}) + \frac{1}{\Omega} \sum_{\alpha} \sum_{lm}^{2l_{max}^{\alpha}} Q_{lm}^{\alpha} e^{-i\boldsymbol{G}\cdot\boldsymbol{\tau}_{\alpha}} 4\pi(-i)^{l} Y_{lm}(\hat{\boldsymbol{G}}) A_{l}^{\alpha}, \qquad (3.48)$$

$$\hat{n}_{ps}(\boldsymbol{0}) = \hat{n}_{PW}(\boldsymbol{0}) + \frac{\sqrt{4\pi}}{\Omega} \sum_{\alpha} q_{00}^{\alpha,ps}, \text{ with}$$

$$A_{l}^{\alpha} := \sum_{r=0}^{N} a_{\eta}^{\alpha} \int_{0}^{GR_{\alpha}} \frac{t^{l+2\eta+2}}{G^{l+2\eta+3}} j_{l}(t) dt. \qquad (3.49)$$

Exploiting the relation $\frac{d}{dt}[t^{l+2}j_{l+1}(t)] = t^{l+2}j_l(t)$ and integrating η times by parts, we compute for the integral in A_l^{α}

$$\int_{0}^{GR_{\alpha}} \frac{t^{l+2\eta+2}}{G^{l+2\eta+3}} j_{l}(t) dt = \frac{R_{\alpha}^{l+2\eta+3}}{GR_{\alpha}} \sum_{\nu=0}^{\eta} \frac{(-1)^{\nu} 2^{\nu} \eta!}{(\eta-\nu)!} \frac{j_{l+\nu+1}(GR_{\alpha})}{(GR_{\alpha})^{\nu}}.$$
 (3.50)

We insert this equation back into A_l^{α} to find after a rearrangement of the sums into same powers of GR_{α} :

$$A_{l}^{\alpha} = R_{\alpha}^{l+3} \sum_{\nu=0}^{N} (-1)^{\nu} 2^{\nu} \frac{j_{l+\nu+1}(GR_{\alpha})}{(GR_{\alpha})^{\nu+1}} \sum_{n=\nu}^{N} \frac{a_{\eta}^{\alpha} \eta! R_{\alpha}^{2\eta}}{(\eta - \nu)!}$$
(3.51)

By choosing

$$a_{\eta}^{\alpha} = (-1)^{N-\eta} R_{\alpha}^{2(N-\eta)} \begin{pmatrix} N \\ \eta \end{pmatrix} a_{N}^{\alpha}$$
 (3.52)

both sums in A_l^{α} collapse and Eqs. (3.47) and (3.51) yield

$$A_l^{\alpha} = \left((-1)^N 2^N R_{\alpha}^{l+3} \right) \frac{j_{l+N+1}(GR_{\alpha})}{(GR_{\alpha})^{N+1}} \left(a_N^{\alpha} N! R_{\alpha}^{2N} \right) \text{ and}$$
 (3.53)

$$Q_{lm}^{\alpha} = \left((-1)^{N} 2^{N} R_{\alpha}^{l+3} \right)^{-1} \frac{(2l+2N+3)!!}{(2l+1)!! R_{\alpha}^{l}} q_{lm}^{\alpha, \text{ps}} \left(a_{N}^{\alpha} N! R_{\alpha}^{2N} \right)^{-1}. \tag{3.54}$$

It becomes apparent that the first and the last factor of both quantities cancel each other in the product of Eq. (3.48), removing the dependence on the coefficients a_{η}^{α} alltogether. Thus, the Fourier coefficients of the pseudodensity become

$$\hat{n}_{\rm ps}(\boldsymbol{G}) = \hat{n}_{\rm PW}(\boldsymbol{G}) + \frac{4\pi}{\Omega} \sum_{\alpha} \sum_{lm}^{2l_{\rm max}^{\alpha}} \frac{(-i)^{l}(2l+2N+3)!!}{(2l+1)!!R_{\alpha}^{l}} \frac{j_{l+N+1}(GR_{\alpha})}{(GR_{\alpha})^{N+1}} \times \dots$$

$$\cdots \times q_{lm}^{\alpha, ps} e^{-i\boldsymbol{G} \cdot \boldsymbol{\tau}_{\alpha}} Y_{lm}(\hat{\boldsymbol{G}}), \qquad (3.55)$$

$$\hat{n}_{\rm ps}(\mathbf{0}) = \hat{n}_{\rm PW}(\mathbf{0}) + \frac{\sqrt{4\pi}}{\Omega} \sum_{\alpha} q_{00}^{\alpha, \rm ps}.$$
 (3.56)

Since the spherical Bessel functions are absolutely bounded by 1 and decay themselves like 1/G, the total coefficients decay like $1/G^{N+2}$. Taking arbitrarily large N to increase the convergence behavior of this part of the Fourier components interferes with the other N-dependent factor (2l+2N+3)!!, though. Instead, Weinert points out that the parameter N can be chosen for each l and each muffin-tin sphere separately and suggests to take a value such that $j_{l+N+1}(z)$ has its first zero in the vicinity of $2G_{\max}R_{\alpha}$. In this way, the largest contribution to the sum from arguments z smaller than the first zero of the spherical Bessel functions is included. For a more detailed view at the choice of N, the reader may be referred to the original publication by Weinert [62].

Apart from the approximation that only the first $2l_{\text{max}}^{\alpha}$ l-channels of the plane-wave density are subtracted from the muffin-tin representation of the pseudodensity, the Coulomb potential in the interstitial region is connected to the pseudodensity via the Poisson equation

$$\Delta V_{\rm C}(\boldsymbol{r}) = -4\pi n_{\rm ps}(\boldsymbol{r}) = -4\pi \sum_{\boldsymbol{G}}^{2G_{\rm max}} \hat{n}_{\rm ps}(\boldsymbol{G}) e^{i\boldsymbol{G}\cdot\boldsymbol{r}}, \text{ or}$$
(3.57)

$$V_{\mathcal{C}}(\boldsymbol{r}) = \hat{V}_{\mathcal{C}}(\boldsymbol{0}) + 4\pi \sum_{\boldsymbol{G} \neq \boldsymbol{0}}^{2G_{\text{max}}} \frac{\hat{n}_{\text{ps}}(\boldsymbol{G})}{G^2} e^{i\boldsymbol{G} \cdot \boldsymbol{r}} = \sum_{\boldsymbol{G}}^{2G_{\text{max}}} \hat{V}_{\mathcal{C}}(\boldsymbol{G}) e^{i\boldsymbol{G} \cdot \boldsymbol{r}}.$$
 (3.58)

A constant shift $\hat{V}_{\rm C}(\mathbf{0})$ in the potential is not determined by this equation.

Now that the Coulomb potential is known in the interstitial region, it is explicitly known on the muffin-tin sphere boundary. We can invert the Poisson equation inside the muffin-tin spheres using the Green function

$$G(\mathbf{r}_{\alpha}, \mathbf{s}_{\alpha}) = 4\pi \sum_{lm} \frac{Y_{lm}^{*}(\hat{\mathbf{s}}_{\alpha}) Y_{lm}(\hat{\mathbf{r}}_{\alpha})}{2l+1} \frac{r_{<}^{l}}{r_{>}^{l+1}} \left[1 - \left(\frac{r_{>}}{R_{\alpha}} \right)^{2l+1} \right]$$
(3.59)

with $r_{<} = \min(r_{\alpha}, s_{\alpha})$ and $r_{>} = \max(r_{\alpha}, s_{\alpha})$, respectively. Its Laplacian is the Dirac- δ -distribution $-4\pi\delta(\mathbf{r}_{\alpha} - \mathbf{s}_{\alpha})$. Green's third identity states that

$$\int_{B_{R_{\alpha}}(\mathbf{0})} G(\mathbf{r}_{\alpha}, \mathbf{s}_{\alpha}) \Delta_{\mathbf{s}_{\alpha}} g(\mathbf{s}_{\alpha}) - g(\mathbf{s}_{\alpha}) \Delta_{\mathbf{s}_{\alpha}} G(\mathbf{r}_{\alpha}, \mathbf{s}_{\alpha}) d^{3} s_{\alpha}$$

$$= \oint_{\partial B_{R_{\alpha}}(\mathbf{0})} G(\mathbf{r}_{\alpha}, \mathbf{s}_{\alpha}) \nabla_{s_{\alpha}} g(\mathbf{s}_{\alpha}) - g(\mathbf{s}_{\alpha}) \nabla_{s_{\alpha}} G(\mathbf{r}_{\alpha}, \mathbf{s}_{\alpha}) dS \tag{3.60}$$

and for $g(s_{\alpha}) = V_{\rm C}(s_{\alpha} + \tau_{\alpha})$ and thus $\Delta_{s_{\alpha}}g(s_{\alpha}) = -4\pi n(s_{\alpha})$ we obtain

$$V_{\rm C}(\boldsymbol{r}_{\alpha} + \boldsymbol{\tau}_{\alpha}) = \int_{B_{R_{\alpha}}(\mathbf{0})} n^{\alpha}(\boldsymbol{s}_{\alpha}) G(\boldsymbol{r}_{\alpha}, \boldsymbol{s}_{\alpha}) d^{3} s_{\alpha}$$
$$-\frac{1}{4\pi} \oint_{\partial B_{R_{\alpha}}(\mathbf{0})} V_{\rm C}(\boldsymbol{s}_{\alpha} + \boldsymbol{\tau}_{\alpha}) \nabla_{s_{\alpha}} G(\boldsymbol{r}_{\alpha}, \boldsymbol{s}_{\alpha}) dS, \tag{3.61}$$

since $G(\mathbf{r}_{\alpha}, \mathbf{s}_{\alpha})$ vanishes at the muffin-tin sphere boundary. The normal derivative of the Green function (3.59) at the muffin-tin sphere boundary is given by

$$\nabla_{s_{\alpha}} G(\boldsymbol{r}_{\alpha}, \boldsymbol{s}_{\alpha})|_{s_{\alpha} = R_{\alpha}} = -\frac{4\pi}{R_{\alpha}^{2}} \sum_{lm} \left(\frac{r_{\alpha}}{R_{\alpha}}\right)^{l} Y_{lm}^{*}(\hat{\boldsymbol{s}}_{\alpha}) Y_{lm}(\hat{\boldsymbol{r}}_{\alpha}). \tag{3.62}$$

This constitutes a Dirichlet boundary-value problem, where the electrostatic potential depends on the local charge density (volume integral) and the potential on the surface of the volume (surface integral). Inserting the interstitial potential (3.58) for the boundary values, the electrostatic potential $V_{\rm C}^{\alpha}(\boldsymbol{r}_{\alpha})$ in the muffin-tin sphere of atom α is determined by the radial coefficients

$$V_{\mathrm{C},lm}^{\alpha}(r_{\alpha}) = \frac{4\pi}{2l+1} \int_{0}^{R_{\alpha}} s_{\alpha}^{2} n_{lm}^{\alpha}(s_{\alpha}) \frac{r_{<}^{l}}{r_{>}^{l+1}} \left[1 - \left(\frac{r_{>}}{R_{\alpha}} \right)^{2l+1} \right] ds_{\alpha}$$

$$+ \left(\frac{r_{\alpha}}{R_{\alpha}} \right)^{l} \cdot \sum_{\boldsymbol{G} \neq \boldsymbol{0}}^{2G_{\max}} e^{i\boldsymbol{G} \cdot \boldsymbol{\tau}_{\alpha}} \hat{V}_{\mathrm{C}}(\boldsymbol{G}) 4\pi i^{l} Y_{lm}^{*}(\hat{\boldsymbol{G}}) j_{l}(GR_{\alpha}).$$

$$(3.63)$$

The expansion into spherical harmonics is applied again up to an angular-momentum cutoff of $2l_{\max}^{\alpha}$. It is thus continuous in the first few l-channels, only.

This concludes the construction of the Coulomb potential in the interstitial and muffin-tin regions. As the multipole moments of the pseudodensity are constructed to reproduce those of the original density, especially the l=0 components that give the total charge within a muffin-tin sphere are given. In the regular case that the input density n(r) is the sum of the electronic and the ionic density, charge neutrality can be deduced from Eq. (3.57). We will apply the same scheme in chapter 7, though, where the input density either originates from only an electronic or a purely ionic source.

3.8. Constructing the Hamilton and overlap matrices

Now that we have defined the LAPW basis functions $\phi_{kG}(r)$ and the potential $V_{\rm eff}(r)$ in the interstitial and muffin-tin sphere regions, we provide the formulas for the contributions to the Hamilton matrix $H_{GG'}(k)$ of Eq. (3.7) and the overlap matrix $S_{GG'}(k)$ of Eq. (3.8).

$$\varphi_{lm}^{\alpha}{}_{\lambda}(\mathbf{r}_{\alpha}) = u_{l\lambda}^{\alpha}(r_{\alpha})Y_{lm}(\hat{\mathbf{r}}_{\alpha}), \tag{3.64}$$

 λ possibly including local orbitals, knowing that for $\lambda \leq 1$ the spherical part of the muffin-tin Hamiltonian produces from it

$$\hat{\mathcal{H}}_{\rm sph}^{\alpha}\varphi_{lm,\lambda}^{\alpha} = E_l^{\alpha}\varphi_{lm,\lambda}^{\alpha} + \delta_{1\lambda}\varphi_{lm,0}^{\alpha}.$$
(3.65)

The result in case of a local orbital depends on what kind of LO was chosen. We leave it to the reader to retrace the following steps for an LO basis function.

For the muffin-tin part of the Hamilton and overlap matrices, we have

$$H_{\mathbf{G}'\mathbf{G}}^{\alpha}(\mathbf{k}) = \sum_{lm\lambda} \sum_{l'm'\lambda'} a_{lm\lambda}^{\alpha\mathbf{k}\mathbf{G}'*} a_{l'm'\lambda'}^{\alpha\mathbf{k}\mathbf{G}} \int_{B_{R_{\alpha}}(\mathbf{0})} \varphi_{lm,\lambda}^{\alpha*}(\mathbf{r}_{\alpha}) \hat{\mathcal{H}}_{\mathrm{MT}}^{\alpha} \varphi_{l'm',\lambda'}^{\alpha}(\mathbf{r}_{\alpha}) d^{3}r_{\alpha}, \qquad (3.66)$$

$$S_{\mathbf{G'G}}^{\alpha}(\mathbf{k}) = \sum_{lm\lambda} \sum_{l'm'\lambda'} a_{lm\lambda}^{\alpha \mathbf{k} \mathbf{G}'} * a_{l'm'\lambda'}^{\alpha \mathbf{k} \mathbf{G}} \int_{B_{R_{\alpha}}(\mathbf{0})} \varphi_{lm,\lambda}^{\alpha *} (\mathbf{r}_{\alpha}) \qquad \varphi_{l'm',\lambda'}^{\alpha}(\mathbf{r}_{\alpha}) d^{3}r_{\alpha}.$$
(3.67)

Apparently, the integrals are independent of the Bloch vector \boldsymbol{k} or the reciprocal vector \boldsymbol{G} and compute to

$$t_{lml'm'}^{\alpha\lambda\lambda'} := \int_{B_{R_{\alpha}}(\mathbf{0})} \varphi_{lm,\lambda}^{\alpha*} (\mathbf{r}_{\alpha}) \hat{\mathcal{H}}_{\mathrm{MT}}^{\alpha} \varphi_{l'm',\lambda'}^{\alpha} (\mathbf{r}_{\alpha}) d^{3} r_{\alpha}$$

$$= \int_{B_{R_{\alpha}}(\mathbf{0})} \varphi_{lm,\lambda}^{\alpha*} (\mathbf{r}_{\alpha}) \hat{\mathcal{H}}_{\mathrm{sph}}^{\alpha} \varphi_{l'm',\lambda'}^{\alpha} (\mathbf{r}_{\alpha}) d^{3} r_{\alpha} + \sum_{l''m''}^{l'' \geq 1} I_{ll'l'm''}^{\alpha\lambda\lambda'} G_{ll'l'}^{mm'm''}$$

$$= E_{l}^{\alpha} \left\langle \varphi_{lm,\lambda}^{\alpha} \middle| \varphi_{l'm',\lambda'}^{\alpha} \right\rangle + \delta_{1\lambda'} \left\langle \varphi_{lm,\lambda}^{\alpha} \middle| \varphi_{l'm',0'}^{\alpha} \right\rangle + \sum_{l''m''}^{l'' \geq 1} I_{ll'l'm''}^{\alpha\lambda\lambda'} G_{ll'l''}^{mm'm''}, \qquad (3.68)$$

$$I_{ll'l'm''}^{\alpha\lambda\lambda'} := \int_{0}^{R_{\alpha}} r_{\alpha}^{2} u_{l\lambda}^{\alpha}(r_{\alpha}) u_{l'\lambda'}^{\alpha}(r_{\alpha}) V_{l''m''}^{\alpha}(r_{\alpha}) dr_{\alpha}$$

$$(3.69)$$

with the overlap matrix elements

$$\left\langle \varphi_{lm,\lambda}^{\alpha} \left| \varphi_{l'm',\lambda'}^{\alpha} \right\rangle = \delta_{ll'} \delta_{mm'} \left(\delta_{0\lambda} \delta_{0\lambda'} + \delta_{1\lambda} \delta_{1\lambda'} \|u_{l1}^{\alpha}\|^2 \right) =: J_{lm}^{\alpha\lambda}. \tag{3.70}$$

Thus, we have

$$H_{\mathbf{G}'\mathbf{G}}^{\alpha}(\mathbf{k}) = \sum_{lm\lambda} \sum_{l'm'\lambda'} a_{lm\lambda}^{\alpha \mathbf{k}\mathbf{G}'*} t_{lml'm'}^{\alpha\lambda\lambda'} a_{l'm'\lambda'}^{\alpha \mathbf{k}\mathbf{G}}, \tag{3.71}$$

$$S_{\mathbf{G}'\mathbf{G}}^{\alpha}(\mathbf{k}) = \sum_{lm\lambda} a_{lm\lambda}^{\alpha \mathbf{k} \mathbf{G}'*} J_{lm}^{\alpha \lambda} a_{lm}^{\alpha \mathbf{k} \mathbf{G}}.$$
 (3.72)

For the contributions from the interstitial region, we use the unit step function $\Theta_{IR}(r)$ to expand the IR integrals over the whole unit cell. It is

$$\Theta_{\rm IR}(r) = 1 - \sum_{\alpha} \Theta(R_{\alpha} - |\boldsymbol{r} - \boldsymbol{\tau}_{\alpha}|), \tag{3.73}$$

$$\hat{\Theta}_{\rm IR}(G) = \delta_{G0} - \sum_{\alpha} e^{-iG \cdot \tau_{\alpha}} \frac{4\pi R_{\alpha}^3}{\Omega} \frac{j_1(GR_{\alpha})}{GR_{\alpha}}.$$
 (3.74)

Plugging in the interstitial representation of the wave functions into Eqs. (3.7) and (3.8) gives the Fourier transforms

$$S_{\mathbf{G}'\mathbf{G}}^{IR}(\mathbf{k}) = \frac{1}{\Omega} \int_{\Omega} e^{-i(\mathbf{G}'-\mathbf{G})\cdot\mathbf{r}} \Theta_{IR}(\mathbf{r}) d^3r = \hat{\Theta}_{IR}(\mathbf{G}'-\mathbf{G}),$$
 (3.75)

$$H_{\mathbf{G}'\mathbf{G}}^{\mathrm{IR}}(\mathbf{k}) = \frac{1}{2}|\mathbf{k} + \mathbf{G}|\hat{\Theta}_{\mathrm{IR}}(\mathbf{G}' - \mathbf{G}) + (\widehat{V_{\mathrm{eff}}\Theta_{\mathrm{IR}}})(\mathbf{G}' - \mathbf{G}). \tag{3.76}$$

Since the plane waves are effectively only used until a cutoff of G_{\max} , the Fourier expansion of the unit step function needs to be generated at least up until $2G_{\max}$. The product between the effective potential and the unit step function is put onto a real space mesh by a Fast Fourier transform, evaluated, and then back-transformed onto the reciprocal mesh.

We wish to explicitly stress once again that the LAPW basis functions within the muffintin spheres are obtained using only the spherical part of the Hamiltonian, but have enough flexibility to allow that the wave functions are constructed to minimize the total energy belonging to the total potential.

3.9. Relativism

The derivations presented so far have been strictly non-relativistic. This is a reasonable approximation for compounds consisting of light atoms, though heavier nuclei imply that their electrons have a high kinetic energy at the atomic positions and thus require relativity to be considered within their description. Thus, the wave functions do not need to solve the single-particle Schrödinger equation (2.4), but instead their relativistic counterpart, the Kohn-Sham-Dirac equation:

$$\left\{c\underline{\alpha} \cdot \hat{p} + (\beta - \underline{1})c^2 + \underline{V}_{\text{eff}}(r)\right\} \psi_i(r) = \epsilon_i \psi_i(r)$$
(3.77)

Herein, $c \approx 1/137$ is the speed of light in Hartree units and the momentum operator \hat{p} is accompanied by the vector of Pauli matrices σ_i

$$\underline{\alpha} = \left(\begin{pmatrix} \underline{0} & \underline{\sigma}_x \\ \underline{\sigma}_x & \underline{0} \end{pmatrix}, \begin{pmatrix} \underline{0} & \underline{\sigma}_y \\ \underline{\sigma}_y & \underline{0} \end{pmatrix}, \begin{pmatrix} \underline{0} & \underline{\sigma}_z \\ \underline{\sigma}_z & \underline{0} \end{pmatrix} \right) = \begin{pmatrix} \underline{0} & \underline{\sigma} \\ \underline{\sigma} & \underline{0} \end{pmatrix}, \tag{3.78}$$

the relativistic four-component wavefunction ψ_i , the effective potential $\underline{V}_{\rm eff}(r) = V_{\rm eff}(r)\underline{1}$ with the unit matrix 1, and

$$\beta = \text{diag}(1, 1, -1, -1).$$
 (3.79)

The Kohn-Sham-Dirac equation, Eq. (3.77), contains all relativistic effects, from mass-velocity over the Darwin-term to spin-orbit coupling. However, it is a partial differential equation of first order in each of its four components, the majority and minority spin channels with their large and small components, which are all coupled. This increases the computational effort of constructing both core and valence states. The core states are obtained in each iteration of the self-consistency cycle directly from the current potential, resulting only in a moderate rise of computational effort. But the effort to find solutions of the Kohn-Sham-Dirac equation self-consistently, as is the case with the valence states, increases tremendously: To work with four instead of one components of a wave function leads to 64 times the non-relativistic computation time for diagonalizing the Hamiltonian, since diagonalization scales to the cube with respect to system size.

3.9.1. The scalar-relativistic approximation

In order to diminish the increment of the computational effort, the valence states can be treated by the so-called scalar-relativistic approximation [109]. In it, the spin-orbit part of the relativistic description is neglected. This in turn leads to a separation of the spin coordinates from the spatial coordinates and decouples the spin channels from each other. In this way, only two times two coupled systems have to be solved, increasing the computational workload by a factor of two times 8 instead of 64.

To reintroduce the spin-orbit coupling to the valence states in the cases where it is needed, it can be considered afterwards via perturbation theory as a small variation of the uncoupled system.

The deviation of a relativistic description from a non-relativistic one is strongest where the kinetic energy of a state ψ_i is large, which is most notably the case in the vicinity of the atomic nuclei. Therefore, the relativistic treatment of the valence states is not only subject to the scalar-relativistic approximation, but also limited to the muffin-tin spheres, while in the interstitial the non-relativistic LAPW wave functions are used. This implies the lack of a small component in the interstitial to which a relativistic radial function from the muffin-tin can be matched to. Instead, only the large component is matched at the muffin-tin sphere boundary and dictates its matching coefficients on the small component.

3.10. The origin of Pulay contributions

The FLAPW approach is constructed to provide a very physical, intuitive, and accurate description of a system given by providing the position dependent representations of basisand wave functions, density, and potential that are advantageous in the different regions of space which the APW method distincts. The quality of this description comes at the price that similar but slightly different systems are not that well represented anymore when using the quantities of the original system. In this thesis, we are interested in atomic forces and phonons, which both are conceptually connected to the displacement of one or more atoms. It is obvious that in the case of a real displacement $\tau_{\alpha} \to \tau_{\alpha} + \delta \tau_{\alpha}$, the original functions cannot be used anymore since parts of them are defined in different regions of space than in the displaced case. For an infinitesimal displacement, this translates to the observation that the variation of a Kohn-Sham state is not fully contained in the Hilbert space provided by the LAPW basis functions. To be more formal, let us assume that the Hamiltonian $\hat{\mathcal{H}}$, its eigenvalues ϵ and eigenfunctions ψ depend on a parameter λ , which could be for example the atomic positions τ_{α} or the effective potential V_{eff} . Let $\psi(\lambda=0)$ be normalized to 1. Applying the derivative with respect to this parameter to the eigenvalue expressed by the Rayleigh coefficient, we find for its change:

$$\frac{d}{d\lambda}\epsilon(\lambda)\bigg|_{\lambda=0} = \frac{d}{d\lambda} \frac{\left\langle \psi(\lambda) \middle| \hat{\mathcal{H}}(\lambda) \middle| \psi(\lambda) \right\rangle}{\left\langle \psi(\lambda) \middle| \psi(\lambda) \right\rangle}\bigg|_{\lambda=0}
= \left\langle \psi \middle| \frac{d}{d\lambda} \left. \hat{\mathcal{H}}(\lambda) \middle|_{\lambda=0} \middle| \psi \right\rangle + \left\langle \frac{d}{d\lambda} \left. \psi(\lambda) \middle|_{\lambda=0} \middle| \hat{\mathcal{H}} - \epsilon \middle| \psi \right\rangle + \text{c.c.}$$
(3.80)

The first term on the right hand side corresponds to the Hellmann-Feynman theorem. The second term and its complex conjugate would vanish if either (a) the wave function does not depend on the parameter λ or if (b) ψ is a true (in the sense of pointwise) eigenfunction of the Hamiltonian. The first statement is not true as pointed out above,

$$\frac{d}{d\lambda} |\psi(\lambda)|_{\lambda=0} = \psi'_{\parallel} + \psi'_{\perp}. \tag{3.81}$$

The second statement is false because the Kohn-Sham states are variational solutions of the Schrödinger equation within the Hilbert space spanned by the LAPW basis functions, i.e.,

$$\hat{\mathcal{H}}\psi = \epsilon\psi + \delta\psi_{\perp}.\tag{3.82}$$

The quantities labeled with \perp are orthogonal to the LAPW Hilbert space. Therefore, the contributions to Eq. (3.80) that exceed the Hellmann-Feynman theorem give

$$\left\langle \frac{d}{d\lambda} \left. \psi(\lambda) \right|_{\lambda=0} \middle| \hat{\mathcal{H}} - \epsilon \middle| \psi \right\rangle = \left\langle \psi'_{\perp} \middle| \delta \psi_{\perp} \right\rangle \neq 0. \tag{3.83}$$

Such a behavior was first pointed out by Pulay in the framework of molecules [55]. He makes note of the reduction of this error term when going from an arbitrary test wave function to a true eigensolution of the molecular Hamiltonian. In the case of solids and the LAPW basis, the transition from a 'test' wave function to a true eigensolution corresponds to a systematic expansion of the LAPW basis space such that $\delta\psi_{\perp}$ becomes smaller and smaller in the process. Of course, when only pure plane-waves are used as basis function, the Pulay contribution also vanishes: The derivative of the wave functions then can be expressed completely within the space spanned by the same plane waves that constitute the basis. Within this space, the variational solution of the Schrödinger equation has the character of a true eigensolution.

3.11. Variational total energy for metals

In the total energy formula (2.14), the factors f_{ik} enter, which weight the occupation of band i at Bloch vector k. In semiconductors and insulators, these occupation numbers are integer and small changes to the system will not affect them. This is because the occupied bands are strictly separated from the conduction bands and the Fermi energy lies in between. For a metal on the other hand, the Fermi energy crosses one or more bands. The crossing point thus depends sensitively on the exact setup of the system. Furthermore, the sharp transition from occupancy to unoccupancy with respect to the k-point path makes Brillouin-zone integration by discretizing the integral to a k-point sum difficult. In order to cope with this circumstance, usually fractional occupation numbers are introduced, which are determined as follows:

Occupy each band at each k-point from bottom to top until all N electrons within the unit cell are distributed.

$$N = \sum_{i\mathbf{k}} f_{i\mathbf{k}}.\tag{3.84}$$

Next, after having chosen a temperature parameter T for good convergence, the Fermi energy $E_{\rm F}$ is determined by requiring that the occupation numbers smeared by a Fermi distribution reproduce the same number of electrons:

$$N = \sum_{i\mathbf{k}} f_{i\mathbf{k}} \frac{1}{e^{(\epsilon_{i\mathbf{k}} - E_{\mathrm{F}})/k_{\mathrm{B}}T} + 1} =: \sum_{i\mathbf{k}} \tilde{f}_{i\mathbf{k}}$$
(3.85)

By the shape of the Fermi distribution, the occupancy of bands far away from $E_{\rm F}$ is virtually not altered, while near the Fermi edge, occupied bands lose a fraction of their electrons, which are collected by the unoccupied bands. The fractional occupation numbers \tilde{f}_{ik} are then used within k-point sums.

Weinert and Davenport pointed out however that the total energy is not variational any more when fractional occupation numbers are employed [113], because the variation of the occupation numbers provides a first order term to the total energy variation when the density used deviates by $\delta\rho$ from the optimal density ρ_0 . To make the total energy variational again, they suggested to add an entropy like term TS with the same temperature broadening T as above and the entropy S given for electron-number conserving deviations as

$$S = k_{\rm B} \sum_{i\mathbf{k}} \left[\tilde{f}_{i\mathbf{k}} \ln(\tilde{f}_{i\mathbf{k}}) + (f_{i\mathbf{k}} - \tilde{f}_{i\mathbf{k}}) \ln(f_{i\mathbf{k}} - \tilde{f}_{i\mathbf{k}}) \right]. \tag{3.86}$$

The response of this term to a variation of the density is

$$\delta S = k_{\rm B} \sum_{i\mathbf{k}} \left[\delta \tilde{f}_{i\mathbf{k}} \ln(\tilde{f}_{i\mathbf{k}}) + \delta \tilde{f}_{i\mathbf{k}} - \delta \tilde{f}_{i\mathbf{k}} \ln(f_{i\mathbf{k}} - \tilde{f}_{i\mathbf{k}}) - \delta \tilde{f}_{i\mathbf{k}} \right]$$

$$= k_{\rm B} \sum_{i\mathbf{k}} \delta \tilde{f}_{i\mathbf{k}} \ln\left(\frac{1}{e^{(\epsilon_{i\mathbf{k}} - E_{\rm F})/k_{\rm B}T} + 1 - 1}\right) = -k_{\rm B} \sum_{i\mathbf{k}} \delta \tilde{f}_{i\mathbf{k}} \epsilon_{i\mathbf{k}}, \tag{3.87}$$

which with the factor T corresponds exactly to the negative of the first order term which would remain with the variation of only the regular total energy. This equation is true in the case of electron-number conserving deviations as the remaining term $k_{\rm B} \sum_{ik} \delta \tilde{f}_{ik} E_{\rm F}$ is the change in the electron number.

By this, we will not consider variations in the occupation number in the forthcoming chapters, since either they vanish because of the system being semiconducting or insulating, or because the addition to the total energy introduced above is applied. Furthermore, knowing that the occupation numbers are fractional, we will denote them without the tilde as f_{ik} again.

The availability of atomic forces in an *ab initio* electronic structure code is an important milestone. Forces are an indispensable tool for geometry optimization, *i.e.*, finding the energetically optimal atomic position within a given unit cell. Instead of displacing each atom manually and scanning the resulting total energies for their minimum and thus the geometric ground state of the system, atomic forces can be used in conjunction with numerical optimization procedures [121] to efficiently navigate in the energy landscape formed by the atomic configurations. Starting from an initial configuration, one moves the atoms in the direction of the atomic forces to obtain a configuration closer to the energetic minimum. At the energetic minimum, the forces F_{α} vanish, since they are the negative first derivatives of the total energy E_{tot} with respect to the atomic positions τ_{α} ,

$$\boldsymbol{F}_{\alpha} = -\frac{dE_{\text{tot}}}{d\boldsymbol{\tau}_{\alpha}}.\tag{4.1}$$

From the advent of the FLAPW method in the 1980's it took about ten years until the seminal work of Soler and Williams [52, 53], and Yu, Singh, and Krakauer [54], in which they independently introduced a force formalism for the FLAPW method. The former group used a slightly different LAPW basis set as the one we presented in chapter 3.2, where the plane-wave representation of the basis functions in Eq. (3.16) is extended into the muffin-tin spheres and the plane-wave parts of the augmented angular-momentum channels are subtracted again from the radial muffin-tin functions. By this, the basis functions are truly continuous up to first order, but the generation of the Hamilton and overlap matrices becomes more involved. The latter group, on whose work the force implementation in the FLEUR-code is based, started from the regular LAPW basis. Both pointed out the importance of an additional contribution to the Hellmann-Feynman force stemming from the dependence of the LAPW basis functions on the atomic position and the property of the wave functions of being variational solutions to the Schrödinger equation and not pointwise exact solutions. This leads to the so-called Pulay-terms, which have already been discussed in section 3.10 of the previous chapter.

In both formulations, force calculations in practice often give rise to an unphysical trait, a violation of the acoustic sum rule, which states that the sum of the forces on all atoms adds up to zero. We address the resulting spurious force

$$F_{\rm D} = \sum_{\alpha} F_{\alpha} \neq 0 \tag{4.2}$$

as the drift force. A non-vanishing drift force directly contradicts Newton's third law of motion. In addition, it leads to a violation of the Goldstone mode of the acoustic phonons, which ensures that the acoustic-phonon branches vanish at the Brillouin-zone center. We will have a more rigorous look into phonons which are collective vibrations of the ions in the following chapters 5 and 7.

In the current chapter, we present a refined derivation of the force formula within the FLAPW method, starting from the regular LAPW basis set as did Yu et al. By comparing their derivation with ours, we identify additional contributions to the forces. Moreover, we show that our force formalism reduces the drift force by two to three orders of magnitude by application to a set of prototype systems. Parts of this chapter are already published in [63].

4.1. Derivative of the total energy

We start the derivation of the atomic force formula by noting that the total energy, Eq. (2.14), contains a number of integrals over the whole unit cell Ω . In the APW type of methods, Ω is divided into atom centered MT spheres and the remaining IR. Since thus the constituents of the total unit-cell volume are dependent on the atomic position, it is important to realize how such an integral behaves under differentiation with respect to τ_{α} . Let f(r) be a generic function defined piecewise as $f^{\text{MT}}(r)$ and $f^{\text{IR}}(r)$ on the different regions of Ω . Then the derivative of an integral containing this function as an integration kernel is

$$\frac{d}{d\boldsymbol{\tau}_{\alpha}} \int_{\Omega} f(\boldsymbol{r}) d^{3}r = \frac{d}{d\boldsymbol{\tau}_{\alpha}} \left[\sum_{\beta} \int_{\mathrm{MT}(\beta)} f(\boldsymbol{r}) d^{3}r + \int_{\mathrm{IR}} f(\boldsymbol{r}) d^{3}r \right]$$

$$= \left[\sum_{\beta} \int_{\mathrm{MT}(\beta)} \frac{df(\boldsymbol{r})}{d\boldsymbol{\tau}_{\alpha}} d^{3}r + \int_{\mathrm{IR}} \frac{df(\boldsymbol{r})}{d\boldsymbol{\tau}_{\alpha}} d^{3}r \right] + \oint_{\partial \mathrm{MT}(\alpha)} [f^{\mathrm{MT}}(\boldsymbol{r}) - f^{\mathrm{IR}}(\boldsymbol{r})] \hat{\boldsymbol{e}} dS \tag{4.3}$$

with the unit normal vector $\hat{\boldsymbol{e}} = (\boldsymbol{r} - \boldsymbol{\tau}_{\alpha})/|\boldsymbol{r} - \boldsymbol{\tau}_{\alpha}|$ pointing from the muffin-tin sphere of atom α into the interstitial region. If the integrand is continuous over the whole domain of integration Ω , the surface integral vanishes. In a FLAPW calculation in practice, however, the finite angular-momentum and reciprocal-lattice cutoffs l_{\max}^{α} and G_{\max} are responsible for rendering the basis- and wave functions, the density, and the potential discontinuous at the muffin-tin sphere boundaries. Hence, the surface term $\oint_{\partial \mathrm{MT}(\alpha)} [f^{\mathrm{MT}}(\boldsymbol{r}) - f^{\mathrm{IR}}(\boldsymbol{r})] \hat{\boldsymbol{e}} dS$ typically does persist.

The derivative of the total energy, Eq. (2.14), with respect to the atomic position τ_{α} becomes

$$\boldsymbol{F}_{\alpha} = -\frac{dE_{\text{tot}}[\rho]}{d\boldsymbol{\tau}_{\alpha}} = \boldsymbol{F}_{\alpha}^{\text{HF}} - \sum_{i\boldsymbol{k}} f_{i\boldsymbol{k}} \frac{d\epsilon_{i\boldsymbol{k}}}{d\boldsymbol{\tau}_{\alpha}} + \int_{\Omega} \rho(\boldsymbol{r}) \frac{dV_{\text{eff}}(\boldsymbol{r})}{d\boldsymbol{\tau}_{\alpha}} d^{3}\boldsymbol{r}$$

$$- \oint_{\partial \text{MT}(\alpha)} \rho^{\text{MT}}(\boldsymbol{r}) \left[\varepsilon_{\text{xc}}^{\text{MT}}(\boldsymbol{r}) - \mu_{\text{xc}}^{\text{MT}}(\boldsymbol{r}) \right] \hat{\boldsymbol{e}} dS$$

$$+ \oint_{\partial \text{MT}(\alpha)} \rho^{\text{IR}}(\boldsymbol{r}) \left[\varepsilon_{\text{xc}}^{\text{IR}}(\boldsymbol{r}) - \mu_{\text{xc}}^{\text{IR}}(\boldsymbol{r}) \right] \hat{\boldsymbol{e}} dS, \tag{4.4}$$

where we have omitted the variation $df_{ik}/d\tau_{\alpha}$ of the occupation number according to chapter 3.11.

The Hellmann-Feynman force acting on atom α is the negative derivative of the Coulomb potential of all charges except the nuclear charge of atom α , evaluated at the position of atom α ,

$$\boldsymbol{F}_{\alpha}^{\mathrm{HF}} = -Z_{\alpha} \left[\sum_{\beta \neq \alpha} \frac{d}{d\boldsymbol{\tau}_{\alpha}} \frac{Z_{\beta}}{|\boldsymbol{\tau}_{\alpha} - \boldsymbol{\tau}_{\beta}|} - \int \frac{d}{d\boldsymbol{\tau}_{\alpha}} \frac{\rho(\boldsymbol{r}')}{|\boldsymbol{\tau}_{\alpha} - \boldsymbol{r}'|} d^{3}r' \right]. \tag{4.5}$$

The derivative of ϵ_{ik} can be found using the Rayleigh coefficient [s. Eq. (3.80)]. Considering also the possible discontinuities leads to

$$\frac{d\epsilon_{ik}}{d\tau_{\alpha}} = \int_{\Omega} |\psi_{ik}(\mathbf{r})|^{2} \frac{dV_{\text{eff}}(\mathbf{r})}{d\tau_{\alpha}} d^{3}r + \left\langle \frac{d\psi_{ik}}{d\tau_{\alpha}} \middle| \hat{\mathcal{H}} - \epsilon_{ik} \middle| \psi_{ik} \right\rangle + \text{c.c.}
+ \oint_{\partial \text{MT}(\alpha)} \left\{ \psi_{ik}^{\text{MT*}}(\mathbf{r}) [\hat{\mathcal{H}} - \epsilon_{ik}] \psi_{ik}^{\text{MT}}(\mathbf{r}) - \psi_{ik}^{\text{IR*}}(\mathbf{r}) [\hat{\mathcal{H}} - \epsilon_{ik}] \psi_{ik}^{\text{IR}}(\mathbf{r}) \right\} \hat{\mathbf{e}} dS.$$
(4.6)

After summing over all states $i\mathbf{k}$, the first term of this expression cancels with the last term of the first line of Eq. (4.4). Then, the total force on atom α can be expressed as the sum of the three terms

$$\boldsymbol{F}_{\alpha} = \boldsymbol{F}_{\alpha}^{\text{HF}} - \boldsymbol{F}_{\alpha}^{\text{Pulay}} - \boldsymbol{F}_{\alpha}^{\text{surface}}, \tag{4.7}$$

where in analogy to Eq. (3.80) the Pulay force is

$$\mathbf{F}_{\alpha}^{\text{Pulay}} = \sum_{i\mathbf{k}} f_{i\mathbf{k}} \left\langle \frac{d\psi_{i\mathbf{k}}}{d\tau_{\alpha}} \middle| \hat{\mathcal{H}} - \epsilon_{i\mathbf{k}} \middle| \psi_{i\mathbf{k}} \right\rangle + \text{c.c.}$$
 (4.8)

and the surface contribution reads

$$\boldsymbol{F}_{\alpha}^{\text{surface}} = \oint_{\partial \text{MT}(\alpha)} \left\{ \rho^{\text{MT}} \left[\varepsilon_{\text{xc}}^{\text{MT}} + V_{\text{eff}}^{\text{MT}} - \mu_{\text{xc}}^{\text{MT}} \right] - \rho^{\text{IR}} \left[\varepsilon_{\text{xc}}^{\text{IR}} + V_{\text{eff}}^{\text{IR}} - \mu_{\text{xc}}^{\text{IR}} \right] \right\} \hat{\boldsymbol{e}} dS$$

$$+ \sum_{i\boldsymbol{k}} f_{i\boldsymbol{k}} \oint_{\partial \text{MT}(\alpha)} \left\{ \psi_{i\boldsymbol{k}}^{\text{MT*}} \left[\hat{T} - \epsilon_{i\boldsymbol{k}} \right] \psi_{i\boldsymbol{k}}^{\text{MT}} - \psi_{i\boldsymbol{k}}^{\text{IR*}} \left[\hat{T} - \epsilon_{i\boldsymbol{k}} \right] \psi_{i\boldsymbol{k}}^{\text{IR}} \right\} \hat{\boldsymbol{e}} dS.$$
 (4.9)

So far, we did not use the exact form of the LAPW basis functions, the density, or the potential; we solely provided that a) the basis functions are dependent on the atomic position, b) the partitioning of space is dependent on the atomic position, and c) the wave functions are only variational solutions of the Schrödinger equation. Therefore, the result is quite general and applicable to other methods with the same set of qualities, like for example the linearized muffin-tin orbital approach [59–61].

linearized muffin-tin orbital approach [59–61]. The importance of the Pulay contribution $F_{\alpha}^{\rm Pulay}$ to the force is one of the central findings in the publication of Yu et al. in case of the FLAPW method. Moreover, they already included the second line of the surface force into their consideration, since the LAPW basis functions are completely discontinuous at second order. In comparison, our surface force contribution $F_{\alpha}^{\rm surface}$ naturally includes this term because it specifically accounts for any discontinuity at the muffin-tin sphere boundary. In addition, our surface contribution includes a correction due to the discontinuity of the potential terms, the density, and the xc energy density. Eq. (4.7) with Eqs. (4.8) and (4.9) thus present a generalization of the force formalism published before.

4.2. Pulay force

The Pulay force arises because the wave functions are dependent on the atomic positions and solve the Schrödinger equation variationally and not pointwise. The effect of the latter we already discussed in chapter 3.10. The Pulay force also involves a sum over all occupied states, which in the FLAPW method are distinguished into core states and valence states.

The former are direct solutions of the scalar-relativistic or fully-relativistic Dirac equation employing the spherical part of the effective potential, while the latter are represented through the LAPW basis set. We will first present the Pulay forces for the valence states and provide the expression for the core states afterwards.

4.2.1. Valence states

The linear combination of the LAPW basis functions ϕ_{kG} according to Eq. (3.24) describes the valence states ψ_{ik} . Thus, their derivative with respect to the atomic position τ_{α} is given by

$$\frac{d\psi_{ik}(\mathbf{r})}{d\boldsymbol{\tau}_{\alpha}} = \sum_{\mathbf{G}} \frac{dz_{ik\mathbf{G}}}{d\boldsymbol{\tau}_{\alpha}} \phi_{k\mathbf{G}}(\mathbf{r}) + z_{ik\mathbf{G}} \frac{d\phi_{k\mathbf{G}}(\mathbf{r})}{d\boldsymbol{\tau}_{\alpha}}.$$
 (4.10)

Inserted into the Pulay force (4.8) it can be seen that only the second part of $d\psi_{ik}/d\tau_{\alpha}$ contributes, which is the variation of the basis functions. The first part is the product of the variation $dz_{ikG}/d\tau_{\alpha}$ of the expansion coefficients times the regular basis functions. Within their Hilbert space, however, the wave functions fulfill the Schrödinger equation exactly, as explained in section 3.10. The variation of the basis function in the second part of Eq. (4.10) can be split into a part that lies within the Hilbert space of the basis functions, which does not add to the Pulay expression, and a part which is orthogonal to the Hilbert space. The latter has a non-vanishing scalar product with the part of $\hat{\mathcal{H}}\psi_{ik}$ that also reaches out of the space spanned by the basis functions.

Recalling the definition of the LAPW basis functions (3.16) allows us to see the independence of their plane-wave representation on the atomic position. In the muffin-tin spheres, the basis functions depend on τ_{α} through the local coordinate frame $r_{\alpha} = r - \tau_{\alpha}$,

$$\phi_{\mathbf{k}\mathbf{G}}^{\mathrm{MT}(\alpha)}(\mathbf{r}) = \sum_{lm} a_{lm\lambda}^{\alpha \mathbf{k}\mathbf{G}} u_{l\lambda}^{\alpha}(r_{\alpha}, E_{l}^{\alpha}) Y_{lm}(\hat{\mathbf{r}}_{\alpha}), \tag{3.16 revisited}$$

and through the phase factor contained in the matching coefficients,

$$\begin{pmatrix} a_{lm0}^{\alpha \mathbf{k} \mathbf{G}} \\ a_{lm1}^{\alpha \mathbf{k} \mathbf{G}} \end{pmatrix} = \frac{4\pi i^{l}}{\sqrt{\Omega}} e^{i(\mathbf{k} + \mathbf{G}) \cdot \boldsymbol{\tau}_{\alpha}} Y_{lm}^{*} (\widehat{\mathbf{k} + \mathbf{G}}) \underline{\boldsymbol{U}}^{-1} \begin{pmatrix} j_{l}(|\mathbf{k} + \mathbf{G}|R_{\alpha}) \\ |\mathbf{k} + \mathbf{G}|j_{l}^{\prime}(|\mathbf{k} + \mathbf{G}|R_{\alpha}) \end{pmatrix}. \quad (3.17 \text{ revisited})$$

Therefore, the derivative of the basis function with respect to the atomic position becomes

$$\frac{d\phi_{kG}(\mathbf{r})}{d\tau_{\alpha}} = \begin{cases} [i(\mathbf{k} + \mathbf{G}) - \nabla]\phi_{kG}(\mathbf{r}) &, \mathbf{r} \in MT(\alpha) \\ 0 &, \text{ else} \end{cases}.$$
 (4.11)

An implicit dependence of the basis functions on τ_{α} is given by the radial functions $u_{l\lambda}^{\beta}$, which are depend on the spherical part of the local effective potential and are thus subjected to variations in the effective potential due to atomic displacements. The impact of this dependence is usually considered to be small compared to the effort necessary to construct the changes in the radial functions as was stated by Yu et al. [54]. Therefore, we stick to this frozen-augmentation approximation and continue from Eq. (4.11) above to find the valence-state contribution to the Pulay force.

Inserting the variation of the basis functions in Eq. (4.8) leads to the Pulay force for the valence (val) states:

$$\boldsymbol{F}_{\alpha,\mathrm{val}}^{\mathrm{Pulay}} = \sum_{i\boldsymbol{k}}^{\mathrm{val}} f_{i\boldsymbol{k}} \sum_{\boldsymbol{G}\boldsymbol{G}'} i(\boldsymbol{G}' - \boldsymbol{G}) z_{i\boldsymbol{k}\boldsymbol{G}}^* \ z_{i\boldsymbol{k}\boldsymbol{G}'} \left\langle \phi_{\boldsymbol{k}\boldsymbol{G}} \ \middle| \hat{\mathcal{H}} - \epsilon_{i\boldsymbol{k}} \middle| \phi_{\boldsymbol{k}\boldsymbol{G}'} \right\rangle_{\mathrm{MT}(\alpha)}$$

$$-\sum_{i\mathbf{k}}^{\text{val}} f_{i\mathbf{k}} \oint_{\partial \text{MT}(\alpha)} \psi_{i\mathbf{k}}^{\text{MT}*} \left[\hat{T} - \epsilon_{i\mathbf{k}} \right] \psi_{i\mathbf{k}}^{\text{MT}} \hat{\mathbf{e}} dS - \int_{\text{MT}(\alpha)} V_{\text{eff}} \nabla \rho_{\text{val}} d^3 r$$
 (4.12)

Since the basis functions depend on τ_{α} only in the muffin-tin sphere of atom α , the bra-ket is confined to this region. To further elaborate the origin of this equation, we note that the first line comes from the $i(\mathbf{k}+\mathbf{G})$ part of Eq. (4.11), while the gradient part directly produces the volume integral of the second line. The remaining sum of $\langle \nabla \phi_{\mathbf{k}\mathbf{G}} | \hat{T} - \epsilon_{i\mathbf{k}} | \phi_{\mathbf{k}\mathbf{G}'} \rangle_{\alpha}$ and $\langle \phi_{\mathbf{k}\mathbf{G}} | \hat{T} - \epsilon_{i\mathbf{k}} | \nabla \phi_{\mathbf{k}\mathbf{G}'} \rangle_{\alpha}$ becomes the surface integral in Eq (4.12) by application of Gauss' theorem, since neither \hat{T} nor $\epsilon_{i\mathbf{k}}$ are affected by the gradient. The surface integral cancels with the muffin-tin part of the valence term in the second line of the surface force (4.9).

The first line of the Pulay contribution from the valence states contains the Hamiltonian and the overlap matrix of Eqs. (3.66) and (3.67). Thus, the bra-ket is

$$\left\langle \phi_{kG} \left| \hat{\mathcal{H}} - \epsilon_{ik} \middle| \phi_{kG'} \right\rangle_{\mathrm{MT}(\alpha)} = H_{GG'}^{\alpha}(k) - \epsilon_{ik} S_{GG'}^{\alpha}(k).$$
 (4.13)

This does scale unfavorably with the system size, though, because of two sums over reciprocal lattice vectors, a sum over bands and the evaluation for each atom. Instead, Yu et al. suggested to precalculate the reciprocal sums by convoluting over G as is done in Eq. (3.23) for the $A_{m\lambda}^{cik}$ -matching coefficients:

$$A_{lm\lambda}^{\alpha ik} = \sum_{G} G z_{ikG} a_{lm\lambda}^{\alpha kG}$$
(4.14)

Splitting the basis function by Eq. (3.64) into the matching coefficients and the radial functions times spherical harmonics, the first line of Eq. (4.12) can be rewritten as

$$\sum_{ik}^{\text{val}} f_{ik} \sum_{GG'} i(G' - G) z_{ikG}^* z_{ikG'} \left\langle \phi_{kG} \middle| \hat{\mathcal{H}} - \epsilon_{ik} \middle| \phi_{kG'} \right\rangle_{\text{MT}(\alpha)}$$

$$= i \sum_{ik}^{\text{val}} f_{ik} \sum_{lm\lambda} \sum_{l'm'\lambda'} \left[A_{lm\lambda}^{\alpha ik} A_{l'm'\lambda'}^{\alpha ik} \left\langle \varphi_{lm\lambda}^{\alpha} \middle| \hat{\mathcal{H}}_{\text{MT}}^{\alpha} - \epsilon_{ik} \middle| \varphi_{l'm'\lambda'}^{\alpha} \right\rangle_{\text{MT}(\alpha)}$$

$$- A_{lm\lambda}^{\alpha ik*} A_{l'm'\lambda'}^{\alpha ik} \left\langle \varphi_{lm\lambda}^{\alpha} \middle| \hat{\mathcal{H}}_{\text{MT}}^{\alpha} - \epsilon_{ik} \middle| \varphi_{l'm'\lambda'}^{\alpha} \right\rangle_{\text{MT}(\alpha)} \right]$$

$$= i \sum_{ik}^{\text{val}} f_{ik} \sum_{lm\lambda} \sum_{l'm'\lambda'} \left[A_{lm\lambda}^{\alpha ik*} A_{l'm'\lambda'}^{\alpha ik} - A_{lm\lambda}^{\alpha ik*} A_{l'm'\lambda'}^{\alpha ik} \right] \left[t_{lml'm'}^{\alpha \lambda \lambda'} - \epsilon_{ik} \delta_{\Sigma\Sigma'} J_{lm}^{\alpha \lambda} \right]$$

$$(4.15)$$

with the matrix elements $t_{lml'm'}^{\alpha\lambda\lambda'}$ and $J_{lm}^{\alpha\lambda}$ from Eqs. (3.68) and (3.70).

To evaluate the integral over the valence-density gradient, we make use of a relation concerning the gradient in natural coordinates given by:

$$\begin{pmatrix} r_{-1} \\ r_{0} \\ r_{1} \end{pmatrix} = \frac{1}{\sqrt{2}} \begin{pmatrix} 1 & -i & 0 \\ 0 & 0 & \sqrt{2} \\ -1 & i & 0 \end{pmatrix} \begin{pmatrix} r_{x} \\ r_{y} \\ r_{z} \end{pmatrix}$$
(4.16)

Then, for $m'' \in \{-1, 0, 1\}$, it is

$$\nabla_{m''} f_{l'm'}(r) Y_{l'm'}(\hat{r}) = \sqrt{\frac{4\pi}{3}} \sum_{l''=-1}^{1,2} G_{l'+l'',l',1}^{m'+m'',m',m'} Y_{l'+l'',m'+m''}(\hat{r}) \times \left[f'_{l'm'}(r) - \left(l''l' + \frac{l''-1}{2} \right) \frac{f_{l'm'}(r)}{r} \right]$$
(4.17)

with the Gaunt coefficients $G_{l''+l'',l',1}^{m'+m''}$ defined as in Eq. (3.30) and the l''-sum running over l''=-1 and 1, only. Effectively, the angular momentum is altered by 1 and the sum in parentheses is either l' or -(l'+1), depending on whether l'' is 1 or -1. The gradient transforms like a vector. Therefore, we have to apply the inverse transformation of Eq. (4.16) in order to obtain the result of the gradient in Cartesian coordinates:

$$\begin{pmatrix}
\nabla_x \\
\nabla_y \\
\nabla_z
\end{pmatrix} = \frac{1}{\sqrt{2}} \begin{pmatrix}
1 & 0 & -1 \\
i & 0 & i \\
0 & \sqrt{2} & 0
\end{pmatrix} \begin{pmatrix}
\nabla_{-1} \\
\nabla_{0} \\
\nabla_{1}
\end{pmatrix} =: \underline{T} \begin{pmatrix}
\nabla_{-1} \\
\nabla_{0} \\
\nabla_{1}
\end{pmatrix} \tag{4.18}$$

Applied to the integral containing the valence-density gradient, this procedure yields

$$\int_{MT(\alpha)} V_{\text{eff}} \nabla \rho_{\text{val}} d^3 r
= \sum_{lm} \sum_{l'm'} \sum_{m''=-1}^{1} \int_{B_{R_{\alpha}}(\mathbf{0})} V_{\text{eff},lm}^{\alpha*}(r_{\alpha}) Y_{lm}^{*}(\hat{r}_{\alpha}) \underline{T} \hat{\mathbf{e}}_{m''} \nabla_{m''} \rho_{\text{val},l'm'}^{\alpha}(r_{\alpha}) Y_{l'm'}(\hat{r}_{\alpha}) d^3 r_{\alpha}
= \sqrt{\frac{4\pi}{3}} \sum_{lm} \sum_{l'm'} \sum_{l''=-1}^{1,2} \sum_{m''=-1}^{1} \underline{T} \hat{\mathbf{e}}_{m''} \delta_{l',l-l''} \delta_{m',m-m''} G_{l,l',1}^{m,m',m''}
\times \int_{0}^{R_{\alpha}} r^2 V_{\text{eff},lm}^{\alpha*}(r) \left[\rho'_{\text{val},l'm'}(r) - \left(l''l' + \frac{l''-1}{2} \right) \frac{\rho_{\text{val},l'm'}(r)}{r} \right] dr. \quad (4.19)$$

The sum over the primed angular and magnetic momenta contracts due to the Kroneckerdeltas, defining them as l-l'' or m-m''.

4.2.2. Core states

The core states $\psi_{ik}(r)$ are strongly bound states, whose wave function is usually assumed to be decayed to zero at the muffin-tin sphere boundary and beyond. Since they are considered to be highly localized at their corresponding atomic nucleus, they are determined only from the spherical potential at this atom. Also, the core states are ideally non-overlapping and thus show no dispersion over the Brillouin zone. Their k dependence is only of formal nature and the band index becomes a superindex $i = (\beta plm_l)$, consisting of the atom index β , the principal and angular quantum numbers p and l as well as the magnetic quantum number m_l . In a practical calculation, however, these prerequisites are only approximately fulfilled, especially the confinement to the muffin-tin sphere.

In analogy to the frozen-augmentation approximation, we will assume that the dependence of the core states on the atomic position τ_{α} does not manifest itself in an implicit change of the form of the state due to the change in the effective potential. As they lack a matching

to plane waves, the only dependence on au_{α} results from the local coordinate frame and we obtain

$$\frac{d\psi_{i\mathbf{k}}(\mathbf{r})}{d\tau_{\alpha}} = -\nabla\psi_{i\mathbf{k}}(\mathbf{r})\delta_{\alpha\beta}.$$
(4.20)

Applying this equation to the Pulay force, Eq. (4.8), we have for its contribution from the core states

$$\boldsymbol{F}_{\alpha,\text{core}}^{\text{Pulay}} = -\sum_{i\boldsymbol{k}} f_{i\boldsymbol{k}} \delta_{\alpha\beta} \left[\left\langle \nabla \psi_{i\boldsymbol{k}} \middle| \hat{\mathcal{H}} - \epsilon_{i\boldsymbol{k}} \middle| \psi_{i\boldsymbol{k}} \right\rangle_{\Omega} + \left\langle \psi_{i\boldsymbol{k}} \middle| \hat{\mathcal{H}} - \epsilon_{i\boldsymbol{k}} \middle| \nabla \psi_{i\boldsymbol{k}} \right\rangle_{\Omega} \right]. \tag{4.21}$$

As ψ_{ik} is a pointwise eigenstate to the spherical Hamiltonian with energy ϵ_{ik} , only the non-spherical part of the effective potential as seen from atom α contributes to the bra-kets. Thus, the wave functions and their gradients can be combined to the density-gradient and yield

$$\mathbf{F}_{\alpha,\text{core}}^{\text{Pulay}} = -\int_{\Omega} V_{\text{nonsph}}(\mathbf{r}) \sum_{i\mathbf{k}} f_{i\mathbf{k}} \delta_{\alpha\beta} \left[\nabla \psi_{i\mathbf{k}}^*(\mathbf{r}) \cdot \psi_{i\mathbf{k}}(\mathbf{r}) + \psi_{i\mathbf{k}}^*(\mathbf{r}) \nabla \psi_{i\mathbf{k}}(\mathbf{r}) \right] d^3r$$

$$= -\int_{\Omega} V_{\text{eff}}(\mathbf{r}) \nabla \rho_{\text{core}}^{\alpha}(\mathbf{r}) d^3r. \tag{4.22}$$

We did not limit ourselves to the non-spherical potential in Eq. (4.22), but it is implicitly included: The core density $\rho_{\text{core}}^{\alpha}(r) = \sum_{ik}^{\text{core}} \delta_{\alpha\beta} f_{ik} |\psi_{ik}(r)|^2$ is spherical. According to the comment concerning the gradient in natural coordinates, Eq. (4.17), application of the gradient produces only contributions to the l=1 channel, from which only the l=1 component of the effective potential is selected from the angular integral centered at τ_{α} . Yu et al. also stated a similar term in their Eq. (20). We note that in contrast to Yu et al., our core contribution is evaluated over the whole unit cell, not only over the muffin-tin sphere of atom α . In their publication, they assume that the core states are confined within the atomic sphere of radius R_{α} .

While it is true that the use of LOs for semi-core states can enforce the remaining core states to be strictly confined, this approach increases the computational cost to calculate systems where many semicore states have to be treated due to the additional basis functions. Also, the inclusion of the whole unit cell in the evaluation of $F_{\alpha,\text{core}}^{\text{Pulay}}$ makes the force calculation more robust and user friendly, since a bad choice of the mulfin-tin radius R_{α} does not exclude the coretail density from the calculation anymore.

Figure 4.1 exemplifies in the case of MgO the leakage of the Mg 2s and 2p core states from the magnesium muffin-tin sphere into the interstitial and even into the neighboring oxygen sphere.

We evaluate Eq. (4.22) by using the pseudodensity $\tilde{\rho}_{\rm core}^{\alpha}$ introduced in section 3.4 which exhibits the same coretail density as the true core-state density $\rho_{\rm core}^{\alpha}$ outside the muffin-tin sphere of atom α by construction. In this way we obtain

$$\mathbf{F}_{\alpha,\text{core}}^{\text{Pulay}} = -\int_{\text{MT}(\alpha)} V_{\text{eff}}(\mathbf{r}) \nabla \rho_{\text{core}}^{\alpha}(\mathbf{r}) d^3 r
- \int_{\text{IR}} V_{\text{eff}}(\mathbf{r}) \nabla \tilde{\rho}_{\text{core}}^{\alpha}(\mathbf{r}) d^3 r - \sum_{\beta \neq \alpha} \int_{\text{MT}(\beta)} V_{\text{eff}}(\mathbf{r}) \nabla \tilde{\rho}_{\text{core}}^{\alpha}(\mathbf{r}) d^3 r.$$
(4.23)

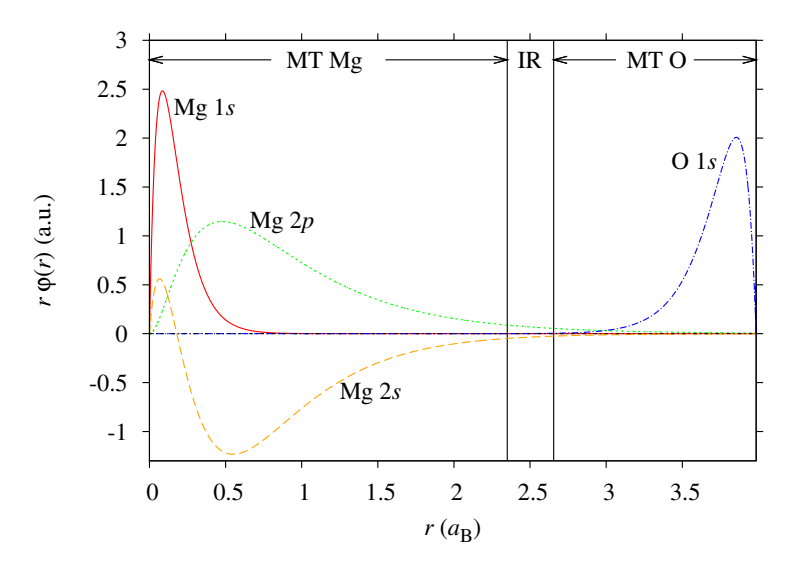


Figure 4.1.: Leakage of core states of MgO.

The pseudodensity is given in terms of a Fourier expansion, so its derivative becomes

$$\nabla \tilde{\rho}_{\text{core}}^{\alpha}(\mathbf{r}) = \sum_{\mathbf{G}} i \mathbf{G} \hat{\rho}_{\text{core}}^{\alpha}(\mathbf{G}) e^{i\mathbf{G}\cdot\mathbf{r}} =: \sum_{\mathbf{G}} \left[\widehat{\boldsymbol{\nabla}}\widehat{\boldsymbol{\rho}_{\text{core}}^{\alpha}}\right] (\mathbf{G}) e^{i\mathbf{G}\cdot\mathbf{r}}.$$
(4.24)

This and the Heaviside step function $\Theta_{\rm IR}(r)$ for the interstitial region given in Eq. (3.74) allow us to express the second term of $F_{\alpha,{\rm core}}^{\rm Pulay}$ by expanding it over the whole unit cell:

$$\int_{\mathrm{IR}} V_{\mathrm{eff}}(\boldsymbol{r}) \nabla \tilde{\rho}_{\mathrm{core}}^{\alpha}(\boldsymbol{r}) d^{3} r = \Omega \sum_{\boldsymbol{G}} \widehat{[\Theta_{\mathrm{IR}} V_{\mathrm{eff}}]}^{*}(\boldsymbol{G}) \widehat{[\boldsymbol{\nabla} \boldsymbol{\widehat{\rho}_{\mathrm{core}}^{\alpha}}]}(\boldsymbol{G})$$
(4.25)

It is advisable to calculate the contributions from all other muffin-tin spheres $\beta \neq \alpha$ by including the integral over the pseudodensity gradient at α and subtracting it later. Then the sum over all atoms can be precalculated independently of atom α :

$$\sum_{\beta} \int_{\mathrm{MT}(\beta)} V_{\mathrm{eff}}(\boldsymbol{r}) \nabla \hat{\rho}_{\mathrm{core}}^{\alpha}(\boldsymbol{r}) d^{3}r$$

$$= \sum_{\boldsymbol{G}} \widehat{[\boldsymbol{\nabla} \hat{\rho}_{\mathrm{core}}^{\alpha}]}(\boldsymbol{G}) \sum_{\beta} e^{i\boldsymbol{G}\cdot\boldsymbol{\tau}_{\beta}} \int_{0}^{R_{\beta}} r_{\beta}^{2} \sum_{lm} 4\pi i^{l} Y_{lm}^{*}(\hat{\boldsymbol{G}}) j_{l}(Gr_{\beta}) V_{\mathrm{eff},lm}^{\beta*}(r_{\beta}) dr \tag{4.26}$$

What is left to calculate now is the integral over the muffin-tin sphere α , both for its real contribution to the force $\boldsymbol{F}_{\alpha}^{\text{Pulay}}$ and for subtracting the pseudodensity from the equation above. For the latter, there are two choices: Either use the last formula explicitly for $\beta = \alpha$, or consider only the Gaussian bell replacement from Eq. (3.36) inside the sphere. In case of

the second approach, the coretails from images of atom α in other unit cells reaching into the muffin-tin sphere of the representative atom are included into the force formula. Since the Gaussian bell is completely spherical, it can be found analogous to

$$\int_{\mathrm{MT}(\alpha)} V_{\mathrm{eff}}(\boldsymbol{r}) \nabla \rho_{\mathrm{core}}^{\alpha}(\boldsymbol{r}) d^{3} r = \sqrt{\frac{4\pi}{3}} \sum_{m''=-1}^{1} \underline{\boldsymbol{T}} \hat{\boldsymbol{e}}_{m''} \int_{0}^{R_{\alpha}} r_{\alpha}^{2} \rho_{\mathrm{core},00}^{\alpha\prime}(r_{\alpha}) V_{\mathrm{eff},1m''}^{\alpha}(r_{\alpha}) dr_{\alpha},$$

$$(4.27)$$

where we used the gradient in natural coordinates as given in Eq. (4.19) letting l'=m'=0. The true core-charge density derivative $\rho_{\mathrm{core},00}^{cl}(r_{\alpha})$ then has to be replaced by $-\sqrt{4\pi}2r_{\alpha}a_{\alpha}A_{\alpha}e^{-a_{\alpha}r_{\alpha}^{2}}$.

4.3. Surface force

We proceed by discussing the evaluation of the remaining surface force term

$$\boldsymbol{F}_{\alpha}^{\text{surface}} = \oint_{\partial MT(\alpha)} \left\{ \rho^{\text{MT}} \left[\varepsilon_{\text{xc}}^{\text{MT}} + V_{\text{eff}}^{\text{MT}} - \mu_{\text{xc}}^{\text{MT}} \right] - \rho^{\text{IR}} \left[\varepsilon_{\text{xc}}^{\text{IR}} + V_{\text{eff}}^{\text{IR}} - \mu_{\text{xc}}^{\text{IR}} \right] \right\} \hat{\boldsymbol{e}} dS$$

$$- \sum_{i\boldsymbol{k}}^{\text{val}} f_{i\boldsymbol{k}} \oint_{\partial MT(\alpha)} \psi_{i\boldsymbol{k}}^{\text{IR*}} \left[\hat{T} - \epsilon_{i\boldsymbol{k}} \right] \psi_{i\boldsymbol{k}}^{\text{IR}} \hat{\boldsymbol{e}} dS, \tag{4.9 revisited}$$

where we have omitted the vanishing contributions from the continuously differentiable core states to the last line as well as the muffin-tin contribution from the valence states, since the latter also appears in the Pulay force term (4.12) with a different sign. This formula contains sphere surface integrals over quantities expressed in spherical coordinates or in terms of a Fourier expansion. Given that the unit normal vector $\hat{\boldsymbol{e}}$ expressed in Cartesian basis vectors $\hat{\boldsymbol{e}}_{i=1,2,3}$ is

$$\hat{\boldsymbol{e}} = \sqrt{\frac{2\pi}{3}} \begin{pmatrix} Y_{1-1}(\hat{\boldsymbol{e}}) - Y_{11}(\hat{\boldsymbol{e}}) \\ iY_{1-1}(\hat{\boldsymbol{e}}) + iY_{11}(\hat{\boldsymbol{e}}) \end{pmatrix} =: \sum_{i=1}^{3} \sum_{m=-1}^{1} c_{i,m} Y_{1m}(\hat{\boldsymbol{e}}) \hat{\boldsymbol{e}}_{i}, \tag{4.28}$$

the first term of Eq. (4.9) containing only muffin-tin quantities yields

$$\oint_{\partial MT(\alpha)} \left\{ \rho^{MT} \left[\varepsilon_{xc}^{MT} + V_{eff}^{MT} - \mu_{xc}^{MT} \right] \right\} \hat{e} dS = R_{\alpha}^{2} \sum_{i=1}^{3} \hat{e}_{i} \sum_{m=-1}^{1} c_{i,m}^{*} \sum_{l'm'} \sum_{l'm'} G_{l'',l',1}^{m'',m} \times \rho_{l'm'}^{\alpha*}(R_{\alpha}) \left[\varepsilon_{xc,l''m''}^{\alpha}(R_{\alpha}) + V_{eff,l''m''}^{\alpha}(R_{\alpha}) - \mu_{xc,l''m''}^{\alpha}(R_{\alpha}) \right]. \tag{4.29}$$

For the interstitial term of opposite sign, it is useful to express the density, potential, and xc energy density in spherical coordinates by making use of a Rayleigh expansion around τ_{α} . We exemplify the resulting expressions and abbreviations by means of the density,

$$\rho^{\text{IR}}(\boldsymbol{r})\big|_{\boldsymbol{r}\in\partial\text{MT}(\alpha)} = \sum_{l'm'} \left[4\pi i^{l'} \sum_{\boldsymbol{G}} \hat{\rho}(\boldsymbol{G}) e^{i\boldsymbol{G}\cdot\boldsymbol{\tau}_{\alpha}} Y_{l'm'}^{*}(\hat{\boldsymbol{G}}) j_{l'}(GR_{\alpha}) \right] Y_{l'm'}(\hat{\boldsymbol{R}}_{\alpha})$$

$$=: \sum_{l'm'} \rho_{l'm'}^{\text{AIR}} Y_{l'm'}(\hat{\boldsymbol{R}}_{\alpha}). \tag{4.30}$$

The contribution from the interstitial is then given analogous to Eq. (4.29) simply by replacing $\rho_{l'm'}^{\alpha*}(R_{\alpha})$, $\varepsilon_{\mathrm{xc},l''m''}^{\alpha}(R_{\alpha})$, $V_{\mathrm{eff},l''m''}^{\alpha}(R_{\alpha})$, and $\mu_{\mathrm{xc},l''m''}^{\alpha}(R_{\alpha})$ by their interstitial counterparts $\rho_{l'm'}^{\alpha\mathrm{IR}*}(R_{\alpha})$, $\varepsilon_{\mathrm{xc},l''m''}^{\alpha\mathrm{IR}}(R_{\alpha})$, $V_{\mathrm{eff},l''m''}^{\alpha\mathrm{IR}}(R_{\alpha})$, and $\mu_{\mathrm{xc},l''m''}^{\alpha\mathrm{IR}}(R_{\alpha})$. The order of the Rayleigh expansion can be chosen arbitrarily, independent of the angular-momentum cutoff $l_{\mathrm{max}}^{\alpha}$, to increase the accuracy of this representation. In this thesis, the order of the Rayleigh expansion is set to $2l_{\mathrm{max}}^{\alpha}$. The Gaunt coefficients effectively limit the range of the sum over l''m'' to $l''=l'\pm 1$ and m''=m+m'.

We also evaluate the remaining surface integral containing the kinetic energy operator analogously by using a Rayleigh expansion of the interstitial representation of the LAPW wave functions. The Bloch factor of the wave functions can be separated after applying the kinetic energy operator. In this way, we obtain:

$$\psi_{i\mathbf{k}}^{*}(\mathbf{r})|_{\mathbf{r}\in\partial\mathrm{MT}(\alpha)} = e^{-i\mathbf{k}\cdot\mathbf{r}} \sum_{lm} \psi_{i\mathbf{k},lm}^{\alpha\mathrm{IR*}}(R_{\alpha}) Y_{lm}^{*}(\hat{\mathbf{R}}_{\alpha}) \tag{4.31}$$

$$:= e^{-i\mathbf{k}\cdot\mathbf{r}} \sum_{lm} \left[4\pi i^{l} \sum_{\mathbf{G}} \frac{z_{i\mathbf{k}\mathbf{G}}}{\sqrt{\Omega}} e^{i\mathbf{G}\cdot\boldsymbol{\tau}_{\alpha}} Y_{lm}^{*}(\hat{\mathbf{G}}) j_{l}(GR_{\alpha}) \right]^{*} Y_{lm}^{*}(\hat{\mathbf{R}}_{\alpha})$$

$$\left[\hat{T} - \epsilon_{i\mathbf{k}} \right] \psi_{i\mathbf{k}}(\mathbf{r})|_{\mathbf{r}\in\partial\mathrm{MT}(\alpha)} = e^{-i\mathbf{k}\cdot\mathbf{r}} \sum_{lm} \left\{ \left[\hat{T} - \epsilon_{i\mathbf{k}} \right] \psi_{i\mathbf{k}} \right\}_{lm}^{\alpha\mathrm{IR}} (R_{\alpha}) Y_{lm}(\hat{\mathbf{R}}_{\alpha}) \tag{4.32}$$

$$:= e^{-i\mathbf{k}\cdot\mathbf{r}} \sum_{lm} \left[4\pi i^{l} \sum_{\mathbf{G}} \frac{z_{i\mathbf{k}\mathbf{G}}}{\sqrt{\Omega}} \left(\frac{1}{2} |\mathbf{k} + \mathbf{G}|^{2} - \epsilon_{i\mathbf{k}} \right) e^{i\mathbf{G}\cdot\boldsymbol{\tau}_{\alpha}} Y_{lm}^{*}(\hat{\mathbf{G}}) j_{l}(GR_{\alpha}) \right] Y_{lm}(\hat{\mathbf{R}}_{\alpha})$$

Inserted into the last line of Eq. (4.9), the Bloch factors cancel and it is

$$\sum_{i\mathbf{k}}^{\text{val}} f_{i\mathbf{k}} \oint_{\partial \text{MT}(\alpha)} \psi_{i\mathbf{k}}^{\text{IR*}} \left[\hat{T} - \epsilon_{i\mathbf{k}} \right] \psi_{i\mathbf{k}}^{\text{IR}} \hat{\mathbf{e}} dS = R_{\alpha}^{2} \sum_{i=1}^{3} \hat{\mathbf{e}}_{i} \sum_{m=-1}^{1} c_{i,m}^{*} \sum_{l'm'} \sum_{l'm'} G_{l'',l',1}^{m'',m',m}$$

$$\times \sum_{i\mathbf{k}}^{\text{val}} f_{i\mathbf{k}} \psi_{i\mathbf{k},l'm'}^{\alpha \text{IR*}} (R_{\alpha}) \left\{ \left[\hat{T} - \epsilon_{i\mathbf{k}} \right] \psi_{i\mathbf{k}} \right\}_{l''m''}^{\alpha \text{IR}} (R_{\alpha}). \tag{4.33}$$

In comparison to Yu et al., our approach differs in a) the existence of the first line of the surface force term Eq. (4.9), which is attributed to the discontinuity of charge density and potential terms, and b) a different treatment of the second line. Yu et al. evaluate it by applying the Laplacian to the interstitial representation of the wave functions first to obtain the factors $|\mathbf{k} + \mathbf{G}|^2/2 - \epsilon_{i\mathbf{k}}$ but then compute the surface integral using the muffintin representation of the basis functions. In light of the discontinuity of the LAPW basis functions at the muffin-tin sphere boundary, this introduces an error to the total force. The continuity between radial and plane-wave representation at $\partial \mathrm{MT}(\alpha)$ is only valid for the l-channels up to $l_{\mathrm{max}}^{\alpha}$, so especially when low angular-momentum cutoff parameters are employed, this difference might be crucial.

4.4. Hellmann-Feynman force

We have found the Hellmann-Feynman force to be the negative gradient of the Coulomb potential generated by all charges except the positively charged nucleus α evaluated at its position τ_{α} :

$$\boldsymbol{F}_{\alpha}^{\mathrm{HF}} = -Z_{\alpha} \left[\sum_{\beta \neq \alpha} \frac{d}{d\boldsymbol{\tau}_{\alpha}} \frac{Z_{\beta}}{|\boldsymbol{\tau}_{\alpha} - \boldsymbol{\tau}_{\beta}|} - \int \frac{d}{d\boldsymbol{\tau}_{\alpha}} \frac{\rho(\boldsymbol{r}')}{|\boldsymbol{\tau}_{\alpha} - \boldsymbol{r}'|} d^{3} r' \right]$$
(4.5 revisited)

Since we have to evaluate the gradient of the Coulomb potential at the position τ_{α} of atom α , we employ Eq. (3.63) of the Weinert approach to obtain the Coulomb potential in $MT(\alpha)$. Together with the gradient, we have to compute

$$F_{\alpha}^{\mathrm{HF}} = Z_{\alpha} \lim_{r \to \tau_{\alpha}} \nabla \int \frac{\rho(r') - \sum_{\beta \neq \alpha} Z_{\beta} \delta(r' - \tau_{\beta})}{|r - r'|} d^{3}r'$$

$$= Z_{\alpha} \lim_{r \to \tau_{\alpha}} \nabla \sum_{lm} Y_{lm}(\hat{r}_{\alpha}) \left\{ \frac{4\pi}{2l+1} \int_{0}^{R_{\alpha}} s_{\alpha}^{2} \rho_{lm}^{\alpha}(s_{\alpha}) \frac{r_{<}^{l}}{r_{>}^{l+1}} \left[1 - \left(\frac{r_{>}}{R_{\alpha}} \right)^{2l+1} \right] ds_{\alpha} + \left(\frac{r_{\alpha}}{R_{\alpha}} \right)^{l} V_{\mathrm{C},lm}^{\alpha}(R_{\alpha}) + \sqrt{4\pi} \frac{Z_{\alpha}}{R_{\alpha}} \delta_{l0} \right\}. \quad (4.34)$$

We know already the value of the Coulomb potential at the muffin-tin sphere boundary expressed in spherical coordinates in the first few l-channels from the determination of the total energy, so we directly inserted $V_{C,lm}^{\alpha}(R_{\alpha})$. The last term excludes the potential generated by the nucleus, but is a constant to the gradient and thus does not contribute to the force. The radial integral has to be split into the ranges from 0 to r_{α} and from r_{α} to R_{α} . However, the former integral does not contribute. The gradient generates terms from application to the integrand as well as from application to the upper border of the integral, which is a onedimensional analogon to Eq. (4.3). For the integrand, application of the gradient reduces the order of r_{α} by one, leading to fractions $(s_{\alpha}/r_{\alpha})^{l+2}$. Since s_{α} is smaller than r_{α} , the integrand is bounded and letting $\mathbf{r}_{\alpha} \to \mathbf{0}$ reduces its contribution to zero. On the other hand, the application of the gradient to the upper border of the integral is canceled by the application of the gradient to the lower border of the integral from r_{α} to R_{α} . Therefore, only the application of the gradient to the integrand of the second integral has to be considered. It yields

$$\boldsymbol{F}_{\alpha}^{\mathrm{HF}} = Z_{\alpha} \sum_{lm} \left\{ \frac{4\pi}{2l+1} \int_{0}^{R_{\alpha}} s_{\alpha}^{1-l} \rho_{lm}^{\alpha}(s_{\alpha}) \left[1 - \left(\frac{s_{\alpha}}{R_{\alpha}} \right)^{2l+1} \right] ds_{\alpha} + \frac{V_{\mathrm{C},lm}^{\alpha}(R_{\alpha})}{R_{\alpha}^{l}} \right\} \times \lim_{\boldsymbol{r}_{\alpha} \to \mathbf{0}} \nabla \left[r_{\alpha}^{l} Y_{lm}(\hat{\boldsymbol{r}}_{\alpha}) \right]. \tag{4.35}$$

Using the formula for applying the gradient in natural coordinates, Eq. (4.17), on the last line suggests that for every l except l=1 the result is zero: For l=0, a constant is differentiated and for $l \geq 2$, the remaining term is of order ≥ 1 and thus vanishes in the limit $r_{\alpha} \to 0$. Expressing the Hellmann-Feynman force in terms of the coordinates of Eq. (4.17) and transforming them back to Cartesian coordinates by the transformation matrix \underline{T} of Eq. (4.18) yields

$$\mathbf{F}_{\alpha}^{\text{HF}} = Z_{\alpha} \sum_{m=-1}^{1} \frac{(-1)^{m}}{\sqrt{12\pi}} \underline{\mathbf{T}} \hat{\mathbf{e}}_{m} \left\{ \frac{4\pi}{3} \int_{0}^{R_{\alpha}} \rho_{1m}^{\alpha}(s_{\alpha}) \left[1 - \left(\frac{s_{\alpha}}{R_{\alpha}} \right)^{3} \right] ds_{\alpha} + \frac{V_{C,1m}^{\alpha}(R_{\alpha})}{R_{\alpha}} \right\}$$
(4.36)

in agreement to what Yu et al. present in their Eq. (A3).

4.5. Summary of differences to Yu, Singh, and Krakauer

We want to prepare a common ground for the following discussion of the upcoming computational results. To summarize our derivation of the atomic force, we introduce the following four levels with which we address our deviations from Yu et al. [54], where at each level the change made to the previous level is described:

- Level 0 is the force formula as given by Yu and coworkers.
- Level 1 includes the tails of core states leaking out of their muffin-tin sphere into the force calculation as presented in Eq. (4.22).
- Level 2 describes the evaluation of the surface contribution to the force containing the kinetic energy operator given in the last line of Eq. (4.9 revisited) in terms of the interstitial basis functions.
- Level 3 finally adds the remaining surface contributions of Eq. (4.9 revisited) to the force formula, which explicitly account for the discontinuity of the charge density, the potential and the exchange-correlation energy density at the muffin-tin sphere boundary.

4.6. Forces using DFT+U

Apart from the changes we distinguish by the different Levels, additional terms have to be included when the DFT+U approach is employed. As we already pointed out in chapter 2.4.1, the inclusion of Hubbard parameters U in the electronic structure calculation yields an additional contribution

$$E_{\rm U}[\rho] = \sum_{\alpha} \left[\frac{U_l^{\alpha}}{2} \sum_{m \neq m'} n_{mm}^{\alpha l} n_{m'm'}^{\alpha l} - \frac{U_l^{\alpha}}{2} n^{\alpha l} (n^{\alpha l} - 1) \right]$$
(4.37)

to the total energy with the occupation numbers of the localized orbitals φ_{lm}^{α} defined by

$$n_{mm'}^{\alpha l} = \sum_{i\mathbf{k}} f_{i\mathbf{k}} \langle \psi_{i\mathbf{k}} | \varphi_{lm'}^{\alpha} \rangle \langle \varphi_{lm}^{\alpha} | \psi_{i\mathbf{k}} \rangle,$$
 (2.18 revisited)

$$n^{\alpha l} = \sum_{m} n_{mm}^{\alpha l}. \tag{2.19 revisited}$$

Also, the Hubbard interaction occurs in the terms replacing the kinetic energy, namely

$$\epsilon_{i\mathbf{k}} = \frac{\left\langle \psi_{i\mathbf{k}} \middle| -\frac{1}{2} \nabla^2 + V_{\text{eff}} + V_{\text{U}} \middle| \psi_{i\mathbf{k}} \right\rangle}{\left\langle \psi_{i\mathbf{k}} \middle| \psi_{i\mathbf{k}} \right\rangle} \tag{4.38}$$

and

$$\sum_{i\mathbf{k}} f_{i\mathbf{k}} \left\langle \psi_{i\mathbf{k}} \middle| -\frac{1}{2} \nabla^2 \middle| \psi_{i\mathbf{k}} \right\rangle = \sum_{i\mathbf{k}} f_{i\mathbf{k}} \left(\epsilon_{i\mathbf{k}} - \langle \psi_{i\mathbf{k}} | V_{\text{eff}} + V_{\text{U}} | \psi_{i\mathbf{k}} \rangle \right) \tag{4.39}$$

with the additional potential

$$V_{\rm U} = \sum_{\alpha} U_l^{\alpha} \left[\frac{1}{2} - n_{mm}^{\alpha l} \right] |\varphi_{lm}^{\alpha}\rangle \langle \varphi_{lm}^{\alpha}|. \tag{2.21 revisited}$$

In the FLAPW method, the projector onto the localized orbitals $\varphi_{lm}^{\alpha}(r)$ is chosen such that it radially integrates the projected angular and magnetic momentum selection:

$$\langle \psi_{i\mathbf{k}} | \varphi_{lm'}^{\alpha} \rangle \langle \varphi_{lm}^{\alpha} | \psi_{i\mathbf{k}} \rangle$$

$$= \int_{0}^{R_{\alpha}} r_{\alpha}^{2} \oint \psi_{i\mathbf{k}}^{*}(\mathbf{r}_{\alpha} + \boldsymbol{\tau}_{\alpha}) Y_{lm'}(\hat{\mathbf{r}}_{\alpha}) dS \oint Y_{lm}^{*}(\hat{\mathbf{r}}_{\alpha}) \psi_{i\mathbf{k}}(\mathbf{r}_{\alpha} + \boldsymbol{\tau}_{\alpha}) dS dr_{\alpha}$$
(4.40)

Tran et al. [122] derived the changes to the FLAPW force formula induced by the use of DFT+U by applying the gradient with respect to the atomic position to all additional terms and collecting the results. In this way, he arrived at the additional contribution

$$\boldsymbol{F}_{\alpha}^{\mathrm{U}} = 2\sum_{i\boldsymbol{k}} f_{i\boldsymbol{k}} \mathrm{Im} \left\{ \sum_{mm'} v_{mm'}^{\alpha l} \left[\sum_{\lambda\lambda'} A_{lm\lambda}^{\alpha i\boldsymbol{k}*} \boldsymbol{A}_{lm'\lambda'}^{\alpha i\boldsymbol{k}} \int_{0}^{R_{\alpha}} r_{\alpha}^{2} u_{l\lambda}^{\alpha}(r_{\alpha}) u_{l\lambda'}^{\alpha}(r_{\alpha}) dr_{\alpha} \right] \right\}. \tag{4.41}$$

The A and A coefficients are the G-sums over the expansion coefficients z_{ikG} and the matching coefficients $a_{lm\lambda}^{\alpha kG}$ of the LAPW basis functions defined in Eqs. (3.23) and (4.14) and $v_{mm'}^{cl}$ is the variation of the additional DFT+U energy term with respect to the orbital occupation number,

$$v_{mm'}^{\alpha l} = \frac{\delta E_{\rm U}[\rho]}{\delta n_{\alpha m'}^{\alpha l}}.$$
(4.42)

The term F^0_{α} has to be added only to the force acting on the atom where the Hubbard parameter U is applied to.

4.7. Computational results

Next, we analyze the precision of the atomic force at the different force Levels summarized in section 4.5 for a set of prototype systems of varying complexity. The systems considered are metallic Al, ionically-bound MgO, covalently-bound GaAs, and the perovskite EuTiO₃. Additionally, we provide results for the strongly correlated material VO₂ with and without Hubbard-U. In any case, the comparison will be with respect to Level 0, the original force formalism of Yu et al. [54]. In detail, we present data on the force calculated analytically by the force formalism(s) versus the numerical differentiation of the total energy with respect to a displacement of an atom. We show the influence of the force Levels on the drift force and provide computation times to estimate the additional workload of using the different Levels.

Table 4.1 summarizes the default settings of each calculation. These parameters are used if not stated otherwise.

Aluminum forms a face-centered cubic (fcc) lattice with a single atom per unit cell. Since a displacement of this atom would correspond to a translation of the whole aluminum lattice and would therefore not yield any forces, we provide two different setups for this material: In the first setup, denoted by $Al_{\rm I}$, we construct the Al unit cell from a simple-cubic (sc) Bravais lattice by explicitly placing four atoms in the sc unit cell, one at the origin and one each at the face-centers. In the second setup, labeled as $Al_{\rm II}$, we stick to the fcc description of the lattice, but repeat the unit cell once in each direction. Thus, we consider eight atoms in the setup instead of one. In both calculations, the $Al\ 1s,\ 2s,\ and\ 2p$ states are treated as core states.

Magnesium oxide crystallizes in rocksalt structure, i.e., in a fcc Bravais lattice, with one atom at the origin and the other atom in the center of the unit cell. Again, we discuss two sets of calculation differing in the treatment of the 2s and 2p Mg semicore states. In one set, in addition to the Mg 1s state, the Mg 2s and 2p states are considered to be core states, while in the other set, the 2s and 2p states are treated in the valence window by using local orbitals. In both calculations, the 1s states of oxygen are set up as core states.

Gallium arsenide is of zinc-blende structure. In an fcc lattice, one atom is placed at the origin, while the other one resides one quarter along the volume diagonal of the cubic unit cell. For both atoms, the core states comprise of the [Ar] states. For As, also the 3d states are described in the core window.

The perovskite europium titanate exhibits a sc lattice structure, where the Eu atom is located at the origin, the three O atoms are at the face-centers of the unit cell and the Ti atom sits in the center of the unit cell. The core states of Eu are given by [Kr]4d, the core states of O by 1s. Also the [Ne]3s states of Ti are treated as core states.

Vanadium dioxide is set up in a simple-monoclinic unit cell, the distorted rutile configuration, within which in total four V atoms and eight O atoms are placed. Since the setup of this system is more involved, we refer to Appendix A.3 for an input file for the input-file generator of FLEUR. The core states are the V [Ne]3s states and the O 1s state. For the DFT+U calculation, a value of $U=4.0~{\rm eV}$ is chosen in accordance to Ref. [123] for the 3d states.

System		Al_{I}	$\mathrm{Al}_{\mathrm{II}}$	MgO
a_0	=	$7.656 \ a_{\rm B}$	$15.311 \ a_{\rm B}$	$7.970 \ a_{\rm B}$
R_1	=	$2.50 \ a_{\rm B}$	$2.50 \ a_{\rm B}$	$2.35 \ a_{\rm B}$
R_2	=	-	-	$1.33 \ a_{\rm B}$
G_{\max}	=	$4.0 \ a_{\rm B}^{-1}$	$4.0 \ a_{\rm B}^{-1}$	$5.5 \ a_{ m B}^{-1}$
$G_{ m max}^{ m dop}$	=	$24.01 \stackrel{\text{B}}{a_{\text{B}}^{-1}}$	$24.01 \stackrel{\mathrm{B}}{a_{\mathrm{B}}^{-1}}$	$22.01 \ a_{\rm B}^{-1}$
$l_{ m max}$	=	12	12	14
Δau	=	$0.07656 \ a_{\rm B}$	$0.05413 \ a_{\rm B}$	$0.19925 \ a_{\rm B}$
Direction		[100]	[011]	[100]
System		GaAs	$EuTiO_3$	VO_2
a_0	=	$10.681 \ a_{\rm B}$	$7.370 \ a_{\rm B}$	see Appendix A.3
R_1	=	$1.99 \ a_{\rm B}$	$2.60 \ a_{\rm B}$	$1.90 \ a_{\rm B}$
R_2	=	$1.99 \ a_{\rm B}$	$2.21 \ a_{\rm B}$	$1.10 \ a_{\rm B}$
R_3	=	-	$1.41 \ a_{\rm B}$	-
G_{max}	=	$4.2 \ a_{\rm B}^{-1}$	$4.8 \ a_{\rm B}^{-1}$	$5.5 \ a_{ m B}^{-1}$
$G_{ m max}^{ m dop}$	=	$12.61 \stackrel{\mathrm{B}}{a_{\mathrm{B}}^{-1}}$	$28.81 \ a_{\rm B}^{-1}$	$15.3 \ a_{\rm B}^{-1}$
$l_{ m max}$	=	12	12	12
Δau	=	$0.42723 \ a_{\rm B}$	$0.02244~a_{ m B}$	$0.05353 \ a_{\rm B}$
Direction		[100]	[100]	[100]

Table 4.1.: Default setup parameters for the different systems considered. The numbering of the muffin-tin radii is according to their appearance in the structure formula. $E.g.~\mathrm{VO_2}$ has $R_1 = R_\mathrm{V},~R_2 = R_\mathrm{O}$.

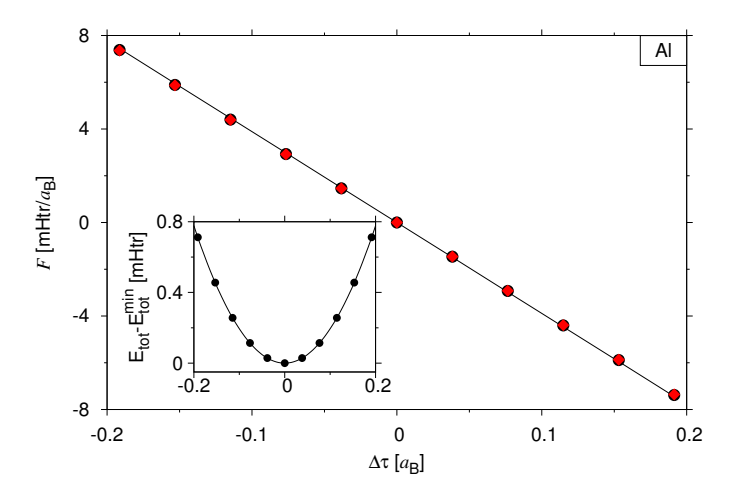
4.7.1. Analytic vs. numerical force

Instead of using the (refined) force formalism, atomic forces can also be calculated by a numerical evaluation of Eq. (4.1), i.e., as the change in energy with respect to a small displacement of atom α . Hence, we displaced for each system the atom located at the origin within a set of different amplitudes, applied a quadratic fit to the resulting energy vs. displacement data, and calculated the force as the derivative of the curve. The forces computed by application of the different force Levels are compared to the derivative of the fit in part (a) of Figs. 4.2, 4.3, 4.4, 4.5, and 4.6 for the five different systems Al_{I/II} to EuTiO₃. The black lines correspond to the derivative of the fits, the black dots to Level 0 of the force formalism. The red diamonds represent the force values calculated using Level 3. On the scale of the graphs, Level 1 and Level 2 can not be resolved from Level 3 and are consequently omitted in the graphs. The insets show the respective energy vs. displacement data and the quadratic fits.

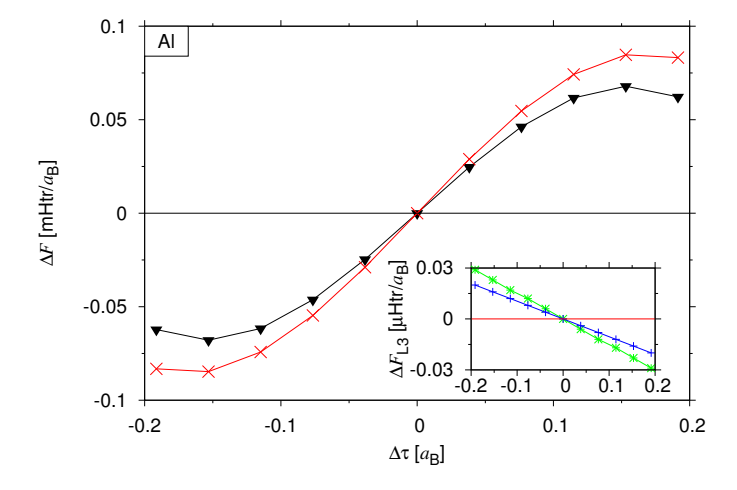
On the scale of the graphs, we notice in general a good agreement of the different force Levels to the numerically computed force at small displacements. For very large displacements as for example in the case of GaAs in Fig. 4.5, the agreement becomes worse, since the harmonic regime is left. In order to analyze the agreement between the force Levels and the fitted curve in more detail, the difference of the Levels to the fitted curve is shown in part (b) of Figs. 4.2, 4.3, 4.4, 4.5, and 4.6. The symbols assigned to the different Levels are black triangles for Level 0, green asterisks for Level 1, blue pluses for Level 2, and red crosses for Level 3. The insets show specifically the difference of the force Levels to Level 3.

For almost all systems, Level 0 agrees slightly better with the numerically calculated force than Level 3 for small displacements. The difference between these Levels is of the order of magnitude of less than 0.1 mHtr/a_B for the largest displacement of each system other than GaAs, though. For GaAs, depicted in Fig. 4.5, the difference is of the order of magnitude of 1 mHtr/a_R, and Level 0 is closer to the numerical force than Level 3 only for large displacements, while Level 3 is in better agreement for small displacements. In addition, in the case of GaAs and MgO presented in Figs. 4.5(b) and 4.4(b), also the force on the second atom is depicted. In these diatomic setups, Newton's third law and the acoustic sum rule, Eq. (4.2), identically imply that the force values of one atom have to be the negative of the force values of the other atom. We realize that this condition is not fulfilled if the analytical forces are produced from Level 0. Instead, at least Level 1 is needed to establish forces on the As or Mg atom to be consistent with the forces on the Ga or O atom, respectively. This can be concluded from the insets which indicate a deviation of Level 1 and Level 2 from Level 3 in the 10 μ Htr/ a_B -regime in the case of the Mg atom, but usually in the 1 μ Htr/ a_B -regime or below. Also, Level 1 mainly affects the force on As and Mg, since these two atoms lose the most core electrons from the MT sphere in their respective setup.

In conclusion, we consider the good agreement of Level 0 with the numerically calculated force to be fortuitous, while applying the different Levels of our refined force formalism enables a consistent description of the atomic force.

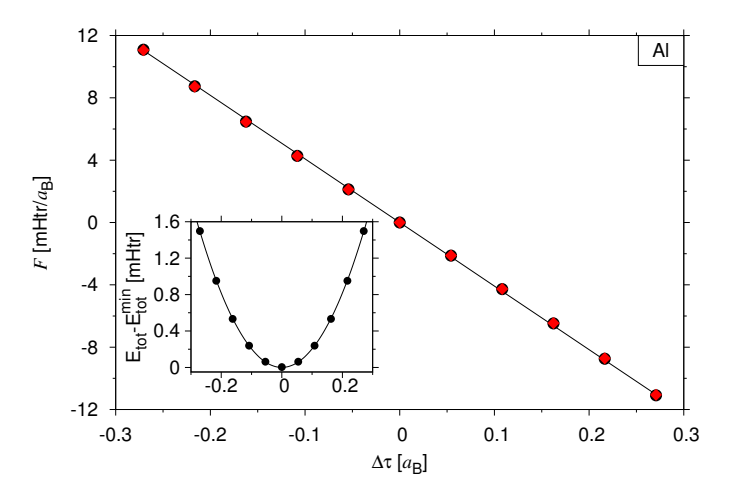


(a) Force on the displaced Al atom. Black dots denote Level 0, red diamonds denote Level 3. The black line corresponds to the derivative of the quadratic energy fit in the inset.

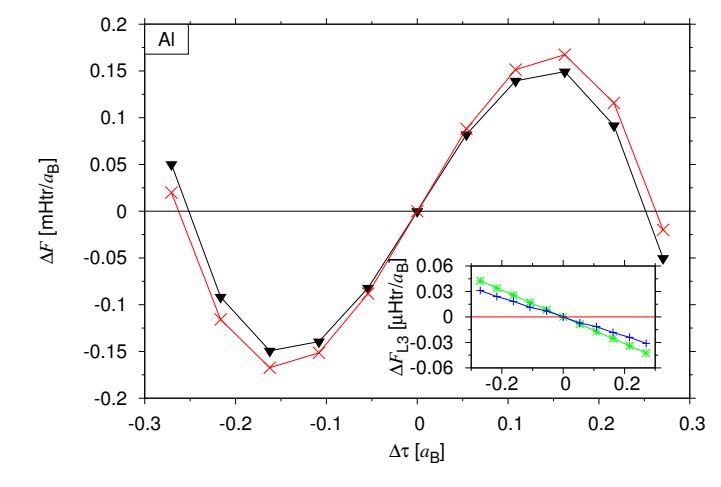


(b) Residual forces with respect to the energy fit (figure) or to Level 3 (inset). Black triangles denote Level 0, green asterisks denote Level 1, blue pluses denote Level 2, and red crosses denote Level 3.

Figure 4.2.: Numerical vs. analytical force for ${\rm Al_I}$.

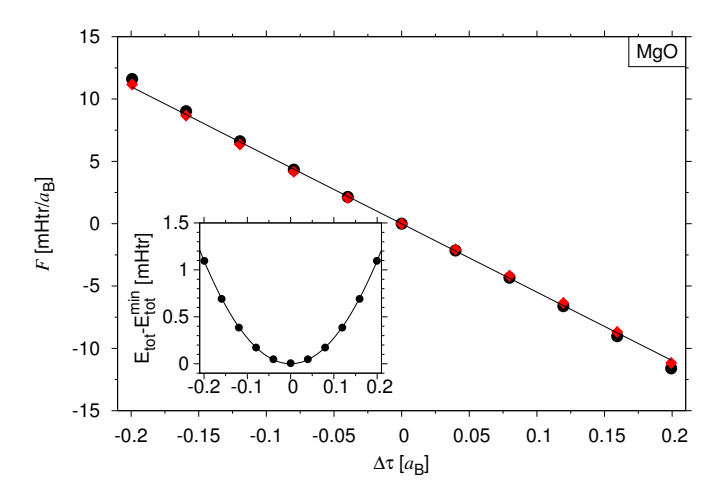


(a) Force on the displaced Al atom. Black dots denote Level 0, red diamonds denote Level 3. The black line corresponds to the derivative of the quadratic energy fit in the inset.

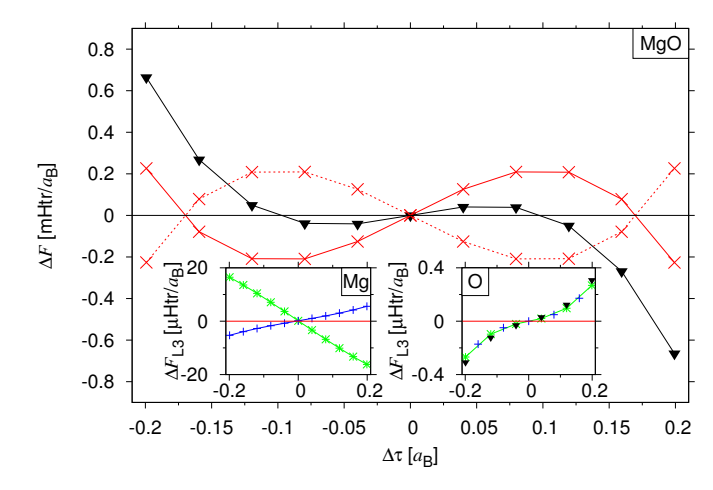


(b) Residual forces with respect to the energy fit (figure) or to Level 3 (inset). Black triangles denote Level 0, green asterisks denote Level 1, blue pluses denote Level 2, and red crosses denote Level 3.

Figure 4.3.: Numerical vs. analytical force for $\mathrm{Al}_{\mathrm{II}}.$

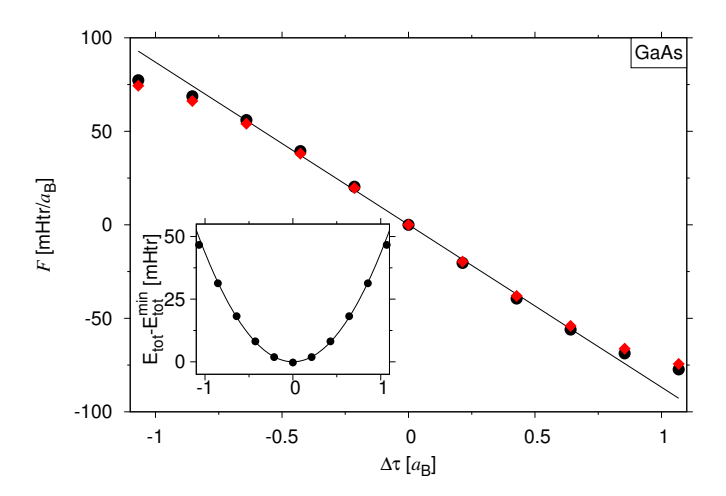


(a) Force on the displaced Mg atom. Black dots denote Level 0, red diamonds denote Level 3. The black line corresponds to the derivative of the quadratic energy fit in the inset.

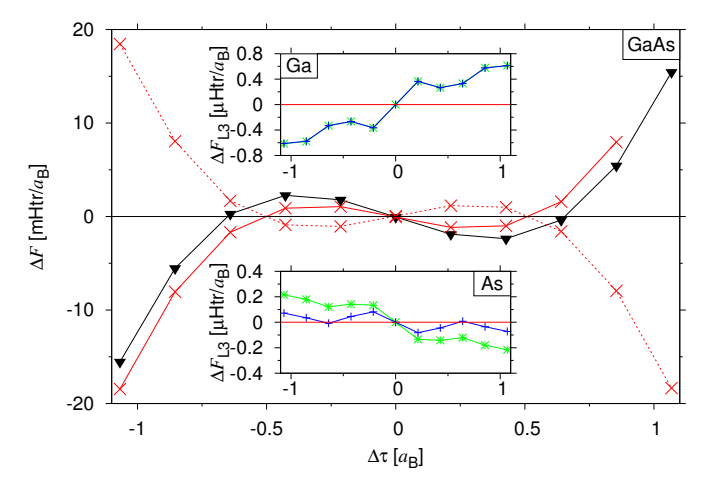


(b) Residual forces on Mg with respect to the energy fit (figure) or to Level 3 (left inset). Black triangles denote Level 0, green asterisks denote Level 1, blue pluses denote Level 2, and red crosses denote Level 3. Dashed lines in the figure and in the right inset denote the corresponding force Level applied to the O atom.

Figure 4.4.: Numerical vs. analytical force for MgO.

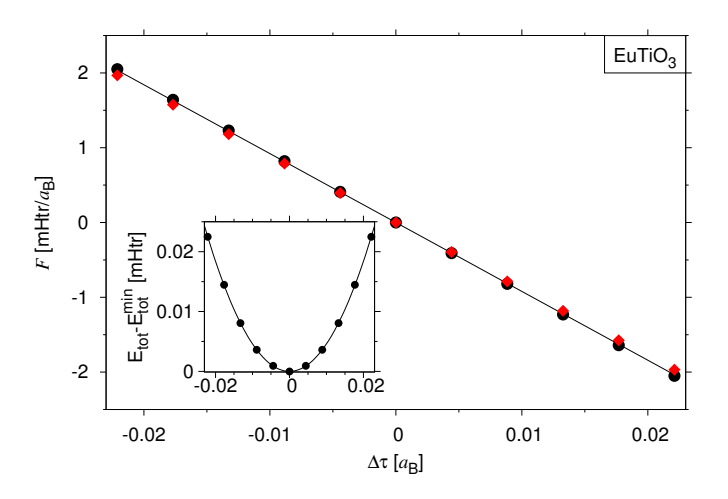


(a) Force on the displaced As atom. Black dots denote Level 0, red diamonds denote Level 3. The black line corresponds to the derivative of the quadratic energy fit in the inset.

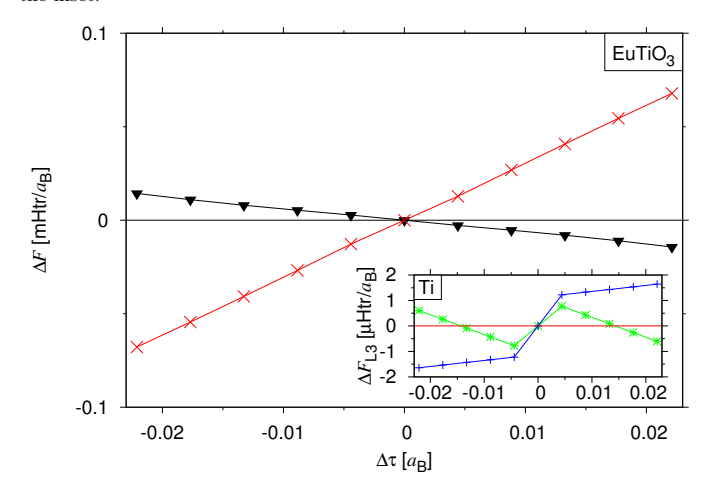


(b) Residual forces on As with respect to the energy fit (figure) or to LEVEL 3 (lower inset). Black triangles denote LEVEL 0, green asterisks denote LEVEL 1, blue pluses denote LEVEL 2, and red crosses denote LEVEL 3. Dashed lines in the figure and in the upper inset denote the corresponding force LEVEL applied to the Ga atom.

Figure 4.5.: Numerical vs. analytical force for GaAs. Due to the large displacement, the quadratic fit is applied only to the seven inner point.



(a) Force on the displaced Ti atom. Black dots denote Level 0, red diamonds denote Level 3. The black line corresponds to the derivative of the quadratic energy fit in the inset.



(b) Residual forces on Ti with respect to the energy fit (figure) or to Level 3 (inset). Black triangles denote Level 0, green asterisks denote Level 1, blue pluses denote Level 2, and red crosses denote Level 3.

Figure 4.6.: Numerical vs. analytical force for ${\rm EuTiO_3}$.

4.7.2. Drift force

As we pointed out at the beginning of this chapter, the total energy of a periodic system is invariant under a translation of the whole system by an arbitrary vector T, *i.e.*, $E[\{\tau_{\alpha}\}] = E[\{\tau_{\alpha} + T\}]$. This prescription implies the acoustic sum rule, which states that the sum of all forces on all atoms of the system has to vanish. If the acoustic sum rule is broken, the spuriously remaining force corresponds to an unphysical energy gain by an arbitrary translation of the whole lattice. In practical calculations, we found such a spuriously remaining force, which we introduced as the drift force in Eq. (4.2).

In this section, we study the effect of the different Levels of our force formalism on the drift force, as well as the dependence of the drift force on the angular momentum cutoff used in the muffin-tin spheres.

We start by demonstrating the influence of the force Levels on the drift force at a particular l_{max} -cutoff in tables 4.2, 4.3, 4.4, 4.5, and 4.6.

(a)	Al_{I}								
Force on	Level 0	Level 1	Level 2	Level 3					
$\overline{\mathrm{Al}_{000}}$	-2.9299	-2.9215	-2.9215	-2.9215					
$Al_{0\frac{1}{2}\frac{1}{2}}$	-0.3654	-0.3643	-0.3643	-0.3642					
$Al_{\frac{1}{2}0\frac{1}{2}}$	1.6476	1.6429	1.6429	1.6429					
$Al_{\frac{1}{2}\frac{1}{2}0}^{\frac{1}{2}}$	1.6476	1.6429	1.6429	1.6429					
Drift	0.0000	0.0000	0.0000	0.0000					

(b)			A	l_{II}		
		Level 0			Level 3	
Force on	F_x	F_y	F_z	F_x	F_y	F_z
Al_{000}	0.0000	-1.5031	-1.5031	0.0000	-1.4989	-1.4989
Al_{011}	0.0000	0.8892	0.8892	0.0000	0.8865	0.8865
Al_{101}	0.4841	-0.1009	0.4027	0.4826	-0.1007	0.4015
Al_{112}	-0.4841	0.4027	-0.1009	-0.4826	0.4015	-0.1007
Al_{110}	0.4841	0.4027	-0.1009	0.4826	0.4015	-0.1007
Al_{121}	-0.4841	-0.1009	0.4027	-0.4826	-0.1007	0.4015
Al_{211}	0.0000	-0.0407	-0.0407	0.0000	-0.0404	-0.0404
Al_{222}	0.0000	0.0511	0.0511	0.0000	0.0510	0.0510
Drift	0.0000	0.0000	0.0000	0.0000	0.0000	0.0000

Table 4.2.: Forces (in $m{\rm Htr}/a_{\rm B}$) in Al at the different Levels of implementation. (a) Setup Al_I: A single fcc unit cell reconstructed in a sc unit cell. (b) Setup Al_{II}: A $2\times2\times2$ grid of fcc unit cells. Only Levels 0 and 3 are shown, since the differences between Level 3 and Levels 1 and 2 are negligible, as suggested by the data in part (a). The angular-momentum cutoff is chosen as $l_{\rm max}=10$ in both cases. The forces presented here are rounded to a precision of $0.1~\mu{\rm Htr}/a_{\rm B}$. Therefore, the data does not add up exactly to a drift force of zero.

For aluminum in both setups, table 4.2 shows that the drift forces are already converged to zero with a precision of $0.1~\mu Htr/a_B$ at Level 0. The application of the higher Levels does not destroy the precision of the drift force. For the Al_{II} setup we present results only for Level 0 and Level 3, since Level 1 and Level 2 do not contain any new information.

Magnesium oxide, presented in table 4.3, shows a stronger dependence on the different Levels of our refined force formalism. The largest drift force of $0.439~m{\rm Htr}/a_{\rm B}$ is realized when the Mg 2s and 2p states are treated as core states at Level 0 in part (a) of the table. Including the whole unit cell into the calculation of the core state contribution to the force at Level 1 or lifting the core states into the valence window by application of LOs to the 2s and 2p states of magnesium reduces the drift force by one order of magnitude to $0.017~m{\rm Htr}/a_{\rm B}$. It is reasonable that the application of Level 1 does not further improve the drift force in the LO calculation. In this setup, only the 1s states of Mg and O contribute to the force contribution stemming from the core electrons. These states are well localized within the muffin-tin sphere of their respective atom and thus the changes of Level 1 are negligible. By the same argument, the force acting on the Mg atom is subject to the biggest changes when the Mg 2s and 2p states are treated in the core, while the force acting on the O atom is affected only slightly. In both setups, the remaining Levels 2 and 3 further decrease the magnitude of the drift force by one order, each.

(a)	Mg core states: $[He]2s2p$							
Force on	Level 0	Level 1	Level 2	Level 3				
Mg	-11.6046	-11.1820	-11.1603	-11.1655				
O	11.1652	11.1652	11.1652	11.1649				
Drift	-0.4394	-0.0168	0.0049	-0.0006				
(b)		Mg core st	tates: [He]					
(b) Force on	Level 0	Mg core st	tates: [He]	Level 3				
	Level 0 -10.8027			Level 3 -10.7861				
Force on		Level 1	Level 2					

Table 4.3.: Forces (in $m{\rm Htr}/a_{\rm B}$) in MgO at the different Levels of implementation. (a) Mg 2s and 2p states are treated as core states. (b) Mg 2s and 2p states are treated using LOs. The angular-momentum cutoff is set to $l_{\rm max}=14$ for both atoms.

Force on	Level 0	Level 1	Level 2	Level 3
Ga	-38.2222	-38.0632	-38.0632	-38.0629
As	39.4411	38.0620	38.0619	38.0618
Drift	1.2189	-0.0012	-0.0013	-0.0011

Table 4.4.: Forces (in $m{\rm Htr}/a_{\rm B}$) in GaAs at the different Levels of implementation. The angular-momentum cutoff is set to $l_{\rm max}=12$ for both atoms.

In the case of gallium arsenide, the data presented in table 4.4 shows an increase in the precision of the drift forces by three orders of magnitude when Level 1 is applied from 1.219 $m{\rm Htr}/a_{\rm B}$ at Level 0 to 0.001 $m{\rm Htr}/a_{\rm B}$. The effect on the force acting on the As atom is strongest, since As loses most core electrons from its core, but also Ga is affected, since in contrast to the oxygen atom in MgO, it also loses core electrons. The higher Levels of our refined force formalism do not further increase the precision of the drift force.

Table 4.5 summarizes the data on EuTiO₃ for an angular momentum cutoff of $l_{\rm max}=10$ and $l_{\rm max}=12$. In both cases, the different force Levels affect mainly the force acting on the Ti atom. For the lower angular-momentum cutoff $l_{\rm max}=10$, the drift force steadily decreases by two orders of magnitude in total from 0.135 $m{\rm Htr}/a_{\rm B}$ to 0.004 $m{\rm Htr}/a_{\rm B}$ between Level 0 and Level 3. For the higher cutoff $l_{\rm max}=12$, the drift force decreases by two orders of magnitude between Levels 0 and 1 already, while the further Levels do not significantly add to the precision of the drift force anymore.

(a)		EuTiO ₃ wit	$h l_{\text{max}} = 10$	1
Force on	Level 0	Level 1	Level 2	Level 3
Eu	0.6215	0.6215	0.6213	0.6214
$O_{0\frac{1}{2}\frac{1}{2}}$	0.8866	0.8866	0.8866	0.8865
$O_{\frac{1}{2}0\frac{1}{2}/\frac{1}{2}\frac{1}{2}0}$	0.2335	0.2335	0.2335	0.2335
Ti	-2.1101	-2.0283	-1.9520	-1.9705
Drift	0.1350	-0.0532	0.0229	0.0044
(b)		EuTiO ₃ wit	$h l_{\text{max}} = 12$	}
(b) Force on	Level 0	EuTiO ₃ wit	$\frac{h \ l_{\text{max}} = 12}{\text{Level 2}}$	Level 3
Force on Eu	Level 0	Level 1	Level 2	Level 3
Force on	LEVEL 0 0.6213	LEVEL 1 0.6213	LEVEL 2 0.6213	LEVEL 3 0.6213
Force on Eu $O_{0\frac{1}{2}\frac{1}{2}}$	LEVEL 0 0.6213 0.8798	LEVEL 1 0.6213 0.8798	LEVEL 2 0.6213 0.8798	LEVEL 3 0.6213 0.8797

Table 4.5.: Forces (in $m{\rm Htr}/a_{\rm B}$) in EuTiO₃ at the different Levels of implementation. The titanium atom Ti has been displaced by 0.022 $a_{\rm B}$ in the [100] direction. The angular momentum cutoff $l_{\rm max}$ is set to 10 in (a) and 12 in (b).

Finally, table 4.6 contains the force data of vanadium dioxide for the different Levels of our force formalism without a Hubbard-U in part (a) and with a Hubbard-U of 4 eV in (b). Since the structure of VO₂ is more involved, displacing an atom along [100]-direction gives rise to forces in different directions, which is why we include also the force components along y and z direction acting on each atom. The largest drift force component of 0.601 mHtr/aB is the drift force in x direction at Level 0 when no Hubbard-U is applied. With the Hubbard-U, the drift force F_x is of comparable size with 0.584 mHtr/aB. In both cases, the x component of the drift force is subsequently decreased by three orders of magnitude when the additional force Levels are included into the calculation, reaching a precision of below μ Htr/aB. The drift force in z direction decreases from around 0.125 mHtr/aB to 0.006 mHtr/aB in both cases; including Level 1 already results in this order of precision for

the drift force F_z . The drift force F_y is already in this regime at Level 0 with and without introducing a Hubbard-U. We note that the effect of the force Levels is most prominent for the vanadium atoms, which is reasonable considering that the 1s states of oxygen are well confined within their respective MT spheres. The data contained in table 4.6 indicates that the Levels of our force formalism also improve the force in DFT+U calculations.

The drift forces presented so far have in common that they are reduced to the $\mu \mathrm{Htr}/a_\mathrm{B}$ -regime when the forces are calculated at Level 3. This indicates that $\mu \mathrm{Htr}/a_\mathrm{B}$ is the precision limit which we can achieve.

We continue our analysis of the drift force by presenting its convergence behavior with respect to the angular-momentum cutoff $l_{\rm max}$ in Figs. 4.7, 4.8, 4.10, 4.12 and 4.11 for the different materials. Since the angular-momentum cutoff directly determines the grade of discontinuity of the wave functions, the density, and the potential at the muffin-tin sphere boundary, we expect that the drift force at Levels 2 and 3 will be affected most by changing $l_{\rm max}$, since these two Levels explicitly account for the discontinuities mentioned above. In agreement to our previous notation used in section 4.7.1, black triangles correspond to Level 0, green asterisks to Level 1, blue pluses to Level 2, and red crosses to Level 3.

All figures have in common that at Level 0 the drift force converges with increasing $l_{\rm max}$ to a constant non-zero value, except for the two aluminum setups. At least Level 1 is required to reduce the drift force to less than 1 μ Htr/ $a_{\rm B}$ per atom. Applying both Level 2 and Level 3 in general increases the rate at which the drift force converges. For small $l_{\rm max}$, the application of only one of the last two Levels would result in deviations from the Level 1 curve which are not beneficial for a small drift force.

We proceed by analyzing the $l_{\rm max}$ convergence of the drift force for the individual systems in more detail.

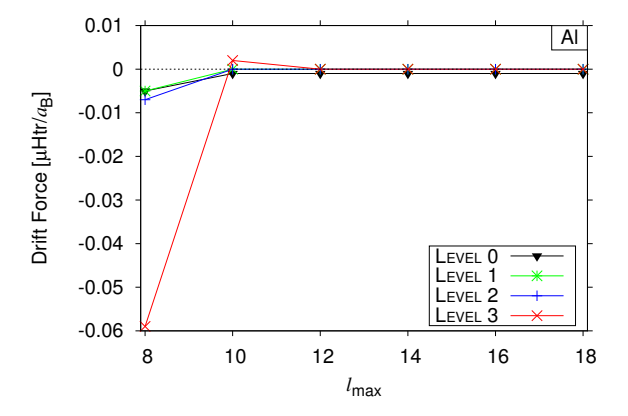


Figure 4.7.: l_{max} convergence of Al_I.

F_y F_z	12.1571 -3.9412 -6.3021	3 -10.2842 -2.5031	1 -4.7801 0.5263 -	5 5.6039 1.9545 11.8221	8.7118 -0.0281	-8.9228 -3.3393	-9.4338	6 9.0196 5.2390 -0.0178	-4.2935 1.2753 -	1.9631 2.1484	0 2.9882 -3.4590 4.8085		9 -0.0037 -0.0067 -0.0008	Level 2 Level 3	F_y	13.9927 -8.5007 -2.8521	-12.8075 -5.7139 -7.5001 $-$	-6.4689 3.8923	8.0524 5.2830	1.1142 9.6497	1.6734 6.2438 -	-0.0788 -1.7517 $-$	-1.4249 -4.3382	0.1537 4.0832 -	-2.2916 6.7844	-2.4401 -7.8610	5 2.7500 -7.7776 -6.2911	-0.0038	Table 4.6.: Forces (in $mHtr/a_{\rm B}$) in VO, at the different Levels of implementation. The atoms appear in the order specified in the	1. (b) DFT+U calculation with U
	-3.9583	-2.5231	0.5463	5.5755 1.9745 11.8185	8.7118 -0.0281 5.9344	-8.9228 -3.3393 -2.2525		9.0196 5.2390 -0.0176		2.1484	2.9882 -3.4590 4.8090	-2.7330 -4.1285 -4.7208	-0.0029 -0.0038 0.0019	LEVEL 1	F_y F_z F_x	-8.5179	-5.7340	3.9124 -	5.3030	-1.1142 9.6497 10.6896	6.2438	-1.7517	-4.3382	4.0832 -	6.7844	-7.8610	2.7500 -7.7776 -6.2915	-0.0031 -0.0039 0.0024	ent LEVELS of implementati	file presented in Appendix A.3. (a) Regular DFT calculation.
F_z	ľ		1.4452 $-$	2.8760 11.8311	-0.0226 5.9344	-3.3330 -2.2525	6.2424	5.2320 -0.0176	1.2760 -2.0599	2.1491	-3.4608 4.8090	-4.1305 -4.7208	0.1276 -0.0102		F_z F_x	ľ		1			6.2501		-4.3452	4.0840 -	6.7852	-7.8629	-7.7796 -6.2915		b) in VO, at the differe	d in Appendix A.3. (a
	31	12	- 69	V 12.0219 3.7118	5.9398 8.7101	O_{II} -2.2582 -8.9224	I	V = -0.0107 = 9.0187	O_V -2.0620 -4.2965		O_{VII} 4.8104 2.9900	O_{VIII} -4.7229 -2.7348	Drift -0.6010 0.0024	PEVEL 0	Force on F_x F_y	09	-7.6329 $-$	-18.0102 -	7 18.4314	10.6950		, 8	4.5671 -	00	_	1	-6.2937 2.7482	ift -0.5841 0.0056	de 4.6.: Forces (in $m{ m Htr}/a$	input file presente

For the Al_I setup, in which the fcc structure of aluminum is reconstructed with four atoms in a sc unit cell, the drift force at Level 0 converges already at $l_{\rm max}=10$ to a non-zero value as can be seen in Fig. 4.7, while Levels 1 and 2 remove the offset of the drift force. However, at Level 3 the drift force converges to zero only at $l_{\rm max}=12$ and shows a larger deviation at smaller $l_{\rm max}$. This larger deviation is only $0.06~\mu {\rm Htr}/a_{\rm B}$, though, and thus still within the precision we expect from our calculation. In the $Al_{\rm II}$ setup presented in Fig. 4.8 that describes a $2\times2\times2$ configuration of the regular fcc unit cell of aluminum, the drift force vanishes at any Level of our force formalism and for any angular-momentum cutoff.

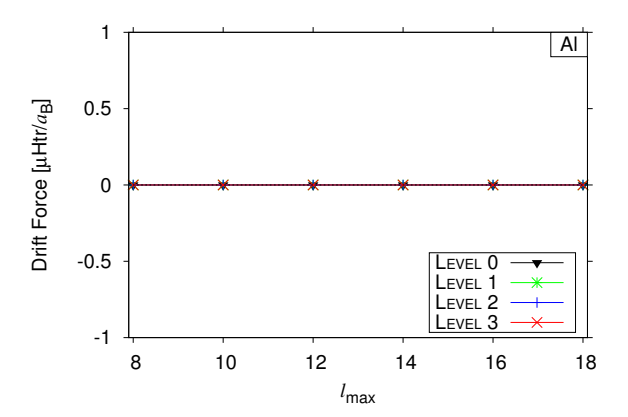


Figure 4.8.: l_{max} convergence of Al_{II}.

The data on MgO shown in Fig. 4.9 includes the drift force calculated with the Mg 2s and 2p states treated with LOs instead of within the core. The corresponding symbols are hollow black triangles (LEVEL 0), hollow blue squares (LEVEL 2), and hollow red diamonds (LEVEL 3). LEVEL 1 with local orbitals is omitted from the graph since this curve lies on top of the Level 0-LO curve and the Level 1 curve from the calculations where the 2sand 2p states of Mg are treated as core states. Apparently, the LO curves lie on top of the corresponding curves from the calculations without LOs from Level 1 onwards. This is surprising in so far as treating the 2s and 2p states of magnesium either by LOs or by LEVEL 1 results nearly in the same drift force. However, starting from the same drift force at LEVEL 1, one can expect that LEVEL 2 and LEVEL 3 have the same effect with or without LOs: The local orbitals vanish at the MT sphere boundary, so they do not alter the discontinuity of wave functions, density, and potential at the MT sphere boundary. Fig. 4.9 demonstrates that a thorough treatment of the leaking core states by either Level 1 or by LOs reduces the offset of the drift force significantly for large l_{max} . A converged drift force is realized at $l_{\text{max}} = 16$. Including both Level 2 and Level 3 accelerates the convergence of the drift force with respect to the angular-momentum cutoff and converged results are produced at $l_{\text{max}} = 12$.

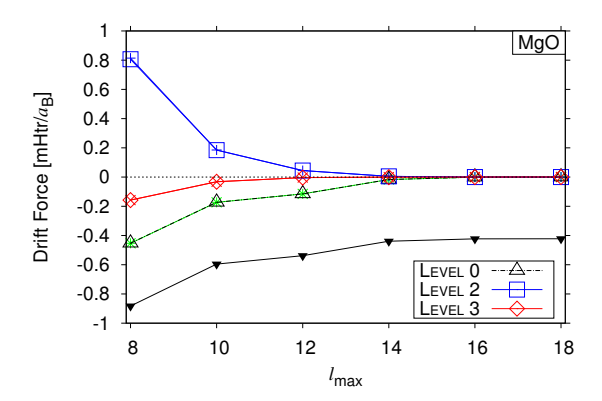


Figure 4.9.: $l_{\rm max}$ convergence of MgO. Labeled symbols: LO calculations. Unlabeled symbols: Mg 2s and 2p states are core states. They are designated as in Fig. 4.8.

In the case of GaAs, the black curve in Fig. 4.10 corresponding to Level 0 has been shifted downwards towards the x-axis by 1200 μ Htr/ $a_{\rm B}$ so that all Levels are visible on the same scale. At $l_{\rm max}=12$, all Levels are converged, but at least Level 1 is necessary for the limit to be in the μ Htr/ $a_{\rm B}$ -regime. Application of Level 2 allows to reduce the angular-momentum cutoff to 10 to achieve a converged drift force, while at Level 3, the drift force is already converged for $l_{\rm max}=8$.

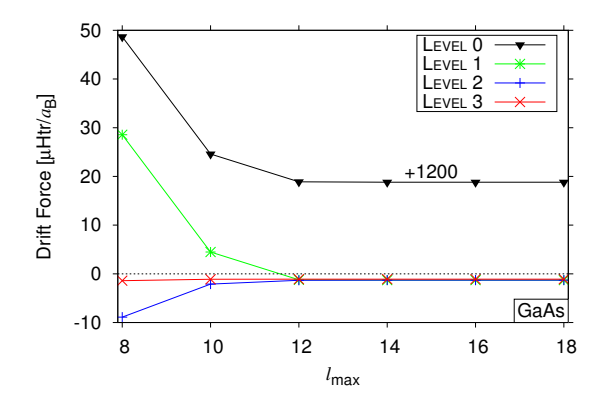


Figure 4.10.: l_{max} convergence of GaAs.

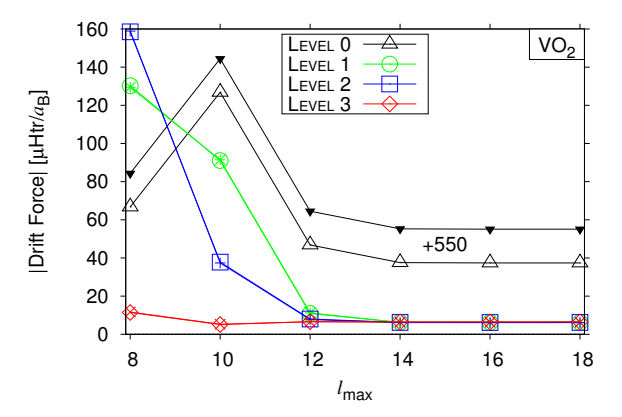
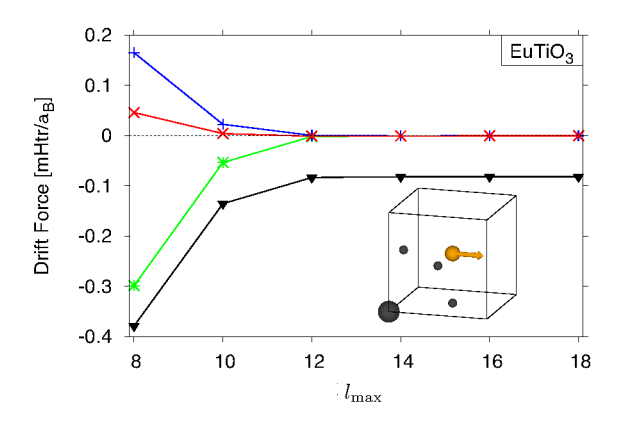


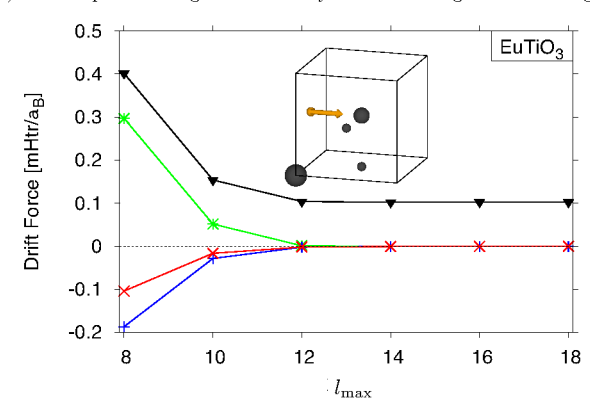
Figure 4.11.: $l_{\rm max}$ convergence of VO₂. Labeled symbols: DFT+U calculations. Unlabeled symbols: Regular LDA calculations. They are designated as in Fig. 4.8.

The convergence behavior of the drift force with respect to $l_{\rm max}$ in the strongly correlated system VO₂ is presented in Fig. 4.11. The figure includes the data obtained from calculations without a Hubbard-U with the regular symbols, as well as the results from calculations with a Hubbard-U of 4 eV. The symbols corresponding to the latter calculations are hollow black triangles (Level 0), hollow green circles (Level 1), hollow blue squares (Level 2), and hollow red diamonds (Level 3). The Level 0 curves have been shifted downwards towards the x-axis by 550 μ Htr/aB each, such that each Level is resolved on the scale of the graph. Convergence of the drift force is achieved at Level 0 and Level 1 at $l_{\rm max}=14$, where the latter Level does reduce the drift force to the regime of μ Htr/aB per atom. Applying Level 2 decreases the angular-momentum cutoff necessary for a converged calculation to 12, while the drift force at Level 3 can be considered to be converged even at $l_{\rm max}=10$.

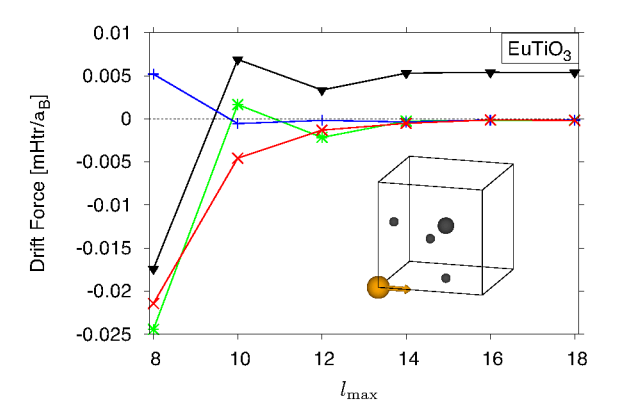
For EuTiO₃, four separate graphs in Fig. 4.12 depict the drift-force convergence depending on the atom displaced. Within the figures, a sketch of the EuTiO₃ unit cell indicates which atom is displaced in the respective set of calculations. All graphs have in common that Level 1 eliminates the offset of the drift force as compared to Level 0. Figs. 4.12(c) and (d), which correspond to the displacement of the europium atom or of an oxygen atom within the europium plane, show drift forces which are already in the μ Htr/a_B-regime. Since we established this regime as the numerical precision which we can achieve with our formalism, it is reasonable that the application of further Levels does not result in the clear ordering of the Levels which we encountered so far. On the other hand, the ordering is present in Figs. 4.12(a) and (b), where either the titanium atom is moved towards an oxygen atom, or an oxygen atom is moved out of the europium plane towards the titanium atom. There, the angular-momentum cutoff necessary for a converged calculation is reduced from $l_{\text{max}} = 12$ at Levels 0 and 1 to $l_{\text{max}} = 10$ at Level 3.



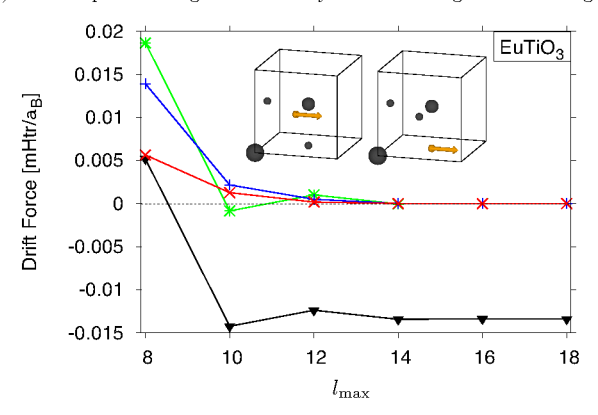
(a) Ti is displaced along the x axis. Symbols are designated as in Fig. 4.8.



(b) O is displaced towards Ti. Symbols are designated as in Fig. 4.8.



(c) Eu is displaced along the x axis. Symbols are designated as in Fig. 4.8.



(d) O is displaced within the Eu plane. Symbols are designated as in Fig. 4.8.

Figure 4.12.: l_{max} convergence of EuTiO₃.

4.7.3. Computation time

In this section, we comment on the computational overhead generated by applying the higher Levels of our force formalism. Since the calculation of the atomic forces is done after the electronic density is determined self-consistently, we compare in table 4.7 the time of a single force iteration, *i.e.*, an iteration with activated force calculations, to the averaged time of a self-consistency iteration without computing the atomic force. In fact, we average the latter over the number of self-consistency steps required to achieve self-consistency, whereas the time of a force iteration is averaged over two iterations. The time of the force calculation is measured for each of the different force Levels. We present the increase in computation time due to the different force Levels as a relative increase compared to a single self-consistency iteration. The percentages of the Levels are additive, *i.e.*, the computation time of each Level increases by the percentage given in the table plus the percentage of each of the previous Levels. Each system is set up according to the default settings presented in table 4.1.

System	Comp. time	Level 0	Level 1	Level 2	Level 3
Al_{I}	$61.7 \ s$	+6.0%	+51.3%	+1.3%	+4.1%
$\mathrm{Al}_{\mathrm{II}}$	$243.5 \ s$	+5.0%	+82.6%	+0.7%	+3.4%
MgO; [Ne] in core	$124.3 \ s$	+15.2%	+3.4%	-0.9%	+0.3%
MgO; [He] in core	$129.2 \ s$	+20.5%	+2.7%	+1.2%	+0.1%
Rel. increase	3.9%	8.8%	8.1%	9.8%	9.7%
GaAs	$68.0 \ s$	+15.9%	+4.3%	+1.8%	-0.1%
EuTiO ₃ ; 28.81 $a_{\rm B}^{-1}$	$825.7 \ s$	+11.2%	+16.7%	+5.8%	+1.4%
EuTiO ₃ ; 19.21 $a_{\rm B}^{-1}$	$746.0 \ s$	+12.8%	+5.3%	+6.5%	+0.8%
VO_2	$6923.8 \ s$	+10.1%	+2.5%	+3.5%	+0.8%
VO_2 ; DFT+U	$7023.7 \ s$	+7.3%	+5.0%	+3.3%	-1.0%

Table 4.7.: Computational overhead for computing the atomic force at the different force Levels for all setups. The percentages are given with respect to the average time of a single step of the self-consistency cycle listed in the column titled 'Comp. time'. The calculations were performed on a single Intel Xeon CPU X5670 @ 2.93 Ghz.

From our refinements, in general Level 1 is the most expensive one, whereas Level 2 and Level 3 in total are about as expensive as Level 1, at most, while usually contributing less to the computation time.

For both Al setups and the EuTiO₃ setup at an expansion cutoff of $G_{\text{max}}^{\text{dop}} = 28.81 \, a_{\text{max}}^{-1}$ for the electronic density and the potential, the time required for Level 1 exceeds that needed by Level 0. These systems have in common that the $G_{\text{max}}^{\text{dop}}$ -cutoff is set to six times the planewave cutoff G_{max} . Level 3 requires a high $G_{\text{max}}^{\text{dop}}$ -cutoff, because the exchange-correlation potential and the xc energy density are non-linear in the electronic density. Therefore, their Fourier expansion contains in principle contributions in all G-channels. In a regular integral over the unit cell, which involves the multiplication of the xc density or potential with the electronic density, the Fourier expansion can be restricted to the regular cutoff for $G_{\text{max}}^{\text{dop}}$ due to the orthogonality of the plane waves. In a surface integral, this argument cannot be used.

For the other systems presented, the $G_{\rm max}^{\rm dop}$ -cutoff is four times $G_{\rm max}$ at most. In order to demonstrate that the drastic increase in computation time at Level 1 for aluminum and europium titanate stems from the choice of a large $G_{\rm max}^{\rm dop}$, we also provide the computation time of a EuTiO₃ calculation where the setup deviates from table 4.1 only by a reduced cutoff value of $G_{\rm max}^{\rm dop}$ to 19.21 $a_{\rm B}^{-1}$, which is four times the plane-wave cutoff. We see that the increase in computation time is reduced by a factor of three from 16.7% to 5.3%.

For MgO, the computation time is given for both sets of calculations: the one where the Mg 2s and 2p states are treated as core states and the one where they are lifted into the valence window by using LOs, which increases the LAPW basis set size. We also include the relative increase in computation time between both setups for each Level. In the LO case, each iteration of the density convergence step is more expensive by 3.9% of the time an average self-consistency step takes when the Mg 2s and 2p states are treated as core states. When atomic forces are calculated, the calculation using LOs takes close to 10% more time. Interestingly, the calculation of Level 2 in the case where no LOs are used decreases the computation time. Since Level 2 replaces the calculation of the kinetic-energy surface-term as implemented at Level 0 and Level 0 instead of adding a new term on top of it, it is plausible that we gain performance in some cases.

Level 3 on the other hand does add new code to calculate the remaining surface terms from Eq. (4.9). We therefore conclude in the case of GaAs, that the additional time needed for Level 3 is small enough to be hidden within small fluctuations in the performance time between different calculations. The calculation of the contribution from Level 3 takes 0.25 s. For vanadium dioxide with $U=4~{\rm eV}$ in the distorted rutile configuration, this contribution takes 7.70 s and also vanishes in the fluctuations of performance, as the total calculation takes more than 7000 s.

Except for the cases of Al and EuTiO₃ at an expansion cutoff of $G_{\rm max}^{\rm dop}=28.81~a_{\rm B}^{-1}$ for the electronic density and the potential, the relative increase in computation time from including Levels 1, 2, and 3 add up to similar values as the increase in computation time from activating a Level 0 force calculation at most. Therefore, we conclude that our force formalism at most doubles the additional time required for the calculation of atomic forces compared to the calculation of a single self-consistency step, when a $G_{\rm max}^{\rm dop}$ -cutoff of about four times the plane-wave cutoff $G_{\rm max}$ is employed. Since the atomic forces are usually calculated after a self-consistent density is found, this increase is negligible, especially compared to the gain of up to three orders of magnitude in the precision of the drift force.

4.8. Summary

The results presented in section 4.7 demonstrate the beneficial effect of the refined force formalism on the calculation of atomic forces within the FLAPW method, which we derived in sections 4.1 to 4.5. By comparing the force obtained by the analytical force formula with the force calculated numerically as the derivative of the total energy with respect to an atomic displacement, we realize that the force formalism is consistent only at Levell 1 and beyond. This can be concluded explicitly from the systems MgO and GaAs, where the force on one atom can be compared directly to the force on the other atom. At Levell 0, the forces are not the opposite of each other. Hence, the good agreement of some Levell 0 curves to the numerical force is considered to be fortuitous. Furthermore, the deviation of our calculated forces at higher Levells from the numerical force is in the same order of magnitude as the deviation of Levell 0 from the numerical force.

The inclusion of the whole unit cell in the calculation of the force contribution stemming from the core electrons by LEVEL 1 is required to allow the angular-momentum convergence of the drift force towards a value significantly closer to zero than the original implementation suggested by Yu et al. [54]. This value is routinely found to be in the regime of $\mu Htr/a_B$ per atom. Therefore, drift forces calculated at Level 1 with a high l_{max} cutoff are in much better agreement to the acoustic sum rule. The reason for the drift-force offset has been identified as the coretails of high lying core states, i.e., the part of a core state that is not contained within its MT sphere. This can be concluded in particular from the MgO system, where we have shown that the treatment of the leaking core states by local orbitals has a similar effect on the drift force as Level 1. However, the LOs have to be included into the calculation during each step of the calculation, also during the self-consistent determination of the electronic density. In total, this makes the treatment of the core states with local orbitals computationally expensive in contrast to the simple inclusion of Level 1. Considering the basis functions to be discontinuous leads to a proper evaluation of the kintic-energy surface term in terms of an interstitial representation at Level 2. The consequent inclusion of surface terms accounting for the slight discontinuities of the electronic density and the potential at Level 3 gives rise to precise atomic forces and a vanishing drift force for a reduced angular-momentum cutoff. For the systems presented in this thesis, the drift force is converged to a precision of $\mu Htr/a_B$ per atom for a modest $l_{max} = 12$. Sometimes, even a smaller cutoff value is sufficient. We conclude from our calculation of VO₂ that the DFT+U implementation in FLEUR according to Tran et al. [122] benefits in the same way from our refined formalism as does the standard FLAPW force. In particular, we achieve converged drift forces of the same precision, indicating that the DFT+U implementation of the atomic forces does not lack further terms. Therefore, our force formalism is a robust scheme for calculating reliable forces which is fairly tolerant to the user input.

Finally, the additional computation time needed for applying the higher Levels of our force formalism is in general a fraction of the time a force calculation at Level 0 takes. The additional computation time is only needed when the atomic forces are actually calculated, which is after the self-consistent electronic density has been determined. Thus, in the perspective of a complete calculation which includes the self-consistency cycle for the electronic density and the force calculation, the additional computation time our formalism requires is negligible. To further reduce the computation time, it might be reasonable to include only Level 2 into the calculation of the atomic forces. This allows to reduce the G_{\max}^{dop} -cutoff if the angular-momentum cutoff is increased.

In total, we have presented in this chapter a robust algorithm for calculating precise atomic forces within the FLAPW method which produces drift forces in the regime of $\mu \mathrm{Htr}/a_\mathrm{B}$ per atom. By employing this algorithm, the muffin-tin radius can be chosen more flexible, since the part of the core states which is lost from the MT sphere is properly taken into account for the force calculation. Furthermore, by taking into account the slight discontinuities of wave functions, density, and potential at the MT sphere boundary, the presented scheme produces reliable results at different MT sphere radii.

Now that we have solidified our understanding of the atomic forces within the FLAPW method in the previous chapter, we want to use the atomic force to calculate the phonon spectrum.

A phononic excitation is a collective displacement of the atomic nuclei of a solid, meaning that they perform vibrations around their equilibrium positions. Different displacement patterns are possible, which define the phonon modes. These modes can be excited by inserting energy into the solid. The quantum of this excitation is called a phonon. Experimentally, phonon spectra can be measured for example by inelastic neutron scattering [1–3], Raman spectroscopy [4–6], infrared absorption [7–9], and x-ray diffraction [10–12].

Phonons are also excited by thermal energy and represent therefore and important contributor to the specific heat of a material. This connection between thermal energy and lattice vibrations directly manifests in the phenomena of thermal expansion and heat conduction. Furthermore, the coupling between phonons and electrons can lead to superconductivity or alters the resistivity of metals, for example.

Phenomenologically, the restoring force on an atom displaced from its ideal position in the crystal is a measure of how tightly it is clamped to its position. If only a small amount of force is required to displace the atomic nucleus, a mode containing this displacement will be easy to excite. Generally, the congregation of information on how easy it is to move atoms in specific directions yields the information needed to determine which phonon modes are available.

In this chapter, we will introduce the force-constant matrix (FCM) and the dynamical matrix (DM) as well as their properties. A set of prototype calculations will be presented to check the fulfillment of these properties and to provide a stock of data to which more elaborate methods of calculating phonon spectra can be compared. Such comparisons will be subject of studies subsequent to this doctoral thesis.

Parts of this chapter are already published in Ref. [63].

5.1. The force-constant matrix

We assume a system where all atoms α in all unit cells R are displaced in direction i by $u_{\alpha Ri}$ from their equilibrium positions. The total energy E of this perturbed system as compared to the total energy E_0 of the system in equilibrium is then given in the harmonic approximation by the Taylor expansion to second order around the optimal positions,

$$E = E_0 + \frac{1}{2} \sum_{\alpha \mathbf{R}i} \sum_{\beta \mathbf{R}'j} \Phi_{\alpha \mathbf{R}i,\beta \mathbf{R}'j} u_{\alpha \mathbf{R}i} u_{\beta \mathbf{R}'j}.$$
 (5.1)

There is no linear term in the displacements due to the equilibrium condition which states that the forces on the atoms - being exactly what would appear as the linear term - vanish. This equation introduces the elements of the force-constant matrix

$$\Phi_{\alpha \mathbf{R}i,\beta \mathbf{R}'j} = \frac{\partial^2 E}{\partial u_{\alpha \mathbf{R}i} \partial u_{\beta \mathbf{R}'j}} = \frac{\partial^2 E_0}{\partial \tau_{\alpha \mathbf{R}i} \partial \tau_{\beta \mathbf{R}'j}}$$
(5.2)

as the second derivative of the total energy with respect to two atomic displacements, or in terms of the Taylor expansion as the second derivative of the equilibrium total energy with respect to two atomic positions, since in the perturbed system, the atomic positions are given by $\tau_{\alpha R} + u_{\alpha R}$ instead of just $\tau_{\alpha R}$. As long as one operates within the harmonic regime, the force-constant matrix can be expressed by the force matrix $F_{\alpha Ri,\beta R'j}$, whose elements are the force components acting on atom α of unit cell R along direction i due to a displacement of atom β in unit cell R' along direction j. In this regime, the connection between the force matrix and the force-constant matrix is given by the difference quotient with respect to the unperturbed system, in which no force or displacement occurs:

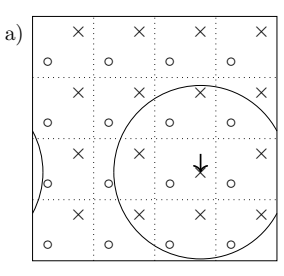
$$\Phi_{\alpha \mathbf{R}i,\beta \mathbf{R}'j} = -\frac{F_{\alpha \mathbf{R}i,\beta \mathbf{R}'j} - 0}{u_{\beta \mathbf{R}'j} - 0} = -\frac{F_{\alpha \mathbf{R}i,\beta \mathbf{R}'j}}{u_{\beta \mathbf{R}'j}}$$
(5.3)

If the displacements are outside of the harmonic regime, the force contains significant anharmonic contributions, which are inherited by the FCM as calculated in Eq. (5.3).

The force-constant matrix is tightly entwined with the dynamical matrix by a Fourier transform as will be demonstrated in the next section. The DM provides the amplitudes and displacement patterns of the phonons. However, this connection calls upon us to analyze Eq (5.3) in more detail:

First of all, Eq. (5.3) suggests that the second order derivative of the total energy that is the FCM is obtained from an analytical first order derivative to calculate the atomic forces as presented in chapter 4, followed by a numerical derivative represented by the difference quotient. This is the core of the finite-displacement (FD) method, which requires to set up a number of displacements and to calculate the force matrix from it. In its purest form, each atom has to be displaced separately in each of the three spatial directions. In practice however, one can exploit the lattice symmetry to reduce the number of analytic derivatives that have to be performed, as we will discuss in more detail in section 5.3. Differentiation however roughens, numerical differentiation even more so, hence it is sensitive to numerical noise in the quantity to be differentiated. Therefore, it is important to have access to accurate forces.

Moreover, R and R' refer to possibly different images of the unit cell. If we naively set up a system and displace one atom from its equilibrium position, we simultaneously displace all of its periodic images by the same amount. Also we would only obtain the force on the atom inside the same unit cell. Therefore, the forces we calculate would not fit to the force (constant) matrix as we defined it. To mitigate this deficiency, instead of the primitive unit cell a supercell needs to be set up. A supercell is an integer repetition of the primitive unit cell in each direction, so it contains different images of the primitive unit cell, as illustrated in Fig. 5.1. For example, if an atom is displaced in a $2 \times 2 \times 2$ supercell, where each integer refers to the number of repetitions of the primitive cell in each direction, its first image in particular is not also displaced, because it is part of the supercell setup, but its second image and all other even images are. Similarly, in a supercell that is $3 \times 3 \times 3$ times the



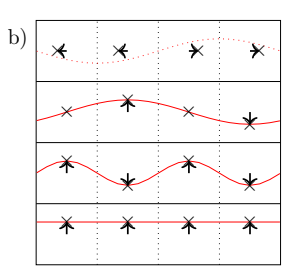


Figure 5.1.: (a) 4×4 supercell and force decay radius with respect to the distance from the atom displaced. (b) 4×1 supercells with commensurable phonon modes. \times and \circ in the figures denote atomic positions of different atom types.

primitive cell, the displacement of an atom would not occur at its first or second true image, but at its third and every further third image, and so on. It is sensible to assume that the force on an atom declines with increasing distance from the atom that is displaced from the equilibrium position. A good choice for the supercell size in terms of approximating the correct FCM thus would be to chose it so large that it includes the first atoms of each type on which the forces due to a displacement have decayed below some small target margin. Fig. 5.1(a) illustrates this concept.

Unfortunately, advancing to a supercell is a direct modification of the system size, in which electronic structure calculations typically scale to the cube. This renders the calculation of forces in a large supercell to be a demanding task. On the other hand, we can interpret the interplay between forces and supercells in a specific way: a displacement in a $1\times1\times1$ supercell (which is equivalent to the primitive unit cell) corresponds to displacing the whole sublattice of the atom which is displaced with respect to all other sublattices. Therefore, such a calculation gives information on vibrations of infinite wavelength, often called the long-wavelength limit in literature. A $2\times2\times2$ supercell allows to decouple an atom from its first image and thus enables information on vibrations where every second atom of a kind vibrates in phase while the direct neighbors of the same kind can vibrate opposite to each other. In this spirit, a given supercell can produce information on those vibrational modes that 'fit' into the supercell, *i.e.*, which can be expressed as a periodic object with respect to the images of the whole supercell. Such phonons are called commensurable with the supercell. Fig. 5.1(b) exemplifies phonons commensurable with a 4×1 supercell.

With the supercell (sc) established, the force on an atom in the unit cell addressed by \mathbf{R}' through the displacement of the atom of the same type in unit cell \mathbf{R} is accessible within the same setup. For any system in equilibrium it holds that if every atom β in each unit cell \mathbf{R}' is displaced by the same amount $u_{\beta \mathbf{R}'j} = \delta_{jk}u$ in the same direction k from its equilibrium position, the force on each atom has to vanish separately:

$$0 = F_{\alpha R i} = -\sum_{\beta R' j}^{\text{sc}} \Phi_{\alpha R i, \beta R' j} \delta_{jk} u = -u \sum_{\beta R'}^{\text{sc}} \Phi_{\alpha R i, \beta R' k}$$
(5.4)

This is the case because the total energy is translational invariant under a rigid shift of the system.

Furthermore, the acoustic sum rule, Eq. (4.2), holds, regardless of whether a single unit cell or a supercell is considered. Hence it is a theoretical prescription that when all atoms are displaced by a small amount $u_{\beta R'j}$, for each i=x,y, and z it has to be

$$0 = \sum_{\alpha \mathbf{R}} F_{\alpha \mathbf{R}i} = -\sum_{\alpha \mathbf{R}}^{\text{sc}} \sum_{\beta \mathbf{R}'j}^{\text{sc}} \Phi_{\alpha \mathbf{R}i,\beta \mathbf{R}'j} u_{\beta \mathbf{R}'j} = -\sum_{\beta \mathbf{R}'j}^{\text{sc}} u_{\beta \mathbf{R}'j} \sum_{\alpha \mathbf{R}}^{\text{sc}} \Phi_{\alpha \mathbf{R}i,\beta \mathbf{R}'j}.$$
 (5.5)

As a last remark on the force-constant matrix, we point out that it has to be symmetric by Young's theorem, since the order of differentiation of the total energy with respect to the displacements $u_{\alpha Ri}$ and $u_{\beta R'j}$ in Eq. (5.2) is arbitrary. Therefore, Eq. (5.5) follows from Eq. (5.4). Consequently, three columns of the FCM (one for each choice of i) are linearly dependent from the other columns, leading to a threefold singular matrix. We will elaborate on the consequences of this prescription in more detail in the next section.

5.2. The dynamical matrix

As was motivated in the introduction of this chapter, the force-constant matrix contains information on how tightly bound an atom is at its equilibrium position with respect to displacements in arbitrary directions. Also, we learned during the introduction of the FCM that when applying the supercell approach, specific phonons can be realized which are commensurable with the supercell lattice. This we can use to formulate the dynamical matrix from the classical equation of motion $\mathbf{F} = m\ddot{\mathbf{x}}$ for the atomic nuclei,

$$\tilde{M}_{\alpha} \ddot{u}_{\alpha R i} = -\sum_{\beta R' j}^{\text{sc}} \Phi_{\alpha R i, \beta R' j} u_{\beta R' j}, \qquad (5.6)$$

where \tilde{M}_{α} is the mass of atom α relative to the electron mass. By the harmonic ansatz

$$u_{\alpha \mathbf{R}i} = \frac{1}{\sqrt{\tilde{M}_{\alpha}}} Q_{\alpha i} e^{i[\mathbf{q} \cdot (\boldsymbol{\tau}_{\alpha} + \mathbf{R}) - \omega(\mathbf{q})t]}$$
(5.7)

with the polarization vector Q_{α} of atom α modulated with position and time by the phase factor, the modulation frequency $\omega(q)$, and the reciprocal lattice vector q defining the wave length of the phonon, the equation of motion transforms to

$$0 = \sum_{\beta j} \left[D_{\alpha i, \beta j}(\mathbf{q}) - \delta_{\alpha \beta} \delta_{ij} \omega^{2}(\mathbf{q}) \right] Q_{\beta j}. \tag{5.8}$$

Herein, the dynamical matrix $D_{\alpha i,\beta j}(q)$ at wave vector q is related to the discrete Fourier transform of the FCM by

$$D_{\alpha i,\beta j}(\mathbf{q}) = \frac{e^{i\mathbf{q}\cdot(\mathbf{\tau}_{\beta} - \mathbf{\tau}_{\alpha})}}{\sqrt{\tilde{M}_{\alpha}\tilde{M}_{\beta}}} \sum_{\mathbf{R}}^{\mathrm{sc}} \Phi_{\alpha \mathbf{R}i,\beta \mathbf{0}j} e^{-i\mathbf{q}\cdot\mathbf{R}}.$$
 (5.9)

We made use of the translational symmetry of the lattice, by which the force on atom α in unit cell \mathbf{R} due to a displacement of atom β in unit cell \mathbf{R}' is the same as the force on atom α in unit cell $\mathbf{R} - \mathbf{R}'$ due to the same displacement of atom β in unit cell $\mathbf{0}$. Therefore, from the force-constant matrix we can easily construct the dynamical matrix at a commensurable

wave vector \boldsymbol{q} , whose eigenvectors and eigenvalues are the polarization of the atoms and the squares of the phonon energies at \boldsymbol{q} . The dimension of this matrix is $3N_{\rm at} \times 3N_{\rm at}$. The phonon band structure at intermediate wave vectors \boldsymbol{q} is approximated by an interpolation between the \boldsymbol{q} -vectors which are commensurable with the supercell. The quality of this approximation is dependent on the supercell size, because larger supercells allow for a finer sampling of the Brillouin zone and thus for more interpolation points. The approximation is done by inserting a wave vector \boldsymbol{q} into Eq. (5.9) which is not commensurable with the supercell. For an incommensurable wave vector, the FCM is only approximate if it is not constructed from a supercell large enough that the forces induced by moving one atom are declined over its length.

The dynamical matrix is Hermitian due to the symmetry of the force-constant matrix and the translational symmetry of the lattice:

$$D_{\beta j,\alpha i}(\mathbf{q}) = \frac{e^{i\mathbf{q}\cdot(\boldsymbol{\tau}_{\alpha}-\boldsymbol{\tau}_{\beta})}}{\sqrt{\tilde{M}_{\alpha}\tilde{M}_{\beta}}} \sum_{\mathbf{R}}^{\mathrm{sc}} \Phi_{\beta \mathbf{R}j,\alpha \mathbf{0}i} e^{-i\mathbf{q}\cdot\mathbf{R}} = \frac{e^{-i\mathbf{q}\cdot(\boldsymbol{\tau}_{\beta}-\boldsymbol{\tau}_{\alpha})}}{\sqrt{\tilde{M}_{\alpha}\tilde{M}_{\beta}}} \sum_{\mathbf{R}}^{\mathrm{sc}} \Phi_{\beta \mathbf{0}j,\alpha-\mathbf{R}i} e^{-i\mathbf{q}\cdot\mathbf{R}}$$
$$= \frac{e^{-i\mathbf{q}\cdot(\boldsymbol{\tau}_{\beta}-\boldsymbol{\tau}_{\alpha})}}{\sqrt{\tilde{M}_{\alpha}\tilde{M}_{\beta}}} \sum_{\mathbf{R}}^{\mathrm{sc}} \Phi_{\alpha \mathbf{R}i,\beta \mathbf{0}j} e^{i\mathbf{q}\cdot\mathbf{R}} = D_{\alpha i,\beta j}^{*}(\mathbf{q})$$
(5.10)

Thus, the eigenvalues $\omega^2(q)$ are real quantities, even though they do not need to be nonnegative. If they are, the corresponding phonon energies are imaginary and indicate an instability of the system. In nature, such an instability would have led to a phase transition of the system into a geometry that is more stable. As such, imaginary modes are only accessible by electronic structure calculations. However, under certain conditions like increasing or decreasing pressure, the softening of a phonon mode can be observed in experiment [124, 125]. In this case, the phonon band structure deforms such that the value of a band at a specific phonon wavelength q becomes smaller and smaller.

To elaborate on this concept in case of an electronic structure calculation, we know for example from the textbook study of the 1D diatomic chain that the acoustic mode at Γ corresponds to a rigid shift of the unit cell, *i.e.*, both atoms vibrate by the same amount in the same direction, while the optic mode advocates a vibration of the two atom types against each other. In the same sense, an imaginary optical mode at Γ in the phonon band structure of a crystal setup suggests that the setup of the calculation was only a metastable equilibrium and that a setup where the relative position of the atoms to each other is different is more stable.

In the last section we discussed that the force-constant matrix exhibits a threefold degenerate eigenvalue of zero due to Eqs. (5.5) and (5.4). A rigid shift of the whole crystal in any direction in space does not alter the total energy and hence the forces. Such a rigid shift corresponds to a phonon of infinite wavelength. The invariance of the total energy translates to the necessity that three of the eigenvalues of the dynamical matrix are zero at the Γ -point q = 0. The phonon modes fulfilling this condition are called the acoustic modes and their slope at the Brillouin-zone center determines the speed of sound in the material,

$$v_{\text{sound}} = \frac{\partial \omega(\mathbf{q})}{\partial q} \Big|_{\mathbf{q} \to \mathbf{0}}.$$
 (5.11)

It is clear that a non-vanishing drift force (5.5) implies that the translational invariance leading to Eq. (5.4) is artificially violated. Therefore, the constituents of the force-constant matrix are not guaranteed to be linearly dependent and the dynamical matrix may show eigenvalues of the acoustic modes that do not vanish at Γ . There are different approaches to deal with this issue: The drift force usually is distributed over and subtracted from the force acting on the atoms, either uniformly or weighted by the mass of the nucleus to enforce the acoustic sum rule. We believe however that in doing so one introduces an uncontrollable error to the FCM and hence to the DM. In our opinion, the most rigorous way to construct the FCM is by more accurate forces, for which we provided a recipe in chapter 4.

If there is more than one atom in the primitive unit cell, the phonon dispersion will consist of $3N_{\rm at}-3$ additional optical phonon modes which are of finite value at the Γ -point. Because photons are massless, their dispersion is very steep, in fact much steeper than the dispersion of the acoustic phonons near the Γ -point. However, as the optical phonons have finite values there at Γ , photons can be used to excite these.

5.3. Exploiting lattice symmetry for the FCM

The basic recipe for obtaining the force-constant matrix $\Phi_{\alpha Ri,\beta R'j}$ in the finite-displacement approach is to separately displace each atom β in each image R' of the primitive unit cell in each direction j by $u_{\beta R'j}$, to compute the forces $F_{\alpha Ri,\beta R'j}$ on every atom and to divide them by the amplitude of the displacement. The symmetry of the lattice allows to reduce the number of calculations needed to be performed, as was presented by Kresse *et al.* [126] and implemented in the PHON-code by Alfe [58].

We already made use of the translational symmetry of the crystal, by which the force matrix and thus the force-constant matrix only depends on the relative position of the different primitive unit cells within the supercell, $\Phi_{\alpha Ri,\beta R'j} = \Phi_{\alpha R-R'i,\beta 0j}$. Therefore, it is sufficient to displace the atoms β within a representative primitive unit cell $\mathbf{0}$ of the supercell.

Furthermore, if β and β' within the representative unit cell of the equilibrium supercell are related by symmetry, *i.e.*, if a transformation \underline{B} exists that maps β' onto β and is a symmetry operation of the crystal, the force-constant matrix generated by displacing β' can be constructed from the one where β was displaced by

$$\underline{\Phi}_{\alpha R, \beta' \mathbf{0}} = \underline{B} \, \underline{\Phi}_{\underline{B}(\alpha R), \beta \mathbf{0}} \, \underline{B}^{-1}, \tag{5.12}$$

where $\underline{\Phi}_{\alpha R,\beta 0}$ is the 3×3 part of the force-constant matrix subsuming the Cartesian components of the entries which belong to atom α in unit cell R and atom β in the representative unit cell. $\underline{B}(\alpha R)$ denotes the image of atom α of unit cell R under the transformation \underline{B} . These simplifications do concern the symmetry of the equilibrium lattice. It might also be useful to consider the symmetry of the system in which an atom is displaced. While the force-constant matrix is constructed from displacements along the Cartesian axes, it is possible that a displacement along an axis which is not one of the Cartesian axes keeps intact more symmetries. Such a setup takes less time to compute. It is therefore favorable. If the atoms are displaced by $u_{\beta 0\mu(\beta)}$ along the three linearly independent directions $\mu(\beta)$, which may be chosen differently for each atom β , the forces from a Cartesian displacement can be reconstructed using

$$F_{\alpha \mathbf{R}, \beta \mathbf{0} j} = \sum_{\mu(\beta)} \left(\underline{\mathbf{A}}(\beta)^{-1} \right)_{j\mu(\beta)} \tilde{F}_{\alpha \mathbf{R}, \beta \mathbf{0} \mu(\beta)}$$
 (5.13)

with

$$\underline{\underline{A}}(\beta) = \left(\frac{\underline{u}_{\beta 0\mu(\beta)=1}}{|\underline{u}_{\beta 0\mu(\beta)=1}|}, \frac{\underline{u}_{\beta 0\mu(\beta)=2}}{|\underline{u}_{\beta 0\mu(\beta)=2}|}, \frac{\underline{u}_{\beta 0\mu(\beta)=3}}{|\underline{u}_{\beta 0\mu(\beta)=3}|}\right)$$
(5.14)

relating between Cartesian coordinates and the ones chosen for the displacement of β . $\tilde{F}_{\alpha R,\beta 0\mu(\beta)}$ are the forces acting on atom α in unit cell R expressed in Cartesian coordinates due to the non-Cartesian set of displacements $u_{\beta 0\mu(\beta)}$. While the non-Cartesian displacements need to be linearly independent, they do not need to be orthogonal. Therefore, the formula above is using the inverse of $\underline{A}(\beta)$ and not its transposed.

Finally, if two linearly independent displacements $u_{\beta 0\mu=1}$ and $u_{\beta 0\mu=2}$ are related by a point group symmetry operation U, also the forces from both displacements can be related to each other:

$$\tilde{\boldsymbol{F}}_{\alpha\boldsymbol{R},\beta\boldsymbol{0}\mu=2} = \underline{\boldsymbol{B}}(U)\tilde{\boldsymbol{F}}_{\boldsymbol{B}(U)^{-1}(\alpha\boldsymbol{R}),\beta\boldsymbol{0}\mu=1}$$
(5.15)

The matrix $\underline{\boldsymbol{B}}(U)$ denotes the transformation matrix going along with the symmetry operation U and $\underline{\boldsymbol{B}}(U)^{-1}(\alpha \boldsymbol{R})$ is the atom which is mapped to α in \boldsymbol{R} by U. μ labels any kind of coordinates here, including Cartesian ones.

Still, since Eq. (5.3) is only an approximation in the case of small displacements within the harmonic regime, the force-constant matrix obtained this way ususally violates the prescription of being invariant under the point group symmetry operations belonging to the crystal lattice. This is the case because anharmonicities contribute to its entries. In order to mitigate the influence of these anharmonicities and to restore the invariance of the FCM, it is averaged over all $N_{\rm PG}$ point group symmetry operations U by

$$\underline{\boldsymbol{\Phi}}_{\alpha\boldsymbol{R},\beta\boldsymbol{0}} = \frac{1}{N_{\text{PG}}} \sum_{U} \underline{\boldsymbol{B}}(U) \underline{\boldsymbol{\Phi}}_{\underline{\boldsymbol{B}}(U)(\alpha\boldsymbol{R}),\beta\boldsymbol{0}} \underline{\boldsymbol{B}}(U^{-1}). \tag{5.16}$$

Using all these techniques, the amount of displacements to construct the full FCM can be reduced drastically. Then, the force-constant matrix is used to calculate the dynamical matrix according to Eq. (5.9). Subsequently, the eigenenergies and displacement patterns of the phonons are extracted from the DM.

5.4. The LO-TO splitting

If phonons are calculated at a finite wave vector \boldsymbol{q} , the overall displacement pattern is such that over certain length-scales or repetitions of what would have been the unperturbed unit cell the displacements nearly average out. This is immediately clear for those \boldsymbol{q} for which a supercell configuration of the lattice exists to which they are commensurable. Then, the average displacements for each atom are exactly zero. Even if the crystal is bound ionically, there will be no macroscopic electric field in it. On the other hand, if \boldsymbol{q} approaches zero, the lengths at which the displacement patterns repeat increase until at $\boldsymbol{q}=\boldsymbol{0}$ sublattices are completely shifted against each other. Now, an ionically bound crystal produces a macroscopic electric field, to which the atoms of the crystal also have to respond.

To provide a crude example, imagine the ionically bound magnesium oxide crystal in rocksalt structure. Along 111-direction, planes of positively charged magnesium atoms alternate with planes of negatively charged oxygen atoms. If we think of these planes as being

homogeneously charged, moving the corresponding sublattices in any direction within the two-dimensional subspace of these planes is the same energetically, but differs from moving the planes towards each other. In the latter case, the polarization of the system is changed and an electric field forms.

This corresponds to the splitting of the longitudinal optical (LO) modes from the transverse optical (TO) modes and is not included into the dynamical matrix for $q \to 0$ presented here. The former modes propagate along the direction of the phonon momentum $q \to 0$ while the latter modes are transverse to it. For $q \neq 0$, a splitting between the longitudinal and transverse modes can typically be observed in the calculations, whereas in the long-wavelength-limit a non-analytical (na) term

$$D_{\alpha i,\beta j}^{\text{na}} = \lim_{\mathbf{q} \to \mathbf{0}} \frac{1}{\sqrt{\tilde{M}_{\alpha} \tilde{M}_{\beta}}} \frac{4\pi}{\Omega} \frac{(\mathbf{q} \cdot \mathbf{Z}_{\alpha}^{*})_{i} (\mathbf{q} \cdot \mathbf{Z}_{\beta}^{*})_{j}}{\mathbf{q} \cdot \underline{\boldsymbol{\epsilon}}^{\infty} \cdot \mathbf{q}}$$
(5.17)

has to be added to the dynamical matrix to properly account for the LO-TO splitting, which results in an energy shift of the longitudinal optical mode. The value of the non-analytical correction depends on the direction from which the Γ -point is approached [127]. Herein, \tilde{M}_{α} is the mass of the nucleus of atom α , Ω is the unit cell volume, and $\underline{\epsilon}^{\infty}$ is the static dielectric tensor with the components

$$\epsilon_{ij}^{\infty} = \frac{\partial \mathcal{E}_{0i}}{\partial \mathcal{E}_{j}} = \frac{\partial (\mathcal{E}_{i} + 4\pi P_{i})}{\partial \mathcal{E}_{j}} = \delta_{ij} + 4\pi \frac{\partial P_{i}}{\partial \mathcal{E}_{j}}$$
(5.18)

evaluated at equilibrium positions u(q=0)=0. The field \mathcal{E}_0 is the macroscopic electric field and \mathcal{E} is the screened field inducing the polarization P. The Born effective charge tensor Z_{α}^* is a measure of how much the polarization of the system changes in a particular direction i if atom α is displaced along direction j at vanishing electric field $\mathcal{E}=0$,

$$Z_{\alpha,ij}^* = \Omega \frac{\partial P_i}{\partial \tau_{\alpha,j}}.$$
 (5.19)

The non-analytical term is not included in the finite-displacement results shown later.

5.5. Computational results

In this section, we discuss the effect of our force formalism on the symmetry of the force-constant matrix of ${\rm EuTiO_3}$ and provide phonon spectra for aluminum, magnesium oxide, gallium arsenide, and europium titanate. The meaning of the different force Levels can be found in chapter 4.5.

5.5.1. The FCM of EuTiO₃

We discuss a part of the force matrix of $EuTiO_3$ with respect to Levels 0 and 3 of our force implementation. In table 5.1, we present in each line the forces in x-direction on every atom in the system caused by a displacement in x-direction of the atom named in the first column of the table. In all setups, the respective atom is displaced by 0.02244 a_B .

(a)			Levi	EL O		
	Eu	$O_{0\frac{1}{2}\frac{1}{2}}$	$O_{\frac{1}{2}0\frac{1}{2}}$	$O_{\frac{1}{2}\frac{1}{2}0}$	Ti	Drift
Eu_{000}	-274.4	200.3	-274.6	-274.6	626.7	3.4
$O_{0\frac{1}{2}\frac{1}{2}}$	199.0	-3208.7	1065.5	1065.5	983.0	104.3
$O_{\frac{1}{2}0\frac{1}{2}}$	-273.0	1067.0	-832.5	-193.4	219.5	-12.4
$O_{\frac{1}{2}\frac{1}{2}0}$	-273.0	1067.0	-194.2	-831.8	219.6	-12.4
$\text{Ti}_{\frac{1}{2}\frac{1}{2}\frac{1}{2}}^{\frac{1}{2}}$	621.3	879.8	233.0	233.0	-2050.1	-83.0
Total	-0.1	5.4	-2.8	-1.3	-1.3	-
Ma	ximal/ave	rage deviat	tion from	symmetry	. 103 2/14	39

(b)			Levi	EL 3		
	Eu	$O_{0\frac{1}{2}\frac{1}{2}}$	$O_{\frac{1}{2}0\frac{1}{2}}$	$O_{\frac{1}{2}\frac{1}{2}0}$	Ti	Drift
Eu_{000}	-272.2	200.3	-274.6	-274.6	619.9	-1.2
$O_{0\frac{1}{2}\frac{1}{2}}$	199.2	-3208.7	1065.5	1065.5	876.9	-1.6
$O_{\frac{1}{2}0^{\frac{1}{2}}}$	-274.3	1067.0	-832.5	-193.4	232.2	-1.0
$O_{\frac{1}{2}\frac{1}{2}0}$	-274.3	1067.0	-194.2	-831.7	232.3	-0.9
$\text{Ti}_{\frac{1}{2}\frac{1}{2}\frac{1}{2}}$	621.3	879.7	233.0	233.0	-1968.0	-1.0
Total	-0.3	5.3	-2.8	-1.2	-6.7	-
N	Iaximal/a	verage devi	ation from	n symmet	ry: 2.8/1.15	

Table 5.1.: x-component of the force matrix of EuTiO₃ in μ Htr/a_B. (a) corresponds to forces obtained at Level 0. (b) corresponds to forces obtained at Level 3. The first column of a row lists the atom which has been displaced by 0.02244 a_B along x-direction. The component of the force along the same direction is then shown for each atom in the unit cell. In the last column (row), the force values of each row (column) are summed up.

We observe that at Level 0, the original force formalism of Yu et al. [54] corresponding to table 5.1(a), a drift force of up to 0.1 mHtr/aB persists. However, each row, which represents a different calculation, adds up already to the margin of μ Htr/aB per atom. This demonstrates the systematic error present in each calculation at Level 0, which is due to the neglect of the coretails. Also, this is an indicator that μ Htr/aB per atom is indeed the precision we can hope to achieve.

Since the applied displacements are of the same amplitude, the x-component of the force-constant matrix is related to the force matrix of table 5.1(a) by a simple factor. Therefore, the data shown in the table has to be symmetric, because the force-constant matrix is a second derivative of the total energy according to Eq. (5.2). The maximal deviation from the symmetry is given by the titanium row and column. The force on titanium caused by a displacement of the oxygen atom towards it and the force on the oxygen atom towards which the titanium is displaced deviate from each other by $103.2~\mu Htr/a_B$. This is reasonable, because the coretail from titanium is affected most strongly by the atoms nearest neighbor, which is the oxygen octaeder in the equilibrium configuration or a particular oxygen atom when a displacement is applied.

Application of our refined force formalism at Level 3 results in table 5.1(b). We immediately see the decrease in the drift force which is in agreement to our results from chapter 4.7. Also, we observe that the effect on the oxygen atoms is negligible, while the forces on eu-

ropium exhibit a small correction. Most importantly, though, the forces on the titanium atom are altered such that not only reliable drift forces are produced, but also that the maximal deviation from symmetry in the force matrix is reduced by two orders of magnitude to $2.8~\mu Htr/a_B$.

In conclusion, the refined force formalism leads to a force-constant matrix which exhibits symmetry to a precision of $\mu {\rm Htr}/a_{\rm B}$ per atom. The effect on the phonon spectrum will be analyzed in the next section.

5.5.2. Phonon spectra

We now make use of the atomic force computed with FLEUR to calculate the phonon spectra of Al, MgO, GaAs, and EuTiO3 employing the finite-displacement method as realized in the PHON code by Alfe [58]. For calculating the phonon spectra, all systems are set up in a $2\times2\times2$ unit cell, i.e., the primitive unit cells are repeated once in x,y, and z direction. For Al, this corresponds to the Al_{II}-setup. All other numerical parameters are set according to table 4.1. The Brillouin zone of the supercell is sampled by a $4\times4\times4$ grid.

Depending on the symmetry of the system, the PHON code suggests a minimal set of atomic displacements as was discussed in section 5.3. For each of the displaced configurations, a FLEUR calculation yields the atomic forces from which the force-constant matrix is constructed by the PHON code. The resulting phonon spectra are shown in Figs. 5.2, 5.4, 5.3, and 5.5. In addition, we include results obtained at the different force Levels we summarized in chapter 4.5. In this context, black lines denote Level 0, and red lines denote Level 3. Level 1 and Level 2 coincide with Level 3 on the scale of the graphs and are thus omitted. When available, experimental data is provided as blue asterisks.

The phonon spectrum of Al (s. Fig. 5.2) shows 3 phonon branches: one longitudinal and two transversal acoustic modes. Depending on the Brillouin-zone path the two transversal modes are degenerate or not. Around the Γ point all three branches exhibit a linear behavior. where the slope of the longitudinal acoustic mode corresponds to the speed of sound in the lattice. The effect of the different force Levels on the phonon dispersion of Al is negligibly small, which agrees with our observation that the forces of Al are mostly unaffected by the higher force Levels. Note that with a $2 \times 2 \times 2$ supercell only the high-symmetry points Γ . X, and L are commensurable with the supercell, i.e., the corresponding phonon eigenmodes exhibit a wavelength that exactly fits in the supercell. This has the consequence that the phonon frequencies at these points are directly accessible by the finite-displacement method. At all other points, the spectrum is obtained from a Fourier interpolation. In order to assess the quality of the interpolation and to demonstrate the effect of the supercell size on the phonon spectrum, Fig. 5.2 also shows the phonon spectrum (black dotted line) resulting from a $4 \times 4 \times 4$ supercell. At the same time the **k**-point mesh of the underlying electronic structure calculation has been reduced to $2 \times 2 \times 2$ to guarantee an equivalent sampling of the Brillouin zone. With this larger supercell, also the phonon energies in the middle of the ΓX , $X(K)\Gamma$, and ΓL path become accessible without interpolation. The effect on the phonon spectrum is most prominently visible at the lowest phonon branch on the $X(K)\Gamma$ path. The kink in the middle of the path is produced by the intermediate point, which is now commensurable with the supercell. In comparison to experiment (blue asterisks) [128], we find a good qualitative agreement. However, the computed phonon energies tend to underestimate the experimental measured one. This is in accordance with the general observation

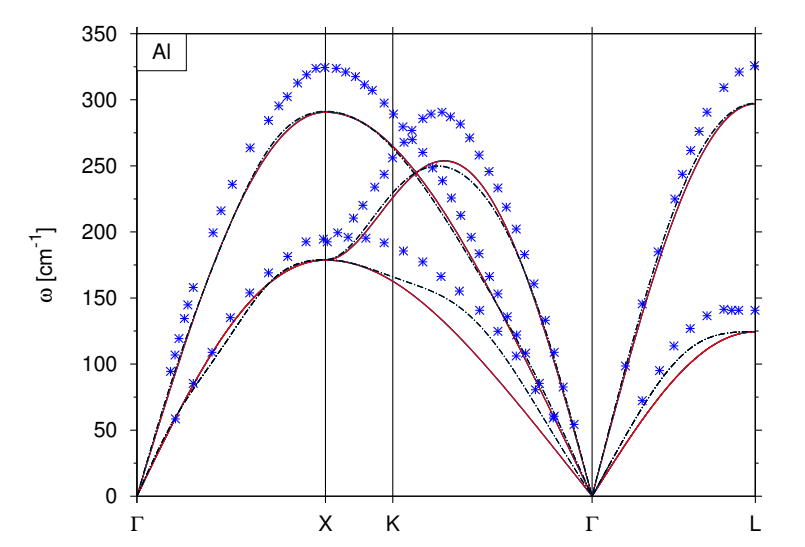


Figure 5.2.: Phonon spectrum of Al obtained from a $2 \times 2 \times 2$ supercell at Level 3 of the force formalism (red solid line) and from a $4 \times 4 \times 4$ supercell at Level 3 (black dashed line). In both cases, Level 3 does not deviate from the other Levels. Blue asterisks mark experimental data.

that LDA phonon frequencies are usually too soft at the experimental lattice constant [129]. A better agreement with the experimental phonon spectrum is typically achieved if the calculation is performed at the theoretically (LDA) predicted equilibrium lattice constant. The latter is usually smaller than the experimental one, which works against the too soft phonon frequencies at the experimental lattice constant.

In contrast to Al, the phonon spectrum of MgO (s. Fig. 5.3) exhibits 6 branches: 3 acoustic and 3 optical modes. The optical branches correspond to a movement of the atoms against each other. A finite, non-zero energy is required to excite these phonons for every q, in particular for the Γ point. At this point, all 3 optical modes are degenerate in our calculation, which is in obvious contraction to the experimental data (taken from Refs. [130–132]), where one optical phonon band is energetically clearly separated from the rest. This band corresponds to the longitudinal optical mode, which is related to a collective movement of the atoms causing a polarization of the ionically bound MgO. In contrast to the transversal ones, this mode requires (significantly) more energy to be excited. As discussed in section 5.4, one has to go beyond the finite-displacement method to properly account for the so-called LO-TO splitting. Hence, we cannot expect that experiment and calculation agree at and in a region around the Γ point, since the interpolation procedure assumes the optical bands to be threefold degenerate at Γ . By using larger and larger supercells for calculating the phonon band structure, the band structure in the vicinity of the Γ point can

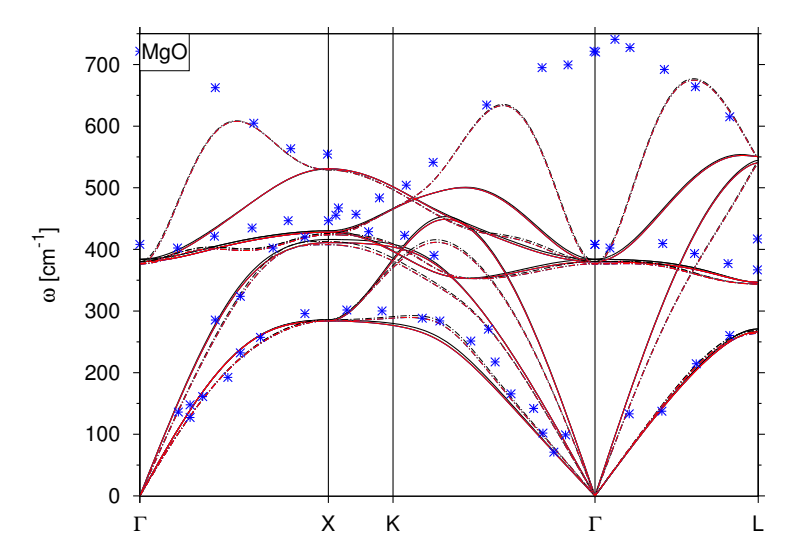


Figure 5.3.: Phonon spectrum of MgO obtained from a $2 \times 2 \times 2$ supercell at Level 0 (black solid line) and at Level 3 (red solid line). Respective data from a $4 \times 4 \times 4$ supercell calculation uses dashed lines. Blue asterisks mark experimental data.

be improved, but not at Γ . We demonstrate this behavior by including the phonon band structure resulting from a $4\times4\times4$ supercell calculation (black and red dotted lines). The k-point mesh of this calculation has been reduced to a $2\times2\times2$ mesh to guarantee an equivalent sampling of the Brillouin zone. In addition to the raise in energy for the longitudinal optical mode in the middle of the high-symmetry points, we see a splitting of the acoustic and optical bands in the middle of the $X(K)\Gamma$ path as well as a kink in the lowest acoustic band on the same path. Both features result from the additional point in the middle of the $X(K)\Gamma$ path at which the phonon frequencies can be calculated exactly with a $4\times4\times4$ supercell.

For both supercell sizes, the acoustic phonon branches of MgO are in reasonable agreement with experiment for both supercell sizes. In general, a slight underestimation of the acoustic and optical phonon energies can be observed, which is again in accordance with the general observation that LDA leads to too soft phonons at the experimental lattice constant.

The dispersion curves belonging to Level 1 and the higher Levels (represented by the red line of Level 3, which are indistinguishable from Level 1 and 2) show a small deviation from Level 0 for both setups. This is expected, because the force formalism at Level 1 adjusts the force acting on the Mg atom, while it keeps the force acting on O unchanged.

The phonon spectrum of GaAs (s. Fig. 5.4) consists of 6 branches as well, from which 3 are acoustic modes while 3 are optical modes. We observe comparably large deviations between Level 0 and Levels 1 to 3 mainly in the optical bands, which agrees to our results

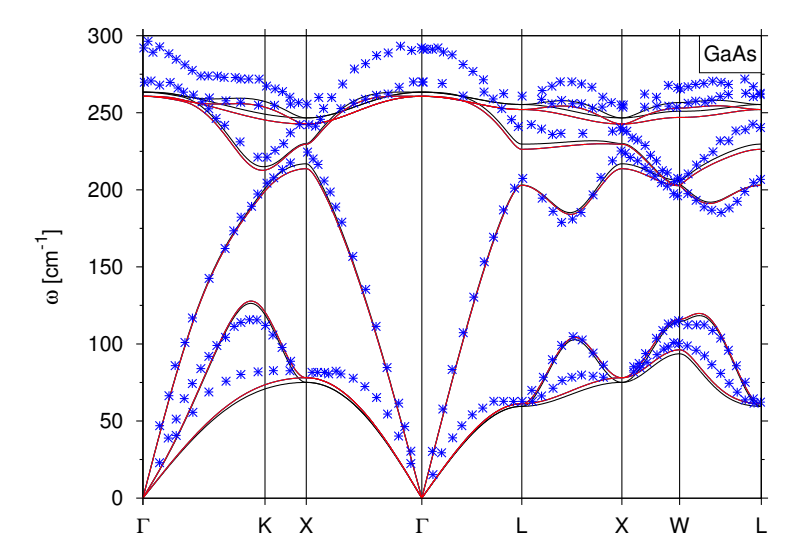


Figure 5.4.: Phonon spectrum of GaAs obtained from a $2 \times 2 \times 2$ supercell at Level 0 (black solid line) and at Level 3 (red solid line). Blue asterisks mark experimental data

from chapter 4.7. Level 1 changes the force acting on As by about 3% as compared to Level 0. If the atoms vibrate out of phase, *i.e.*, if an optical mode is excited, the amount of the coretail of As entering the Ga muffin-tin sphere changes during the vibration. Apart from the LO-TO splitting at Γ (s. discussion of MgO), our calculation is in good agreement with the experimental data of Ref. [133]. The features of the experimental band structure are well reproduced also in between the high-symmetry points Γ , X, and L, at which the phonon frequencies are directly accessible via the finite-displacement method due to their commensurability with the $2 \times 2 \times 2$ supercell used for the calculation. Quantitatively, a slight underestimation of the experimental phonon energies can be observed again.

Having five atoms in the chemical unit cell, $EuTiO_3$ has a phonon band structure which contains 15 branches (3 acoustic modes and 12 optical modes). The phonon dispersion exhibits soft modes at the high-symmetry points M and R and on the high-symmetry line between these points, which reveals a structural instability that breaks the translational symmetry of the primitive unit cell. Interestingly, we observe negative phonon frequencies at the Γ , R, and M point of the BZ. These negative frequencies occur mathematically if the dynamical matrix, which is a Hermitian matrix, has negative eigenvalues. As the eigenvalues of the dynamical matrix correspond to the phonon frequencies squared, a negative value is related to an imaginary frequency, which is then depicted as a negative energy in the phonon band structure. Physically these imaginary frequencies indicate a structural instability of the system and are called soft modes. The soft modes at the high-symmetry points M and

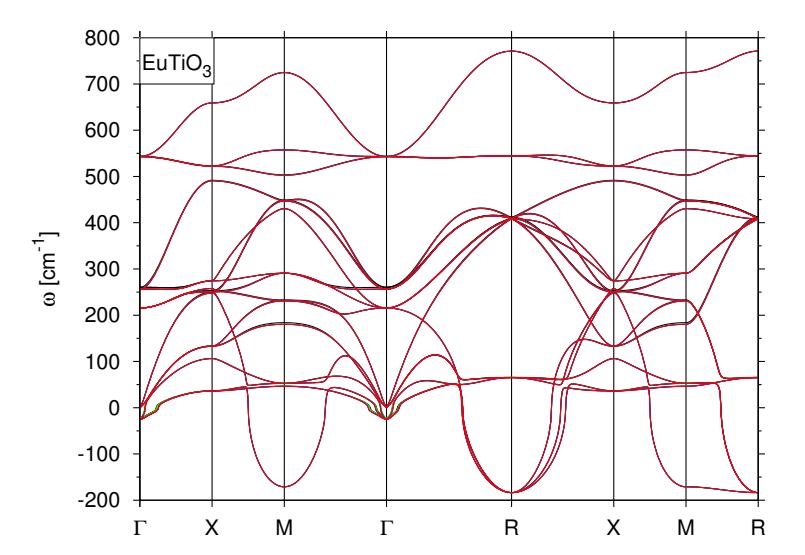


Figure 5.5.: Phonon spectrum of EuTiO $_3$ obtained from a $2\times2\times2$ supercell at Level 0 (black solid line) and at Level 3 (red solid line). The Levels are nearly indistinguishable.

R and on the high-symmetry line between these points reveal a structural instability that breaks the translational symmetry of the primitive unit cell. The new distorted geometric structure exhibits a translational symmetry that is restored in the $2\times2\times2$ super cell. The eigenvectors of the soft modes reveal that these point at configurations where the oxygen octahedra are tilted and rotated around the titanium atom within the europium planes. In addition, a threefold degenerate soft mode is present at the Γ point, albeit not as pronounced as those at M and R. This soft mode consists of optical bands, which indicate a structural instability where the atoms of the primitive unit cell are shifted against each other but which keeps the translational symmetry of the primitive unit cell intact. Overall, the perfect cubic perovskite structure is not the ground state of EuTiO₃.

The phonon spectrum shows small deviations between the different force Levels.

Our observations agree quite well with those of Rushchanskii et al. [134]. Rushchanskii et al. performed a detailed study on europium titanate using the vienna ab initio simulation package (VASP) and the projector augmented-wave method (PAW) [135–138]. They employed a GGA xc functional, a Hubbard-U of U=5.7 eV and a Hund's exchange of J=1.0 eV. Despite these differences, the qualitative results are very similar: they found soft phonon modes at M and R as well as a soft mode at Γ at a lattice constant of $a_0=3.95$ Å = 7.47 $a_{\rm B}$. By reducing the lattice constant to $a_0=3.90$ Å = 7.37 $a_{\rm B}$ the instability at Γ vanishes. As we already mentioned, LDA is usually considered to overbind atoms and thus to underestimate the lattice constant. Therefore, we assume that our LDA calculation is still in the regime where the instability at Γ can be expected.

While we observe deviations between the phonon spectra obtained from force constants at different implementation Levels, these deviations are minor and do not result in a qualitatively different interpretation of the spectra. In conjunction with the improvement of the force-constant matrix demonstrated in table 5.1, this is surprising. Instead of a homogeneous change of the force-constant matrix of EuTiO₃, a particular column is affected by our corrections, while the other rows are largely unchanged. Therefore, we would have expected a more prominent change in the eigenvalues of the dynamical matrix. We assume that the symmetry exploits and the final symmetrization of the force-constant matrix discussed in section 5.3 reduces the impact of our refinement of the force formalism.

6. Density functional perturbation theory and the FLAPW method

So far, we have employed the finite-displacement (FD) method to calculate phonon band structures. This requires the setup of a supercell and only allows the exact computation of phonons whose wave vector is commensurable with the supercell. While the FD method can be used with any electronic structure code that can calculate reliable atomic forces and in addition it incorporates anharmonic effects if the atomic displacements are outside of the harmonic regime, the supercell setup increases the computation time of the underlying calculations unfavorably. The need of a supercell makes phonon calculations at small q-vectors computationally very expensive, nearly impossible.

A different approach to calculate phonon spectra is the usage of density functional perturbation theory (DFPT) [34, 36, 139]. In contrast to the FD approach, DFPT allows to obtain the dynamical matrix (DM) at any wave vector \boldsymbol{q} from computing a single unit cell in equilibrium. There is no need for a supercell. In DFPT, the linear response of the system due to a phonon of wave vector \boldsymbol{q} is computed by applying perturbation theory. Since it can be formulated variationally, the resulting scheme is very robust.

In this chapter, we first present the general theory of DFPT independent of the underlying electronic structure formalism and irrespective of the applied perturbation. Then, we focus on the FLAPW method and discuss Pulay and surface corrections that arise from the properties of the LAPW basis and wave functions. We are interested in phonons, which are specified by the eigenvectors and eigenvalues of the dynamical matrix. Since the DM is related to a second-order derivative of the total energy by Eqs. (5.2) and (5.9), we restrict ourselves to the second order in the responses. However, to keep this chapter as a general introduction to DFPT within the FLAPW method, the application of the results of this chapter to a phononic perturbation is presented in the next chapter.

6.1. Density functional perturbation theory

DFPT is the application of perturbation theory to the density functional formalism. Assume a system described by a Hamiltonian $\hat{\mathcal{H}}_0$ and a slightly different system $\hat{\mathcal{H}} = \hat{\mathcal{H}}_0 + [V_{\rm ext}(r) - V_{\rm ext}^{(0)}(r)]$, where the potential difference is a small perturbation of the original system. We will denote quantities belonging to the original unperturbed system with the label (0). In case of phonons, this perturbation is induced by a collective displacement of the atomic positions. Then, the external potential and all quantities X of the perturbed system can be expressed in terms of a small parameter λ that scales the perturbation:

$$V_{\text{ext}}(\mathbf{r}) = V_{\text{ext}}^{(0)}(\mathbf{r}) + \lambda V_{\text{ext}}^{(1)}(\mathbf{r}) + \frac{1}{2!} \lambda^2 V_{\text{ext}}^{(2)}(\mathbf{r}) + \dots$$
 (6.1)

6. Density functional perturbation theory and the FLAPW method

$$X(\lambda) = X^{(0)} + \lambda X^{(1)} + \frac{1}{2!} \lambda^2 X^{(2)} + \dots$$
 (6.2)

For example, the expansion of the DFT total energy $E_{\rm tot}$, Eq. (2.14), reads

$$E_{\text{tot,basic}} = E_{\text{tot,basic}}^{(0)} + \lambda E_{\text{tot,basic}}^{(1)} + \frac{\lambda^2}{2} E_{\text{tot,basic}}^{(2)} + \mathcal{O}(\lambda^3)$$
 (6.3)

with

$$E_{\text{tot,basic}}^{(0)} = \sum_{i} f_{i}^{(0)} \epsilon_{i}^{(0)} - \int \rho^{(0)}(\mathbf{r}) V_{\text{eff}}^{(0)}(\mathbf{r}) d^{3}r + \frac{1}{2} \iint \frac{\rho^{(0)}(\mathbf{r})\rho^{(0)}(\mathbf{r}')}{|\mathbf{r} - \mathbf{r}'|} d^{3}r' d^{3}r$$

$$+ \int \rho^{(0)}(\mathbf{r}) V_{\text{ext}}^{(0)}(\mathbf{r}) d^{3}r + \int \rho^{(0)}(\mathbf{r}) \varepsilon_{\text{xc}}^{(0)}[\rho^{(0)}](\mathbf{r}) d^{3}r + E_{\text{ii}}^{(0)}, \qquad (6.4)$$

$$E_{\text{tot,basic}}^{(1)} = \sum_{i} f_{i}^{(0)} \epsilon_{i}^{(1)} - \int \rho^{(1)}(\mathbf{r}) V_{\text{eff}}^{(0)}(\mathbf{r}) d^{3}r - \int \rho^{(0)}(\mathbf{r}) V_{\text{eff}}^{(1)}(\mathbf{r}) d^{3}r$$

$$+ \int \rho^{(1)}(\mathbf{r}) \int \frac{\rho^{(0)}(\mathbf{r}')}{|\mathbf{r} - \mathbf{r}'|} d^{3}r' d^{3}r + \int \rho^{(1)}(\mathbf{r}) V_{\text{ext}}^{(0)}(\mathbf{r}) d^{3}r$$

$$+ \int \rho^{(0)}(\mathbf{r}) V_{\text{ext}}^{(1)}(\mathbf{r}) d^{3}r + \int \rho^{(1)}(\mathbf{r}) \mu_{\text{xc}}^{(0)}[\rho^{(0)}](\mathbf{r}) d^{3}r + E_{\text{ii}}^{(1)}$$

$$= \sum_{i} f_{i}^{(0)} \epsilon_{i}^{(1)} - \int \rho^{(0)}(\mathbf{r}) V_{\text{eff}}^{(1)}(\mathbf{r}) d^{3}r + \int \rho^{(0)}(\mathbf{r}) V_{\text{ext}}^{(1)}(\mathbf{r}) d^{3}r + E_{\text{ii}}^{(1)}, \qquad (6.5)$$

and

$$\begin{split} E_{\rm tot,basic}^{(2)} &= \sum_{i} f_{i}^{(0)} \epsilon_{i}^{(2)} - \int \rho^{(2)}(\boldsymbol{r}) V_{\rm eff}^{(0)}(\boldsymbol{r}) d^{3}r - 2 \int \rho^{(1)}(\boldsymbol{r}) V_{\rm eff}^{(1)}(\boldsymbol{r}) d^{3}r \\ &- \int \rho^{(0)}(\boldsymbol{r}) V_{\rm eff}^{(2)}(\boldsymbol{r}) d^{3}r + \int \rho^{(2)}(\boldsymbol{r}) \int \frac{\rho^{(0)}(\boldsymbol{r'})}{|\boldsymbol{r} - \boldsymbol{r'}|} d^{3}r' d^{3}r \\ &+ \int \int \frac{\rho^{(1)}(\boldsymbol{r}) \rho^{(1)}(\boldsymbol{r'})}{|\boldsymbol{r} - \boldsymbol{r'}|} d^{3}r' d^{3}r + \int \rho^{(2)}(\boldsymbol{r}) V_{\rm ext}^{(0)}(\boldsymbol{r}) d^{3}r \\ &+ 2 \int \rho^{(1)}(\boldsymbol{r}) V_{\rm ext}^{(1)}(\boldsymbol{r}) d^{3}r + \int \rho^{(0)}(\boldsymbol{r}) V_{\rm ext}^{(2)}(\boldsymbol{r}) d^{3}r \\ &+ \int \rho^{(2)}(\boldsymbol{r}) \mu_{\rm xc}^{(0)}[\rho^{(0)}](\boldsymbol{r}) d^{3}r + \int \rho^{(1)}(\boldsymbol{r}) \mu_{\rm xc}^{(1)}[\rho^{(0)}](\boldsymbol{r}) d^{3}r + E_{\rm ii}^{(2)} \\ &= \sum_{i} f_{i}^{(0)} \epsilon_{i}^{(2)} - \int \rho^{(1)}(\boldsymbol{r}) V_{\rm eff}^{(1)}(\boldsymbol{r}) d^{3}r - \int \rho^{(0)}(\boldsymbol{r}) V_{\rm eff}^{(2)}(\boldsymbol{r}) d^{3}r \\ &+ \int \rho^{(1)}(\boldsymbol{r}) V_{\rm ext}^{(1)}(\boldsymbol{r}) d^{3}r + \int \rho^{(0)}(\boldsymbol{r}) V_{\rm ext}^{(2)}(\boldsymbol{r}) d^{3}r + E_{\rm ii}^{(2)}. \end{split} \tag{6.6}$$

Here, we made use of the fact that the occupation numbers do not contribute to the first-order change in energy as discussed in chapter 3.11, which is specifically true for phonons of non-vanishing q-vector in Refs. [34, 36]. We will mostly concentrate on $q \neq 0$. The energy contributions $E_{\rm ii}^{(i)}$ denote the ith order change in the ion-ion energy part. For $E_{\rm tot,basic}^{(1)}$, we employed Eq. (2.13) to obtain $\mu_{\rm xc}^{(0)}[\rho^{(0)}](r)$ from $\epsilon_{\rm xc}^{(0)}[\rho^{(0)}](r)$ and the integrals explicitly containing the first order density response $\rho^{(1)}$ cancel. Therefore, only the linear changes in

the eigenenergy $\epsilon_i^{(1)}$, in the effective potential $V_{\rm eff}^{(1)}(\boldsymbol{r})$ and external potential $V_{\rm ext}^{(1)}(\boldsymbol{r})$, and in the ion-ion energy $E_{\rm ii}^{(1)}$ have to be calculated. In the same manner, terms containing the second-order density response $\rho^{(2)}$ in the formula for $E_{\rm tot,basic}^{(2)}$ vanish, such that in addition $\rho^{(1)}(\boldsymbol{r})$, $\epsilon_i^{(2)}$, $V_{\rm eff}^{(2)}(\boldsymbol{r})$, $V_{\rm ext}^{(2)}(\boldsymbol{r})$, and $E_{\rm ii}^{(2)}$ need to be determined. We use the label 'basic' in light of the modifications that will be introduced when we consider the FLAPW method.

In the following, we will construct the first- and second-order changes of the KS eigenvalues and KS wave functions. The latter are required to construct the corresponding changes in the density.

6.1.1. First-order changes

From the prescription that the perturbed Kohn-Sham system is governed by the Schrödinger equation $\,$

$$\hat{\mathcal{H}}\psi_i(\mathbf{r}) = (\hat{T} + V_{\text{eff}}(\mathbf{r}))\psi_i(\mathbf{r}) = \epsilon_i\psi_i(\mathbf{r}), \tag{6.7}$$

and the orthonormalization of the states

$$\langle \psi_i | \psi_j \rangle = \delta_{ij}, \tag{6.8}$$

we reconstruct the unperturbed equations as the zeroth-order expansion in λ , when the λ expansion of all quantities involved is inserted:

$$(\hat{\mathcal{H}}_0 - \epsilon_i^{(0)})\psi_i^{(0)}(\mathbf{r}) = 0 \text{ and}$$
 (6.9)

$$\left\langle \psi_i^{(0)} \middle| \psi_j^{(0)} \right\rangle = \delta_{ij}$$
 (6.10)

The linearized Schrödinger equation is obtained from Eq. (6.7) by only considering the terms linear in the parameter λ . In this way, we obtain

$$(\hat{\mathcal{H}}_0 - \epsilon_i^{(0)})\psi_i^{(1)}(\mathbf{r}) = -(V_{\text{eff}}^{(1)}(\mathbf{r}) - \epsilon_i^{(1)})\psi_i^{(0)}(\mathbf{r}). \tag{6.11}$$

Eq. (6.11) is called the Sternheimer equation. It was first used to calculate atomic polarizabilities [37–40].

The first-order change in the eigenvalue $\epsilon_i^{(0)}$ is extracted from this equation by projecting it onto the state $\psi_i^{(0)}(\mathbf{r})$,

$$\epsilon_{i}^{(1)} = \left\langle \psi_{i}^{(0)} \middle| V_{\text{eff}}^{(1)} \middle| \psi_{i}^{(0)} \right\rangle + \left\langle \psi_{i}^{(0)} \middle| \hat{\mathcal{H}}_{0} - \epsilon_{i}^{(0)} \middle| \psi_{i}^{(1)} \right\rangle = \left\langle \psi_{i}^{(0)} \middle| V_{\text{eff}}^{(1)} \middle| \psi_{i}^{(0)} \right\rangle, \tag{6.12}$$

in accordance to the Hellmann-Feynman theorem. Here, we made use of the fact that $\psi_i^{(0)}(r)$ solves the unperturbed Schrödinger equation, Eq. (6.9), and applied the Hamiltonian to the left. We see now that a sum over all states as present in Eq. (6.5) turns the scalar product into $\int \rho^{(0)} V_{cl}^{(1)} d^3 r$. Therefore, Eq. (6.5) defining the first-order change in the total energy simplifies to

$$E_{\text{tot,basic}}^{(1),\text{simple}} = \int \rho^{(0)}(\mathbf{r}) V_{\text{ext}}^{(1)}(\mathbf{r}) d^3 r + E_{\text{ii}}^{(1)}.$$
 (6.13)

6. Density functional perturbation theory and the FLAPW method

This formula is reminiscent of Eq. (4.5), the Hellmann-Feynman part of the atomic force formula, if one considers the perturbation to be an atomic displacement.

The linearization of the orthonormality condition, Eq. (6.8), yields

$$\left\langle \psi_i^{(1)} \middle| \psi_j^{(0)} \right\rangle + \left\langle \psi_i^{(0)} \middle| \psi_j^{(1)} \right\rangle = 0. \tag{6.14}$$

The Sternheimer equation, Eq. (6.11), contains the linear response of the effective potential, which is the sum of the external, the Hartree, and the xc potential. Because the Hartree and xc potentials depend on the density, their first-order variations have to be determined self-consistently.

6.1.1.1. The self-consistent Sternheimer loop

Formally, the first-order change in the effective potential is given by the corresponding first-order changes of its components,

$$V_{\text{eff}}^{(1)}(\mathbf{r}) = V_{\text{H}}^{(1)}(\mathbf{r}) + V_{\text{ext}}^{(1)}(\mathbf{r}) + \mu_{\text{xc}}^{(1)}(\mathbf{r}), \tag{6.15a}$$

$$V_{\rm H}^{(1)}(\mathbf{r}) = \int \frac{\rho^{(1)}(\mathbf{r}')}{|\mathbf{r} - \mathbf{r}'|} d^3 r',$$
 (6.15b)

and

$$\mu_{\rm xc}^{(1)}(\mathbf{r}) = \rho^{(1)}(\mathbf{r}) \left. \frac{\delta \mu_{\rm xc}^{(0)}[\rho](\mathbf{r})}{\delta \rho(\mathbf{r})} \right|_{\rho = \rho^{(0)}}.$$
 (6.15c)

Physically, $V_{\rm H}^{(1)}({\bm r})$ and $\mu_{\rm xc}^{(1)}({\bm r})$ describe the screening of the external perturbation due to a rearrangement of the electrons. The variation of the xc potential $\delta\mu_{\rm xc}^{(0)}[\rho]({\bm r})/\delta\rho({\bm r})$, sometimes referred to as the (trace of the) exchange-correlation kernel, is independent of the actual perturbation. In Appendix A.2 we provide the formulas necessary to calculate the xc kernel for the LDA functional by Vosko, Wilk, and Nusair, to which we restrict ourselves in this work.

The first-order change in the electronic density is given by

$$\rho^{(1)}(\mathbf{r}) = \sum_{i}^{\text{occ}} f_i^{(0)} \left(\psi_i^{(1)*}(\mathbf{r}) \psi_i^{(0)}(\mathbf{r}) + \psi_i^{(0)*}(\mathbf{r}) \psi_i^{(1)}(\mathbf{r}) \right). \tag{6.16}$$

We see from Eq. (6.14) with i=j that the spatially averaged first-order change in density vanishes.

Together with Eq. (6.11), Eqs. (6.15) and (6.16) form a set of equations that has to be solved self-consistently, because the linear response of the wave functions depends on the linear response of the full effective potential, which in turn depends on the linear response of the density. The effort to obtain the density response is similar to the effort necessary to find the ground state density of a system.

To solve the Sternheimer equation, we expand the linear response $\psi_i^{(1)}(\mathbf{r})$ in terms of the unperturbed wave functions. Then we have for the first-order wave function response

$$\psi_i^{(1)}(\mathbf{r}) = \sum_j \psi_j^{(0)}(\mathbf{r}) \left\langle \psi_j^{(0)} \middle| \psi_i^{(1)} \right\rangle. \tag{6.17}$$

In the case of i=j, the linearized orthonormalization condition given in Eq. (6.14) is the sum of a complex number and its complex conjugate. Hence Eq. (6.14) indicates that the real part of $\langle \psi_i^{(0)} | \psi_i^{(1)} \rangle$ vanishes. Since $\psi_i^{(0)}(\mathbf{r})$ is defined only up to a phase factor, we can set it such that also the imaginary part of $\langle \psi_i^{(0)} | \psi_i^{(1)} \rangle$ is zero. Therefore, we can assume that $\psi_i^{(1)}(\mathbf{r})$ and $\psi_i^{(0)}(\mathbf{r})$ are orthogonal. For $i \neq j$, the expansion coefficient of the first-order change in the wave function can be found by projecting the Sternheimer equation onto $\psi_i^{(0)}(\mathbf{r})$. In this way, we obtain

$$\psi_i^{(1)}(\mathbf{r}) = \sum_{j \neq i} \psi_j^{(0)}(\mathbf{r}) \frac{\left\langle \psi_j^{(0)} \middle| V_{\text{eff}}^{(1)} \middle| \psi_i^{(0)} \right\rangle}{\epsilon_i^{(0)} - \epsilon_j^{(0)}}, \tag{6.18}$$

where we assumed non-degenerate states.

As an alternative way of solving the Sternheimer equation, one can invert it. However, the left-hand side of Eq. (6.11) is singular since $\epsilon_i^{(0)}$ is an eigenvalue of the unperturbed Hamiltonian $\hat{\mathcal{H}}_0$. Therefore, the Sternheimer equation has to be modified. To motivate an appropriate modification, we insert the expansion of the wave function response in terms of the unperturbed wave functions given by Eq. (6.18) into the density response, Eq. (6.16):

$$\rho^{(1)}(\mathbf{r}) = 2\Re\left(\sum_{i}^{\text{occ}} f_{i} \sum_{j}^{\text{unocc}} \psi_{i}^{(0)*}(\mathbf{r}) \psi_{j}^{(0)}(\mathbf{r}) \frac{\left\langle \psi_{j}^{(0)} \middle| V_{\text{eff}}^{(1)} \middle| \psi_{i}^{(0)} \right\rangle}{\epsilon_{i}^{(0)} - \epsilon_{j}^{(0)}} \right). \tag{6.19}$$

The part containing the j of the occupied states cancels out, because within the sum over the i, these terms appear twice, but with different sign. Therefore, the density response couples only occupied with unoccupied states. The Sternheimer equation consequently can be modified to generate the wave function response in the unoccupied or conduction bands by means of projectors \hat{P}_c :

$$\hat{P}_{c}(\hat{\mathcal{H}}_{0} - \epsilon_{i}^{(0)})\hat{P}_{c}\psi_{i}^{(1)}(\mathbf{r}) = -\hat{P}_{c}V_{\text{eff}}^{(1)}(\mathbf{r})\psi_{i}^{(0)}(\mathbf{r})$$
(6.20)

Since $\epsilon_i^{(0)}$ is the energy of an occupied state according to Eq. (6.19), the restriction of $(\hat{\mathcal{H}}_0 - \epsilon_i^{(0)})$ to the unoccupied states lifts its singularity.

Baroni et~al. state though [36], that the iterative algorithms commonly used to solve the Sternheimer equation, like the conjugate gradient [140–142] or minimal residual methods [143], maintain orthogonality to the occupied manifold during the iteration process if the starting solution was already orthogonal to it, regardless of whether the projectors are employed or not.

6.1.2. Second-order changes

In order to find the second-order change in eigenvalues and wave functions, which are for example required for Eq. (6.6), we consider the second-order expansion of the perturbed Schrödinger equation, Eq. (6.7), in terms of the parameter λ , which yields

$$(\hat{\mathcal{H}}_{0} - \epsilon_{i}^{(0)})\psi_{i}^{(2)}(\mathbf{r}) = -2(V_{\text{eff}}^{(1)}(\mathbf{r}) - \epsilon_{i}^{(1)})\psi_{i}^{(1)}(\mathbf{r}) - (V_{\text{off}}^{(2)}(\mathbf{r}) - \epsilon_{i}^{(2)})\psi_{i}^{(0)}(\mathbf{r}).$$
(6.21)

6. Density functional perturbation theory and the FLAPW method

In analogy to the calculation of the first-order variation $\epsilon_i^{(1)}$ in Eq. (6.12), we project Eq. (6.21) onto $\psi_i^{(0)}(\mathbf{r})$ and obtain

$$\epsilon_{i}^{(2)} = \left\langle \psi_{i}^{(0)} \middle| V_{\text{eff}}^{(2)} \middle| \psi_{i}^{(0)} \right\rangle + \left\langle \psi_{i}^{(0)} \middle| \hat{\mathcal{H}}_{0} - \epsilon_{i}^{(0)} \middle| \psi_{i}^{(2)} \right\rangle + 2 \left\langle \psi_{i}^{(0)} \middle| V_{\text{eff}}^{(1)} - \epsilon_{i}^{(1)} \middle| \psi_{i}^{(1)} \right\rangle. \tag{6.22a}$$

The term containing the second-order variation in the wave function vanishes when the Hamiltonian is applied to the left. A more convenient form can be obtained by introducing the term $2\left\langle \psi_i^{(1)} \middle| \hat{\mathcal{H}}_0 - \epsilon_i^{(0)} \middle| \psi_i^{(1)} \right\rangle + 2\left\langle \psi_i^{(1)} \middle| V_{\text{eff}}^{(1)} - \epsilon_i^{(1)} \middle| \psi_i^{(0)} \right\rangle$ into the expression, which is zero due to the Sternheimer equation, Eq. (6.11), giving rise to

$$\begin{split} \epsilon_{i}^{(2)} &= \left\langle \psi_{i}^{(0)} \middle| V_{\text{eff}}^{(2)} \middle| \psi_{i}^{(0)} \right\rangle + 2 \left\langle \psi_{i}^{(1)} \middle| \hat{\mathcal{H}}_{0} - \epsilon_{i}^{(0)} \middle| \psi_{i}^{(1)} \right\rangle \\ &+ 2 \left\langle \psi_{i}^{(1)} \middle| V_{\text{eff}}^{(1)} - \epsilon_{i}^{(1)} \middle| \psi_{i}^{(0)} \right\rangle + 2 \left\langle \psi_{i}^{(0)} \middle| V_{\text{eff}}^{(1)} - \epsilon_{i}^{(1)} \middle| \psi_{i}^{(1)} \right\rangle. \end{split} \tag{6.22b}$$

This form of $\epsilon_i^{(2)}$ is variational with respect to the first-order changes in the wave functions, $\psi_i^{(1)}(\mathbf{r})$. Variation of it with respect to $\psi_i^{(1)*}(\mathbf{r})$ or its complex conjugate reproduces the Sternheimer equation for $\psi_i^{(1)}(\mathbf{r})$ or $\psi_i^{(1)*}(\mathbf{r})$. The benefit from having a variational form of $\epsilon_i^{(2)}$ lies in the fact that small errors in $\psi_i^{(1)}(\mathbf{r})$ are further dampened when the second-order variation of the energy eigenvalues is calculated.

Finally, we apply once more the Sternheimer equation to $\epsilon_i^{(2)}$. Thereby, we transform the term containing $\psi_i^{(1)}(\boldsymbol{r})$ on both sides of the scalar product, $2\left\langle \psi_i^{(1)} \middle| \hat{\mathcal{H}}_0 - \epsilon_i^{(0)} \middle| \psi_i^{(1)} \right\rangle$, into $-\left\langle \psi_i^{(1)} \middle| V_{\text{eff}}^{(1)} - \epsilon_i^{(1)} \middle| \psi_i^{(0)} \right\rangle - \left\langle \psi_i^{(0)} \middle| V_{\text{eff}}^{(1)} - \epsilon_i^{(1)} \middle| \psi_i^{(1)} \right\rangle$. In this way, we obtain

$$\begin{split} \epsilon_{i}^{(2)} = & \left\langle \psi_{i}^{(0)} \middle| V_{\text{eff}}^{(2)} \middle| \psi_{i}^{(0)} \right\rangle + \int \left[\psi_{i}^{(1)*}(\boldsymbol{r}) \psi_{i}^{(0)}(\boldsymbol{r}) + \psi_{i}^{(0)*}(\boldsymbol{r}) \psi_{i}^{(1)}(\boldsymbol{r}) \right] V_{\text{eff}}^{(1)}(\boldsymbol{r}) d^{3}r \\ & - \epsilon_{i}^{(1)} \left[\left\langle \psi_{i}^{(1)} \middle| \psi_{i}^{(0)} \right\rangle + \left\langle \psi_{i}^{(0)} \middle| \psi_{i}^{(1)} \right\rangle \right]. \end{split} \tag{6.22c}$$

With the first-order variation in the orthonormality condition, Eq. (6.14), we find that the last term in the previous equation vanishes. Introducing $\rho_i^{(1)}(\mathbf{r}) = \psi_i^{(1)*}(\mathbf{r})\psi_i^{(0)}(\mathbf{r}) + \psi_i^{(0)*}(\mathbf{r})\psi_i^{(1)}(\mathbf{r})$ we have

$$\epsilon_i^{(2)} = \left\langle \psi_i^{(0)} \middle| V_{\text{eff}}^{(2)} \middle| \psi_i^{(0)} \right\rangle + \int \rho_i^{(1)}(\mathbf{r}) V_{\text{eff}}^{(1)}(\mathbf{r}) d^3 r. \tag{6.22d}$$

Employing this equation in the sum-over-states of Eq. (6.6), the integral containing the linear response in the effective potential cancels. Thus, the second-order change in the total energy simplifies to

$$E_{\text{tot,basic}}^{(2),\text{simple}} = \int \rho^{(1)}(\mathbf{r}) V_{\text{ext}}^{(1)}(\mathbf{r}) d^3 r + \int \rho^{(0)}(\mathbf{r}) V_{\text{ext}}^{(2)}(\mathbf{r}) d^3 r + E_{\text{ii}}^{(2)}.$$
(6.23)

Therefore, the calculation of $E_{\rm tot}^{(2)}$ requires the first-order changes in the density and the external potential and only the second-order changes in the external potential and in the ion-ion energy. Specifically, it does not require knowledge of the second-order variation in the wave functions. This observation is part of a more general theorem, which we discuss in the next section.

6.1.3. The 2n + 1 theorem

When we compare the expressions for the first- and second-order changes in the energy eigenvalues, Eqs. (6.12) and (6.22b), we observe that $\epsilon_i^{(1)}$ can be determined from the unperturbed wave functions $\psi_i^{(0)}(\mathbf{r})$ alone, while $\epsilon_i^{(2)}$ requires knowledge of the linear response $\psi_i^{(1)}(\mathbf{r})$ of the wave functions. This observation condensates in the '2n+1 theorem': The 2n+1st variation in the eigenenergy can be produced from the first n variations in the wave function corresponding to that eigenvalue [144–147].

This statement is true for any functional dependent on $\psi_i(\mathbf{r})$ [148], not only for the energy functional of the KS system. Thus, it holds also for the DFT total energy. The independence of Eqs. (6.13) and (6.23) from $\rho^{(1)}(\mathbf{r})$ and $\rho^{(2)}(\mathbf{r})$, respectively, supports the validity of the 2n+1 theorem.

6.2. Adjustment to the FLAPW method

In the following sections, we adapt the DFPT formalism to comply with the properties of the FLAPW method.

The LAPW basis functions $\phi_{kG}(r)$ depend on the perturbation. Hence, for the wave functions expressed in terms of the LAPW basis, the expansion into orders of λ introduced in Eqs. (6.1) and (6.2) holds on the level of the expansion coefficients z_{ikG} and the basis functions. If we allow that the perturbation changes the Bloch character of the unperturbed state $\psi_{ik}^{(0)}(r)$ from k to a linear combination of vectors K, we can write for the perturbed state

$$\psi_{i\mathbf{k}}(\mathbf{r}) = \sum_{\mathbf{G}} z_{\mathbf{k}\mathbf{G}}^{i\mathbf{k}(0)} \phi_{\mathbf{k}\mathbf{G}}^{(0)}(\mathbf{r}) + \lambda \sum_{\mathbf{K}\mathbf{G}} \left[z_{\mathbf{K}\mathbf{G}}^{i\mathbf{k}(1)} \phi_{\mathbf{K}\mathbf{G}}^{(0)}(\mathbf{r}) + z_{\mathbf{K}\mathbf{G}}^{i\mathbf{k}(0)} \phi_{\mathbf{K}\mathbf{G}}^{(1)}(\mathbf{r}) \right]$$

$$+ \frac{1}{2!} \lambda^{2} \sum_{\mathbf{K}\mathbf{G}} \left[z_{\mathbf{K}\mathbf{G}}^{i\mathbf{k}(2)} \phi_{\mathbf{K}\mathbf{G}}^{(0)}(\mathbf{r}) + 2 z_{\mathbf{K}\mathbf{G}}^{i\mathbf{k}(1)} \phi_{\mathbf{K}\mathbf{G}}^{(1)}(\mathbf{r}) + z_{\mathbf{K}\mathbf{G}}^{i\mathbf{k}(0)} \phi_{\mathbf{K}\mathbf{G}}^{(2)}(\mathbf{r}) \right] + \mathcal{O}(\lambda^{3}). \quad (6.24)$$

We introduced here the uniform notation $z_{KG}^{ik(n)}$ for the *n*th-order variation in the expansion coefficient of the state $\psi_{ik}^{(0)}(r)$. K is a particular Bloch vector, into which the perturbation scatters the unperturbed wave function. For n=0, it holds that

$$z_{KG}^{ik(0)} = \delta_{kK} z_{ikG}^{(0)} \tag{6.25}$$

with the unperturbed expansion coefficient $z_{i\mathbf{k}\mathbf{G}}^{(0)}$.

The term in Eq. (6.24) which is linear in λ indicates that the first-order change of the wave function decomposes into a component $\hat{\psi}_{ik}^{(1)}(r)$ that is contained within the Hilbert space spanned by the LAPW basis functions and a component $\tilde{\psi}_{ik}^{(1)}(r)$ which lives at least partly outside of the LAPW basis space:

$$\hat{\psi}_{ik}^{(1)}(\mathbf{r}) := \sum_{KG} z_{KG}^{ik(1)} \phi_{KG}^{(0)}(\mathbf{r})$$
 (6.26a)

$$\tilde{\psi}_{i\mathbf{k}}^{(1)}(\mathbf{r}) := \sum_{\mathbf{K}\mathbf{G}} z_{\mathbf{K}\mathbf{G}}^{i\mathbf{k}(0)} \phi_{\mathbf{K}\mathbf{G}}^{(1)}(\mathbf{r})$$
(6.26b)

$$\psi_{ik}^{(1)}(\mathbf{r}) = \hat{\psi}_{ik}^{(1)}(\mathbf{r}) + \tilde{\psi}_{ik}^{(1)}(\mathbf{r})$$
(6.26c)

6. Density functional perturbation theory and the FLAPW method

For the moment, we assume $\tilde{\psi}_{ik}^{(1)}(r)$ to be known already. Its exact form depends on the perturbation, which we do not specify until the next chapter to keep the generality of this chapter.

During the derivation of DFPT in the last section we made use of

$$\left\langle \psi_{ik}^{(1)} \middle| \hat{\mathcal{H}}_0 \middle| \psi_{ik}^{(0)} \right\rangle = \epsilon_{ik}^{(0)} \left\langle \psi_{ik}^{(1)} \middle| \psi_{ik}^{(0)} \right\rangle. \tag{6.27}$$

However, this equation does only hold for the part $\hat{\psi}_{ik}^{(1)}(r)$ which is contained in the LAPW basis space. Hence, we need to consider additional Pulay terms as discussed in chapter 3.10 when we apply DFPT within the FLAPW method.

In addition we need to take into account surface terms if the perturbation arises from a displacement of the atomic positions, as is the case for example for forces or phonons. The reason for this is that the LAPW basis functions are constructed to be continuous only up to first order at the muffin-tin sphere boundaries, while the Hamiltonian contains the Laplace operator and thus generates the second derivative of the wave functions. Also, the FLAPW method uses a different representation of its functions in terms of radial functions times spherical harmonics in the atom centered muffin-tin spheres and in terms of a Fourier expansion in the interstitial region which does only match up to an angular-momentum cutoff of $l_{\rm max}^{\alpha}$. Thus, a slight discontinuity of the functions is also present in zeroth and first order

In case of a displacive perturbation, we assume that the displacement is mediated by a shift of the atoms from their position τ_{α} to $\tau_{\alpha} + w_{\alpha}$, were w_{α} is a real-valued vector. Also, we introduce the short hand notation

$$[f(\mathbf{r})]_{SF} := f^{MT}(\mathbf{r}) - f^{IR}(\mathbf{r})$$
(6.28)

for the difference between the muffin-tin sphere and the interstitial representation of a quantity f(r).

As we did in the previous section 6.1, we devote separate subsections to the first-order changes and the second-order changes.

6.2.1. Additional first-order changes

In contrast to Eq. (6.12), we have to account for Pulay terms when we calculate the first-order variation in the eigenenergies within the FLAPW method. Since the wave functions are solutions to the Schrödinger equation only within the LAPW basis space, we have to calculate $\epsilon_{ik}^{(1)}$ from the Rayleigh quotient, as we did in Eq. (3.80):

$$\epsilon_{i\mathbf{k},\text{FLAPW}}^{(1)} = \left\langle \psi_{i\mathbf{k}}^{(0)} \middle| V_{\text{eff}}^{(1)} \middle| \psi_{i\mathbf{k}}^{(0)} \right\rangle + \left\langle \psi_{i\mathbf{k}}^{(1)} \middle| \hat{\mathcal{H}}_{0} - \epsilon_{i\mathbf{k}}^{(0)} \middle| \psi_{i\mathbf{k}}^{(0)} \right\rangle + \left\langle \psi_{i\mathbf{k}}^{(0)} \middle| \hat{\mathcal{H}}_{0} - \epsilon_{i\mathbf{k}}^{(0)} \middle| \psi_{i\mathbf{k}}^{(1)} \right\rangle
+ \sum_{\alpha} \mathbf{w}_{\alpha}^{\text{T}} \cdot \oint_{\partial \text{MT}(\alpha)} \hat{\mathbf{e}} \left[\psi_{i\mathbf{k}}^{(0)*}(\mathbf{r}) \left(\hat{\mathcal{H}}_{0} - \epsilon_{i\mathbf{k}}^{(0)} \right) \psi_{i\mathbf{k}}^{(0)}(\mathbf{r}) \right]_{\text{SF}} dS$$
(6.29)

The surface integral appears analogously to Eq. (4.3) only in case of a displacive perturbation. \hat{e} is the unit normal vector $(r - \tau_{\alpha})/|r - \tau_{\alpha}|$ pointing out of the MT sphere of

atom α . The sum-over-states in Eq. (6.5) defining $E_{\rm tot,basic}^{(1)}$, into which we have to insert Eq. (6.29), transforms the first term of $\epsilon_{i\mathbf{k},{\rm FLAPW}}^{(1)}$ into $\int \rho^{(0)}(r)V_{\rm eff}^{(1)}(r)d^3r$. Thus it cancels with its counterpart in Eq. (6.5). We extract the other two scalar products from Eq. (6.29) and define the Pulay correction

$$E_{\text{tot,Pulay}}^{(1)} = \sum_{i\mathbf{k}} f_{i\mathbf{k}}^{(0)} \left[\left\langle \psi_{i\mathbf{k}}^{(1)} \middle| \hat{\mathcal{H}}_0 - \epsilon_{i\mathbf{k}}^{(0)} \middle| \psi_{i\mathbf{k}}^{(0)} \right\rangle + \left\langle \psi_{i\mathbf{k}}^{(0)} \middle| \hat{\mathcal{H}}_0 - \epsilon_{i\mathbf{k}}^{(0)} \middle| \psi_{i\mathbf{k}}^{(1)} \right\rangle \right]. \tag{6.30}$$

If the perturbation affects the atomic positions, the complete surface correction follows from collecting the surface integrals generated by the linear variation of the unperturbed total energy, Eq. (6.4). The surface term in the variation of the eigenenergies, Eq. (6.29), is then accompanied by the surface terms which are generated by separating the domains of integration in the volume integrals of Eq. (6.4) into MT and IR volumes and applying the variation. This procedure yields

$$E_{\text{tot,SF}}^{(1)} = \sum_{i\boldsymbol{k}} f_{i\boldsymbol{k}}^{(0)} \sum_{\alpha} \boldsymbol{w}_{\alpha}^{\text{T}} \cdot \oint_{\partial MT(\alpha)} \hat{\boldsymbol{e}} \left[\psi_{i\boldsymbol{k}}^{(0)*}(\boldsymbol{r}) \left(\hat{\mathcal{H}}_{0} - \epsilon_{i\boldsymbol{k}}^{(0)} \right) \psi_{i\boldsymbol{k}}^{(0)}(\boldsymbol{r}) \right]_{\text{SF}} dS$$

$$- \sum_{\alpha} \boldsymbol{w}_{\alpha}^{\text{T}} \cdot \oint_{\partial MT(\alpha)} \hat{\boldsymbol{e}} \left[\rho^{(0)}(\boldsymbol{r}) V_{\text{eff}}^{(0)}(\boldsymbol{r}) \right]_{\text{SF}} dS$$

$$+ \sum_{\alpha} \boldsymbol{w}_{\alpha}^{\text{T}} \cdot \oint_{\partial MT(\alpha)} \hat{\boldsymbol{e}} \left[\rho^{(0)}(\boldsymbol{r}) \left\{ V_{\text{H}}^{(0)}(\boldsymbol{r}) + V_{\text{ext}}^{(0)}(\boldsymbol{r}) + \varepsilon_{\text{xc}}^{(0)}(\boldsymbol{r}) \right\} \right]_{\text{SF}} dS$$

$$= \sum_{i\boldsymbol{k}} f_{i\boldsymbol{k}}^{(0)} \sum_{\alpha} \boldsymbol{w}_{\alpha}^{\text{T}} \cdot \oint_{\partial MT(\alpha)} \hat{\boldsymbol{e}} \left[\psi_{i\boldsymbol{k}}^{(0)*}(\boldsymbol{r}) \left(\hat{\mathcal{H}}_{0} - \epsilon_{i\boldsymbol{k}}^{(0)} \right) \psi_{i\boldsymbol{k}}^{(0)}(\boldsymbol{r}) \right]_{\text{SF}} dS$$

$$+ \sum_{\alpha} \boldsymbol{w}_{\alpha}^{\text{T}} \cdot \oint_{\partial MT(\alpha)} \hat{\boldsymbol{e}} \left[\rho^{(0)}(\boldsymbol{r}) \left\{ \varepsilon_{\text{xc}}^{(0)}(\boldsymbol{r}) - \mu_{\text{xc}}^{(0)}(\boldsymbol{r}) \right\} \right]_{\text{SF}} dS. \tag{6.31}$$

In total, starting from the simplified formula for the first-order change $E_{\rm tot,basic}^{(1),\rm simple}$ of the total energy given in Eq. (6.13), its FLAPW counterpart is complemented by a Pulay and a surface term,

$$E_{\text{tot}}^{(1)} = E_{\text{tot,basic}}^{(1),\text{simple}} + E_{\text{tot,Pulay}}^{(1)} + E_{\text{tot,SF}}^{(1)}.$$
 (6.32)

In case of atomic displacements, the first-order change in the total energy within the FLAPW method corresponds exactly to the force formulas in Eqs. (4.7)-(4.9).

We also present the form which the linearized orthonormalization condition takes in the FLAPW method:

$$\left\langle \psi_{jl}^{(1)} \middle| \psi_{ik}^{(0)} \right\rangle + \left\langle \psi_{jl}^{(0)} \middle| \psi_{ik}^{(1)} \right\rangle + \sum_{\alpha} \boldsymbol{w}_{\alpha}^{\mathrm{T}} \cdot \oint_{\partial \mathrm{MT}(\alpha)} \hat{\boldsymbol{e}} \left[\psi_{jl}^{(0)*} \psi_{ik}^{(0)} \right]_{\mathrm{SF}} dS = 0 \tag{6.33}$$

Also here, a surface integral has to be added if the perturbation affects the domain of integration, since the orthonormalization condition is an integral. For $(i\mathbf{k})=(j\mathbf{l})$, the expression transforms into

$$2\Re\left(\left\langle \psi_{i\boldsymbol{k}}^{(0)} \middle| \psi_{i\boldsymbol{k}}^{(1)} \right\rangle\right) + \sum_{\alpha} \boldsymbol{w}_{\alpha}^{\mathrm{T}} \cdot \oint_{\partial \mathrm{MT}(\alpha)} \hat{\boldsymbol{e}} \left[\rho_{i\boldsymbol{k}}^{(0)}(\boldsymbol{r})\right]_{\mathrm{SF}} dS = 0 \tag{6.34}$$

6. Density functional perturbation theory and the FLAPW method

with the $(i\mathbf{k})$ component of the unperturbed density defined by $\rho^{(0)}(\mathbf{r}) = \sum_{i\mathbf{k}} f_{i\mathbf{k}}^{(0)} \rho_{i\mathbf{k}}^{(0)}(\mathbf{r})$. We have the liberty to choose the phase of $\psi_{i\mathbf{k}}^{(0)}(\mathbf{r})$ such that $\langle \psi_{i\mathbf{k}}^{(0)} | \psi_{i\mathbf{k}}^{(1)} \rangle$ is real-valued itself. The linearized orthonormalization condition then takes the form

$$\left\langle \psi_{i\mathbf{k}}^{(0)} \middle| \psi_{i\mathbf{k}}^{(1)} \right\rangle = -\frac{1}{2} \sum_{\alpha} \mathbf{w}_{\alpha}^{\mathrm{T}} \cdot \oint_{\partial \mathrm{MT}(\alpha)} \hat{\mathbf{e}} \left[\rho_{i\mathbf{k}}^{(0)}(\mathbf{r}) \right]_{\mathrm{SF}} dS. \tag{6.35}$$

Therefore, if the perturbation affects the atomic positions, the first-order change of the wave function is not orthogonal to the unperturbed wave function anymore. Though we expect the projection to be small.

6.2.1.1. The Sternheimer loop within the FLAPW method

Since in the FLAPW method the wave functions are variational solutions of the Schrödinger equation, the derivation of the Sternheimer equation, Eq. (6.11), is more complex. We start the derivation by projecting the Sternheimer equation onto the LAPW basis function $\phi_{LG'}(r)$, since the Schrödinger equation is fulfilled in the LAPW basis space. This yields the matrix equation

$$\left\langle \phi_{LG'} \middle| \hat{\mathcal{H}} - \epsilon_{ik} \middle| \psi_{ik} \right\rangle = \sum_{KG} \left\langle \phi_{LG'} \middle| \hat{\mathcal{H}} - \epsilon_{ik} \middle| \phi_{KG} \right\rangle z_{KG}^{ik} = 0.$$
 (6.36)

The linearized form of this equation is the Sternheimer equation for the first-order responses of the expansion coefficients:

$$\sum_{KG} \left\langle \phi_{LG'}^{(0)} \middle| \hat{\mathcal{H}}_{0} - \epsilon_{ik}^{(0)} \middle| \phi_{KG}^{(0)} \right\rangle z_{KG}^{ik(1)}$$

$$= -\sum_{KG} \left\{ \left\langle \phi_{LG'}^{(0)} \middle| V_{\text{eff}}^{(1)} - \epsilon_{ik}^{(1)} \middle| \phi_{KG}^{(0)} \right\rangle + \left\langle \phi_{LG'}^{(0)} \middle| \hat{\mathcal{H}}_{0} - \epsilon_{ik}^{(0)} \middle| \phi_{KG}^{(1)} \right\rangle + \left\langle \phi_{LG'}^{(0)} \middle| \hat{\mathcal{H}}_{0} - \epsilon_{ik}^{(0)} \middle| \phi_{KG}^{(1)} \right\rangle + \sum_{\alpha} w_{\alpha}^{\text{T}} \cdot \oint_{\partial \text{MT}(\alpha)} \hat{e} \left[\phi_{LG'}^{(0)*} (\hat{\mathcal{H}}_{0} - \epsilon_{ik}^{(0)}) \phi_{KG}^{(0)} \right]_{\text{SF}} dS \right\} z_{KG}^{ik(0)}, \tag{6.37}$$

In order to solve the Sternheimer equation, we need knowledge about the variation of the effective potential and of the electronic density. To this end, we reuse Eqs. (6.15a) and (6.16). However, in the case of a displacive perturbation, the linear change in the Hartree potential contributes an additional surface term in the FLAPW framework, since the electronic density is slightly discontinuous at the MT sphere boundary. Therefore, the adjusted set of equations is given by

$$V_{\text{eff}}^{(1)}(\mathbf{r}) = V_{\text{H}}^{(1)}(\mathbf{r}) + V_{\text{ext}}^{(1)}(\mathbf{r}) + \rho^{(1)}(\mathbf{r}) \left. \frac{\delta \mu_{\text{xc}}^{(0)}[\rho](\mathbf{r})}{\delta \rho(\mathbf{r})} \right|_{\rho = \rho^{(0)}}, \tag{6.15a revisited}$$

$$V_{\mathrm{H}}^{(1)}(\boldsymbol{r}) = \sum_{\alpha} \boldsymbol{w}_{\alpha}^{\mathrm{T}} \cdot \oint_{\partial \mathrm{MT}(\alpha)} \hat{\boldsymbol{e}}' \frac{\left[\rho^{(0)}(\boldsymbol{r}')\right]_{\mathrm{SF}}}{|\boldsymbol{r} - \boldsymbol{r}'|} dS' + \int \frac{\rho^{(1)}(\boldsymbol{r}')}{|\boldsymbol{r} - \boldsymbol{r}'|} d^{3}r', \tag{6.38}$$

$$\rho^{(1)}(\mathbf{r}) = \sum_{i\mathbf{k}} f_{i\mathbf{k}}^{(0)} \left(\psi_{i\mathbf{k}}^{(1)*}(\mathbf{r}) \psi_{i\mathbf{k}}^{(0)}(\mathbf{r}) + \psi_{i\mathbf{k}}^{(0)*}(\mathbf{r}) \psi_{i\mathbf{k}}^{(1)}(\mathbf{r}) \right). \tag{6.16 revisited}$$

It is instructive to transform Eq. (6.37), the Sternheimer matrix equation, into a form more reminiscent of the standard perturbation theory expression, Eq. (6.18). In order to do so, we recall the separation of $\psi_{ik}^{(1)}(r)$ into $\hat{\psi}_{ik}^{(1)}(r)$ and $\hat{\psi}_{ik}^{(1)}(r)$ as introduced in Eq. (6.26). The component $\hat{\psi}_{ik}^{(1)}(r)$ is a linear combination of LAPW basis functions and thus completely contained in the LAPW basis space. Therefore, it can be expanded purely in terms of the LAPW wave functions:

$$\hat{\psi}_{ik}^{(1)}(r) = \sum_{il} \psi_{jl}^{(0)}(r) \left\langle \psi_{jl}^{(0)} \middle| \hat{\psi}_{ik}^{(1)} \right\rangle$$
(6.39)

The component $\tilde{\psi}_{ik}^{(1)}(r)$ in general is not confined to the Hilbert space spanned by the LAPW basis functions.

We now operate with $\sum_{LG'} z_{LG'}^{jl(0)*}$ on Eq. (6.36). A contraction of the sums yields

$$\sum_{\mathbf{L}\mathbf{G}'} \sum_{\mathbf{K}\mathbf{G}} z_{\mathbf{L}\mathbf{G}'}^{jl(0)*} \left\langle \phi_{\mathbf{L}\mathbf{G}'}^{(0)} | \hat{\mathcal{H}}_{0} - \epsilon_{i\mathbf{k}}^{(0)} | \phi_{\mathbf{K}\mathbf{G}}^{(0)} \right\rangle z_{\mathbf{K}\mathbf{G}}^{i\mathbf{k}(1)} = \left\langle \psi_{jl}^{(0)} | \epsilon_{jl}^{(0)} - \epsilon_{i\mathbf{k}}^{(0)} | \hat{\psi}_{i\mathbf{k}}^{(1)} \right\rangle
= -\left\langle \psi_{jl}^{(0)} | V_{\text{eff}}^{(1)} - \epsilon_{i\mathbf{k}}^{(1)} | \psi_{i\mathbf{k}}^{(0)} \right\rangle - \left\langle \tilde{\psi}_{jl}^{(1)} | \hat{\mathcal{H}}_{0} - \epsilon_{i\mathbf{k}}^{(0)} | \psi_{i\mathbf{k}}^{(0)} \right\rangle - \left\langle \psi_{jl}^{(0)} | \hat{\mathcal{H}}_{0} - \epsilon_{i\mathbf{k}}^{(0)} | \tilde{\psi}_{i\mathbf{k}}^{(1)} \right\rangle
- \sum_{\alpha} \mathbf{w}_{\alpha} \cdot \oint_{\partial \mathbf{MT}(\alpha)} \hat{\mathbf{e}} \left[\psi_{jl}^{(0)*} (\hat{\mathcal{H}}_{0} - \epsilon_{i\mathbf{k}}^{(0)}) \psi_{i\mathbf{k}}^{(0)} \right]_{\text{SF}} dS,$$
(6.40)

or equivalently for $(j\mathbf{l}) \neq (i\mathbf{k})$:

$$\left\langle \psi_{jl}^{(0)} \middle| \hat{\psi}_{ik}^{(1)} \right\rangle = \frac{\left\langle \psi_{jl}^{(0)} \middle| \psi_{ik}^{(0)} \right\rangle}{\epsilon_{ik}^{(0)} - \epsilon_{jl}^{(0)}} + \frac{\left\langle \tilde{\psi}_{jl}^{(1)} \middle| \hat{\mathcal{H}}_{0} - \epsilon_{ik}^{(0)} \middle| \psi_{ik}^{(0)} \right\rangle}{\epsilon_{ik}^{(0)} - \epsilon_{jl}^{(0)}} + \frac{\left\langle \psi_{jl}^{(0)} \middle| \hat{\mathcal{H}}_{0} - \epsilon_{jl}^{(0)} \middle| \hat{\psi}_{ik}^{(1)} \right\rangle}{\epsilon_{ik}^{(0)} - \epsilon_{jl}^{(0)}} + \sum_{\alpha} w_{\alpha} \cdot \oint_{\partial \text{MT}(\alpha)} \hat{e} \left[\frac{\psi_{jl}^{(0)*} (\hat{\mathcal{H}}_{0} - \epsilon_{ik}^{(0)}) \psi_{ik}^{(0)}}{\epsilon_{ik}^{(0)} - \epsilon_{jl}^{(0)}} \right]_{\text{SF}} dS - \left\langle \psi_{jl}^{(0)} \middle| \tilde{\psi}_{ik}^{(1)} \right\rangle$$
(6.41)

In the case $(j\mathbf{l}) = (i\mathbf{k})$ we apply Eq. (6.35) and find the relation

$$\left\langle \psi_{i\boldsymbol{k}}^{(0)} \middle| \hat{\psi}_{i\boldsymbol{k}}^{(1)} \right\rangle = -\left\langle \psi_{i\boldsymbol{k}}^{(0)} \middle| \tilde{\psi}_{i\boldsymbol{k}}^{(1)} \right\rangle - \frac{1}{2} \sum_{\alpha} \boldsymbol{w}_{\alpha}^{\mathrm{T}} \cdot \oint_{\partial \mathrm{MT}(\alpha)} \hat{\boldsymbol{e}} \left[\rho_{i\boldsymbol{k}}^{(0)}(\boldsymbol{r}) \right]_{\mathrm{SF}} dS. \tag{6.42}$$

Using Eq. (6.39) we can now express the first-order change in the wave function as

$$\begin{split} \psi_{i\boldsymbol{k}}^{(1)}(\boldsymbol{r}) &= \sum_{jl} \psi_{jl}^{(0)}(\boldsymbol{r}) \left\langle \psi_{jl}^{(0)} \middle| \hat{\psi}_{i\boldsymbol{k}}^{(1)} \right\rangle + \tilde{\psi}_{i\boldsymbol{k}}^{(1)}(\boldsymbol{r}) \\ &= \sum_{jl \neq i\boldsymbol{k}} \psi_{jl}^{(0)}(\boldsymbol{r}) \left\{ C_{i\boldsymbol{k}jl}^{\text{PT}} + C_{i\boldsymbol{k}jl}^{\text{Pulay}} + C_{i\boldsymbol{k}jl}^{\text{surface}} \right\} + \psi_{i\boldsymbol{k}}^{(0)}(\boldsymbol{r}) C_{i\boldsymbol{k}}^{\text{surface}} + \psi_{i\boldsymbol{k}}^{\text{IBC}}(\boldsymbol{r}) \end{split}$$
(6.43)

which dismantles $\psi_{i\mathbf{k}}^{(1)}(\mathbf{r})$ into four parts:

• The regular perturbation theory coefficients $C^{\rm PT}_{ikjl}$ we already found in Eq. (6.18) in chapter 6.1.1,

$$C_{ikjl}^{\text{PT}} = \frac{\left\langle \psi_{jl}^{(0)} \middle| V_{\text{eff}}^{(1)} \middle| \psi_{ik}^{(0)} \right\rangle}{\epsilon_{ik}^{(0)} - \epsilon_{il}^{(0)}}.$$
 (6.44)

- 6. Density functional perturbation theory and the FLAPW method
 - The Pulay contribution C_{kil}^{Pulay} discussed in chapter 3.10, which arises because the LAPW basis is dependent on the perturbation and the wave functions are only variational solutions of the Schrödinger equation,

$$C_{ikjl}^{\text{Pulay}} = \frac{\left\langle \tilde{\psi}_{jl}^{(1)} \middle| \hat{\mathcal{H}}_{0} - \epsilon_{ik}^{(0)} \middle| \psi_{ik}^{(0)} \right\rangle}{\epsilon_{ik}^{(0)} - \epsilon_{jl}^{(0)}} + \frac{\left\langle \psi_{jl}^{(0)} \middle| \hat{\mathcal{H}}_{0} - \epsilon_{jl}^{(0)} \middle| \tilde{\psi}_{ik}^{(1)} \right\rangle}{\epsilon_{ik}^{(0)} - \epsilon_{jl}^{(0)}}. \tag{6.45}$$

• The surface terms $C^{\text{surface}}_{ikjl}$ and C^{surface}_{ik} that take into account the small discontinuities of the wave functions at the muffin-tin sphere boundary,

$$C_{ikjl}^{\text{surface}} = \sum_{\alpha} \boldsymbol{w}_{\alpha} \cdot \oint_{\partial \text{MT}(\alpha)} \hat{\boldsymbol{e}} \left[\frac{\psi_{jl}^{(0)*} (\hat{\mathcal{H}}_{0} - \epsilon_{ik}^{(0)}) \psi_{ik}^{(0)}}{\epsilon_{ik}^{(0)} - \epsilon_{jl}^{(0)}} \right]_{\text{SF}} dS$$
(6.46a)

and

$$C_{i\boldsymbol{k}}^{\text{surface}} = -\frac{1}{2} \sum_{\alpha} \boldsymbol{w}_{\alpha} \cdot \oint_{\partial \text{MT}(\alpha)} \hat{\boldsymbol{e}} \left[\rho_{i\boldsymbol{k}}^{(0)}(\boldsymbol{r}) \right]_{\text{SF}} dS.$$
 (6.46b)

• The function $\psi_{ik}^{\mathrm{IBC}}(r)$ which results from the explicit response of the LAPW basis functions which is not contained in the LAPW basis space and which thus compensates the incompleteness of the basis functions,

$$\psi_{i\mathbf{k}}^{\text{IBC}}(\mathbf{r}) = \int \left(\delta(\mathbf{r} - \mathbf{r}') - \sum_{jl} \psi_{jl}^{(0)}(\mathbf{r}) \psi_{jl}^{(0)*}(\mathbf{r}') \right) \tilde{\psi}_{i\mathbf{k}}^{(1)}(\mathbf{r}') d^3 r'.$$
 (6.47)

The terms $C_{ikjl}^{\rm surface}$ and $C_{ik}^{\rm surface}$ only arise when the perturbation alters the domains of integration, which is the case for phonons. Betzinger *et al.* [149] presented a similar decomposition in the context of the optimized-effective potential approach. In this method, the perturbation does not affect the domains of integration, hence the surface terms do not appear.

Making the basis set more and more complete, the contributions of C^{Pulay}_{ik} and $\psi^{\text{IBC}}_{ik}(r)$ will become smaller. If specifically more l-channels are considered in the spherical-harmonics expansion within the muffin-tin spheres, the surface contributions C^{surface}_{ik} and C^{surface}_{ik} will diminish and only the result of conventional perturbation theory will persist.

Eqs. (6.35) and (6.43) guarantee that the number of electrons $N_{\rm el}$ is conserved within the FLAPW method also by a displacive perturbation. Applying a variation to

$$N_{\rm el} = \int \rho^{(0)}(\mathbf{r})d^3r$$
 (6.48)

yields the expression

$$0 = \sum_{i\mathbf{k}} f_{i\mathbf{k}}^{(0)} \left[\left\langle \psi_{i\mathbf{k}}^{(1)} \middle| \psi_{i\mathbf{k}}^{(0)} \right\rangle + \left\langle \psi_{i\mathbf{k}}^{(0)} \middle| \psi_{i\mathbf{k}}^{(1)} \right\rangle \right] + \sum_{\alpha} \boldsymbol{w}_{\alpha}^{\mathrm{T}} \cdot \oint_{\partial \mathrm{MT}(\alpha)} \hat{\boldsymbol{e}} \left[\rho^{(0)}(\boldsymbol{r}) \right]_{\mathrm{SF}} dS, \quad (6.49)$$

which is true for $\psi_{i\mathbf{k}}^{(1)}(\mathbf{r})$ as defined in Eq. (6.43).

6.2.2. Additional second-order changes

The second-order change in the total energy obtained within the FLAPW method is also affected by Pulay corrections and in case of a displacive perturbation also by surface corrections. The latter are obtained in second order not only from a variation of the response of the energy eigenvalues and a variation of the volume integrals in Eq. (6.5), but also from an additional variation of the surface terms $E_{\text{tot,SF}}^{(1)}$. To avoid miscounting these terms, we postpone the calculation of $E_{\text{tot,SF}}^{(2)}$ to the end of this section.

We first construct the second-order Pulay correction under the assumption that the perturbation is non-displacive. To this end, we apply an additional variation to the first-order variation of the eigenenergies, Eq. (6.29), and omit any surface terms in the original and resulting equation. In this way, we obtain

$$\epsilon_{i\mathbf{k},\text{FLAPW}}^{(2)} = \left\langle \psi_{i\mathbf{k}}^{(0)} \middle| V_{\text{eff}}^{(0)} \middle| \psi_{i\mathbf{k}}^{(0)} \right\rangle + 2 \int \rho_{i\mathbf{k}}^{(1)}(r) V_{\text{eff}}^{(1)}(r) d^3 r + 2 \left\langle \psi_{i\mathbf{k}}^{(1)} \middle| \hat{\mathcal{H}}_0 - \epsilon_{i\mathbf{k}}^{(0)} \middle| \psi_{i\mathbf{k}}^{(1)} \right\rangle \\
+ \left\langle \psi_{i\mathbf{k}}^{(2)} \middle| \hat{\mathcal{H}}_0 - \epsilon_{i\mathbf{k}}^{(0)} \middle| \psi_{i\mathbf{k}}^{(0)} \right\rangle + \left\langle \psi_{i\mathbf{k}}^{(0)} \middle| \hat{\mathcal{H}}_0 - \epsilon_{i\mathbf{k}}^{(0)} \middle| \psi_{i\mathbf{k}}^{(2)} \right\rangle \tag{6.50}$$

For a more compact notation, we define the contribution $\rho_{ik}^{(1)}(r)$ to the total density variation

$$\rho_{i\mathbf{k}}^{(1)}(\mathbf{r}) = \psi_{i\mathbf{k}}^{(1)*}(\mathbf{r})\psi_{i\mathbf{k}}^{(0)}(\mathbf{r}) + \psi_{i\mathbf{k}}^{(0)*}(\mathbf{r})\psi_{i\mathbf{k}}^{(1)}(\mathbf{r}), \tag{6.51}$$

so that $\rho^{(1)}(\mathbf{r}) = \sum_{i\mathbf{k}} f_{i\mathbf{k}}^{(0)} \rho_{i\mathbf{k}}^{(1)}(\mathbf{r})$. In order to find the second-order Pulay correction to the total energy, we insert Eq. (6.50) into the second-order variation of the total energy, Eq. (6.6), and compare the resulting equation with its simplified form in Eq. (6.23). We obtain for the Pulay correction

$$E_{\text{tot,Pulay}}^{(2)} = \int \rho^{(1)}(\mathbf{r}) V_{\text{eff}}^{(1)}(\mathbf{r}) d^3 \mathbf{r} + \sum_{i\mathbf{k}} f_{i\mathbf{k}}^{(0)} \left[2 \left\langle \psi_{i\mathbf{k}}^{(1)} \middle| \hat{\mathcal{H}}_0 - \epsilon_{i\mathbf{k}}^{(0)} \middle| \psi_{i\mathbf{k}}^{(1)} \right\rangle + \left\langle \psi_{i\mathbf{k}}^{(2)} \middle| \hat{\mathcal{H}}_0 - \epsilon_{i\mathbf{k}}^{(0)} \middle| \psi_{i\mathbf{k}}^{(2)} \right\rangle \right].$$
(6.52)

Apparently, the second-order change in the wave functions is needed to calculate the Pulay correction $E_{\rm tot,Pulay}^{(2)}$. However, according to Eq. (6.24), the second-order change in the wave function is given by

$$\psi_{ik}^{(2)}(\mathbf{r}) = \sum_{KG} \left[z_{KG}^{ik(2)} \phi_{KG}^{(0)}(\mathbf{r}) + 2z_{KG}^{ik(1)} \phi_{KG}^{(1)}(\mathbf{r}) + z_{KG}^{ik(0)} \phi_{KG}^{(2)}(\mathbf{r}) \right]. \tag{6.53}$$

Therein, the only second-order variations are of the expansion coefficients, $z_{KG}^{ik(2)}$, and of the basis functions $\phi_{KG}^{(2)}(r)$. The former are factors to the unperturbed basis functions, for which $\langle \phi_{KG}^{(0)} | \hat{\mathcal{H}}_0 - \epsilon_{ik}^{(0)} | \psi_{ik}^{(0)} \rangle$ vanishes. Hence, the 2n+1 theorem still holds with respect to the LAPW expansion coefficients.

6. Density functional perturbation theory and the FLAPW method

Now we turn to the calculation of the second-order surface terms which appear in case of a displacive perturbation. To this end, we need to apply a variation to the first-order change in the total energy, Eq. (6.5) using $\epsilon_{ik,\mathrm{FLAPW}}^{(1)}$ without its surface terms in the sum-overstates, and extract from this the surface terms. These are due to the volume integrals in $E_{\mathrm{tot,basic}}^{(1)}$, not from any surface (nsf) terms subsumed in $E_{\mathrm{tot,SF}}^{(1)}$. We obtain the contribution

$$E_{\text{tot,SF}}^{(2),\text{nsf}} = \sum_{\alpha} \boldsymbol{w}_{\alpha}^{\text{T}} \cdot \oint_{\partial \text{MT}(\alpha)} \hat{\boldsymbol{e}} \left[\rho^{(0)}(\boldsymbol{r}) V_{\text{eff}}^{(1)}(\boldsymbol{r}) \right]_{\text{SF}} dS$$

$$+ \sum_{\alpha} \boldsymbol{w}_{\alpha}^{\text{T}} \cdot \sum_{i\boldsymbol{k}} f_{i\boldsymbol{k}}^{(0)} \oint_{\partial \text{MT}(\alpha)} \hat{\boldsymbol{e}} \left[\psi_{i\boldsymbol{k}}^{(1)*}(\boldsymbol{r}) \left(\hat{\mathcal{H}}_{0} - \epsilon_{i\boldsymbol{k}}^{(0)} \right) \psi_{i\boldsymbol{k}}^{(0)}(\boldsymbol{r}) \right]_{\text{SF}} dS$$

$$+ \sum_{\alpha} \boldsymbol{w}_{\alpha}^{\text{T}} \cdot \sum_{i\boldsymbol{k}} f_{i\boldsymbol{k}}^{(0)} \oint_{\partial \text{MT}(\alpha)} \hat{\boldsymbol{e}} \left[\psi_{i\boldsymbol{k}}^{(0)*}(\boldsymbol{r}) \left(\hat{\mathcal{H}}_{0} - \epsilon_{i\boldsymbol{k}}^{(0)} \right) \psi_{i\boldsymbol{k}}^{(1)}(\boldsymbol{r}) \right]_{\text{SF}} dS$$

$$- \sum_{\alpha} \boldsymbol{w}_{\alpha}^{\text{T}} \cdot \oint_{\partial \text{MT}(\alpha)} \hat{\boldsymbol{e}} \left[\rho^{(0)}(\boldsymbol{r}) \left\{ V_{\text{eff}}^{(1)}(\boldsymbol{r}) - V_{\text{ext}}^{(1)}(\boldsymbol{r}) \right\} \right]_{\text{SF}} dS. \tag{6.54}$$

Additionally, we need to apply a variation to Eq. (6.31), which contains the surface terms that occurred when we constructed the first-order change in the total energy. A variation of such a surface term will produce two components. One accounts for an additional variation of the domain of integration, the other one comes from the variation of the integrand. In general, these two terms can be obtained by applying Gauss' theorem to the first-order surface term beforehand:

$$\sum_{\alpha} \boldsymbol{w}_{\alpha}^{\mathrm{T}} \cdot \left(\oint_{\partial \mathrm{MT}(\alpha)} \hat{\boldsymbol{e}} \left[f^{(0)}(\boldsymbol{r}) \right]_{\mathrm{SF}} dS \right)^{(1)} = \sum_{\alpha} \boldsymbol{w}_{\alpha}^{\mathrm{T}} \cdot \left(\int_{\mathrm{MT}(\alpha)} \nabla \left[f^{(0)}(\boldsymbol{r}) \right]_{\mathrm{SF}} d^{3} r \right)^{(1)} \\
= \sum_{\alpha} \boldsymbol{w}_{\alpha}^{\mathrm{T}} \cdot \oint_{\partial \mathrm{MT}(\alpha)} \nabla \left[f^{(0)}(\boldsymbol{r}) \right]_{\mathrm{SF}} \hat{\boldsymbol{e}}^{\mathrm{T}} dS \cdot \boldsymbol{w}_{\alpha} + \sum_{\alpha} \boldsymbol{w}_{\alpha}^{\mathrm{T}} \cdot \oint_{\partial \mathrm{MT}(\alpha)} \hat{\boldsymbol{e}} \left[f^{(1)}(\boldsymbol{r}) \right]_{\mathrm{SF}} dS \quad (6.55)$$

Using this formula on $E_{\text{tot,SF}}^{(1)}$ yields for the higher order surface (hosf) terms

$$E_{\text{tot,SF}}^{(2),\text{hosf}} = \sum_{\alpha} \boldsymbol{w}_{\alpha}^{\text{T}} \cdot \sum_{i\boldsymbol{k}} f_{i\boldsymbol{k}}^{(0)} \oint_{\partial \text{MT}(\alpha)} \hat{\boldsymbol{e}} \left[\psi_{i\boldsymbol{k}}^{(0)*}(\boldsymbol{r}) \left(\hat{\mathcal{H}}_{0} - \epsilon_{i\boldsymbol{k}}^{(0)} \right) \psi_{i\boldsymbol{k}}^{(0)}(\boldsymbol{r}) \right]_{\text{SF}} \hat{\boldsymbol{e}}^{\text{T}} dS \cdot \boldsymbol{w}_{\alpha}$$

$$+ \sum_{\alpha} \boldsymbol{w}_{\alpha}^{\text{T}} \cdot \oint_{\partial \text{MT}(\alpha)} \hat{\boldsymbol{e}} \left[\rho^{(0)}(\boldsymbol{r}) V_{\text{eff}}^{(1)}(\boldsymbol{r}) \right]_{\text{SF}} dS$$

$$+ \sum_{\alpha} \boldsymbol{w}_{\alpha}^{\text{T}} \cdot \sum_{i\boldsymbol{k}} f_{i\boldsymbol{k}}^{(0)} \oint_{\partial \text{MT}(\alpha)} \hat{\boldsymbol{e}} \left[\psi_{i\boldsymbol{k}}^{(1)*}(\boldsymbol{r}) \left(\hat{\mathcal{H}}_{0} - \epsilon_{i\boldsymbol{k}}^{(0)} \right) \psi_{i\boldsymbol{k}}^{(0)}(\boldsymbol{r}) \right]_{\text{SF}} dS$$

$$+ \sum_{\alpha} \boldsymbol{w}_{\alpha}^{\text{T}} \cdot \sum_{i\boldsymbol{k}} f_{i\boldsymbol{k}}^{(0)} \oint_{\partial \text{MT}(\alpha)} \hat{\boldsymbol{e}} \left[\psi_{i\boldsymbol{k}}^{(0)*}(\boldsymbol{r}) \left(\hat{\mathcal{H}}_{0} - \epsilon_{i\boldsymbol{k}}^{(0)} \right) \psi_{i\boldsymbol{k}}^{(1)}(\boldsymbol{r}) \right]_{\text{SF}} dS$$

$$+ \sum_{\alpha} \boldsymbol{w}_{\alpha}^{\text{T}} \cdot \oint_{\partial \text{MT}(\alpha)} \hat{\boldsymbol{e}} \left[\rho^{(0)}(\boldsymbol{r}) \left\{ \varepsilon_{\text{xc}}^{(0)}(\boldsymbol{r}) - \mu_{\text{xc}}^{(0)}(\boldsymbol{r}) \right\} \right]_{\text{SF}} \hat{\boldsymbol{e}}^{\text{T}} dS \cdot \boldsymbol{w}_{\alpha}$$

$$- \sum_{\alpha} \boldsymbol{w}_{\alpha}^{\text{T}} \cdot \oint_{\partial \text{MT}(\alpha)} \hat{\boldsymbol{e}} \left[\rho^{(0)}(\boldsymbol{r}) \rho^{(1)}(\boldsymbol{r}) \left[\frac{\delta \mu_{\text{xc}}^{(0)}[\boldsymbol{\rho}](\boldsymbol{r})}{\delta \rho(\boldsymbol{r})} \right]_{\rho = \rho^{(0)}} \right]_{\text{SF}} dS. \tag{6.56}$$

The total surface correction of the second-order total energy formula is now the sum

$$E_{\text{tot,SF}}^{(2)} = E_{\text{tot,SF}}^{(2),\text{nsf}} + E_{\text{tot,SF}}^{(2),\text{hosf}}$$

$$= 2 \sum_{ik} f_{ik}^{(0)} \sum_{\alpha} \boldsymbol{w}_{\alpha}^{\text{T}} \cdot \oint_{\partial MT(\alpha)} \hat{\boldsymbol{e}} \left[\psi_{ik}^{(1)*}(\boldsymbol{r}) \left(\hat{\mathcal{H}}_{0} - \epsilon_{ik}^{(0)} \right) \psi_{ik}^{(0)}(\boldsymbol{r}) \right]_{\text{SF}} dS$$

$$+ 2 \sum_{ik} f_{ik}^{(0)} \sum_{\alpha} \boldsymbol{w}_{\alpha}^{\text{T}} \cdot \oint_{\partial MT(\alpha)} \hat{\boldsymbol{e}} \left[\psi_{ik}^{(0)*}(\boldsymbol{r}) \left(\hat{\mathcal{H}}_{0} - \epsilon_{ik}^{(0)} \right) \psi_{ik}^{(1)}(\boldsymbol{r}) \right]_{\text{SF}} dS$$

$$+ \sum_{ik} f_{ik}^{(0)} \sum_{\alpha} \boldsymbol{w}_{\alpha}^{\text{T}} \cdot \oint_{\partial MT(\alpha)} \nabla \left[\psi_{ik}^{(0)*}(\boldsymbol{r}) \left(\hat{\mathcal{H}}_{0} - \epsilon_{ik}^{(0)} \right) \psi_{ik}^{(0)}(\boldsymbol{r}) \right]_{\text{SF}} \hat{\boldsymbol{e}}^{\text{T}} dS \cdot \boldsymbol{w}_{\alpha}$$

$$+ \sum_{\alpha} \boldsymbol{w}_{\alpha}^{\text{T}} \cdot \oint_{\partial MT(\alpha)} \nabla \left[\rho^{(0)}(\boldsymbol{r}) \left\{ \varepsilon_{\text{xc}}^{(0)}(\boldsymbol{r}) - \mu_{\text{xc}}^{(0)}(\boldsymbol{r}) \right\} \right]_{\text{SF}} \hat{\boldsymbol{e}}^{\text{T}} dS \cdot \boldsymbol{w}_{\alpha}$$

$$+ \sum_{\alpha} \boldsymbol{w}_{\alpha}^{\text{T}} \cdot \oint_{\partial MT(\alpha)} \hat{\boldsymbol{e}} \left[\rho^{(0)}(\boldsymbol{r}) \left\{ 2V_{\text{ext}}^{(1)}(\boldsymbol{r}) + V_{\text{H}}^{(1)}(\boldsymbol{r}) \right\} \right]_{\text{SF}} dS. \tag{6.57}$$

Adding the Pulay and surface contributions to the second-order change $E_{\rm tot,basic}^{(2),\rm simple}$ in the total energy in its simplified form, Eq. (6.23), the second-order change in the total energy obtained from the FLAPW method becomes

$$E_{\text{tot}}^{(2)} = E_{\text{tot,basic}}^{(2),\text{simple}} + E_{\text{tot,Pulay}}^{(2)} + E_{\text{tot,SF}}^{(2)}.$$
 (6.58)

We point out once more that the surface correction only applies in case of a perturbation which affects the position of the atoms. From all contributions to the surface correction, we assume that the ones containing the Hamiltonian (more specifically the Laplacian) are most relevant, since the second derivative of the LAPW basis functions is discontinuous at the MT sphere boundary in all angular-momentum channels.

6.3. Summary

So far, we discussed the DFPT formalism and provided explicit formulas for the variations of the total energy up to second order. We presented the Sternheimer equation, which is the linearized Schrödinger equation. It allows to calculate the first-order change in the wave functions. The Sternheimer equation has to be solved self-consistently to obtain the change in the wave functions due to an external perturbation in order to account for a screening of the external perturbation through a rearrangement of the electrons. Furthermore, we gave formulas defining the second-order variation of the total energy and identified the necessary quantities to calculate $E_{\text{tot}}^{(2)}$. We made notion of the 2n+1 theorem, by which a given order of variation in the total energy can be expressed by variations in the wave functions of half that order. In the last part of this chapter, we extended the DFPT formalism to be applicable to the FLAPW method. The changes to the general DFPT formalism consist of Pulav and surface terms. With chapter 3.10 in mind, the former have to be included because the LAPW basis functions are not pointwise solutions to the Schrödinger equation and depend themselves on the perturbation. The latter take into account the small discontinuities of the LAPW basis functions and the quantities derived from them, which manifest at the muffin-tin sphere boundaries due to a different representation of the basis functions in the IR and MT regions.

6. Density functional perturbation theory and the FLAPW method

The results of this chapter are employed in the next chapter using specifically a phononic perturbation. Since we exclusively treat phonons in the FLAPW method there, we omit any labels 'FLAPW' in the following.

In the last chapter, we introduced DFPT and its adaptation to the FLAPW method. So far, the perturbation has been quite general. We now focus on a phononic perturbation and discuss how DFPT can be used to construct the dynamical matrix $\underline{\mathcal{D}}(q)$, which is related to the second-order derivative of the total energy with respect to the atomic positions by a Fourier transform of the force-constant matrix as presented in Eqs. (5.2) and (5.9).

Let us assume a finite but large solid consisting of N primitive, unperturbed unit cells, where the atomic arrangement results in the unperturbed external potential $V_{\rm ext}^{(0)}(r)$. In the end, we will consider the limit $N \to \infty$. Furthermore, we assume a perturbation \boldsymbol{w} where every atom α in every unit cell \boldsymbol{R} is displaced from its equilibrium position by a vector

$$\boldsymbol{w}_{\alpha \boldsymbol{R}} = \boldsymbol{w}_{\alpha \boldsymbol{R}}^{+} + \boldsymbol{w}_{\alpha \boldsymbol{R}}^{-} := \boldsymbol{Q}_{\alpha} e^{i\boldsymbol{q} \cdot \boldsymbol{R}} + \boldsymbol{Q}_{\alpha}^{*} e^{-i\boldsymbol{q} \cdot \boldsymbol{R}}. \tag{7.1}$$

This is a monochromatic perturbation of wave vector \boldsymbol{q} and polarization vector \boldsymbol{Q}_{α} , which we do not explicitly specify at this point. The dependence of the polarization vector on the wave vector is implicitly denoted by the capital Q instead of the lower case q. Furthermore, we omit the argument \boldsymbol{q} for the perturbation vector \boldsymbol{w} since we keep the value of \boldsymbol{q} fixed. The displacement $\boldsymbol{w}_{\alpha R}$ is real valued and its components obey

$$\boldsymbol{w}_{\alpha\boldsymbol{R}}^{+*} = \boldsymbol{w}_{\alpha\boldsymbol{R}}^{-}.\tag{7.2}$$

From this perturbation, we construct the changes in the wave functions, the density and the potential to first and second order. We follow the structure of chapter 6 and derive equations for the first-order changes in $V_{\rm ext}^{(1)}(r)$, $\phi_{KG}^{(1)}(r)$, $z_{KG}^{ik(1)}$, $\rho^{(1)}(r)$, $V_{\rm H}^{(1)}(r)$, and $V_{\rm eff}^{(1)}(r)$ first, which we obtain from the self-consistent solution of the Sternheimer equation, Eqs. (6.37), (6.15a), and (6.16). Afterwards, we present formulas for the second-order quantities $V_{\rm ext}^{(2)}(r)$, $E_{\rm ii}^{(2)}$, and $\phi_{KG}^{(2)}(r)$. According to Eq. (6.58) and its constituents defined in Eqs. (6.23), (6.52), and (6.57) of the last chapter, these quantities allow us to calculate the second-order change in the total energy.

Before we start with the evaluation of the first-order terms, we demonstrate that each order of perturbation introduces a shift in the Bloch vector of a function by $\pm q$, *i.e.*, that the response of a Bloch function of wave vector k is a combination of Bloch functions of wave vector $k \pm q$. We do so by expanding the perturbed external potential in orders of the perturbation:

$$\begin{aligned} V_{\text{ext}}(r) &= -\sum_{\alpha R} \frac{Z_{\alpha}}{|r - (\tau_{\alpha} + R + w_{\alpha R})|} \\ &= -\sum_{\alpha R} \frac{Z_{\alpha}}{|r - (\tau_{\alpha} + R)|} - \sum_{\alpha R} w_{\alpha R}^{\text{T}} \cdot \frac{d}{dw_{\alpha R}} \frac{Z_{\alpha}}{|r - (\tau_{\alpha} + R + w_{\alpha R})|} \bigg|_{w=0} + \dots \end{aligned}$$

$$\cdots - \frac{1}{2} \sum_{\alpha \mathbf{R}} \mathbf{w}_{\alpha \mathbf{R}}^{\mathrm{T}} \cdot \left[\left(\frac{d}{d\mathbf{w}_{\alpha \mathbf{R}}} \right) \cdot \left(\frac{d}{d\mathbf{w}_{\alpha \mathbf{R}}} \right)^{\mathrm{T}} \left(\frac{Z_{\alpha}}{|\mathbf{r} - (\boldsymbol{\tau}_{\alpha} + \mathbf{R} + \mathbf{w}_{\alpha \mathbf{R}})|} \right) \Big|_{\mathbf{w} = \mathbf{0}} \right] \cdot \mathbf{w}_{\alpha \mathbf{R}}$$

$$+ \mathcal{O}(\mathbf{w}^{3})$$

$$(7.3)$$

By redirecting the differentiation with respect to $w_{\alpha R}$ towards r and by expanding the displacement vector following its definition, we arrive at

$$V_{\text{ext}}(\mathbf{r}) = V_{\text{ext}}^{(0)}(\mathbf{r}) + V_{\text{ext}}^{(1)}(\mathbf{r}) + \frac{1}{2}V_{\text{ext}}^{(2)}(\mathbf{r}) + \mathcal{O}(\mathbf{w}^3), \tag{7.4}$$

where the respective orders are given by

$$V_{\text{ext}}^{(0)}(\mathbf{r}) = -\sum_{\alpha \mathbf{R}} \frac{Z_{\alpha}}{|\mathbf{r} - (\mathbf{\tau}_{\alpha} + \mathbf{R})|} =: \sum_{\alpha \mathbf{R}} V_{\text{ext}}^{\alpha \mathbf{R}}(\mathbf{r}),$$

$$V_{\text{ext}}^{(1)}(\mathbf{r}) = \sum_{\alpha} \mathbf{Q}_{\alpha}^{\text{T}} \cdot \sum_{\mathbf{R}} e^{i\mathbf{q}\cdot\mathbf{R}} \nabla \frac{Z_{\alpha}}{|\mathbf{r} - (\mathbf{\tau}_{\alpha} + \mathbf{R})|} + \sum_{\alpha} \mathbf{Q}_{\alpha}^{*\text{T}} \cdot \sum_{\mathbf{R}} e^{-i\mathbf{q}\cdot\mathbf{R}} \nabla \frac{Z_{\alpha}}{|\mathbf{r} - (\mathbf{\tau}_{\alpha} + \mathbf{R})|}$$

$$=: \sum_{\alpha} \mathbf{Q}_{\alpha}^{\text{T}} \cdot V_{\text{ext}}^{(1)\alpha+}(\mathbf{r}) + \sum_{\alpha} \mathbf{Q}_{\alpha}^{*\text{T}} \cdot V_{\text{ext}}^{(1)\alpha-}(\mathbf{r}), \text{ and}$$

$$(7.6)$$

$$V_{\rm ext}^{(2)}(\boldsymbol{r}) = \sum_{\alpha \boldsymbol{R}ij} \left[Q_{\alpha i} Q_{\alpha j} e^{2i\boldsymbol{q}\cdot\boldsymbol{R}} + Q_{\alpha i} Q_{\alpha j}^* + Q_{\alpha i}^* Q_{\alpha j} + Q_{\alpha i}^* Q_{\alpha j}^* e^{-2i\boldsymbol{q}\cdot\boldsymbol{R}} \right]$$

$$\times \left[\partial_i \partial_j V_{\text{ext}}^{\alpha \mathbf{R}}(\mathbf{r}) \right]. \tag{7.7}$$

From the definition

$$V_{\text{ext}}^{(1)\alpha\pm}(\mathbf{r}) = -\sum_{\mathbf{R}} e^{\pm i\mathbf{q}\cdot\mathbf{R}} \nabla V_{\text{ext}}^{\alpha\mathbf{R}}(\mathbf{r}), \tag{7.8}$$

and the fact that $\nabla V_{\text{ext}}^{QR}(r)$ is a real quantity immediately follows that the parts of the linear perturbation are complex conjugates to each other,

$$\left(\boldsymbol{V}_{\mathrm{ext}}^{(1)\alpha+}(\boldsymbol{r})\right)^* = \boldsymbol{V}_{\mathrm{ext}}^{(1)\alpha-}(\boldsymbol{r}). \tag{7.9}$$

Moreover, $V_{\mathrm{ext}}^{(1)\alpha\pm}(r)$ is a Bloch function of wave vector q or -q:

$$V_{\text{ext}}^{(1)\alpha\pm}(\mathbf{r}+\mathbf{R}') = -\sum_{\mathbf{R}} e^{\pm i\mathbf{q}\cdot\mathbf{R}} \nabla V_{\text{ext}}^{\alpha\mathbf{R}}(\mathbf{r}+\mathbf{R}')$$

$$= -e^{\pm i\mathbf{q}\cdot\mathbf{R}'} \sum_{\mathbf{R}} e^{\pm i\mathbf{q}\cdot(\mathbf{R}-\mathbf{R}')} \nabla V_{\text{ext}}^{\alpha(\mathbf{R}-\mathbf{R}')}(\mathbf{r}) = e^{\pm i\mathbf{q}\cdot\mathbf{R}'} \mathbf{V}_{\text{ext}}^{(1)\alpha\pm}(\mathbf{r}) \qquad (7.10)$$

We made use of the fact that the lattice translations R form a group in the case of the infinite bulk system by using R - R' as the summation variable instead of R. Similarly, the second order perturbation $V_{\rm ext}^{(2)}(r)$ is a linear combination of three Bloch waves of wave vectors $\mathbf{0}$ and $\pm 2q$.

7.1. First-order changes

Because the electronic system will adjust to the external perturbation, the Sternheimer equation has to be solved self-consistently. In order to calculate the first iteration of the

Sternheimer equation, where the linear change in the potential $V_{\text{eff}}^{(1)}(r)$ is given by the first-order perturbation $V_{\text{ext}}^{(1)}(r)$, we need in addition to the unperturbed quantities and the external perturbation the linear response of the basis functions, $\phi_{KG}^{(1)}(r)$. This can be seen from

$$\sum_{KG} \left\langle \phi_{LG'}^{(0)} \middle| \hat{\mathcal{H}}_{0} - \epsilon_{ik}^{(0)} \middle| \phi_{KG}^{(0)} \right\rangle_{V} z_{KG}^{ik(1)}$$

$$= -\sum_{KG} \left\{ \left\langle \phi_{LG'}^{(0)} \middle| V_{\text{eff}}^{(1)} - \epsilon_{ik}^{(1)} \middle| \phi_{KG}^{(0)} \right\rangle_{V}$$

$$+ \left\langle \phi_{LG'}^{(1)} \middle| \hat{\mathcal{H}}_{0} - \epsilon_{ik}^{(0)} \middle| \phi_{KG}^{(0)} \right\rangle_{V} + \left\langle \phi_{LG'}^{(0)} \middle| \hat{\mathcal{H}}_{0} - \epsilon_{ik}^{(0)} \middle| \phi_{KG}^{(1)} \right\rangle_{V}$$

$$+ \sum_{CR} w_{\alpha R}^{T} \cdot \oint_{\partial MT(\alpha, R)} \hat{e} \left[\phi_{LG'}^{(0)*} (\hat{\mathcal{H}}_{0} - \epsilon_{ik}^{(0)}) \phi_{KG}^{(0)} \right]_{SF} dS \right\} z_{KG}^{ik(0)}, \qquad (6.37 \text{ revisited})$$

where $V = N\Omega$ is the total volume of the large, but finite lattice. The sum over K allows that the wave function response is a superposition of Bloch waves with different wave vectors. For the later iterations, we also need the first-order responses of the Hartree potential $V_{\rm H}^{(1)}(r)$ and the xc potential $\mu_{\rm xc}^{(1)}(r)$, for which we will derive formulas in sections 7.1.4.2 and 7.1.4.3.

Before we discuss the calculation of the basis function response in section 7.1.1, we show now that the sums over K in Eq. (6.37 revisited) actually collapse to $K = k \pm q$ (l.h.s.) or K = k (r.h.s.). We assume for the moment that $\phi_{KG}^{(1)}(r)$ decomposes similarly to $V_{\rm ext}^{(1)}(r)$ into

$$\phi_{KG}^{(1)}(r) = \sum_{\alpha} Q_{\alpha}^{T} \cdot \phi_{KG}^{(1)\alpha+}(r) + \sum_{\alpha} Q_{\alpha}^{*T} \cdot \phi_{KG}^{(1)\alpha-}(r)$$
 (7.11)

with $\phi_{KG}^{(1)\alpha\pm}(r)$ being Bloch waves of wave vector $K\pm q$. This will be proven in section 7.1.1. In addition, we concentrate for now on the case $q\neq 0$ and neglect any contribution from $\epsilon_{ik}^{(1)}$. Then, also the expansion coefficients can be decomposed into q and -q components, or into components belonging to Q_{α} and Q_{α}^{*} , respectively:

$$z_{KG}^{ik(1)} = \sum_{\alpha} Q_{\alpha}^{\mathrm{T}} \cdot z_{KG}^{ik(1)\alpha+} + \sum_{\alpha} Q_{\alpha}^{*\mathrm{T}} \cdot z_{KG}^{ik(1)\alpha-}.$$
 (7.12)

The Sternheimer equation to determine the response of the expansion coefficients $z_{KG}^{ik(1)\alpha\pm}$ being factors of a particular $Q_{\alpha}^{(*)T}$ consequently takes the form

$$\sum_{KG} \left\langle \phi_{LG'}^{(0)} \middle| \hat{\mathcal{H}}_{0} - \epsilon_{ik}^{(0)} \middle| \phi_{KG}^{(0)} \right\rangle_{V} z_{KG}^{ik(1)\alpha\pm}$$

$$= -\sum_{KG} \left\{ \left\langle \phi_{LG'}^{(0)} \middle| V_{\text{eff}}^{(1)\alpha\pm} \middle| \phi_{KG}^{(0)} \right\rangle_{V} + \left\langle \phi_{LG'}^{(0)} \middle| \hat{\mathcal{H}}_{0} - \epsilon_{ik}^{(0)} \middle| \phi_{KG}^{(1)\alpha\pm} \right\rangle_{V} + \left\langle \phi_{LG'}^{(0)} \middle| \hat{\mathcal{H}}_{0} - \epsilon_{ik}^{(0)} \middle| \phi_{KG}^{(1)\alpha\pm} \right\rangle_{V} + \sum_{R} e^{\pm iq \cdot R} \cdot \oint_{\partial MT(\alpha, R)} \hat{e} \left[\phi_{LG'}^{(0)*} (\hat{\mathcal{H}}_{0} - \epsilon_{ik}^{(0)}) \phi_{KG}^{(0)} \right]_{SF} dS \right\} z_{KG}^{ik(0)}.$$
(7.13)

Making use of the fact that the integral over a Bloch function of non-vanishing Bloch vector is identically zero (and treating the surface integral as a volume integral by Gauss' theorem), we realize that the right-hand side of Eq. (7.13) only contributes in the case $L = K \pm q$. Moreover, the definition $z_{KG}^{ik(0)} = \delta_{kK} z_{ikG}^{(0)}$ from Eq. (6.25) implies for the r.h.s. that $L = k \pm q$. For this choice of L, on the l.h.s. also $K = k \pm q$ holds and the Sternheimer equation defining the components of the expansion-coefficient response $z_{KG}^{ik(1)\alpha\pm}$ becomes

$$\sum_{G} \left\langle \phi_{\mathbf{k}\pm\mathbf{q},G'}^{(0)} \middle| \hat{\mathcal{H}}_{0} - \epsilon_{i\mathbf{k}}^{(0)} \middle| \phi_{\mathbf{k}\pm\mathbf{q},G}^{(0)} \right\rangle_{V} z_{\mathbf{k}\pm\mathbf{q},G}^{i\mathbf{k}(1)\alpha\pm}$$

$$= -\sum_{G} \left\{ \left\langle \phi_{\mathbf{k}\pm\mathbf{q},G'}^{(0)} \middle| V_{\text{eff}}^{(1)\alpha\pm} \middle| \phi_{\mathbf{k}G}^{(0)} \right\rangle_{V} + \left\langle \phi_{\mathbf{k}\pm\mathbf{q},G'}^{(1)\alpha\mp} \middle| \hat{\mathcal{H}}_{0} - \epsilon_{i\mathbf{k}}^{(0)} \middle| \phi_{\mathbf{k}G}^{(0)} \right\rangle_{V} + \left\langle \phi_{\mathbf{k}\pm\mathbf{q},G'}^{(0)} \middle| \hat{\mathcal{H}}_{0} - \epsilon_{i\mathbf{k}}^{(0)} \middle| \phi_{\mathbf{k}G}^{(1)\alpha\pm} \right\rangle_{V}$$

$$+\sum_{R} e^{\pm i\mathbf{q}\cdot\mathbf{R}} \cdot \oint_{\partial \text{MT}(\alpha,R)} \hat{e} \left[\phi_{\mathbf{k}\pm\mathbf{q},G'}^{(0)*} (\hat{\mathcal{H}}_{0} - \epsilon_{i\mathbf{k}}^{(0)}) \phi_{\mathbf{k}G}^{(0)} \right]_{\text{SF}} dS \right\} z_{\mathbf{k}G}^{i\mathbf{k}(0)}. \tag{7.14}$$

For any other choice of L, the first-order change in the expansion coefficients vanishes. This we see by operating from the left with $\sum_{G'} z_{LG'}^{jl(0)*}$ on Eq. (7.13), where by $L = l \neq k \pm q$ the right-hand side of this equation is zero. We obtain

$$\sum_{GG'} z_{LG'}^{jl(0)*} \left\langle \phi_{LG'}^{(0)} \middle| \hat{\mathcal{H}}_{0} - \epsilon_{ik}^{(0)} \middle| \phi_{LG}^{(0)} \right\rangle_{V} z_{LG}^{ik(1)\alpha\pm} = \sum_{G} \left\langle \psi_{jl}^{(0)} \middle| \hat{\mathcal{H}}_{0} - \epsilon_{ik}^{(0)} \middle| \phi_{lG}^{(0)} \right\rangle_{V} z_{lG}^{ik(1)\alpha\pm} \\
= \left(\epsilon_{jl}^{(0)} - \epsilon_{ik}^{(0)} \right) \sum_{G} \left\langle \psi_{jl}^{(0)} \middle| \phi_{lG}^{(0)} \right\rangle_{V} z_{lG}^{ik(1)\alpha\pm} = 0.$$
(7.15)

This is true for all j at a chosen l, implying $z_{lG}^{ik(1)\alpha\pm}=0$ for all $l\neq k\pm q$.

Furthermore, we can use the periodicity of the integrands in Eq. (7.14) to limit the evaluation of the integrals to the representative unit cell Ω at $\mathbf{R} = \mathbf{0}$. In the picture of the large, but finite system, the integrals then have to be multiplied by the factor N defining the size of the system. Since in this picture, the wave functions are normalized with respect to $N\Omega$, the evaluation of the Sternheimer equation can be performed per unit cell using the regular LAPW wave functions and thus omitting the factor N alltogether.

The neglect of a contribution from $\epsilon_{ik}^{(1)}$ does not limit the generality of the results above, as long as $q \neq 0$, since for non-vanishing q, $\epsilon_{ik}^{(1)}$ is zero. In order to prove this statement, we operate with $\sum_{\mathbf{G}'} z_{k\mathbf{G}'}^{ik(0)*}$ on Eq. (6.37 revisited). Then, the left-hand side yields zero in analogy to Eq. (7.15) and the right-hand side gives $\epsilon_{ik}^{(1)}$:

$$\sum_{GG'} z_{kG'}^{ik(0)*} \left\langle \phi_{kG'}^{(0)} \middle| \hat{\mathcal{H}}_{0} - \epsilon_{ik}^{(0)} \middle| \phi_{kG}^{(0)} \right\rangle_{V} z_{kG}^{ik(1)}$$

$$= \sum_{G} \left\langle \psi_{ik}^{(0)} \middle| \hat{\mathcal{H}}_{0} - \epsilon_{ik}^{(0)} \middle| \phi_{kG}^{(0)} \right\rangle_{V} z_{kG}^{ik(1)}$$

$$= \left(\epsilon_{ik}^{(0)} - \epsilon_{ik}^{(0)} \right) \left\langle \psi_{ik}^{(0)} \middle| \phi_{kG}^{(0)} \right\rangle_{V} z_{kG}^{ik(1)} = 0 = \epsilon_{ik}^{(1)} \tag{7.16}$$

For q=0 on the other hand, the same procedure yields zero for the left-hand side of the equation again. However, the right-hand side defines $\epsilon_{ik}^{(1)}$ as

$$\begin{split} \epsilon_{ik}^{(1)} &= \left\langle \psi_{ik}^{(0)} \middle| V_{\text{eff}}^{(1)} \middle| \psi_{ik}^{(0)} \right\rangle_{V} + \left\langle \tilde{\psi}_{ik}^{(1)} \middle| \hat{\mathcal{H}}_{0} - \epsilon_{ik}^{(0)} \middle| \psi_{ik}^{(0)} \right\rangle_{V} + \left\langle \psi_{ik}^{(0)} \middle| \hat{\mathcal{H}}_{0} - \epsilon_{ik}^{(0)} \middle| \tilde{\psi}_{ik}^{(1)} \right\rangle_{V} \\ &+ \sum_{\alpha R} \boldsymbol{w}_{\alpha R}^{\mathsf{T}} \cdot \oint_{\partial \mathrm{MT}(\alpha, R)} \hat{\boldsymbol{e}} \left[\psi_{ik}^{(0)*} (\hat{\mathcal{H}}_{0} - \epsilon_{ik}^{(0)}) \psi_{ik}^{(0)} \right]_{\mathrm{SF}} dS \end{aligned} \tag{7.17a} \\ &= \sum_{\alpha} \boldsymbol{Q}_{\alpha}^{\mathsf{T}} \cdot \left\{ \left\langle \psi_{ik}^{(0)} \middle| \boldsymbol{V}_{\mathrm{eff}}^{(1)\alpha+} \middle| \psi_{ik}^{(0)} \right\rangle_{V} + \sum_{G'} z_{kG'}^{ik(0)*} \left\langle \boldsymbol{\phi}_{kG'}^{(1)\alpha-} \middle| \hat{\mathcal{H}}_{0} - \epsilon_{ik}^{(0)} \middle| \psi_{ik}^{(0)} \right\rangle_{V} \\ &+ \sum_{G} \left\langle \psi_{ik}^{(0)} \middle| \hat{\mathcal{H}}_{0} - \epsilon_{ik}^{(0)} \middle| \boldsymbol{\phi}_{kG}^{(1)\alpha+} \right\rangle_{V} z_{kG}^{ik(0)} \\ &+ N \oint_{\partial \mathrm{MT}(\alpha, 0)} \hat{\boldsymbol{e}} \left[\psi_{ik}^{(0)*} (\hat{\mathcal{H}}_{0} - \epsilon_{ik}^{(0)}) \psi_{ik}^{(0)} \right]_{\mathrm{SF}} dS \right\} \tag{7.17b} \\ &+ \sum_{\alpha} \left\langle \boldsymbol{\psi}_{ik}^{(0)} \middle| \boldsymbol{V}_{\mathrm{eff}}^{(1)\alpha-} \middle| \psi_{ik}^{(0)} \right\rangle_{V} + \sum_{G'} z_{kG'}^{ik(0)*} \left\langle \boldsymbol{\phi}_{kG'}^{(1)\alpha+} \middle| \hat{\mathcal{H}}_{0} - \epsilon_{ik}^{(0)} \middle| \psi_{ik}^{(0)} \right\rangle_{V} \\ &+ \sum_{G} \left\langle \psi_{ik}^{(0)} \middle| \hat{\mathcal{H}}_{0} - \epsilon_{ik}^{(0)} \middle| \boldsymbol{\phi}_{kG}^{(1)\alpha-} \right\rangle_{V} z_{kG}^{ik(0)} \\ &+ N \oint_{\partial \mathrm{MT}(\alpha, 0)} \hat{\boldsymbol{e}} \left[\psi_{ik}^{(0)*} (\hat{\mathcal{H}}_{0} - \epsilon_{ik}^{(0)}) \psi_{ik}^{(0)} \right]_{\mathrm{SF}} dS \right\} \tag{7.17c} \end{aligned}$$

Here, the \pm does not denote a shift in the wave vector of a Bloch function, but indicates only the affiliation to \mathbf{Q}_{α} or \mathbf{Q}_{α}^{*} . Also, the linear response of the eigenenergy can be evaluated considering only a single unit cell. The integrals are periodic, yielding a factor N when the domain of integration is reduced to Ω , while the normalization of the wave functions cancels this factor. We define

$$\epsilon_{i\boldsymbol{k}}^{(1)\alpha\pm} = \left\langle \psi_{i\boldsymbol{k}}^{(0)} \middle| \boldsymbol{V}_{\text{eff}}^{(1)\alpha\pm} \middle| \psi_{i\boldsymbol{k}}^{(0)} \right\rangle + \oint_{\partial \text{MT}(\alpha)} \hat{e} \left[\psi_{i\boldsymbol{k}}^{(0)*} (\hat{\mathcal{H}}_0 - \epsilon_{i\boldsymbol{k}}^{(0)}) \psi_{i\boldsymbol{k}}^{(0)} \right]_{\text{SF}} dS
+ \sum_{\boldsymbol{G}'} z_{\boldsymbol{k}\boldsymbol{G}'}^{i\boldsymbol{k}(0)*} \left\langle \boldsymbol{\phi}_{\boldsymbol{k}\boldsymbol{G}'}^{(1)\alpha\mp} \middle| \hat{\mathcal{H}}_0 - \epsilon_{i\boldsymbol{k}}^{(0)} \middle| \psi_{i\boldsymbol{k}}^{(0)} \right\rangle + \sum_{\boldsymbol{G}} \left\langle \psi_{i\boldsymbol{k}}^{(0)} \middle| \hat{\mathcal{H}}_0 - \epsilon_{i\boldsymbol{k}}^{(0)} \middle| \boldsymbol{\phi}_{\boldsymbol{k}\boldsymbol{G}}^{(1)\alpha\pm} \right\rangle z_{\boldsymbol{k}\boldsymbol{G}}^{i\boldsymbol{k}(0)} \quad (7.18)$$

and include this term into Eq. (7.14). Thus, the Sternheimer equation, which determines the first-order changes in the wave functions, and thus subsequently in the density, and in the potential is given by

$$\sum_{G} \left\langle \phi_{\mathbf{k}\pm\mathbf{q},G'}^{(0)} \middle| \hat{\mathcal{H}}_{0} - \epsilon_{i\mathbf{k}}^{(0)} \middle| \phi_{\mathbf{k}\pm\mathbf{q},G}^{(0)} \right\rangle z_{\mathbf{k}\pm\mathbf{q},G}^{i\mathbf{k}(1)\alpha\pm}$$

$$= -\sum_{G} \left\{ \left\langle \phi_{\mathbf{k}\pm\mathbf{q},G'}^{(0)} \middle| V_{\text{eff}}^{(1)\alpha\pm} - \delta_{\mathbf{q}0} \epsilon_{i\mathbf{k}}^{(1)\alpha\pm} \middle| \phi_{\mathbf{k}G}^{(0)} \right\rangle \right.$$

$$+ \left\langle \phi_{\mathbf{k}\pm\mathbf{q},G'}^{(1)\alpha\mp} \middle| \hat{\mathcal{H}}_{0} - \epsilon_{i\mathbf{k}}^{(0)} \middle| \phi_{\mathbf{k}G}^{(0)} \right\rangle + \left\langle \phi_{\mathbf{k}\pm\mathbf{q},G'}^{(0)} \middle| \hat{\mathcal{H}}_{0} - \epsilon_{i\mathbf{k}}^{(0)} \middle| \phi_{\mathbf{k}G}^{(1)\alpha\pm} \right\rangle$$

$$+ \oint_{\partial \mathbf{MT}(\alpha,\mathbf{0})} \hat{\mathbf{e}} \left[\phi_{\mathbf{k}\pm\mathbf{q},G'}^{(0)*} (\hat{\mathcal{H}}_{0} - \epsilon_{i\mathbf{k}}^{(0)}) \phi_{\mathbf{k}G}^{(0)} \right]_{\text{SF}} dS \right\} z_{\mathbf{k}G}^{i\mathbf{k}(0)}. \tag{7.19}$$

As the next step, we derive the first-order variation of the basis functions in the frozenaugmentation approximation. Afterwards, we present the linear response of the electronic density, and the effective potential.

7.1.1. Evaluation of $\phi_{KG}^{(1)}(r)$

The LAPW basis functions are constructed from plane waves in the interstitial region to which radial functions and spherical harmonics are matched in the muffin-tin spheres. In the current setting of a large but finite structure containing N unit cells, we define the perturbed basis functions to be normalized over the whole structure. Abbreviating the positions of the atomic nuclei in the perturbed system by $r_{\alpha Rw} = \tau_{\alpha} + R + w_{\alpha R}$, the basis functions take the form

$$\phi_{kG}(\mathbf{r}) = \begin{cases} \frac{1}{\sqrt{N\Omega}} e^{i(\mathbf{k} + \mathbf{G}) \cdot \mathbf{r}} &, \mathbf{r} \in \mathbf{IR} \\ \frac{1}{\sqrt{N}} \sum_{lm\lambda} a_{lm\lambda}^{\alpha \mathbf{R}kG} u_{l\lambda}^{\alpha \mathbf{R}} (|\mathbf{r} - \mathbf{r}_{\alpha \mathbf{R}w}|) Y_{lm} (\widehat{\mathbf{r} - \mathbf{r}_{\alpha \mathbf{R}w}}) &, \mathbf{r} \in \mathbf{MT}(\alpha, \mathbf{R}) \end{cases}, (7.20)$$

where we explicitly denote the unit cell R in which we evaluate the muffin-tin contribution. We construct the variation of the basis functions $\phi_{kG}^{(1)}$ within the frozen-augmentation approximation. Within this approximation, only the explicit dependence of the basis functions on the perturbation is taken into account for determining $\phi_{kG}^{(1)}$. A change in the radial functions due to an adjustment of the effective potential is neglected. The linear response in the basis functions in turn leads to the part $\tilde{\psi}_{ik}^{(1)}$ of the wave function response that is not completely contained in the LAPW basis space, according to Eq. (6.26). From Eq. (3.17) we know that the explicit dependence of the matching coefficients $a_{lm\lambda}^{\alpha RkG}$ on the perturbation w is given through the phase factor $\exp[i(k+G)\cdot r_{\alpha Rw}]$, which characterizes ϕ_{kG} as a Bloch function of wave vector k. An explicit dependence of the radial function $u_{l\lambda}^{\alpha R}$ and the spherical harmonic Y_{lm} exists due to the local coordinate frame. Hence, at the level of the frozen-augmentation approximation, at which the change in the potential does not affect the radial functions, the linear response of the basis functions due to a displacive response w is

$$\phi_{\mathbf{k}\mathbf{G}}^{(1)}(\mathbf{r}) = \begin{cases} 0 &, \mathbf{r} \in \mathrm{IR} \\ \mathbf{w}_{\alpha\mathbf{R}}^{\mathrm{T}} \cdot [i(\mathbf{k} + \mathbf{G}) - \nabla]\phi_{\mathbf{k}\mathbf{G}}^{(0)}(\mathbf{r}) &, \mathbf{r} \in \mathrm{MT}(\alpha, \mathbf{R}) \end{cases}$$
(7.21)

The MT part of $\phi_{\boldsymbol{k}\boldsymbol{G}}^{(1)}(\boldsymbol{r})$ can be rewritten as

$$\phi_{\mathbf{k}\mathbf{G}}^{(1)}(\mathbf{r}) = \sum_{\alpha \mathbf{R}} \Theta(R_{\alpha} - |\mathbf{r} - \boldsymbol{\tau}_{\alpha} - \mathbf{R}|) \mathbf{Q}_{\alpha}^{\mathrm{T}} \cdot [i(\mathbf{k} + \mathbf{G}) - \nabla] e^{i\mathbf{q} \cdot \mathbf{R}} \phi_{\mathbf{k}\mathbf{G}}^{(0)}(\mathbf{r})$$

$$+ \sum_{\alpha \mathbf{R}} \Theta(R_{\alpha} - |\mathbf{r} - \boldsymbol{\tau}_{\alpha} - \mathbf{R}|) \mathbf{Q}_{\alpha}^{*\mathrm{T}} \cdot [i(\mathbf{k} + \mathbf{G}) - \nabla] e^{-i\mathbf{q} \cdot \mathbf{R}} \phi_{\mathbf{k}\mathbf{G}}^{(0)}(\mathbf{r}) \qquad (7.22a)$$

$$=: \sum_{\alpha} \mathbf{Q}_{\alpha}^{\mathrm{T}} \cdot \phi_{\mathbf{k}\mathbf{G}}^{(1)\alpha+}(\mathbf{r}) + \sum_{\alpha} \mathbf{Q}_{\alpha}^{*\mathrm{T}} \cdot \phi_{\mathbf{k}\mathbf{G}}^{(1)\alpha-}(\mathbf{r}) \qquad (7.22b)$$

which is a superposition of Bloch waves $\phi_{kG}^{(1)\alpha\pm}$ of wave vector $k\pm q$. Rigorously, also the variation in the shape of the basis function due to the change in the potential has to be calculated. This corresponds to a lifting of the frozen-augmentation approximation. Such a

¹The limit $N \to \infty$ is taken at the end.

change of the basis functions has been discussed by Betzinger et al. [149, 150] in the context of the exact-exchange optimized-effective-potential approach.

We insert the variation of the (unit-cell normalized) basis functions into the Sternheimer equation, Eq. (7.19), to obtain

$$\sum_{G} \left\langle \phi_{k\pm q,G'}^{(0)} \middle| \hat{\mathcal{H}}_{0} - \epsilon_{ik}^{(0)} \middle| \phi_{k\pm q,G}^{(0)} \right\rangle z_{k\pm q,G}^{ik(1)\alpha\pm}$$

$$= -\sum_{G} \left\{ \left\langle \phi_{k\pm q,G'}^{(0)} \middle| V_{\text{eff}}^{(1)\alpha\pm} - \delta_{q0} \epsilon_{ik}^{(1)\alpha\pm} \middle| \phi_{kG}^{(0)} \right\rangle$$

$$+ i(G - G' \mp q) \left\langle \phi_{k\pm q,G'}^{(0)} \middle| \hat{\mathcal{H}}_{0} - \epsilon_{ik}^{(0)} \middle| \phi_{kG}^{(0)} \right\rangle_{\alpha}$$

$$- \left\langle \nabla \phi_{k\pm q,G'}^{(0)} \middle| \hat{\mathcal{H}}_{0} - \epsilon_{ik}^{(0)} \middle| \phi_{kG}^{(0)} \right\rangle_{\alpha} - \left\langle \phi_{k\pm q,G'}^{(0)} \middle| \hat{\mathcal{H}}_{0} - \epsilon_{ik}^{(0)} \middle| \nabla \phi_{kG}^{(0)} \right\rangle_{\alpha}$$

$$+ \oint_{\partial MT(\alpha,0)} \hat{e} \left[\phi_{k\pm q,G'}^{(0)*} (\hat{\mathcal{H}}_{0} - \epsilon_{ik}^{(0)}) \phi_{kG}^{(0)} \right]_{SF} dS \right\} z_{kG}^{ik(0)}. \tag{7.23}$$

Adding and subtracting $\langle \phi^{(0)}_{\mathbf{k} \pm \mathbf{q}, \mathbf{G}'} | \nabla V^{(0)}_{\mathrm{eff}} | \phi^{(0)}_{\mathbf{k} \mathbf{G}} \rangle_{\alpha}$ to the third line of the right-hand side of the previous equation allows us to apply Gauss' theorem. After all surface terms have been taken into account, this procedure transforms the Sternheimer equation into

$$\sum_{\mathbf{G}} \left\langle \phi_{\mathbf{k}\pm\mathbf{q},\mathbf{G}'}^{(0)} \middle| \hat{\mathcal{H}}_{0} - \epsilon_{i\mathbf{k}}^{(0)} \middle| \phi_{\mathbf{k}\pm\mathbf{q},\mathbf{G}}^{(0)} \right\rangle z_{\mathbf{k}\pm\mathbf{q},\mathbf{G}}^{i\mathbf{k}(1)\alpha\pm}$$

$$= -\sum_{\mathbf{G}} \left\{ \left\langle \phi_{\mathbf{k}\pm\mathbf{q},\mathbf{G}'}^{(0)} \middle| V_{\text{eff}}^{(1)\alpha\pm} - \delta_{\mathbf{q}0} \epsilon_{i\mathbf{k}}^{(1)\alpha\pm} \middle| \phi_{\mathbf{k}\mathbf{G}}^{(0)} \right\rangle + \left\langle \phi_{\mathbf{k}\pm\mathbf{q},\mathbf{G}'}^{(0)} \middle| \nabla V_{\text{eff}}^{(0)} \middle| \phi_{\mathbf{k}\mathbf{G}}^{(0)} \right\rangle_{\alpha}$$

$$- i(\mathbf{G}' \pm \mathbf{q} - \mathbf{G}) \left\langle \phi_{\mathbf{k}\pm\mathbf{q},\mathbf{G}'}^{(0)} \middle| \hat{\mathcal{H}}_{0} - \epsilon_{i\mathbf{k}}^{(0)} \middle| \phi_{\mathbf{k}\mathbf{G}}^{(0)} \right\rangle_{\alpha}$$

$$- \oint_{\partial \mathbf{MT}(\alpha,\mathbf{0})} \hat{\mathbf{e}} \left[\phi_{\mathbf{k}\pm\mathbf{q},\mathbf{G}'}^{\mathbf{IR}(0)*} (\hat{\mathcal{H}}_{0} - \epsilon_{i\mathbf{k}}^{(0)}) \phi_{\mathbf{k}\mathbf{G}}^{\mathbf{IR}(0)} \right] dS \right\} z_{\mathbf{k}\mathbf{G}}^{i\mathbf{k}(0)}. \tag{7.24}$$

In the first line of the right-hand side of this equation, the linear response of the effective potential $V_{\rm eff}^{(1)\alpha\pm}(r)$ occurs together with the gradient of the effective potential $\nabla V_{\rm eff}^{(0)}(r)$ in the muffin-tin sphere of the displaced atom α . During the self-consistency cycle to solve the Sternheimer equation, this can be useful as it avoids the delicacy to numerically calculate the gradient of the effective potential. Therefore, it is possible to solve the Sternheimer equation numerically stable. In Eqs. (6.23) and (6.52), which define the contributions to the second-order variation of the total energy, such a cancellation does not occur, though.

7.1.2. Evaluation of the core state change $\psi_{ik}^{(1)}(r)$

Similar to the frozen-augmentation approximation for the valence states, we employ the frozen-core approximation for the core states, *i.e.*, the change in the wave functions of the core states is only due to the explicit dependence of the core states on the perturbation \boldsymbol{w} , not due to the adjustment of the effective potential caused by the perturbation. This explicit dependence occurs only by means of the local coordinate system $\boldsymbol{r} - \boldsymbol{r}_{\alpha \boldsymbol{R} \boldsymbol{w}}, \boldsymbol{r}_{\alpha \boldsymbol{R} \boldsymbol{w}} = \boldsymbol{\tau}_{\alpha} + \boldsymbol{R} + \boldsymbol{w}_{\alpha \boldsymbol{R}}$, of the atom the core state is attached to. We remind the reader that the

multiindex $i = (\beta p l m_l)$ specifying the core state comprises of the atom index β and the prime, angular momentum, and magnetic quantum numbers p, l, and m_l . Since according to chapter 3.4 the core states in different unit cells \mathbf{R}' are multiplied by a Bloch factor $\exp(i\mathbf{k} \cdot \mathbf{R}')$, the first-order variation of the core states can be extracted from

$$\psi_{i\mathbf{k}}(\mathbf{r}) = \frac{1}{\sqrt{N}} \sum_{\mathbf{R}'} u_l^{\beta} (|\mathbf{r} - \mathbf{r}_{\beta \mathbf{R}' \mathbf{w}}|) Y_{lm} (\widehat{\mathbf{r} - \mathbf{r}_{\beta \mathbf{R}' \mathbf{w}}}) e^{i\mathbf{k} \cdot \mathbf{R}'}.$$
(7.25)

The first-order variation of this expression is given by

$$\psi_{i\mathbf{k}}^{(1)}(\mathbf{r}) = -\mathbf{Q}_{\beta}^{\mathrm{T}} \cdot \nabla \psi_{i\mathbf{k}+\mathbf{q}}^{(0)}(\mathbf{r}) - \mathbf{Q}_{\beta}^{*\mathrm{T}} \cdot \nabla \psi_{i\mathbf{k}-\mathbf{q}}^{(0)}(\mathbf{r})$$
(7.26)

and defines the vector valued quantities

$$\psi_{i\mathbf{k}}^{(1)\alpha\pm}(\mathbf{r}) = -\delta_{\alpha\beta}\nabla\psi_{i\mathbf{k}\pm\mathbf{q}}^{(0)}(\mathbf{r}),\tag{7.27}$$

which are Bloch functions of wave vector $\mathbf{k} \pm \mathbf{q}$.

The first-order change $\psi_{ik}^{(1)}(r)$ of the core state does contribute to the first-order change in the density and subsequently in the Hartree and xc potentials. Other than that, it does not explicitly appear within the Sternheimer equation that determines the first-order variation of the expansion coefficients $z_{KG}^{(1)}$ of the valence states. Moreover, the calculation of the core state response does not involve the Sternheimer matrix equation, Eq. (7.19), since they are not represented by a basis. In addition, the response of the core states does not need to be determined self-consistently within the frozen-core approximation. We proceed by presenting the first-order change in the electronic density.

7.1.3. Evaluation of $\rho^{(1)}(\boldsymbol{r})$

Eqs. (7.15) and (7.22) suggest that just as the response of the expansion coefficients and the response of the basis functions, the first-order change in the valence wave functions is separable into two Bloch waves $\psi_{ik}^{(1)a\pm}$ of wave vectors $k \pm q$:

$$\begin{split} \psi_{ik}^{(1)}(r) &= \sum_{KG} \left[z_{KG}^{ik(1)} \phi_{KG}^{(0)}(r) + z_{KG}^{ik(0)} \phi_{KG}^{(1)}(r) \right] \\ &= \sum_{\alpha} Q_{\alpha}^{\mathrm{T}} \cdot \sum_{G} \left[z_{k+q,G}^{ik(1)\alpha +} \phi_{k+q,G}^{(0)}(r) + z_{kG}^{ik(0)} \phi_{kG}^{(1)\alpha +}(r) \right] \\ &+ \sum_{\alpha} Q_{\alpha}^{*\mathrm{T}} \cdot \sum_{G} \left[z_{k-q,G}^{ik(1)\alpha -} \phi_{k-q,G}^{(0)}(r) + z_{kG}^{ik(0)} \phi_{kG}^{(1)\alpha -}(r) \right] \\ &= : \sum_{\alpha} Q_{\alpha}^{\mathrm{T}} \cdot \psi_{ik}^{(1)\alpha +} + \sum_{\alpha} Q_{\alpha}^{*\mathrm{T}} \cdot \psi_{ik}^{(1)\alpha -} \end{split} \tag{7.28}$$

Provided that time-reversal symmetry holds, the variation of the conjugated wave function is connected with the variation of the regular wave function by

$$\left(\psi_{i\mathbf{k}}^{(1)\alpha\pm}(\mathbf{r})\right)^* = \psi_{i\mathbf{k}}^{*(1)\alpha\mp}(\mathbf{r}) \tag{7.29}$$

as is stated for example in Ref. [36].

Consequently, also the density variation decomposes into two Bloch functions of wave vectors $\pm q$ according to

$$\rho^{(1)}(\mathbf{r}) = \rho^{(1)+}(\mathbf{r}) + \rho^{(1)-}(\mathbf{r}) = \sum_{\alpha} \mathbf{Q}_{\alpha}^{\mathrm{T}} \cdot \boldsymbol{\rho}^{(1)\alpha+}(\mathbf{r}) + \sum_{\alpha} \mathbf{Q}_{\alpha}^{*\mathrm{T}} \cdot \boldsymbol{\rho}^{(1)\alpha-}(\mathbf{r})$$
(7.30)

with the density response vectors given by

$$\rho^{(1)\alpha\pm}(\mathbf{r}) = \sum_{i\mathbf{k}} f_{i\mathbf{k}}^{(0)} \left\{ \psi_{i\mathbf{k}}^{*(1)\alpha\pm}(\mathbf{r})\psi_{i\mathbf{k}}^{(0)}(\mathbf{r}) + \psi_{i\mathbf{k}}^{(0)*}(\mathbf{r})\psi_{i\mathbf{k}}^{(1)\alpha\pm}(\mathbf{r}) \right\}. \tag{7.31a}$$

Thus, the $\pm q$ -part of the density response has contributions from the $\mp q$ wave functions. Using time-reversal symmetry, we can simplify this equation to yield

$$\rho^{(1)\alpha\pm}(\mathbf{r}) = \sum_{i\mathbf{k}} f_{i\mathbf{k}}^{(0)} \left\{ \psi_{i-\mathbf{k}}^{(1)\alpha\pm}(\mathbf{r}) \psi_{i-\mathbf{k}}^{(0)*}(\mathbf{r}) + \psi_{i\mathbf{k}}^{(0)*}(\mathbf{r}) \psi_{i\mathbf{k}}^{(1)\alpha\pm}(\mathbf{r}) \right\}
= 2 \sum_{i\mathbf{k}} f_{i\mathbf{k}}^{(0)} \psi_{i\mathbf{k}}^{(0)*}(\mathbf{r}) \psi_{i\mathbf{k}}^{(1)\alpha\pm}(\mathbf{r}).$$
(7.31b)

By inserting the wave function response according to Eqs. (6.26) and (7.22) into Eq. (7.31b) we obtain

$$\rho^{(1)\alpha\pm}(\mathbf{r}) = -\sum_{i\mathbf{k}}^{\text{core}} f_{i\mathbf{k}}^{(0)} \delta_{\alpha\beta} \sum_{\mathbf{R}} e^{\pm i\mathbf{q}\cdot\mathbf{R}} \nabla \rho_{i\mathbf{k}}^{(0)}(\mathbf{r})
+ 2 \sum_{i\mathbf{k}}^{\text{val}} f_{i\mathbf{k}}^{(0)} \sum_{\mathbf{G}\mathbf{G}'} \left\{ z_{\mathbf{k}\mathbf{G}'}^{i\mathbf{k}(0)*} z_{\mathbf{k}\pm\mathbf{q},\mathbf{G}}^{i\mathbf{k}(1)\alpha\pm} \phi_{\mathbf{k}\mathbf{G}'}^{(0)*}(\mathbf{r}) \phi_{\mathbf{k}\pm\mathbf{q},\mathbf{G}}^{(0)}(\mathbf{r})
+ \sum_{\mathbf{R}} \Theta(R_{\alpha} - |\mathbf{r} - \boldsymbol{\tau}_{\alpha} - \mathbf{R}|) e^{\pm i\mathbf{q}\cdot\mathbf{R}} z_{\mathbf{k}\mathbf{G}'}^{i\mathbf{k}(0)*} z_{\mathbf{k}\mathbf{G}}^{i\mathbf{k}(0)} \phi_{\mathbf{k}\mathbf{G}'}^{(0)*}(\mathbf{r}) [i(\mathbf{k} + \mathbf{G}) - \nabla] \phi_{\mathbf{k}\mathbf{G}}^{(0)}(\mathbf{r}) \right\}.$$
(7.32)

The first term in curly brackets is due to the variation in the expansion coefficients, while the third line results from the variation in the basis functions. When the summations are executed, the very last term including the gradient ∇ becomes the gradient of the unperturbed valence density. In general, $\rho_{ik}^{(0)}(r)$ denotes the part of the density generated by the state (ik), without the weighting factor $f_{ik}^{(0)}$. In the first line, (ik) refers to the core states. We explicitly separate the shift in the Bloch wave vector by including $\sum_{\mathbf{R}} \exp(\pm i\mathbf{q} \cdot \mathbf{R})$ in the formula. Furthermore, to properly consider the coretail in this term, we convolute the summation over the core states to yield the pseudo core density of atom α , $\rho_{\text{core}}^{\alpha(0)}(r-\tau_{\alpha})$, which we introduced in Eq. (3.36). In this equation, the density of the core states within their native muffin-tin sphere is replaced by a Gaussian to allow for a rapidly convergent Fourier expansion of the core density. We undo this replacement when we discuss the density response within the MT sphere of atom α .

In the following, we develop the explicit formulas for the density response in the IR and MT spheres by substituting the basis functions by their corresponding IR and MT representation. Since we can restrict the density times potential integrals over the whole lattice to a single unit cell by changing the normalization of the LAPW basis function to Ω , we will only consider the representative unit cell R=0.

Interstitial region

In the interstitial region, the density response is composed of the response of the coretail density and the response of the expansion coefficients, since the last line of Eq. (7.32) is only non-zero in the MT spheres. The interstitial density response takes the form

$$\rho^{(1)\alpha\pm}(\mathbf{r}) = -\sum_{\mathbf{G}} i(\mathbf{G} \pm \mathbf{q}) \hat{\rho}_{\text{core}}^{\alpha(0)}(\mathbf{G}) e^{i(\mathbf{G} \pm \mathbf{q}) \cdot \mathbf{r}}$$

$$+ 2 \sum_{i\mathbf{k}}^{\text{val}} f_{i\mathbf{k}}^{(0)} \sum_{\mathbf{G}\mathbf{G}'} z_{\mathbf{k}\mathbf{G}'}^{i\mathbf{k}(0)*} z_{\mathbf{k}\pm\mathbf{q},\mathbf{G}}^{i\mathbf{k}(1)\alpha\pm} \frac{1}{\Omega} e^{i(\mathbf{G} \pm \mathbf{q} - \mathbf{G}') \cdot \mathbf{r}}.$$
(7.33a)

By rearranging the sums such that the reciprocal summation comes first, we find

$$\rho^{(1)\alpha\pm}(\mathbf{r}) = -\sum_{\mathbf{G}} i(\mathbf{G} \pm \mathbf{q}) \hat{\rho}_{\text{core}}^{(0)}(\mathbf{G}) e^{i(\mathbf{G} \pm \mathbf{q}) \cdot \mathbf{r}}$$

$$+ \sum_{\mathbf{G}\mathbf{G}'} 2 \sum_{i\mathbf{k}}^{\text{val}} f_{i\mathbf{k}}^{(0)} z_{\mathbf{k}\mathbf{G}'}^{i\mathbf{k}(0)*} z_{\mathbf{k} \pm \mathbf{q}, \mathbf{G}}^{i\mathbf{k}(1)\alpha\pm} \frac{1}{\Omega} e^{i(\mathbf{G} \pm \mathbf{q} - \mathbf{G}') \cdot \mathbf{r}}$$

$$= \sum_{\mathbf{G}''} \hat{\rho}^{(1)\alpha\pm}(\mathbf{G}'') e^{i(\mathbf{G}'' \pm \mathbf{q}) \cdot \mathbf{r}}. \tag{7.33b}$$

We have subsumed the remaining terms in the Fourier coefficient

$$\hat{\rho}^{(1)\alpha\pm}(\mathbf{G}'') = -i(\mathbf{G}''\pm\mathbf{q})\hat{\rho}_{\text{core}}^{\alpha(0)}(\mathbf{G}'') + \frac{2}{\Omega} \sum_{\mathbf{G}'} \sum_{i\mathbf{k}}^{\text{val}} f_{i\mathbf{k}}^{(0)} z_{\mathbf{k}\mathbf{G}'}^{i\mathbf{k}(0)*} z_{\mathbf{k}\pm\mathbf{q},\mathbf{G}''+\mathbf{G}'}^{i\mathbf{k}(1)\alpha\pm}.$$
(7.33c)

Muffin-tin spheres

We calculate first the spherical harmonic expansion of the first-order change in the density due to a displacement of the atomic nucleus α at an arbitrary muffin-tin sphere $\beta \neq \alpha$. According to Eq. (7.32), it is given by

$$\boldsymbol{\rho}^{(1)\alpha\pm}(\boldsymbol{r}) = \sum_{lm} \boldsymbol{\rho}_{lm\beta}^{(1)\alpha\pm}(r_{\beta}) Y_{lm}(\hat{\boldsymbol{r}}_{\beta})$$
 (7.34a)

with the local coordinates $r_{\beta} = r - \tau_{\beta}$ and the expansion coefficients

$$\rho_{lm\beta}^{(1)\alpha\pm}(r_{\beta}) = -4\pi i^{l} \sum_{\mathbf{G}} i(\mathbf{G} \pm \mathbf{q}) e^{i(\mathbf{G} \pm \mathbf{q}) \cdot \boldsymbol{\tau}_{\beta}} \hat{\rho}_{\text{core}}^{\alpha(0)}(\mathbf{G}) Y_{lm}^{*}(\widehat{\mathbf{G}} \pm \mathbf{q}) j_{l}(|\mathbf{G} \pm \mathbf{q}| r_{\beta})$$

$$+ 2 \sum_{i\mathbf{k}}^{\text{val}} f_{i\mathbf{k}}^{(0)} \sum_{\mathbf{G}\mathbf{G}' \ l'm'\lambda'l''m''\lambda''} G_{l'',l,l'}^{m'',m,m'} u_{l'\lambda'}^{\beta}(r_{\beta}) u_{l''\lambda''}^{\beta}(r_{\beta})$$

$$\times z_{\mathbf{k}\mathbf{G}'}^{i\mathbf{k}(0)*} z_{\mathbf{k}\pm\mathbf{q},\mathbf{G}}^{i\mathbf{k}(1)\alpha\pm} a_{l'm'\lambda'}^{\beta\mathbf{k}\mathbf{G}'*} a_{l'm''\lambda''}^{\beta,\mathbf{k}\pm\mathbf{q},\mathbf{G}}. \tag{7.34b}$$

We introduce the G contraction of the perturbed expansion coefficients with the unperturbed matching coefficients in analogy to Eq. (3.23) for the unperturbed expansion and matching coefficients:

$$A_{lm\lambda\beta}^{\alpha ik\pm} = \sum_{G} z_{k\pm q,G}^{ik(1)\alpha\pm} a_{lm\lambda}^{\beta,k\pm q,G}$$
 (7.34c)

Using these coefficients, the density response simplifies to

$$\rho_{lm\beta}^{(1)\alpha\pm}(r_{\beta}) = -4\pi i^{l} \sum_{\mathbf{G}} i(\mathbf{G} \pm \mathbf{q}) e^{i(\mathbf{G} \pm \mathbf{q}) \cdot \boldsymbol{\tau}_{\beta}} Y_{lm}^{*}(\widehat{\mathbf{G}} \pm \mathbf{q}) j_{l}(|\mathbf{G} \pm \mathbf{q}| r_{\beta}) \hat{\rho}_{\text{core}}^{\alpha(0)}(\mathbf{G})
+ \sum_{l'\lambda'l''\lambda''} u_{l'\lambda'}^{\beta}(r_{\beta}) u_{l''\lambda''}^{\beta}(r_{\beta}) \sum_{m'm''} G_{l'',l,l'}^{m'',m,m'} 2 \sum_{i\mathbf{k}}^{\text{val}} f_{i\mathbf{k}}^{(0)} A_{l'm'\lambda'}^{\beta i\mathbf{k}*} A_{l''m''\lambda''\beta}^{\alpha i\mathbf{k} \pm}.$$
(7.34d)

At muffin-tin sphere α of the representative unit cell $\mathbf{R}=\mathbf{0}$, the expansion coefficients $\rho_{lm\alpha}^{(1)\alpha\pm}$ have to be further modified. For once, we added the Fourier expansion of the pseudo core density response at all muffin-tin spheres. This has to be corrected in the muffin-tin sphere of atom α by replacing the pseudo core density by the original core density. Second, at the muffin-tin sphere of atom α , the last line of Eq. (7.32) contributes. Therefore, we have to complement Eq. (7.34d) in the MT sphere of atom α by

$$\left\{2\sum_{ik}^{\text{val}} f_{ik}^{(0)} \sum_{\boldsymbol{G}\boldsymbol{G}'} z_{k\boldsymbol{G}}^{ik(0)*} z_{k\boldsymbol{G}'}^{ik(0)} \phi_{k\boldsymbol{G}}^{\alpha(0)*}(\boldsymbol{r}_{\alpha}) \left[i(\boldsymbol{k}+\boldsymbol{G})-\nabla\right] \phi_{k\boldsymbol{G}'}^{\alpha(0)}(\boldsymbol{r}_{\alpha}) - \nabla\rho_{\text{core}}^{\alpha(0)}(\boldsymbol{r}_{\alpha}) + \nabla\tilde{\rho}_{\text{core}}^{\alpha(0)}(\boldsymbol{r}_{\alpha})\right\}_{lm} \\
= 2i\sum_{l'\lambda'l''\lambda''} u_{l'\lambda'}^{\alpha}(r_{\alpha}) u_{l''\lambda''}^{\alpha}(r_{\alpha}) \sum_{m'm''} G_{l'',l,l'}^{m'',m,m'} \\
\times \sum_{ik} f_{ik}^{(0)} A_{l'm'\lambda'}^{\alpha ik*} \left[kA_{l''m''\lambda''}^{\alpha ik} + A_{l''m''\lambda''}^{\alpha ik}\right] \\
- \underline{T}\sqrt{\frac{4\pi}{3}} \sum_{l'm'} \sum_{m''} \hat{e}_{m''} \sum_{l''=-1}^{1,2} G_{l,l',1}^{m,m',m''} \delta_{l,l'+l''} \delta_{m,m'+m''} \\
\times \left[\rho_{l'm'}^{\alpha(0)'}(r_{\alpha}) - \left(l''l' + \frac{l''-1}{2}\right) \frac{\rho_{l'm'}^{\alpha(0)}(r_{\alpha})}{r_{\alpha}}\right] \\
- 2r_{\alpha} a_{\alpha} A_{\alpha} e^{-a_{\alpha} r_{\alpha}^{2}} \sum_{i=1}^{3} \hat{e}_{i} c_{i,m} \delta_{1l}. \tag{7.34e}$$

The second term, which includes the transformation matrix \underline{T} from the natural coordinates to Cartesian coordinates defined in Eq. (4.18), subsumes the gradient of the valence density and of the original core density of atom α , while the last term accounts for the gradient of the pseudo core density.

With the response of the density due to a collective displacement of the atoms modulated by a wave vector \mathbf{q} at hand, we are now in the position to calculate the linear change in the Hartree and the xc potential.

7.1.4. Evaluation of the first-order changes of the potential

According to Eq. (6.15a revisited), the first-order change of the effective potential decomposes into first-order changes in the external potential, the Hartree potential, and the xc potential. We will discuss each component separately in the following sections.

7.1.4.1. The first-order change $V_{ m ext}^{(1)}({m r})$ of the external potential

The first-order change in the external potential is special for two reasons. First, it is the pure perturbation and does not change during the iterations of the Sternheimer equation. Therefore, it has to be calculated only once at the beginning of the calculation. Second, it represents the starting 'guess' for the change in the effective potential to initialize the SCF cycle, *i.e.*, in the first iteration, it is $V_{\rm eff}^{(1)}(r) = V_{\rm ext}^{(1)}(r)$. Formally, we have given the first-order change in the external potential in Eq. (7.6). How-

Formally, we have given the first-order change in the external potential in Eq. (7.6). However, in order to use it in the Sternheimer equation, Eq. (7.24), we need to express it in terms of radial functions times spherical harmonics in the muffin-tin spheres and in terms of a Fourier expansion in the interstitial region, as is the common procedure in the FLAPW method. The respective representations of $V_{\rm ext}^{(1)}(r)$ can be obtained using the procedure by Weinert as introduced in chapter 3.7. In the Weinert scheme, the electrostatic potential in the interstitial region is constructed from the interstitial charge density and from a pseudodensity in the muffin-tin spheres which has the same multipole moments as the original density, but has a rapidly converging Fourier expansion. The MT potential is then constructed from a Dirichlet boundary value problem using the correct local density in the MT sphere and the potential from the IR as boundary values.

Construction of the pseudodensity

In order to use the Weinert method, we first need to identify the density in the muffin-tin spheres from which we construct a smooth pseudodensity with the same multipole moments. According to Eqs. (7.6) and (7.8), the linear change of the external potential can be written as

$$V_{\text{ext}}^{(1)\alpha\pm}(\mathbf{r}) = -\sum_{\mathbf{R}} e^{\pm i\mathbf{q}\cdot\mathbf{R}} \nabla V_{\text{ext}}^{\alpha\mathbf{R}}(\mathbf{r})$$

$$= \int \frac{\sum_{\mathbf{R}} Z_{\alpha} e^{\pm i\mathbf{q}\cdot\mathbf{R}} \nabla' \delta(\mathbf{r}' - \boldsymbol{\tau}_{\alpha} - \mathbf{R})}{|\mathbf{r} - \mathbf{r}'|} d^{3}r'. \tag{7.35}$$

Similarly, the gradient of the external potential can be expressed by

$$\nabla V_{\text{ext}}^{(0)}(\mathbf{r}) = \sum_{\alpha \mathbf{R}} \nabla V_{\text{ext}}^{\alpha \mathbf{R}}(\mathbf{r}) = -\sum_{\alpha} \int \nabla \frac{\sum_{\mathbf{R}} Z_{\alpha} \delta(\mathbf{r}' - \boldsymbol{\tau}_{\alpha} - \mathbf{R})}{|\mathbf{r} - \mathbf{r}'|} d^{3} r'$$

$$= -\sum_{\alpha} \int \frac{\sum_{\mathbf{R}} Z_{\alpha} \nabla' \delta(\mathbf{r}' - \boldsymbol{\tau}_{\alpha} - \mathbf{R})}{|\mathbf{r} - \mathbf{r}'|} d^{3} r'.$$
(7.36)

The atomic-density gradients within the integrals deviate from each other by a sign and by the factor $\exp(\pm i q \cdot R)$. Therefore, we can define a general ion-density response $n^{\alpha \bar{q}}(r)$ as

$$n^{\alpha \tilde{q}}(r) = \sum_{R} Z_{\alpha} e^{i\tilde{q} \cdot R} \nabla \delta(r - \tau_{\alpha} - R),$$
 (7.37)

which corresponds to the nominator occurring in Eq. (7.36) for $\tilde{q} = 0$ and in Eq. (7.35) for $\tilde{q} = \pm q$. It is this expression which we have to replace by a pseudodensity. We use the symbols n and q_{lm} in analogy to the notation of chapter 3.7, where they denoted the electrostatic density and its multipole moments, even though $n^{\alpha\tilde{q}}(r)$ is technically the derivative of a δ -density. The multipole moments caused by displacing atom α and its images according to a perturbation of wave vector \tilde{q} in the multipole moments of a tom β in unit cell R' are

$$q_{lm}^{\alpha\bar{\mathbf{q}}}(\beta, \mathbf{R}') = \int_{\mathrm{MT}(\beta, \mathbf{R}')} Y_{lm}^*(\mathbf{r} - \widehat{\boldsymbol{\tau}_{\beta}} - \mathbf{R}') |\mathbf{r} - \boldsymbol{\tau}_{\beta} - \mathbf{R}'|^l n^{\alpha\bar{\mathbf{q}}}(\mathbf{r}) d^3 r$$

$$= \sum_{\mathbf{R}} Z_{\alpha} e^{i\bar{\mathbf{q}} \cdot \mathbf{R}} \int_{B_{R_{\beta}}(\mathbf{0})} Y_{lm}^*(\hat{\mathbf{r}}_{\beta}) r_{\beta}^l \nabla_{\beta} \delta(\mathbf{r}_{\beta} - (\boldsymbol{\tau}_{\alpha} - \boldsymbol{\tau}_{\beta}) - (\mathbf{R} - \mathbf{R}')) d^3 r_{\beta}$$

$$= -Z_{\alpha} e^{i\bar{\mathbf{q}} \cdot \mathbf{R}'} \delta_{\alpha\beta} \nabla [r^l Y_{lm}^*(\hat{\mathbf{r}})]_{r=\mathbf{0}}. \tag{7.38}$$

We obtained this result by an integration by parts and by realizing that the argument of the Dirac- δ can only be zero for $\alpha=\beta$ and for $\mathbf{R}=\mathbf{R}'$, since the muffin-tin spheres are not overlapping. The multipole moments contain a phase factor $\exp(i\tilde{\mathbf{q}}\cdot\mathbf{R}')$ corresponding to the unit cell \mathbf{R}' at which the ion-density response is evaluated. The l=1 component is selected because for l=0, the gradient acts on a constant, while for $l\geq 2$ the contribution is suppressed by the term proportional to r^{l-1} that remains after application of the gradient, since the expression is evaluated at the muffin-tin sphere center, i.e., at r=0. The ion-density response is zero at every place other than the muffin-tin sphere centers of atom α and its images, in particular the interstitial contribution to $\mathbf{n}^{\alpha\bar{\mathbf{q}}}(\mathbf{r})$ is zero. Therefore, no multipole moments from a plane wave extension into the MT sphere has to be subtracted. By Eqs. (3.46) and following, the pseudodensity in the muffin-tin sphere of atom α in unit cell \mathbf{R} is given by

$$n_{\text{ps}}^{\alpha R\tilde{\mathbf{q}}}(\mathbf{r}_{\alpha}) = \sum_{m=-1}^{1} \mathbf{q}_{1m}^{\alpha\tilde{\mathbf{q}}}(\alpha, \mathbf{R}) Y_{1m}(\hat{\mathbf{r}}_{\alpha}) \left[\sum_{\eta=0}^{N} a_{\eta}^{\alpha} \frac{R_{\alpha}^{2\eta+5}}{2\eta+5} \right]^{-1} \left[\sum_{\eta=0}^{N} a_{\eta}^{\alpha} r_{\alpha}^{2\eta+1} \right]$$
$$= e^{i\tilde{\mathbf{q}} \cdot \mathbf{R}} n_{\text{ps}}^{\alpha 0\tilde{\mathbf{q}}}(\mathbf{r}_{\alpha})$$
(7.39)

and the Fourier transform of the lattice periodic part over the representative unit cell Ω (i.e., R = 0) yields

$$n_{\text{ps}}^{\alpha\tilde{\mathbf{q}}}(\mathbf{r}) = e^{i\tilde{\mathbf{q}}\cdot\mathbf{r}} e^{-i\tilde{\mathbf{q}}\cdot\mathbf{r}} \sum_{\mathbf{R}} n_{\text{ps}}^{\alpha\mathbf{R}\tilde{\mathbf{q}}}(\mathbf{r})\Theta(R_{\alpha} - |\mathbf{r} - \boldsymbol{\tau}_{\alpha} - \mathbf{R}|)$$

$$= e^{i\tilde{\mathbf{q}}\cdot\mathbf{r}} \sum_{\mathbf{G}} e^{i\mathbf{G}\cdot\mathbf{r}} \frac{1}{\Omega} \int_{\Omega} e^{-i\mathbf{G}\cdot\mathbf{r}'} e^{-i\tilde{\mathbf{q}}\cdot\mathbf{r}'} \sum_{\mathbf{R}} n_{\text{ps}}^{\alpha\mathbf{R}\tilde{\mathbf{q}}}(\mathbf{r}')\Theta(R_{\alpha} - |\mathbf{r}' - \boldsymbol{\tau}_{\alpha} - \mathbf{R}|) d^{3}r'$$

$$= \sum_{\mathbf{G}} e^{i(\mathbf{G}+\tilde{\mathbf{q}})\cdot\mathbf{r}} \hat{\mathbf{n}}_{\text{ps}}^{\alpha\tilde{\mathbf{q}}}(\mathbf{G}). \tag{7.40}$$

Following the scheme of Weinert, the Fourier coefficients are given by

$$\hat{\boldsymbol{n}}_{\mathrm{ps}}^{\alpha\tilde{\boldsymbol{q}}}(\boldsymbol{G}) = \frac{1}{\Omega} \int_{\Omega} e^{-i(\boldsymbol{G} + \tilde{\boldsymbol{q}}) \cdot \boldsymbol{r}'} \sum_{\boldsymbol{R}} n_{\mathrm{ps}}^{\alpha\boldsymbol{R}\tilde{\boldsymbol{q}}}(\boldsymbol{r}') \Theta(R_{\alpha} - |\boldsymbol{r}' - \boldsymbol{\tau}_{\alpha} - \boldsymbol{R}|) d^{3}r'$$

$$= -\frac{4\pi i}{\Omega} \sum_{m=-1}^{1} \frac{(2N+5)!!}{3R_{\alpha}} \frac{j_{N+2}(|\boldsymbol{G} + \tilde{\boldsymbol{q}}|R_{\alpha})}{(|\boldsymbol{G} + \tilde{\boldsymbol{q}}|R_{\alpha})^{N+1}} q_{1m}^{\alpha\tilde{\boldsymbol{q}}}(\alpha, \boldsymbol{0}) e^{-i(\boldsymbol{G} + \tilde{\boldsymbol{q}}) \cdot \boldsymbol{\tau}_{\alpha}} Y_{1m}(\widehat{\boldsymbol{G} + \tilde{\boldsymbol{q}}}). \tag{7.41}$$

This can be further simplified by inserting the multipole moment from Eq. (7.38) and summing over m:

$$\sum_{m=-1}^{1} q_{1m}^{\alpha \tilde{\mathbf{q}}}(\alpha, \mathbf{0}) Y_{1m}(\widehat{\mathbf{G}} + \widehat{\tilde{\mathbf{q}}}) = -Z_{\alpha} \sum_{m=-1}^{1} \nabla \left[r Y_{1m}^{*}(\hat{\mathbf{r}}) \right]_{r=\mathbf{0}} Y_{1m}(\widehat{\mathbf{G}} + \widehat{\tilde{\mathbf{q}}})$$

$$= -Z_{\alpha} \nabla \left[r \sum_{m=-1}^{1} Y_{1m}^{*}(\hat{\mathbf{r}}) Y_{1m}(\widehat{\mathbf{G}} + \widehat{\tilde{\mathbf{q}}}) \right]_{r=\mathbf{0}} = -Z_{\alpha} \nabla \left[r \frac{3}{4\pi} P_{1}(\hat{\mathbf{r}} \cdot (\widehat{\mathbf{G}} + \widehat{\tilde{\mathbf{q}}})) \right]_{r=\mathbf{0}}$$

$$= -Z_{\alpha} \frac{3}{4\pi} \nabla \left[r \cdot (\widehat{\mathbf{G}} + \widehat{\tilde{\mathbf{q}}}) \right] = -Z_{\alpha} \frac{3}{4\pi} (\widehat{\mathbf{G}} + \widehat{\tilde{\mathbf{q}}}) \tag{7.42}$$

Here, we used the addition theorem for spherical harmonics $P_l(\hat{x} \cdot \hat{y}) = 4\pi/(2l+1) \cdot \sum_m Y_{lm}^*(\hat{x}) Y_{lm}(\hat{y})$ with the Legendre polynomials $P_l(r)$, $P_1(r)$ equaling r. With this, the Fourier coefficients become

$$\hat{\boldsymbol{n}}_{\mathrm{ps}}^{\alpha\tilde{\boldsymbol{q}}}(\boldsymbol{G}) = \frac{iZ_{\alpha}}{\Omega}(2N+5)!!\frac{j_{N+2}(|\boldsymbol{G}+\tilde{\boldsymbol{q}}|R_{\alpha})}{(|\boldsymbol{G}+\tilde{\boldsymbol{q}}|R_{\alpha})^{N+2}}e^{-i(\boldsymbol{G}+\tilde{\boldsymbol{q}})\cdot\boldsymbol{\tau}_{\alpha}}(\boldsymbol{G}+\tilde{\boldsymbol{q}}). \tag{7.43a}$$

This expression is undefined for $\tilde{q} = G = 0$. In this case, we have

$$\hat{\boldsymbol{n}}_{\mathrm{ps}}^{\alpha\tilde{\boldsymbol{q}}}(\mathbf{0}) = \mathbf{0},\tag{7.43b}$$

as can be verified by explicitly calculating the Fourier component for G = 0 of $n_{\rm ps}^{\alpha 0}(r)$ and realizing that the angular integral is only over $Y_{1m}(\hat{r})$, thus yielding zero, or by showing that the fraction in Eq. (7.43a) containing the spherical Bessel function is bounded. In this case, the vector $G + \tilde{q}$ directly makes the right hand side of the equation zero. In the limit $t \to 0$, L'Hôspital's rule states that

$$\frac{j_{N+2}(t)}{t^{N+2}} \to \frac{t^{N+3}j_{N+2}(t)}{t^{2N+5}} \to \frac{t^{N+3}j_{N+1}(t)}{(2N+5)t^{2N+4}} = \frac{t^{N+2}j_{N+1}(t)}{(2N+5)t^{2N+3}}
\to \frac{t^{N+2}j_{N}(t)}{(2N+5)(2N+3)t^{2N+2}} \to \cdots \to \frac{1}{(2N+5)!!}.$$
(7.44)

It is no surprise that the **0**-component of the ion-density response vanishes. It contains the average alteration of ionic charge in the system. However, the phononic perturbation does not add or remove charges from the system, but only displaces the atoms in the unit cells.

The interstitial contributions

Having knowledge about the Fourier components of the pseudodensity representing the ion-density response, we can express the interstitial part of the linear change in the external potential:

$$V_{\text{ext}}^{(1)\alpha\pm}(\mathbf{r}) = 4\pi \sum_{\mathbf{G},\mathbf{G}\pm\mathbf{q}\neq\mathbf{0}} \frac{\hat{\mathbf{n}}_{\text{ps}}^{\alpha\pm\mathbf{q}}(\mathbf{G})}{|\mathbf{G}\pm\mathbf{q}|^2} e^{i(\mathbf{G}\pm\mathbf{q})\cdot\mathbf{r}}$$

$$=: \sum_{\mathbf{G},\mathbf{G}\pm\mathbf{q}\neq\mathbf{0}} \hat{\mathbf{V}}_{\text{ext}}^{(1)\alpha\pm}(\mathbf{G}) e^{i(\mathbf{G}\pm\mathbf{q})\cdot\mathbf{r}}$$
(7.45a)

$$\nabla V_{\text{ext}}^{(0)}(\mathbf{r}) = 4\pi \sum_{\mathbf{G} \neq \mathbf{0}} \frac{-\sum_{\alpha} \hat{\mathbf{n}}_{\text{ps}}^{\alpha \mathbf{0}}(\mathbf{G})}{G^2} e^{i\mathbf{G} \cdot \mathbf{r}} =: \sum_{\mathbf{G} \neq \mathbf{0}} \widehat{[\nabla V_{\text{ext}}^{(\mathbf{0})}]}(\mathbf{G}) e^{i\mathbf{G} \cdot \mathbf{r}}$$
(7.45b)

We use these results to develop formulas for the muffin-tin parts of $V_{\rm ext}^{(1)\alpha\pm}(r)$ and $\nabla V_{\rm ext}^{(0)}(r)$ in the following.

The muffin-tin contributions

From the IR representation of the perturbed potential we can calculate the MT part by making use of the Green function technique as proposed by Weinert. The latter requires the potential (response) on the surface of the MT sphere, given by Eq. (7.45), and the true charge density (response) inside the corresponding sphere. In order to make use of Eq. (3.61), we have to Rayleigh-expand Eq. (7.45). We start the derivation of $V_{\text{ext}}^{(1)\alpha\pm}(r)$ from the Dirichlet boundary-value problem defining the MT change of the external potential in the MT sphere of atom β in unit cell R',

$$\mathbf{V}_{\text{ext}}^{(1)\alpha\pm}(\mathbf{r}_{\beta}+\mathbf{\tau}_{\beta}+\mathbf{R}') = \int_{B_{R_{\beta}}(\mathbf{0})} \mathbf{n}^{\alpha\pm\mathbf{q}}(\mathbf{s}_{\beta}+\mathbf{\tau}_{\beta}+\mathbf{R}')G(\mathbf{r}_{\beta},\mathbf{s}_{\beta})d^{3}\mathbf{s}_{\beta}$$
$$-\frac{1}{4\pi} \oint_{\partial B_{R_{\beta}}(\mathbf{0})} \mathbf{V}_{\text{ext}}^{(1)\alpha\pm}(\mathbf{s}_{\beta}+\mathbf{\tau}_{\beta}+\mathbf{R}')\nabla_{\mathbf{s}_{\beta}}G(\mathbf{r}_{\beta},\mathbf{s}_{\beta})dS. \quad (7.46)$$

Inserting the Green function and its radial derivative defined in Eqs. (3.59) and (3.62), an integration by parts of the gradient contained in the ion-density response $n^{\alpha \pm q}(s_{\beta} + \tau_{\beta} + R')$ yields

$$V_{\text{ext}}^{(1)\alpha\pm}(\boldsymbol{r}_{\beta} + \boldsymbol{\tau}_{\beta} + \boldsymbol{R}')$$

$$= -e^{\pm i\boldsymbol{q}\cdot\boldsymbol{R}'}Z_{\alpha}\delta_{\alpha\beta}\frac{4\pi}{3}\frac{1}{r_{\alpha}^{2}}\left[1 - \left(\frac{r_{\alpha}}{R_{\alpha}}\right)^{3}\right]\sum_{m=-1}^{1}Y_{1m}(\hat{\boldsymbol{r}}_{\alpha})\nabla_{\boldsymbol{s}}\left[sY_{1m}^{*}(\hat{\boldsymbol{s}})\right]_{\boldsymbol{s}=\boldsymbol{0}}$$

$$+ e^{\pm i\boldsymbol{q}\cdot\boldsymbol{R}'}\sum_{\boldsymbol{G},\boldsymbol{G}\pm\boldsymbol{q}\neq\boldsymbol{0}}e^{i(\boldsymbol{G}\pm\boldsymbol{q})\cdot\boldsymbol{\tau}_{\beta}}\hat{\boldsymbol{V}}_{\text{ext}}^{(1)\alpha\pm}(\boldsymbol{G}\pm\boldsymbol{q})$$

$$\times\sum_{lm}\left(\frac{r_{\beta}}{R_{\beta}}\right)^{l}4\pi i^{l}Y_{lm}^{*}(\widehat{\boldsymbol{G}\pm\boldsymbol{q}})j_{l}(|\boldsymbol{G}\pm\boldsymbol{q}|R_{\beta})Y_{lm}(\hat{\boldsymbol{r}}_{\beta}). \tag{7.47}$$

The first part of the equation stems from the volume integral containing the true iondensity response, while the second part is due to the surface integral. Similarly, we find for the gradient of the external potential

$$\nabla V_{\text{ext}}^{(0)}(\boldsymbol{r}_{\beta} + \boldsymbol{\tau}_{\beta} + \boldsymbol{R}')$$

$$= Z_{\alpha} \delta_{\alpha\beta} \frac{4\pi}{3} \frac{1}{r_{\alpha}^{2}} \left[1 - \left(\frac{r_{\alpha}}{R_{\alpha}} \right)^{3} \right] \sum_{m=-1}^{1} Y_{1m}(\hat{\boldsymbol{r}}_{\alpha}) \nabla_{\boldsymbol{s}} \left[s Y_{1m}^{*}(\hat{\boldsymbol{s}}) \right]_{\boldsymbol{s}=\boldsymbol{0}}$$

$$+ \sum_{\boldsymbol{G} \neq \boldsymbol{0}} e^{i\boldsymbol{G} \cdot \boldsymbol{\tau}_{\beta}} \left[\widehat{\boldsymbol{\nabla} V_{\text{ext}}^{(0)}} \right] (\boldsymbol{G}) \sum_{lm} \left(\frac{r_{\beta}}{R_{\beta}} \right)^{l} 4\pi i^{l} Y_{lm}^{*}(\hat{\boldsymbol{G}}) j_{l}(GR_{\beta}) Y_{lm}(\hat{\boldsymbol{r}}_{\beta}). \tag{7.48}$$

The gradient of sY_{1m}^* can be combined with the sum over m to yield \hat{r}_{α} as was done in Eq. (7.42). A subsequent expansion of \hat{r}_{α} in terms of spherical harmonics results in the equality

$$\sum_{m=-1}^{1} Y_{1m}(\hat{\boldsymbol{r}}_{\alpha}) \nabla_{\boldsymbol{s}} \left[s Y_{1m}^{*}(\hat{\boldsymbol{s}}) \right]_{\boldsymbol{s}=\boldsymbol{0}} = \frac{3}{4\pi} \hat{\boldsymbol{r}}_{\alpha} = \frac{3}{4\pi} \sum_{m=-1}^{1} Y_{1m}(\hat{\boldsymbol{r}}_{\alpha}) \sum_{i=1}^{3} \hat{\boldsymbol{e}}_{i} c_{i,m}$$
(7.49)

with the Cartesian basis vectors \hat{e}_i and the coefficients $c_{i,m}$ from Eq. (4.28).

When the linear perturbation of the external potential and the gradient of the unperturbed external potential are combined in Eq. (7.24) for evaluating the muffin-tin sphere contribution of atom α in the representative unit cell $\mathbf{R}' = \mathbf{0}$, the contributions from $\mathbf{V}_{\mathrm{ext}}^{(1)\alpha\pm}$ and $\nabla V_{\mathrm{ext}}^{(0)}$ stemming from the volume integral over the local ion-density response cancel, leaving only the surface terms to be considered. Hence, the numerically delicate step of calculating the gradient of $V_{\mathrm{ext}}^{(0)}(\mathbf{r})$ can be completely avoided for evaluating the Sternheimer equation.

7.1.4.2. The first-order change $V_{\mathbf{H}}^{(1)}(r)$ of the Hartree potential

To obtain all ingredients for the Sternheimer equation, Eq. (7.24), we also need the response of the Hartree potential, which, according to Eq. (6.38), is given as

$$\boldsymbol{V}_{\mathrm{H}}^{(1)\alpha\pm}(\boldsymbol{r}) = \int \frac{\boldsymbol{\rho}^{(1)\alpha\pm}(\boldsymbol{r}')}{|\boldsymbol{r}-\boldsymbol{r}'|} d^{3}r' + \sum_{\boldsymbol{R}} e^{\pm i\boldsymbol{q}\cdot\boldsymbol{R}} \oint_{\partial \mathrm{MT}(\alpha,\boldsymbol{R})} \hat{\boldsymbol{e}}' \frac{\left[\boldsymbol{\rho}^{(0)}(\boldsymbol{r}')\right]_{\mathrm{SF}}}{|\boldsymbol{r}-\boldsymbol{r}'|} dS', \tag{7.50}$$

as well as the gradient of the Hartree potential in the muffin-tin sphere of atom α ,

$$\nabla V_{\rm H}(\boldsymbol{r}) = \nabla \int \frac{\rho(\boldsymbol{r}')}{|\boldsymbol{r} - \boldsymbol{r}'|} d^3 r'$$

$$= \int \frac{\nabla' \rho(\boldsymbol{r}')}{|\boldsymbol{r} - \boldsymbol{r}'|} d^3 r' - \sum_{\beta \boldsymbol{R}} \oint_{\mathrm{MT}(\beta, \boldsymbol{R})} \hat{\boldsymbol{e}}' \frac{\left[\rho^{(0)}(\boldsymbol{r}')\right]_{\mathrm{SF}}}{|\boldsymbol{r} - \boldsymbol{r}'|} dS'. \tag{7.51}$$

We obtained the second line of the right-hand side by an integration by parts. In this form, it is explicitly visible how the density response $\rho^{(1)\alpha\pm}$ and the density gradient $\nabla'\rho$ interact when the Hartree response and the gradient of the Hartree potential come together in the Sternheimer equation, Eq. (7.24); also the density terms add up to $\rho^{(1)\alpha\pm}(\mathbf{r}') + \nabla'\rho(\mathbf{r}')$, similar to the potential terms. In Eq. (7.32), $\rho^{(1)\alpha\pm}(\mathbf{r}')$ is shown to contain the negative gradient of the density in the MT spheres of atom α and its images.

Construction of the pseudodensity

We want to use the Weinert method introduced in chapter 3.7 to construct expressions for the Hartree response and the gradient of the Hartree potential. Before we do so, we need to rewrite the surface integrals in terms of a volume integral in order to include them into the construction of the pseudodensity response. If we denote with \tilde{q} any of 0 or $\pm q$, the surface terms of the Hartree response and the gradient of the Hartree potential can be written as

$$\sum_{\boldsymbol{R}} e^{i\tilde{\boldsymbol{q}}\cdot\boldsymbol{R}} \oint_{\partial \mathrm{MT}(\alpha,\boldsymbol{R})} \hat{\boldsymbol{e}}' \frac{\left[\rho^{(0)}(\boldsymbol{r}')\right]_{\mathrm{SF}}}{|\boldsymbol{r}-\boldsymbol{r}'|} dS'$$

$$= \int \frac{\left[\rho^{(0)}(\mathbf{r}')\right]_{SF} \sum_{\mathbf{R}} e^{i\tilde{\mathbf{q}} \cdot \mathbf{R}} (\mathbf{r}' - \boldsymbol{\tau}_{\alpha} - \mathbf{R}) \delta(R_{\alpha} - |\mathbf{r}' - \boldsymbol{\tau}_{\alpha} - \mathbf{R}|)}{|\mathbf{r} - \mathbf{r}'|} d^{3}r'.$$
(7.52)

Therefore, we define as the density response from the surface integrals the term

$$\boldsymbol{n}^{\alpha \tilde{\boldsymbol{q}}}(\boldsymbol{r}) = \left[\rho^{(0)}(\boldsymbol{r})\right]_{\mathrm{SF}} \sum_{\boldsymbol{R}} e^{i\tilde{\boldsymbol{q}} \cdot \boldsymbol{R}} (\boldsymbol{r} - \boldsymbol{\tau}_{\alpha} - \boldsymbol{R}) \delta(R_{\alpha} - |\boldsymbol{r} - \boldsymbol{\tau}_{\alpha} - \boldsymbol{R}|). \tag{7.53}$$

In the MT sphere of atom β in unit cell \mathbf{R}' , it gives rise to the multipole moments

$$\mathbf{q}_{lm}^{\alpha\bar{\mathbf{q}}}(\beta, \mathbf{R}') = \int_{\mathrm{MT}(\beta, \mathbf{R}')} Y_{lm}^*(\mathbf{r} - \widehat{\boldsymbol{\tau}_{\beta}} - \mathbf{R}') |\mathbf{r} - \boldsymbol{\tau}_{\beta} - \mathbf{R}'|^l \mathbf{n}^{\alpha\bar{\mathbf{q}}}(\mathbf{r}) d^3 r$$

$$= \delta_{\alpha\beta} \oint_{\partial B_{R_{\alpha}}(\mathbf{0})} Y_{lm}^*(\widehat{\boldsymbol{r}}_{\alpha}) r_{\alpha}^l \left[\rho^{(0)}(\mathbf{r}_{\alpha} + \boldsymbol{\tau}_{\alpha}) \right]_{\mathrm{SF}} e^{i\bar{\mathbf{q}} \cdot \mathbf{R}'} \hat{\mathbf{e}} dS_{\alpha}$$

$$= \delta_{\alpha\beta} e^{i\bar{\mathbf{q}} \cdot \mathbf{R}'} R_{\alpha}^l \sum_{i=1}^3 \hat{\mathbf{e}}_i \sum_{m''=-1}^1 c_{i,m''} \sum_{l'=|l-1|}^{l+1,2} G_{l,l',1}^{m,m-m'',m''} \left[\rho_{l',m-m''}^{\alpha(0)}(R_{\alpha}) \right]_{\mathrm{SF}}$$

$$(7.54)$$

In addition, the multipole moments from the density terms in the volume integrals of Eqs. (7.50) and (7.51) have to be constructed. In contrast to the ion-density response, the electronic density response and the gradient of the electronic density are non-zero in the interstitial region. Therefore, also the multipole moments of the plane wave terms extended into the muffin-tin spheres must be included. For the density response $\rho^{(1)\alpha\pm}(r)$, the multipole moments in MT sphere β of unit cell R' are given by

$$q_{lm,\delta\rho}^{\alpha\pm\boldsymbol{q}}(\beta,\boldsymbol{R}') = \int_{\mathrm{MT}(\beta,\boldsymbol{R}')} Y_{lm}^*(\boldsymbol{r} - \widehat{\boldsymbol{\tau}_{\beta}} - \boldsymbol{R}') |\boldsymbol{r} - \boldsymbol{\tau}_{\beta} - \boldsymbol{R}'|^l [\boldsymbol{\rho}^{(1)\alpha\pm}(\boldsymbol{r}) - \boldsymbol{\rho}_{\mathrm{PW}}^{(1)\alpha\pm}(\boldsymbol{r})] d^3r$$

$$= \int_{B_{R_{\beta}}(0)} Y_{lm}^*(\hat{\boldsymbol{r}}_{\beta}) r_{\beta}^l e^{\pm i\boldsymbol{q}\cdot\boldsymbol{R}'} [\boldsymbol{\rho}^{(1)\alpha\pm}(\boldsymbol{r}_{\beta} + \boldsymbol{\tau}_{\beta}) - \boldsymbol{\rho}_{\mathrm{PW}}^{(1)\alpha\pm}(\boldsymbol{r}_{\beta} + \boldsymbol{\tau}_{\beta})] d^3r_{\beta} \quad (7.55)$$

The formula for the MT representation of the density response is given in Eq. (7.34), while its IR representation is expressed in Eq. (7.33). In order to use the latter in the equation above, the $\exp[i(\mathbf{G} \pm \mathbf{q}) \cdot \mathbf{r}]$ have to be Rayleigh-expanded to

$$e^{i(\mathbf{G}\pm\mathbf{q})\cdot\mathbf{r}} = e^{i(\mathbf{G}\pm\mathbf{q})\cdot\boldsymbol{\tau}_{\beta}} \sum_{lm} 4\pi i^{l} Y_{lm}^{*}(\widehat{\mathbf{G}\pm\mathbf{q}}) j_{l}(|\mathbf{G}\pm\mathbf{q}|r_{\beta}) Y_{lm}(\hat{\mathbf{r}}_{\beta}). \tag{7.56}$$

Then the multipole moments of the density response become

$$\begin{aligned} \boldsymbol{q}_{lm,\delta\rho}^{\alpha\pm\boldsymbol{q}}(\boldsymbol{\beta},\boldsymbol{R}') &= e^{\pm i\boldsymbol{q}\cdot\boldsymbol{R}'} \int_{0}^{R_{\beta}} r_{\beta}^{l+2} \boldsymbol{\rho}_{lm\beta}^{(1)\alpha\pm}(\boldsymbol{r}_{\beta}) dr_{\beta} \\ &- e^{\pm i\boldsymbol{q}\cdot\boldsymbol{R}'} \sum_{\boldsymbol{G}} \hat{\boldsymbol{\rho}}_{\mathrm{PW}}^{(1)\alpha\pm}(\boldsymbol{G}) e^{i(\boldsymbol{G}\pm\boldsymbol{q})\cdot\boldsymbol{\tau}_{\beta}} 4\pi i^{l} Y_{lm}^{*}(\widehat{\boldsymbol{G}\pm\boldsymbol{q}}) \\ &\times \int_{0}^{R_{\beta}} r_{\beta}^{l+2} j_{l}(|\boldsymbol{G}\pm\boldsymbol{q}|r_{\beta}) dr_{\beta} \end{aligned}$$

$$= e^{\pm i\boldsymbol{q}\cdot\boldsymbol{R}'} \int_{0}^{R_{\beta}} r_{\beta}^{l+2} \rho_{lm\beta}^{(1)\alpha\pm}(\boldsymbol{r}_{\beta}) dr_{\beta} - 4\pi i^{l} R_{\beta}^{l+3} e^{\pm i\boldsymbol{q}\cdot\boldsymbol{R}'}$$

$$\times \sum_{\boldsymbol{G}} \hat{\rho}_{PW}^{(1)\alpha\pm}(\boldsymbol{G}) e^{i(\boldsymbol{G}\pm\boldsymbol{q})\cdot\boldsymbol{\tau}_{\beta}} Y_{lm}^{*}(\widehat{\boldsymbol{G}\pm\boldsymbol{q}}) \frac{j_{l+1}(|\boldsymbol{G}\pm\boldsymbol{q}|R_{\beta})}{|\boldsymbol{G}\pm\boldsymbol{q}|R_{\beta}}.$$
 (7.57)

Similarly, the multipole moments due to the periodic density gradient are given by

$$q_{lm,\nabla\rho}^{\mathbf{0}}(\beta) = \int_{B_{R_{\beta}}(\mathbf{0})} Y_{lm}^{*}(\hat{\boldsymbol{r}}_{\beta}) r_{\beta}^{l} [\nabla_{\beta}\rho^{(0)}(\boldsymbol{r}_{\beta} + \boldsymbol{\tau}_{\beta}) - \nabla_{\beta}\rho_{\mathrm{PW}}^{(0)}(\boldsymbol{r}_{\beta} + \boldsymbol{\tau}_{\beta})] d^{3}r_{\beta}$$

$$= \int_{0}^{R_{\beta}} r_{\beta}^{l+2} \left\{ [\nabla \boldsymbol{\rho}^{(0)}]_{lm}^{\beta}(r_{\beta}) - [\nabla \boldsymbol{\rho}_{\mathrm{PW}}^{(0)}]_{lm}^{\beta}(r_{\beta}) \right\} dr_{\beta}, \tag{7.58}$$

where we abbreviated the gradient of the MT and IR representation of the density evaluated in the MT sphere of atom β as

$$\begin{split} \left[\nabla \boldsymbol{\rho}^{(0)}\right]_{lm}^{\beta}(r_{\beta}) &= \oint_{\partial B_{1}(0)} Y_{lm}^{*}(\hat{\boldsymbol{r}}_{\beta}) \nabla_{\beta} \sum_{l'm'} \rho_{l'm'}^{\beta(0)}(r_{\beta}) Y_{l'm'}(\hat{\boldsymbol{r}}_{\beta}) dS_{\beta} \\ &= \sqrt{\frac{4\pi}{3}} \sum_{m''=-1}^{1} \underline{\boldsymbol{T}} \hat{\boldsymbol{e}}_{m''} \left\{ G_{l,l-1,1}^{m,m-m'',m''} \left[\rho_{l-1,m-m''}^{\beta(0)}(r_{\beta}) - (l-1) \frac{\rho_{l-1,m-m''}^{\beta(0)}(r_{\beta})}{r_{\beta}} \right] + G_{l,l+1,1}^{m,m-m'',m''} \left[\rho_{l+1,m-m''}^{\beta(0)}(r_{\beta}) + (l+2) \frac{\rho_{l+1,m-m''}^{\beta(0)}(r_{\beta})}{r_{\beta}} \right] \right\} (7.59) \end{split}$$

and

$$\left[\nabla \boldsymbol{\rho}_{\mathrm{PW}}^{(0)}\right]_{lm}^{\beta}(r_{\beta}) = \oint_{\partial B_{1}(\mathbf{0})} Y_{lm}^{*}(\hat{\boldsymbol{r}}_{\beta}) \nabla_{\beta} \sum_{\boldsymbol{G}} \hat{\rho}^{(0)}(\boldsymbol{G}) e^{i\boldsymbol{G}\cdot(\boldsymbol{r}_{\beta}+\boldsymbol{\tau}_{\beta})} dS_{\beta}$$
$$= e^{i\boldsymbol{G}\cdot\boldsymbol{\tau}_{\beta}} 4\pi i^{l} \sum_{\boldsymbol{G}} i\boldsymbol{G} \hat{\rho}^{(0)}(\boldsymbol{G}) Y_{lm}^{*}(\hat{\boldsymbol{G}}) j_{l}(Gr_{\beta}). \tag{7.60}$$

The total multipole moments from which the pseudodensities for constructing $V_{\rm H}^{(1)\alpha\pm}(r)$ and $\nabla V_{\rm H}^{(0)}(r)$ are determined, are the sums of Eqs. (7.54) and (7.57) for $\tilde{q}=\pm q$ and of Eqs. (7.54) and (7.58) for $\tilde{q}=0$:

$$q_{lm.\delta\rho,\text{tot}}^{\alpha \pm q}(\beta, \mathbf{R}') = q_{lm.\delta\rho}^{\alpha \pm q}(\beta, \mathbf{R}') + q_{lm}^{\alpha \pm q}(\beta, \mathbf{R}')$$
(7.61)

$$q_{lm,\nabla\rho,\text{tot}}^{\mathbf{0}}(\beta) = q_{lm,\nabla\rho}^{\mathbf{0}}(\beta) - \sum_{\alpha} q_{lm}^{\alpha \mathbf{0}}(\beta, \mathbf{0})$$
 (7.62)

Inserting these multipole moments into Eq. (3.55), the Fourier coefficients of the corresponding pseudodensities are given by

$$\hat{\rho}_{ps}^{(1)\alpha\pm}(\boldsymbol{G}) = \hat{\rho}_{PW}^{(1)\alpha\pm}(\boldsymbol{G}) + \frac{4\pi}{\Omega} \sum_{\beta} \sum_{lm} \frac{(-i)^{l}(2l+2N+3)!!}{(2l+1)!!R_{\beta}^{l}} \frac{j_{l+N+1}(|\boldsymbol{G}\pm\boldsymbol{q}|R_{\beta})}{(|\boldsymbol{G}\pm\boldsymbol{q}|R_{\beta})^{N+1}} \times \boldsymbol{q}_{lm,\delta_{0},\text{tot}}^{\alpha\pm\boldsymbol{q}}(\boldsymbol{\beta},\boldsymbol{0}) e^{-i(\boldsymbol{G}\pm\boldsymbol{q})\cdot\boldsymbol{\tau}_{\beta}} Y_{lm}(\widehat{\boldsymbol{G}\pm\boldsymbol{q}})$$
(7.63)

an

$$\widehat{[\nabla \rho_{\rm ps}^{(0)}]}(G) = \widehat{[\nabla \rho_{\rm PW}^{(0)}]}(G) + \frac{4\pi}{\Omega} \sum_{\beta} \sum_{lm} \frac{(-i)^l (2l+2N+3)!!}{(2l+1)!! R_{\beta}^l} \frac{j_{l+N+1}(GR_{\beta})}{(GR_{\beta})^{N+1}}$$

$$\times \mathbf{q}_{lm,\nabla\rho,\text{tot}}^{\mathbf{0}}(\beta)e^{-i\mathbf{G}\cdot\boldsymbol{\tau}_{\beta}}Y_{lm}(\hat{\mathbf{G}}). \tag{7.64}$$

For $G = \tilde{q} = 0$, we recover an analogon to Eq. (3.56) by applying L'Hôspital's rule as in Eq. (7.44).

The interstitial contributions

From the pseudodensity, we construct the response and the gradient of the Hartree potential in the interstitial by inverting Poisson's equation:

$$V_{\mathrm{H}}^{(1)\alpha\pm}(\mathbf{r}) = \sum_{\mathbf{G},\mathbf{G}\pm\mathbf{q}\neq\mathbf{0}} \hat{V}_{\mathrm{H}}^{(1)\alpha\pm}(\mathbf{G})e^{i(\mathbf{G}\pm\mathbf{q})\cdot\mathbf{r}} = \sum_{\mathbf{G},\mathbf{G}\pm\mathbf{q}\neq\mathbf{0}} \frac{4\pi\hat{\boldsymbol{\rho}}_{\mathrm{ps}}^{(1)\alpha\pm}(\mathbf{G})}{|\mathbf{G}\pm\mathbf{q}|^2}e^{i(\mathbf{G}\pm\mathbf{q})\cdot\mathbf{r}}$$
(7.65a)

$$\nabla V_{\mathrm{H}}^{(0)}(\mathbf{r}) = \sum_{\mathbf{G} \neq \mathbf{0}} \widehat{[\nabla V_{\mathrm{H}}^{(0)}]}(\mathbf{G}) e^{i\mathbf{G} \cdot \mathbf{r}} = \sum_{\mathbf{G} \neq \mathbf{0}} \frac{4\pi \widehat{[\nabla \rho_{\mathrm{ps}}^{(0)}]}(\mathbf{G})}{G^2} e^{i\mathbf{G} \cdot \mathbf{r}}$$
(7.65b)

Evaluated at the MT sphere boundaries, these expressions define the boundary values to formulate the response and the gradient of the Hartree potential in the MT spheres in terms of a Dirichlet boundary-value problem.

The muffin-tin contributions

To construct the spherical-harmonics representation of $V_{\rm H}^{(1)\alpha\pm}(r)$ and $\nabla V_{\rm H}^{(0)}(r)$ within the MT sphere of atom β of the representative unit cell R'=0, we insert the true local density response $\rho^{(1)\alpha\pm}(r)$ and the true local density gradient $\nabla \rho^{(0)}(r)$ into Eq. (3.63) for the volume integral. Furthermore, we insert the response and the gradient of the Hartree potential given in Eq. (7.65) into the part of Eq. (3.63) stemming from the surface integral and we obtain

$$V_{\mathrm{H},lm\beta}^{(1)\alpha\pm}(r_{\beta}) = \frac{4\pi}{2l+1} \int_{0}^{R_{\beta}} s_{\beta}^{2} \boldsymbol{\rho}_{lm\beta}^{(1)\alpha\pm}(s_{\beta}) \frac{r_{\leq}^{l}}{r_{>}^{l+1}} \left[1 - \left(\frac{r_{>}}{R_{\beta}} \right)^{2l+1} \right] ds_{\beta}$$

$$+ \left(\frac{r_{\beta}}{R_{\beta}} \right)^{l} \sum_{\boldsymbol{G},\boldsymbol{G} \pm \boldsymbol{q} \neq \boldsymbol{0}} e^{i(\boldsymbol{G} \pm \boldsymbol{q}) \cdot \boldsymbol{\tau}_{\beta}} \hat{\boldsymbol{V}}_{\mathrm{H}}^{(1)\alpha\pm}(\boldsymbol{G}) 4\pi i^{l} Y_{lm}^{*}(\widehat{\boldsymbol{G}} \pm \boldsymbol{q}) j_{l}(|\boldsymbol{G} \pm \boldsymbol{q}|R_{\beta})$$

$$(7.66)$$

and

$$\nabla V_{\mathrm{H},lm\beta}^{(0)}(r_{\beta}) = \frac{4\pi}{2l+1} \int_{0}^{R_{\beta}} s_{\beta}^{2} \left[\nabla \boldsymbol{\rho}^{(0)} \right]_{lm}^{\beta} \left(s_{\beta} \right) \frac{r_{<}^{l}}{r_{>}^{l+1}} \left[1 - \left(\frac{r_{>}}{R_{\beta}} \right)^{2l+1} \right] ds_{\beta}$$

$$+ \left(\frac{r_{\beta}}{R_{\beta}} \right)^{l} \sum_{\boldsymbol{G} \neq \boldsymbol{0}} e^{i\boldsymbol{G} \cdot \boldsymbol{\tau}_{\beta}} \left[\widehat{\boldsymbol{\nabla} \boldsymbol{V}_{\mathrm{H}}^{(0)}} \right] (\boldsymbol{G}) 4\pi i^{l} Y_{lm}^{*}(\hat{\boldsymbol{G}}) j_{l}(\boldsymbol{G}R_{\beta})$$

$$(7.67)$$

We remark two things regarding the last two equations. First of all, according to the Sternheimer matrix equation, Eq. (7.24), $\nabla V_{\mathrm{H},lm\beta}^{(0)}(r_{\beta})$ has to be calculated only for $\beta=\alpha$. Second, the density response $\boldsymbol{\rho}^{(1)\alpha\pm}(\boldsymbol{r})$ as given in Eq. (7.32) includes the negative gradient

of the electronic density in the MT sphere of atom α . Therefore, the first line defining $\nabla V_{\mathrm{H},lm\beta}^{(0)}(r_{\beta})$ cancels with a part of the first line defining $V_{\mathrm{H},lm\beta}^{(1)\alpha\pm}(r_{\beta})$, when the Hartree response is calculated for solving the Sternheimer equation. From the gradient of the Hartree potential, only the term stemming from the boundary values has to be evaluated.

7.1.4.3. The first-order change $\mu_{xc}^{(1)}(r)$ of the xc potential

According to Eq. (6.15c), the variation of the exchange-correlation potential is given by

$$\mu_{\mathrm{xc}}^{(1)\alpha\pm}(\mathbf{r}) = \rho^{(1)\alpha\pm}(\mathbf{r}) \left. \frac{\delta \mu_{\mathrm{xc}}^{(0)}[\rho](\mathbf{r})}{\delta \rho(\mathbf{r})} \right|_{\rho=\rho^{(0)}}.$$
 (7.68)

By applying the chain rule, a similar expression can be found for the gradient of the xc potential, which we need within the MT sphere of atom α :

$$\nabla \mu_{\mathrm{xc}}^{(0)}(\boldsymbol{r}) = \left[\nabla \rho^{(0)}(\boldsymbol{r})\right] \left. \frac{\delta \mu_{\mathrm{xc}}^{(0)}[\rho](\boldsymbol{r})}{\delta \rho(\boldsymbol{r})} \right|_{\rho = \rho^{(0)}}$$
(7.69)

We have derived formulas for describing the density response $\rho^{(1)\alpha\pm}(r)$ in the interstitial region and in the muffin-tin spheres with Eqs. (7.33) and (7.34), respectively, in section 7.1.3. Specifically, we remarked for the MT representation at the displaced atom α that the density response contains the negative gradient of the unperturbed density. Therefore, this contribution cancels with $\nabla \rho^{(0)}(r)$ and we do not need to calculate the gradient of the density explicitly while we solve the Sternheimer equation self-consistently. The exact form of the xc kernel $\delta \mu_{\rm xc}[\rho](r)/\delta \rho(r)$ is dependent on the choice of the xc functional. For the LDA functional of Vosko, Wilk, and Nusair [74], which has been used throughout this thesis, we provide an explicit formula for the kernel in Appendix A.2.

The kernel is generated by applying the formula for $f_{xc}(\mathbf{r}, \mathbf{r}) = \delta \mu_{xc}[\rho](\mathbf{r})/\delta \rho(\mathbf{r})$ given in Appendix A.2 at every point of a real-space mesh and then recollecting the results in terms of plane waves in the IR and in terms of radial functions times spherical harmonics in the MT spheres. In other words, the kernel is generated using the same scheme as applied for constructing the xc energy-density and the xc potential, which is explained in chapter 3.6. By convoluting the representations of the density response and the xc kernel, the response of the xc potential finally takes the form

$$\boldsymbol{\mu}_{\mathrm{xc}}^{(1)\alpha\pm}(\boldsymbol{r}) = \sum_{\boldsymbol{G}\boldsymbol{G}'} \hat{\boldsymbol{\rho}}^{(1)\alpha\pm}(\boldsymbol{G}) \hat{f}_{\mathrm{xc}}(\boldsymbol{G}') e^{i(\boldsymbol{G}+\boldsymbol{G}')\cdot\boldsymbol{r}}$$
(7.70a)

in the interstitial region and

$$\mu_{\text{xc}}^{(1)\alpha\pm}(\mathbf{r}) = \sum_{lml'm'} \rho_{lm\beta}^{(1)\alpha\pm}(r_{\beta}) f_{\text{xc},l'm'}(r_{\beta},r_{\beta}) \sum_{s=|l-l'|}^{l+l',2} G_{s,l,l'}^{m+m',m,m'} Y_{s,m+m'}(\mathbf{r}_{\beta})$$
(7.70b)

in the muffin-tin sphere of atom β .

7.1.5. Solving the Sternheimer equation

In the previous sections, we constructed every quantity needed for the self-consistent solution of the Sternheimer equation ${\bf r}$

$$\sum_{\boldsymbol{G}} \left\langle \phi_{\boldsymbol{k} \pm \boldsymbol{q}, \boldsymbol{G}'}^{(0)} \middle| \hat{\mathcal{H}}_{0} - \epsilon_{i\boldsymbol{k}}^{(0)} \middle| \phi_{\boldsymbol{k} \pm \boldsymbol{q}, \boldsymbol{G}}^{(0)} \right\rangle z_{\boldsymbol{k} \pm \boldsymbol{q}, \boldsymbol{G}}^{i\boldsymbol{k}(1)\alpha \pm}$$

$$= -\sum_{\boldsymbol{G}} \left\{ \left\langle \phi_{\boldsymbol{k} \pm \boldsymbol{q}, \boldsymbol{G}'}^{(0)} \middle| \boldsymbol{V}_{\text{eff}}^{(1)\alpha \pm} - \delta_{\boldsymbol{q}0} \boldsymbol{\epsilon}_{i\boldsymbol{k}}^{(1)\alpha \pm} \middle| \phi_{\boldsymbol{k}\boldsymbol{G}}^{(0)} \right\rangle + \left\langle \phi_{\boldsymbol{k} \pm \boldsymbol{q}, \boldsymbol{G}'}^{(0)} \middle| \nabla V_{\text{eff}}^{(0)} \middle| \phi_{\boldsymbol{k}\boldsymbol{G}}^{(0)} \right\rangle_{\alpha} \\ - i(\boldsymbol{G}' \pm \boldsymbol{q} - \boldsymbol{G}) \left\langle \phi_{\boldsymbol{k} \pm \boldsymbol{q}, \boldsymbol{G}'}^{(0)} \middle| \hat{\mathcal{H}}_{0} - \epsilon_{i\boldsymbol{k}}^{(0)} \middle| \phi_{\boldsymbol{k}\boldsymbol{G}}^{(0)} \right\rangle_{\alpha} \\ - \oint_{\partial \text{MT}(\boldsymbol{\alpha}, \boldsymbol{0})} \hat{\boldsymbol{e}} \left[\phi_{\boldsymbol{k} \pm \boldsymbol{q}, \boldsymbol{G}'}^{\text{IR}(0)*} (\hat{\mathcal{H}}_{0} - \epsilon_{i\boldsymbol{k}}^{(0)}) \phi_{\boldsymbol{k}\boldsymbol{G}}^{\text{IR}(0)} \right] dS \right\} z_{\boldsymbol{k}\boldsymbol{G}}^{i\boldsymbol{k}(0)}.$$
 (7.24 revisited)

We stressed in particular the cancellation of the rigid part $\nabla f(\mathbf{r})$ in the density and potential with the respective responses $\mathbf{f}^{(1)\alpha\pm}(\mathbf{r})$ within the muffin-tin sphere of atom α , which omits the necessity to explicitly calculate the respective gradient. We therefore expect that the Sternheimer equation represents a stable algorithm to construct the first-order changes of wave functions, density, and potential.

In Fig. 7.1 we sketch the program flow to solve the Sternheimer equation self-consistently. For any perturbation vector \mathbf{q} and for any atom α , starting from the external perturbation $V^{(1)\alpha\pm}(\mathbf{r})$ as the first potential response $V^{(1)\alpha\pm}_{\mathrm{eff}}(\mathbf{r})$, the wave-function response $\psi^{(1)\alpha\pm}_{ik}(\mathbf{r})$ is constructed. From the wave-function response, the density response $\rho^{(1)\alpha\pm}(\mathbf{r})$ follows, which in turn determines the screening of the external perturbation by the Hartree and xc potential responses $V_{\mathrm{H}}^{(1)\alpha\pm}(\mathbf{r})$ and $\mu_{\mathrm{xc}}^{(1)\alpha\pm}(\mathbf{r})$. Together with the external perturbation, these constitute the response of the effective potential $V_{\mathrm{eff}}^{(1)\alpha\pm}(\mathbf{r})$ used in any subsequent steps of solving the Sternheimer equation. The algorithm is repeated until the input and output density response equal each other within a given numerical precision.

7.2. Second-order changes

In addition to the unperturbed quantities available from a regular electronic structure calculation and the first-order changes which we discussed in the previous section 7.1, the calculation of the second-order change in the total energy within the FLAPW method requires knowledge of the second-order changes in the external potential, $V_{\rm ext}^{(2)}(r)$, in the ion-ion energy $E_{\rm ii}^{(2)}$, and in the basis functions, $\phi_{kG}^{(2)}(r)$. This can be seen from the constituents of the second-order total energy variation $E_{\rm tot}^{(2)}$, Eq. (6.58), which we recapitulate to be

$$E_{\text{tot,basic}}^{(2),\text{simple}} = \int \rho^{(1)}(\mathbf{r}) V_{\text{ext}}^{(1)}(\mathbf{r}) d^3 r + \int \rho^{(0)}(\mathbf{r}) V_{\text{ext}}^{(2)}(\mathbf{r}) d^3 r + E_{\text{ii}}^{(2)}, \qquad (6.23 \text{ revisited})$$

$$E_{\text{tot,Pulay}}^{(2)} = \int \rho^{(1)}(\mathbf{r}) V_{\text{eff}}^{(1)}(\mathbf{r}) d^3 r + \sum_{i\mathbf{k}} f_{i\mathbf{k}}^{(0)} \left[2 \left\langle \psi_{i\mathbf{k}}^{(1)} \middle| \hat{\mathcal{H}}_0 - \epsilon_{i\mathbf{k}}^{(0)} \middle| \psi_{i\mathbf{k}}^{(1)} \right\rangle \right.$$

$$\left. + \left\langle \psi_{i\mathbf{k}}^{(2)} \middle| \hat{\mathcal{H}}_0 - \epsilon_{i\mathbf{k}}^{(0)} \middle| \psi_{i\mathbf{k}}^{(0)} \right\rangle + \left\langle \psi_{i\mathbf{k}}^{(0)} \middle| \hat{\mathcal{H}}_0 - \epsilon_{i\mathbf{k}}^{(0)} \middle| \psi_{i\mathbf{k}}^{(2)} \right\rangle \right], \qquad (6.52 \text{ revisited})$$

where the only relevant second-order change within $\psi_{ik}^{(2)}(r)$ is given by $\phi_{kG}^{(2)}(r)$, and

$$\begin{split} E_{\text{tot,SF}}^{(2)} = & 2\sum_{i\boldsymbol{k}} f_{i\boldsymbol{k}}^{(0)} \sum_{\alpha} \boldsymbol{w}_{\alpha}^{\text{T}} \cdot \oint_{\partial \text{MT}(\alpha)} \hat{\boldsymbol{e}} \left[\psi_{i\boldsymbol{k}}^{(1)*}(\boldsymbol{r}) \left(\hat{\mathcal{H}}_{0} - \epsilon_{i\boldsymbol{k}}^{(0)} \right) \psi_{i\boldsymbol{k}}^{(0)}(\boldsymbol{r}) \right]_{\text{SF}} dS \\ & + 2\sum_{i\boldsymbol{k}} f_{i\boldsymbol{k}}^{(0)} \sum_{\alpha} \boldsymbol{w}_{\alpha}^{\text{T}} \cdot \oint_{\partial \text{MT}(\alpha)} \hat{\boldsymbol{e}} \left[\psi_{i\boldsymbol{k}}^{(0)*}(\boldsymbol{r}) \left(\hat{\mathcal{H}}_{0} - \epsilon_{i\boldsymbol{k}}^{(0)} \right) \psi_{i\boldsymbol{k}}^{(1)}(\boldsymbol{r}) \right]_{\text{SF}} dS + \dots \end{split}$$

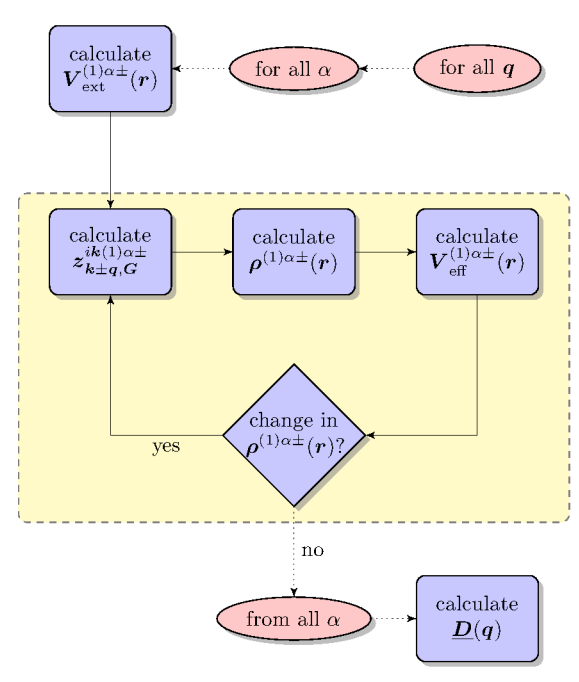


Figure 7.1.: Flowchart depicting the algorithm to solve the Sternheimer equation, Eq. (7.24), self-consistently. Parallelization can be applied for every q and for every α . Within the Sternheimer loop (yellow box), k-point parallelization can be performed for fixed q and α .

$$\dots + \sum_{ik} f_{ik}^{(0)} \sum_{\alpha} \boldsymbol{w}_{\alpha}^{\mathrm{T}} \cdot \oint_{\partial \mathrm{MT}(\alpha)} \nabla \left[\psi_{ik}^{(0)*}(\boldsymbol{r}) \left(\hat{\mathcal{H}}_{0} - \epsilon_{ik}^{(0)} \right) \psi_{ik}^{(0)}(\boldsymbol{r}) \right]_{\mathrm{SF}} \hat{\boldsymbol{e}}^{\mathrm{T}} dS \cdot \boldsymbol{w}_{\alpha} \\
+ \sum_{\alpha} \boldsymbol{w}_{\alpha}^{\mathrm{T}} \cdot \oint_{\partial \mathrm{MT}(\alpha)} \nabla \left[\rho^{(0)}(\boldsymbol{r}) \left\{ \varepsilon_{\mathrm{xc}}^{(0)}(\boldsymbol{r}) - \mu_{\mathrm{xc}}^{(0)}(\boldsymbol{r}) \right\} \right]_{\mathrm{SF}} \hat{\boldsymbol{e}}^{\mathrm{T}} dS \cdot \boldsymbol{w}_{\alpha} \\
+ \sum_{\alpha} \boldsymbol{w}_{\alpha}^{\mathrm{T}} \cdot \oint_{\partial \mathrm{MT}(\alpha)} \hat{\boldsymbol{e}} \left[\rho^{(0)}(\boldsymbol{r}) \left\{ 2V_{\mathrm{ext}}^{(1)}(\boldsymbol{r}) + V_{\mathrm{H}}^{(1)}(\boldsymbol{r}) \right\} \right]_{\mathrm{SF}} dS. \quad (6.57 \text{ revisited})$$

From these expressions, we will eventually derive the dynamical matrix $\underline{D}(q)$. Before we do so, however, we first construct the missing second-order changes mentioned above. Although we will sometimes mention the case q=0, the derivation of the second-order quantities presented here does not focus on this case. On the contrary, a rigorous treatment of q=0 would require to include the first-order variation of the occupation numbers $f_{ik}^{(1)}$ to be calculated, since chapter 3.11 only guarantees that $f_{ik}^{(1)}$ vanishes in the first-order derivative of the total energy. However, $f_{ik}^{(1)}$ is always zero for the important case $q \neq 0$ [34, 36].

7.2.1. Evaluation of $V_{\mathbf{ext}}^{(2)}(\boldsymbol{r})$

The evaluation of the second-order variation in the external potential appearing within a volume integral in Eq. (6.23),

$$V_{\text{ext}}^{(2)}(\mathbf{r}) = \sum_{\alpha \mathbf{R}ij} \left[Q_{\alpha i} Q_{\alpha j} e^{2i\mathbf{q} \cdot \mathbf{R}} + Q_{\alpha i} Q_{\alpha j}^* + Q_{\alpha i}^* Q_{\alpha j} + Q_{\alpha i}^* Q_{\alpha j}^* e^{-2i\mathbf{q} \cdot \mathbf{R}} \right] \times \left[\partial_i \partial_j V_{\text{ext}}^{\alpha \mathbf{R}}(\mathbf{r}) \right], \qquad (7.7 \text{ revisited})$$

can be simplified by realizing that only $Q_{\alpha i}Q_{\alpha j}^* + Q_{\alpha i}^*Q_{\alpha j}$ from the sum in the square brackets contributes if q is not 0 or half of a reciprocal lattice vector. Both other terms then result in Bloch waves of non-vanishing wave vector. In this case, the second-order change in the external potential can be summarized as

$$V_{\text{ext}}^{(2)}(\mathbf{r}) = \sum_{\alpha} \left\{ \mathbf{Q}_{\alpha}^{\text{T}} \cdot \left[\sum_{\mathbf{R}} \nabla \nabla^{\text{T}} V_{\text{ext}}^{\alpha \mathbf{R}}(\mathbf{r}) \right] \cdot \mathbf{Q}_{\alpha}^{*} + \mathbf{Q}_{\alpha}^{*\text{T}} \cdot \left[\sum_{\mathbf{R}} \nabla \nabla^{\text{T}} V_{\text{ext}}^{\alpha \mathbf{R}}(\mathbf{r}) \right] \cdot \mathbf{Q}_{\alpha} \right\}. \quad (7.71)$$

In the case that q is 0 or half of a reciprocal lattice vector, the exponentials become 1 and the periodic second-order change in the external potential is given by

$$V_{\text{ext}}^{(2)}(\boldsymbol{r}) = 4\sum_{\alpha} \left\{ \Re(\boldsymbol{Q}_{\alpha}^{\text{T}}) \cdot \left[\sum_{\boldsymbol{R}} \nabla \nabla^{\text{T}} V_{\text{ext}}^{\alpha \boldsymbol{R}}(\boldsymbol{r}) \right] \cdot \Re(\boldsymbol{Q}_{\alpha}) \right\}.$$
(7.72)

In both cases, the term involving the sum over R needs to be calculated. We abbreviate it with

$$\underline{V}_{\text{ext}}^{(2)\alpha}(\mathbf{r}) = \sum_{\mathbf{R}} \nabla \nabla^{\text{T}} V_{\text{ext}}^{\alpha \mathbf{R}}(\mathbf{r})$$
(7.73)

In analogy to the evaluation of $V_{\rm ext}^{(1)}(r)$ in section 7.1.4.1, we express the external potential in terms of a Dirac- δ density, redirect the derivatives to this density and use the Weinert method. In this way, we have access to interstitial and muffin-tin representations of $\underline{V}_{\rm ext}^{(2)\alpha}(r)$. The second-order derivative $\underline{n}^{\alpha}(r)$ of the ion-density is extracted from

$$\underline{V}_{\text{ext}}^{(2)\alpha}(\mathbf{r}) = -\int \nabla \nabla^{\text{T}} \frac{\sum_{\mathbf{R}} Z_{\alpha} \delta(\mathbf{r}' - \boldsymbol{\tau}_{\alpha} - \mathbf{R})}{|\mathbf{r} - \mathbf{r}'|} d^{3}r'$$

$$= -\int \frac{\sum_{\mathbf{R}} Z_{\alpha} \nabla' \nabla'^{\text{T}} \delta(\mathbf{r}' - \boldsymbol{\tau}_{\alpha} - \mathbf{R})}{|\mathbf{r} - \mathbf{r}'|} d^{3}r' \tag{7.74}$$

and yields

$$\underline{n}^{\alpha}(\mathbf{r}) = -\sum_{\mathbf{R}} Z_{\alpha} \nabla \nabla^{\mathrm{T}} \delta(\mathbf{r} - \boldsymbol{\tau}_{\alpha} - \mathbf{R}). \tag{7.75}$$

From this expression, we construct a pseudodensity which exhibits the same multipole moments, but which has a fast converging Fourier-expansion.

Construction of the pseudodensity

The multipole moments of $\underline{n}^{\alpha}(r)$ at the muffin-tin sphere of atom β in unit cell R' are determined after two integrations by parts as

$$\underline{\boldsymbol{q}}_{lm}^{\alpha}(\beta, \boldsymbol{R}') = \int_{\mathrm{MT}(\beta, \boldsymbol{R}')} Y_{lm}^{*}(\boldsymbol{r} - \widehat{\boldsymbol{\tau}_{\beta}} - \boldsymbol{R}') |\boldsymbol{r} - \boldsymbol{\tau}_{\beta} - \boldsymbol{R}'|^{l} \underline{\boldsymbol{n}}^{\alpha}(\boldsymbol{r}) d^{3} \boldsymbol{r}$$

$$= -Z_{\alpha} \delta_{\alpha\beta} \nabla \nabla^{\mathrm{T}} \left[r^{l} Y_{lm}^{*}(\hat{\boldsymbol{r}}) \right]_{\boldsymbol{r}=0}. \tag{7.76}$$

The $\underline{q}_{lm}^{\alpha}(\beta, \mathbf{R}')$ are independent of \mathbf{R} and \mathbf{R}' , since $\underline{n}^{\alpha}(\mathbf{r})$ exhibits the same periodicity as the unperturbed lattice. Being evaluated at the center of the sphere, $\mathbf{r} = \mathbf{0}$, the multipole moments vanish for all angular momenta except for l = 2. The second-order ion-density response $\underline{n}^{\alpha}(\mathbf{r})$ does not have any contributions in the interstitial region. According to Eqs. (3.46)-(3.56), the Fourier components of the pseudodensity are

$$\hat{\underline{n}}_{ps}^{\alpha}(G) = -\frac{4\pi}{\Omega} \frac{(2N+7)!!}{5!! R_{\alpha}^{2}} \frac{j_{N+3}(GR_{\alpha})}{(GR_{\alpha})^{N+1}} e^{-iG \cdot \boldsymbol{\tau}_{\alpha}} \sum_{m=-2}^{2} Y_{2m}(\hat{G}) \underline{q}_{2m}^{\alpha}(\alpha, \mathbf{0})
= \frac{4\pi}{\Omega} Z_{\alpha} \frac{(2N+7)!!}{5!! R_{\alpha}^{2}} \frac{j_{N+3}(GR_{\alpha})}{(GR_{\alpha})^{N+1}} e^{-iG \cdot \boldsymbol{\tau}_{\alpha}} \frac{5}{4\pi} \nabla \nabla^{T} \left[r^{2} P_{2}(\hat{r} \cdot \hat{G}) \right] \Big|_{r=0}.$$
(7.77)

We made use of the addition theorem for spherical harmonics; $P_2(r) = (3r^2 - 1)/2$ is a Legendre polynomial. Performing the derivatives yields

$$\underline{\hat{n}}_{ps}^{\alpha}(\mathbf{G}) = \frac{Z_{\alpha}}{\Omega} \frac{(2N+7)!!j_{N+3}(GR_{\alpha})}{(GR_{\alpha})^{N+3}} e^{-i\mathbf{G}\cdot\boldsymbol{\tau}_{\alpha}} \left[\mathbf{G}\mathbf{G}^{\mathrm{T}} - G^{2}\underline{\boldsymbol{E}}_{3}/3\right]$$
(7.78)

and

$$\hat{\underline{n}}_{ps}^{\alpha}(\mathbf{0}) = \underline{\mathbf{0}}_{3} \tag{7.79}$$

where \underline{E}_3 is the 3×3 unit matrix and $\underline{0}_3$ is the zero matrix of the same dimensions. The vanishing of the G=0 component can be confirmed analogously to Eq. (7.44) by realizing that the fraction in Eq. (7.78) becomes 1 for $G\to 0$ by use of L'Hôspital's rule, while the last factor is of order G^2 . Since no ions are added or subtracted from the system by the phononic perturbation, it is plausible that the average second-order variation in the ion density is zero.

The interstitial contribution

The second-order perturbation $\underline{V}_{\mathrm{ext}}^{(2)lpha}(r)$ in the IR takes the form

$$\underline{\underline{V}}_{\text{ext}}^{(2)\alpha}(r) = \sum_{\underline{G} \neq 0} \frac{4\pi \underline{\hat{n}}_{\text{ps}}^{\alpha}(\underline{G})}{G^2} e^{i\underline{G} \cdot r} =: \sum_{\underline{G} \neq 0} \underline{\hat{V}}_{\text{ext}}^{(2)\alpha}(\underline{G}) e^{i\underline{G} \cdot r},$$
(7.80)

which we subsequently use as boundary values on the muffin-tin spheres to construct the muffin-tin representation of $\underline{V}_{\text{ext}}^{(2)\alpha}(r)$.

The muffin-tin contribution

In the muffin-tin sphere of atom β , the second-order change of $V_{\rm ext}(r)$ is composed of a contribution generated by the local density and the contribution of all other spheres taken into account by the sphere surface term as seen in Eq. (3.61). The surface contribution is obtained easily by using Eq. (7.80). The volume contribution on the other hand is found by redirecting the twofold derivative in the local density towards the Green function, which we use here in conjunction with the Legendre polynomials:

$$\begin{split} \underline{\boldsymbol{V}}_{\mathrm{ext}}^{(2)\alpha}(\boldsymbol{r}_{\beta} + \boldsymbol{\tau}_{\beta}) &= -Z_{\alpha} \int_{B_{R_{\beta}}(\boldsymbol{0})} \sum_{R} \delta(\boldsymbol{s}_{\beta} - (\boldsymbol{\tau}_{\alpha} - \boldsymbol{\tau}_{\beta}) - \boldsymbol{R}) \\ &\times \nabla_{\boldsymbol{s}_{\beta}} \nabla_{\boldsymbol{s}_{\beta}}^{\mathrm{T}} \sum_{l} P_{l}(\hat{\boldsymbol{r}}_{\beta} \cdot \hat{\boldsymbol{s}}_{\beta}) \frac{r_{<}^{l}}{r_{>}^{l+1}} \left[1 - \left(\frac{r_{>}}{R_{\beta}} \right)^{2l+1} \right] d^{3} \boldsymbol{s}_{\beta} \\ &+ \sum_{l_{m}} \left(\frac{r_{\beta}}{R_{\beta}} \right)^{l} \cdot \sum_{\boldsymbol{G} \neq \boldsymbol{0}} e^{i\boldsymbol{G} \cdot \boldsymbol{\tau}_{\beta}} \underline{\hat{\boldsymbol{V}}}_{\mathrm{ext}}^{(2)\alpha}(\boldsymbol{G}) 4\pi i^{l} Y_{l_{m}}^{*}(\hat{\boldsymbol{G}}) j_{l}(\boldsymbol{G}R_{\beta}) Y_{l_{m}}(\hat{\boldsymbol{r}}_{\beta}) \end{split}$$

We abbreviate the radial part of the last line by

$$\underline{\boldsymbol{V}}_{\text{ext},lm,\beta}^{(2)\alpha}(r_{\beta}) = \left(\frac{r_{\beta}}{R_{\beta}}\right)^{l} \cdot \sum_{\boldsymbol{G} \neq \boldsymbol{0}} e^{i\boldsymbol{G} \cdot \boldsymbol{\tau}_{\beta}} \underline{\hat{\boldsymbol{V}}}_{\text{ext}}^{(2)\alpha}(\boldsymbol{G}) 4\pi i^{l} Y_{lm}^{*}(\hat{\boldsymbol{G}}) j_{l}(GR_{\beta}). \tag{7.81}$$

Further manipulation of the volume integral then yields

$$\underline{V}_{\text{ext}}^{(2)\alpha}(r_{\beta} + \tau_{\beta}) = -Z_{\alpha}\delta_{\alpha\beta} \frac{1}{r_{\alpha}^{3}} \left[1 - \left(\frac{r_{\alpha}}{R_{\alpha}} \right)^{5} \right] \nabla_{s_{\alpha}} \nabla_{s_{\alpha}}^{T} \left[\frac{s_{\alpha}^{2}}{2} \left(3(\hat{r}_{\alpha} \cdot \hat{s}_{\alpha})^{2} - 1 \right) \right]_{s_{\alpha} = 0}
+ \sum_{lm} \underline{V}_{\text{ext},lm,\beta}^{(2)\alpha}(r_{\beta}) Y_{lm}(\hat{r}_{\beta})
= -\delta_{\alpha\beta} \frac{Z_{\alpha}}{r_{\alpha}^{5}} \left[1 - \left(\frac{r_{\alpha}}{R_{\alpha}} \right)^{5} \right] \left[3r_{\alpha} r_{\alpha}^{T} - r_{\alpha}^{2} \underline{E}_{3} \right]
+ \sum_{lm} \underline{V}_{\text{ext},lm,\beta}^{(2)\alpha}(r_{\beta}) Y_{lm}(\hat{r}_{\beta}).$$
(7.82)

In order to determine a spherical harmonic representation of the volume integral part, we express the unit vectors $\hat{\mathbf{r}}_{\alpha}$ in terms of spherical harmonics by

$$\hat{r}_{\alpha} = \sum_{i=1}^{3} \hat{e}_{i} \sum_{t=-1}^{1} c_{i,t} Y_{1,t}(\hat{r}_{\alpha}).$$
 (4.28 revisited)

We plug this into the dyadic product $r_{\alpha}r_{\alpha}^{\mathrm{T}}$ and find

$$\boldsymbol{r}_{\alpha}\boldsymbol{r}_{\alpha}^{\mathrm{T}} = r_{\alpha}^{2} \sum_{ij} \hat{\boldsymbol{e}}_{i} \hat{\boldsymbol{e}}_{j}^{\mathrm{T}} \sum_{t,t'=-1}^{1} c_{i,t} c_{j,t'} \sum_{s=0}^{2,2} G_{s,1,1}^{t+t',t,t'} Y_{s,t+t'}(\hat{\boldsymbol{r}}_{\alpha}). \tag{7.83}$$

7. Phonons in FLAPW using DFPT

In total, the matrices appearing in the second-order perturbation $V_{\rm ext}^{(2)}(\boldsymbol{r})$ are given by

$$\underline{\boldsymbol{V}}_{\text{ext}}^{(2)\alpha}(\boldsymbol{r}_{\beta} + \boldsymbol{\tau}_{\beta}) = -\delta_{\alpha\beta} \frac{Z_{\alpha}}{r_{\alpha}^{3}} \left[1 - \left(\frac{r_{\alpha}}{R_{\alpha}} \right)^{5} \right] \sum_{s=0}^{2,2} \sum_{t,t'=-1}^{1} Y_{s,t+t'}(\hat{\boldsymbol{r}}_{\alpha})$$

$$\times \sum_{ij} \hat{\boldsymbol{e}}_{i} \hat{\boldsymbol{e}}_{j}^{T} \left(3c_{i,t}c_{j,t'}G_{s,1,1}^{t+t',t,t'} - \sqrt{4\pi}\delta_{ij}\delta_{s0} \right)$$

$$+ \sum_{lm} \underline{\boldsymbol{V}}_{\text{ext},lm,\beta}^{(2)\alpha}(r_{\beta})Y_{lm}(\hat{\boldsymbol{r}}_{\beta}) \tag{7.84}$$

in the muffin-tin sphere of atom β . From the surface term, all l channels contribute, while the volume term is limited to l=0 and l=2.

7.2.2. Evaluation of $E_{ii}^{(2)}$

In order to evaluate the second-order response of the ion-ion energy appearing in Eq. (6.23), we start from the ion-ion energy of a finite solid consisting of N unit cells that is perturbed by a phonon of wave vector q. The interaction-energy of each atom with each atom in the whole solid other than itself is given as

$$E_{ii} = \frac{1}{2} \sum_{\alpha R} \sum_{\beta R'} \frac{Z_{\alpha} Z_{\beta}}{|\boldsymbol{\tau}_{\alpha} + \boldsymbol{R} + \boldsymbol{w}_{\alpha R} - \boldsymbol{\tau}_{\beta} - \boldsymbol{R}' - \boldsymbol{w}_{\beta R'}|},$$
(7.85)

where the prime next to the sum indicates the exclusion of $(\beta \mathbf{R}') = (\alpha \mathbf{R})$. The second-order variation of this expression can be transformed to yield the ion-ion-contribution to the dynamical matrix:

$$E_{ii}^{(2)} = \sum_{\gamma R''} \sum_{\delta R'''} \mathbf{w}_{\gamma R''}^{\mathrm{T}} \cdot \left[\left(\frac{d}{d \mathbf{w}_{\gamma R''}} \right) \cdot \left(\frac{d}{d \mathbf{w}_{\delta R'''}} \right)^{\mathrm{T}} E_{ii} \Big|_{\mathbf{w} = 0} \right] \cdot \mathbf{w}_{\delta R'''}$$

$$= \frac{1}{2} \sum_{\alpha R} \sum_{\beta R'} {}' Z_{\alpha} Z_{\beta} \left[\mathbf{w}_{\alpha R}^{\mathrm{T}} \cdot \nabla_{\alpha} \nabla_{\alpha}^{\mathrm{T}} \frac{1}{|\boldsymbol{\tau}_{\alpha} + \boldsymbol{R} - \boldsymbol{\tau}_{\beta} - \boldsymbol{R'}|} \cdot \boldsymbol{w}_{\alpha R} \right.$$

$$+ \mathbf{w}_{\alpha R}^{\mathrm{T}} \cdot \nabla_{\alpha} \nabla_{\beta}^{\mathrm{T}} \frac{1}{|\boldsymbol{\tau}_{\alpha} + \boldsymbol{R} - \boldsymbol{\tau}_{\beta} - \boldsymbol{R'}|} \cdot \boldsymbol{w}_{\beta R'}$$

$$+ \mathbf{w}_{\beta R'}^{\mathrm{T}} \cdot \nabla_{\beta} \nabla_{\alpha}^{\mathrm{T}} \frac{1}{|\boldsymbol{\tau}_{\alpha} + \boldsymbol{R} - \boldsymbol{\tau}_{\beta} - \boldsymbol{R'}|} \cdot \boldsymbol{w}_{\alpha R}$$

$$+ \mathbf{w}_{\beta R'}^{\mathrm{T}} \cdot \nabla_{\beta} \nabla_{\beta}^{\mathrm{T}} \frac{1}{|\boldsymbol{\tau}_{\alpha} + \boldsymbol{R} - \boldsymbol{\tau}_{\beta} - \boldsymbol{R'}|} \cdot \boldsymbol{w}_{\beta R'}$$

$$(7.87)$$

 ∇_{α} denotes the gradient with respect to atomic position $\boldsymbol{\tau}_{\alpha}$. Interchanging α with β and \boldsymbol{R} with \boldsymbol{R}' in the third and fourth line and inserting the displacements gives rise to:

$$\begin{split} E_{\text{ii}}^{(2)} = & \sum_{\alpha \boldsymbol{R}} \sum_{\beta \boldsymbol{R}'} Z_{\alpha} Z_{\beta} \Bigg[\boldsymbol{Q}_{\alpha}^{*\text{T}} \cdot \nabla_{\alpha} \nabla_{\alpha}^{\text{T}} \frac{e^{-2i\boldsymbol{q} \cdot \boldsymbol{R}}}{|\boldsymbol{\tau}_{\alpha} + \boldsymbol{R} - \boldsymbol{\tau}_{\beta} - \boldsymbol{R}'|} \cdot \boldsymbol{Q}_{\alpha}^{*} \\ & + \boldsymbol{Q}_{\alpha}^{*\text{T}} \cdot \nabla_{\alpha} \nabla_{\alpha}^{\text{T}} \frac{1}{|\boldsymbol{\tau}_{\alpha} + \boldsymbol{R} - \boldsymbol{\tau}_{\beta} - \boldsymbol{R}'|} \cdot \boldsymbol{Q}_{\alpha} \end{split}$$

7.2. Second-order changes

$$+ \mathbf{Q}_{\beta}^{*T} \cdot \nabla_{\alpha} \nabla_{\beta}^{T} \frac{e^{-i\mathbf{q}\cdot(\mathbf{R}'+\mathbf{R})}}{|\boldsymbol{\tau}_{\alpha} + \mathbf{R} - \boldsymbol{\tau}_{\beta} - \mathbf{R}'|} \cdot \mathbf{Q}_{\alpha}^{*}$$

$$+ \mathbf{Q}_{\beta}^{*T} \cdot \nabla_{\alpha} \nabla_{\beta}^{T} \frac{e^{-i\mathbf{q}\cdot(\mathbf{R}'-\mathbf{R})}}{|\boldsymbol{\tau}_{\alpha} + \mathbf{R} - \boldsymbol{\tau}_{\beta} - \mathbf{R}'|} \cdot \mathbf{Q}_{\alpha} + \text{c.c.}$$
(7.88)

By manipulating the equation to create only occurrences of $\mathbf{R}'' = \mathbf{R}' - \mathbf{R}$ and $\mathbf{R}''' = \mathbf{R}'$ and renaming the lattice vectors accordingly, we find

$$E_{ii}^{(2)} = \sum_{\alpha\beta} Z_{\alpha} Z_{\beta} \left[\left\{ \sum_{\boldsymbol{R}'''} e^{-2i\boldsymbol{q}\cdot\boldsymbol{R}'''} \right\} \boldsymbol{Q}_{\alpha}^{*T} \cdot \nabla_{\alpha} \nabla_{\alpha}^{T} \sum_{\boldsymbol{R}''} ' \frac{e^{2i\boldsymbol{q}\cdot\boldsymbol{R}''}}{|\boldsymbol{\tau}_{\alpha} - \boldsymbol{\tau}_{\beta} - \boldsymbol{R}''|} \cdot \boldsymbol{Q}_{\alpha}^{*} + N \cdot \boldsymbol{Q}_{\alpha}^{*T} \cdot \nabla_{\alpha} \nabla_{\alpha}^{T} \sum_{\boldsymbol{R}''} ' \frac{1}{|\boldsymbol{\tau}_{\alpha} - \boldsymbol{\tau}_{\beta} - \boldsymbol{R}''|} \cdot \boldsymbol{Q}_{\alpha} + \left\{ \sum_{\boldsymbol{R}'''} e^{-2i\boldsymbol{q}\cdot\boldsymbol{R}'''} \right\} \boldsymbol{Q}_{\beta}^{*T} \cdot \nabla_{\alpha} \nabla_{\beta}^{T} \sum_{\boldsymbol{R}''} ' \frac{e^{i\boldsymbol{q}\cdot\boldsymbol{R}''}}{|\boldsymbol{\tau}_{\alpha} - \boldsymbol{\tau}_{\beta} - \boldsymbol{R}''|} \cdot \boldsymbol{Q}_{\alpha}^{*} + N \cdot \boldsymbol{Q}_{\beta}^{*T} \cdot \nabla_{\alpha} \nabla_{\beta}^{T} \sum_{\boldsymbol{R}''} ' \frac{e^{-i\boldsymbol{q}\cdot\boldsymbol{R}''}}{|\boldsymbol{\tau}_{\alpha} - \boldsymbol{\tau}_{\beta} - \boldsymbol{R}''|} \cdot \boldsymbol{Q}_{\alpha} \right] + \text{c.c.}, \quad (7.89)$$

where the prime next to the sum now consistently indicates $\mathbf{R}'' \neq \mathbf{0}$ if $\alpha = \beta$, such that the denominator stays non-zero. The first and third lines contain a factor $\sum_{\mathbf{R}'''} \exp(-2i\mathbf{q}\cdot\mathbf{R}''')$, which contributes only if $2\mathbf{q}$ is a reciprocal lattice vector and then is the number of unit cells in the solid. In this case, the nominator $\exp(2i\mathbf{q}\cdot\mathbf{R}'')$ is 1 and the equation becomes

$$E_{ii}^{(2)} = 4N \sum_{\alpha\beta} Z_{\alpha} Z_{\beta} \left[\Re(Q_{\alpha}^{\mathrm{T}}) \cdot \nabla_{\alpha} \nabla_{\beta}^{\mathrm{T}} \sum_{\mathbf{R''}} ' \frac{1}{|\boldsymbol{\tau}_{\alpha} - \boldsymbol{\tau}_{\beta} - \mathbf{R''}|} \cdot \Re(Q_{\alpha}) + \Re(Q_{\beta}^{\mathrm{T}}) \cdot \nabla_{\alpha} \nabla_{\beta}^{\mathrm{T}} \sum_{\mathbf{R''}} ' \frac{e^{-i\boldsymbol{q}\cdot\mathbf{R''}}}{|\boldsymbol{\tau}_{\alpha} - \boldsymbol{\tau}_{\beta} - \mathbf{R''}|} \cdot \Re(Q_{\alpha}) \right]$$
(7.90)

due to $\exp(i\boldsymbol{q}\cdot\boldsymbol{R}'')=\exp(-i\boldsymbol{q}\cdot\boldsymbol{R}'')=\pm 1$ for such a \boldsymbol{q} . Also, by dividing the factor N out of the equation, we obtain the second-order ion-ion energy response per unit cell. In any case, we need to express the matrices

$$\nabla_{\alpha}\nabla_{\alpha}^{T}\sum_{\mathbf{R}}'\frac{Z_{\alpha}Z_{\beta}e^{i\bar{\mathbf{q}}\cdot\mathbf{R}}}{|\boldsymbol{\tau}_{\alpha}-\boldsymbol{\tau}_{\beta}-\mathbf{R}|} = \lim_{\mathbf{r}\to\boldsymbol{\tau}_{\alpha}}\nabla\nabla^{T}\sum_{\mathbf{R}}'\frac{Z_{\alpha}Z_{\beta}e^{i\bar{\mathbf{q}}\cdot\mathbf{R}}}{|\mathbf{r}-\boldsymbol{\tau}_{\beta}-\mathbf{R}|}$$

$$= Z_{\alpha}\lim_{\mathbf{r}\to\boldsymbol{\tau}_{\alpha}}\int\frac{\sum_{\mathbf{R}}'Z_{\beta}e^{i\bar{\mathbf{q}}\cdot\mathbf{R}}\nabla'\nabla'^{T}\delta(\mathbf{r}'-\boldsymbol{\tau}_{\beta}-\mathbf{R})}{|\mathbf{r}-\mathbf{r}'|}d^{3}r', \quad (7.91)$$

$$\nabla_{\alpha}\nabla_{\beta}^{T}\sum_{\mathbf{R}}'\frac{Z_{\alpha}Z_{\beta}e^{i\bar{\mathbf{q}}\cdot\mathbf{R}}}{|\boldsymbol{\tau}_{\alpha}-\boldsymbol{\tau}_{\beta}-\mathbf{R}|} = -\nabla_{\alpha}\nabla_{\alpha}^{T}\sum_{\mathbf{R}}'\frac{Z_{\alpha}Z_{\beta}e^{i\bar{\mathbf{q}}\cdot\mathbf{R}}}{|\boldsymbol{\tau}_{\alpha}-\boldsymbol{\tau}_{\beta}-\mathbf{R}|}$$

$$= -Z_{\alpha}\lim_{\mathbf{r}\to\boldsymbol{\tau}_{\alpha}}\int\frac{\sum_{\mathbf{R}}'Z_{\beta}e^{i\bar{\mathbf{q}}\cdot\mathbf{R}}\nabla'\nabla'^{T}\delta(\mathbf{r}'-\boldsymbol{\tau}_{\beta}-\mathbf{R})}{|\mathbf{r}-\mathbf{r}'|}d^{3}r', \quad (7.92)$$

where \tilde{q} is 0 or -q and the sum over lattice vectors excludes R = 0 if α and β refer to the same atom. We will discuss the case $\alpha \neq \beta$ first and modify the results for $\alpha = \beta$ later. We

7. Phonons in FLAPW using DFPT

make use of the Weinert method of chapter 3.7 to construct IR and MT representations for these expressions. The quantity taking the role of the density in the Weinert method is the nominator in the integral of Eqs. (7.91) and (7.92),

$$\underline{n}^{\beta \tilde{q}}(r) = \sum_{R} {}' Z_{\beta} e^{i \tilde{q} \cdot R} \nabla \nabla^{T} \delta(r - \tau_{\beta} - R)$$
(7.93)

From this quantity, we construct a pseudodensity with the same multipole moments, which has a rapidly converging Fourier expansion. This Fourier expansion is used to determine the integral of Eqs. (7.91) and (7.92) in the IR. Subsequently, the MT representation of the integrals is generated.

Construction of the pseudodensity & the interstitial contribution

Since the integral common to Eqs. (7.91) and (7.92) is reminiscent of Eq. (7.75), we can modify the formulas discussed there to express the interstitial representation of the integral. The density $\underline{n}^{\beta\bar{q}}(r)$ inside the MT sphere of an atom α in unit cell \mathbf{R}' gives rise to the multipole moments

$$\underline{q}_{lm}^{\beta \tilde{q}}(\alpha, \mathbf{R}') = Z_{\beta} \delta_{\alpha \beta} e^{i \tilde{q} \cdot \mathbf{R}'} \nabla \nabla^{\mathrm{T}} \left[r^{l} Y_{lm}^{*}(\hat{r}) \right]_{r=0}.$$
 (7.94)

This leads to the Fourier components of the pseudodensity being

$$\underline{\boldsymbol{n}}_{\mathrm{ps}}^{\beta\tilde{\boldsymbol{q}}}(\boldsymbol{G}) = \frac{Z_{\beta}}{\Omega} (2N+7)!! \frac{j_{N+3}(|\boldsymbol{G}+\tilde{\boldsymbol{q}}|R_{\beta})}{(|\boldsymbol{G}+\tilde{\boldsymbol{q}}|R_{\beta})^{N+3}} \times \left[(\boldsymbol{G}+\tilde{\boldsymbol{q}})(\boldsymbol{G}+\tilde{\boldsymbol{q}})^{\mathrm{T}} - |\boldsymbol{G}+\tilde{\boldsymbol{q}}|^{2} \underline{\boldsymbol{E}}_{3}/3 \right] e^{-i(\boldsymbol{G}+\tilde{\boldsymbol{q}})\cdot\boldsymbol{\tau}_{\beta}}$$
(7.95)

$$= \underline{n}_{ps}^{\beta 0}(G + \tilde{q}) =: \underline{n}_{ps}^{\beta}(G + \tilde{q}), \tag{7.96}$$

$$\underline{\boldsymbol{n}}_{\mathrm{ps}}^{\beta}(\mathbf{0}) = \underline{\mathbf{0}}_{3} \tag{7.97}$$

and finally yields the interstitial representation of the integral

$$\int \frac{\sum_{\boldsymbol{R}} Z_{\beta} e^{i\tilde{\boldsymbol{q}} \cdot \boldsymbol{R}} \nabla' \nabla'^{T} \delta(\boldsymbol{r}' - \boldsymbol{\tau}_{\beta} - \boldsymbol{R})}{|\boldsymbol{r} - \boldsymbol{r}'|} d^{3} r'
= \sum_{\boldsymbol{G}, \boldsymbol{G} + \tilde{\boldsymbol{q}} \neq \boldsymbol{0}} \frac{4\pi \underline{\boldsymbol{n}}_{ps}^{\beta} (\boldsymbol{G} + \tilde{\boldsymbol{q}}) e^{i(\boldsymbol{G} + \tilde{\boldsymbol{q}}) \cdot \boldsymbol{\tau}_{\beta}}}{|\boldsymbol{G} + \tilde{\boldsymbol{q}}|^{2}} e^{i(\boldsymbol{G} + \tilde{\boldsymbol{q}}) \cdot (\boldsymbol{r} - \boldsymbol{\tau}_{\beta})}.$$
(7.98)

More precisely, we have evaluated the integral whose integrand is generated by atom β and its images at any point outside of their atomic spheres. This includes the interstitial, but also any point in a muffin-tin sphere which is not associated with atom β or any of its images. For $\alpha \neq \beta$ we can thus let $r \to \tau_{\alpha}$ and we obtain

$$\nabla_{\alpha}\nabla_{\alpha}^{\mathrm{T}}\sum_{\mathbf{R}}\frac{Z_{\alpha}Z_{\beta}e^{i\tilde{\mathbf{q}}\cdot\mathbf{R}}}{|\boldsymbol{\tau}_{\alpha}-\boldsymbol{\tau}_{\beta}-\mathbf{R}|}=Z_{\alpha}\sum_{\mathbf{G},\mathbf{G}+\tilde{\mathbf{q}}\neq\mathbf{0}}\frac{4\pi\underline{\boldsymbol{n}}_{\mathrm{ps}}^{\beta}(\mathbf{G}+\tilde{\mathbf{q}})e^{i(\mathbf{G}+\tilde{\mathbf{q}})\cdot\boldsymbol{\tau}_{\beta}}}{|\mathbf{G}+\tilde{\mathbf{q}}|^{2}}e^{i(\mathbf{G}+\tilde{\mathbf{q}})\cdot(\boldsymbol{\tau}_{\alpha}-\boldsymbol{\tau}_{\beta})}. \quad (7.99)$$

For the case $\alpha = \beta$, we continue with the regular procedure of the Weinert method by constructing the MT representation of the integral from a Dirichlet boundary-value problem.

The muffin-tin contribution

In order to find an expression in the muffin-tin sphere of atom β for the integral common to Eqs. (7.91) and (7.92) for $\alpha=\beta$, where the representative atom α in unit cell ${\bf R}={\bf 0}$ is explicitly excluded from the density response, we apply a technique which has been suggested by Weinert et al. [43] to calculate the ion-ion energy $E_{\rm ii}^{(0)}$ in the first place. In this technique, it is assumed that the potential still is a Bloch function in order to construct its IR representation as usual. However, when the MT representation is constructed from a Dirichlet boundary-value problem, the critical atom is excluded from the local density in the volume integral of Eq. (3.61) and the potential defining the boundary-values is adjusted by removing the contribution generated by the local density to it. Applying this technique yields

$$\int \frac{\sum_{\mathbf{R}}' Z_{\beta} e^{i\hat{\mathbf{q}} \cdot \mathbf{R}} \nabla' \nabla'^{\mathsf{T}} \delta(\mathbf{r}' - \boldsymbol{\tau}_{\beta} - \mathbf{R})}{|\mathbf{r}_{\beta} + \boldsymbol{\tau}_{\beta} - \mathbf{r}'|} d^{3}r'$$

$$= \int_{B_{R_{\beta}}(\mathbf{0})} \sum_{\mathbf{R} \neq \mathbf{0}} Z_{\beta} e^{i\hat{\mathbf{q}} \cdot \mathbf{R}} \nabla_{\mathbf{s}_{\beta}} \nabla_{\mathbf{s}_{\beta}}^{\mathsf{T}} \delta(\mathbf{s}_{\beta} - (\mathbf{R} - \mathbf{0})) G(\mathbf{r}_{\beta}, \mathbf{s}_{\beta}) d^{3}s_{\beta}$$

$$+ \oint_{\partial B_{1}(\mathbf{0})} \int \frac{\sum_{\mathbf{R}} Z_{\beta} e^{i\hat{\mathbf{q}} \cdot \mathbf{R}} \nabla' \nabla'^{\mathsf{T}} \delta(\mathbf{r}' - \boldsymbol{\tau}_{\beta} - \mathbf{R}) - Z_{\beta} \nabla' \nabla'^{\mathsf{T}} \delta(\mathbf{r}' - \boldsymbol{\tau}_{\beta})}{|R_{\beta}\mathbf{s} + \boldsymbol{\tau}_{\beta} - \mathbf{r}'|} d^{3}r'$$

$$\times \sum_{lm} \left(\frac{r_{\beta}}{R_{\beta}}\right)^{l} Y_{lm}^{*}(\hat{\mathbf{s}}) Y_{lm}(\hat{\mathbf{r}}_{\beta}) dS. \quad (7.100)$$

The volume integral vanishes since the integrand is 0 due to $\mathbf{R} \neq \mathbf{0}$. To completely evaluate the surface integral, we have to calculate the second term in the second line of the r.h.s. By expanding the denominator into Legendre polynomials, we obtain with $\mathbf{r}_{\beta} = \mathbf{r}' - \mathbf{\tau}_{\beta}$

$$\int \frac{Z_{\beta} \nabla' \nabla'^{\mathrm{T}} \delta(\mathbf{r}' - \boldsymbol{\tau}_{\beta})}{|R_{\beta} \mathbf{s} + \boldsymbol{\tau}_{\beta} - \mathbf{r}'|} d^{3} r' = Z_{\beta} \sum_{l} \int \frac{r_{<}^{l}}{r_{>}^{l+1}} P_{l}(\hat{\mathbf{s}} \cdot \hat{\mathbf{r}}_{\beta}) \nabla_{\mathbf{r}_{\beta}} \nabla_{\mathbf{r}_{\beta}}^{\mathrm{T}} \delta(\mathbf{r}_{\beta}) d^{3} r_{\beta}$$

$$= Z_{\beta} \sum_{l} \frac{1}{R_{\beta}^{l+1}} \nabla \nabla^{\mathrm{T}} \left[r^{l} P_{l}(\hat{\mathbf{s}} \cdot \hat{\mathbf{r}}) \right]_{\mathbf{r} = \mathbf{0}}$$

$$= \frac{Z_{\beta}}{R_{\beta}^{3}} \sum_{s=0}^{2,2} \sum_{t,t'=-1}^{1} Y_{s,t+t'}(\hat{\mathbf{s}}) \sum_{i,i} \hat{\mathbf{e}}_{i} \hat{\mathbf{e}}_{j}^{\mathrm{T}} \left(3c_{i,t}c_{j,t'} G_{s,1,1}^{t+t',t,t'} - \sqrt{4\pi}\delta_{ij}\delta_{s0} \right). \tag{7.101}$$

Plugging this and the Fourier transform of Eq. (7.98) into the Dirichlet boundary-value problem, Eq. (7.100), we find in the case $\alpha = \beta$

$$\nabla_{\alpha}\nabla_{\alpha}^{\mathrm{T}} \sum_{\boldsymbol{R}}' \frac{Z_{\alpha}Z_{\beta}e^{i\hat{\boldsymbol{q}}\cdot\boldsymbol{R}}}{|\boldsymbol{\tau}_{\alpha} - \boldsymbol{\tau}_{\beta} - \boldsymbol{R}|}$$

$$= Z_{\alpha} \lim_{\boldsymbol{r}_{\beta} \to \boldsymbol{0}} \left\{ \sum_{lm} \left[\sum_{\boldsymbol{G}, \boldsymbol{G} + \tilde{\boldsymbol{q}} \neq \boldsymbol{0}} \frac{4\pi \underline{\boldsymbol{n}}_{\mathrm{ps}}^{\beta}(\boldsymbol{G} + \tilde{\boldsymbol{q}})e^{i(\boldsymbol{G} + \tilde{\boldsymbol{q}})\cdot\boldsymbol{\tau}_{\beta}}}{|\boldsymbol{G} + \tilde{\boldsymbol{q}}|^{2}} 4\pi i^{l} Y_{lm}^{*}(\widehat{\boldsymbol{G}} + \tilde{\boldsymbol{q}})j_{l}(|\boldsymbol{G} + \tilde{\boldsymbol{q}}|R_{\beta}) \right] \times \left(\frac{r_{\beta}}{R_{\beta}} \right)^{l} Y_{lm}(\hat{\boldsymbol{r}}_{\beta}) + \dots$$

7. Phonons in FLAPW using DFPT

$$\cdots - \frac{Z_{\beta}}{R_{\beta}^{3}} \sum_{s=0}^{2,2} \sum_{t,t'=-1}^{1} \left[\sum_{ij} \hat{\boldsymbol{e}}_{i} \hat{\boldsymbol{e}}_{j}^{T} \left(3c_{i,t} c_{j,t'} G_{s,1,1}^{t+t',t,t'} - \sqrt{4\pi} \delta_{ij} \delta_{s0} \right) \right] \left(\frac{r_{\beta}}{R_{\beta}} \right)^{s} Y_{s,t+t'}(\hat{r}_{\beta}) \right\}.$$
(7.102)

Since technically the denominator of the matrix $\nabla_{\alpha}\nabla_{\alpha}^{\mathrm{T}}\sum_{\mathbf{R}}'\frac{Z_{\alpha}Z_{\beta}e^{i\mathbf{q}\cdot\mathbf{R}}}{|\mathbf{\tau}_{\alpha}-\mathbf{\tau}_{\beta}-\mathbf{R}|}$ is just the lattice vector $|\mathbf{R}|$, we keep both labels α and β to remind on which part of the denominator the differential operators act and which parameters have to be used for the calculation of the matrix value. In the limit $\mathbf{r}_{\beta} = \mathbf{0}$, only the l = s = 0 parts of the sums contribute, such that we have for the matrix elements:

$$\nabla_{\alpha} \nabla_{\alpha}^{\mathrm{T}} \sum_{\mathbf{R}} \frac{Z_{\alpha} Z_{\beta} e^{i\tilde{\mathbf{q}} \cdot \mathbf{R}}}{|\boldsymbol{\tau}_{\alpha} - \boldsymbol{\tau}_{\beta} - \mathbf{R}|} = Z_{\alpha} \left\{ \sum_{\mathbf{G}, \mathbf{G} + \tilde{\mathbf{q}} \neq \mathbf{0}} \frac{4\pi \underline{n}_{\mathrm{ps}}^{\beta} (\mathbf{G} + \tilde{\mathbf{q}}) e^{i(\mathbf{G} + \tilde{\mathbf{q}}) \cdot \boldsymbol{\tau}_{\beta}}}{|\mathbf{G} + \tilde{\mathbf{q}}|^{2}} j_{0} (|\mathbf{G} + \tilde{\mathbf{q}}| R_{\beta}) - \frac{Z_{\beta}}{R_{\beta}^{3}} \sum_{t=-1}^{1} \sum_{ij} \hat{\mathbf{e}}_{i} \hat{\mathbf{e}}_{j}^{\mathrm{T}} \left(\frac{3}{4\pi} c_{i,t} c_{j,-t} (-1)^{t} - \delta_{ij} \right) \right\}$$
(7.103)

Reinstating Eqs. (7.99) and (7.103) in the expression for the second-order variation in the ion-ion energy, Eq. (7.89), we are able to explicitly calculate its contribution to the dynamical matrix.

7.2.3. Evaluation of $\phi_{m{k}m{G}}^{(2)}(m{r})$

By the same line of arguments that led to Eq. (7.21) defining the first-order variation of the basis functions, the second-order variation of the basis functions within the frozenaugmentation approximation is given by

$$\phi_{\mathbf{k}\mathbf{G}}^{(2)}(\mathbf{r}) = \begin{cases} 0 &, \mathbf{r} \in \mathrm{IR} \\ \mathbf{w}_{\alpha\mathbf{R}}^{\mathrm{T}} \cdot [i(\mathbf{k} + \mathbf{G}) - \nabla] [i(\mathbf{k} + \mathbf{G}) - \nabla]^{\mathrm{T}} \phi_{\mathbf{k}\mathbf{G}}^{(0)}(\mathbf{r}) \cdot \mathbf{w}_{\alpha\mathbf{R}} &, \mathbf{r} \in \mathrm{MT}(\alpha, \mathbf{R}) \end{cases},$$
(7.104)

because the dependence of the basis functions on the perturbation manifests in the phase factor $\exp(i(k+G)\cdot r_{\alpha Rw})$ of the matching coefficients and in the local coordinate frame $r-r_{\alpha Rw}$ in which the radial functions and spherical harmonics are expressed.

By virtue of the perturbation vectors $\boldsymbol{w}_{\alpha R}$, $\phi_{kG}^{(2)}(r)$ consists of components which are Bloch functions of wave vectors $\boldsymbol{k} + 2\boldsymbol{q}$, $\boldsymbol{k} - 2\boldsymbol{q}$ and \boldsymbol{k} . However, the second-order change of the basis functions only occurs within an integral in Eq. (6.50). The rest of the integrand is a Bloch function of wave vector $-\boldsymbol{k}$, so that only the \boldsymbol{k} -component of $\phi_{kG}^{(2)}(r)$ needs to be known, if $2\boldsymbol{q}$ is not a reciprocal lattice vector. Therefore, we only consider

$$\phi_{\mathbf{k}\mathbf{G}}^{(2)\alpha}(\mathbf{r})\Big|_{\mathbf{r}\in\mathrm{MT}(\alpha,\mathbf{0})} = \mathbf{Q}_{\alpha}^{*\mathrm{T}}\cdot\left[i(\mathbf{k}+\mathbf{G})-\nabla\right]\left[i(\mathbf{k}+\mathbf{G})-\nabla\right]^{\mathrm{T}}\phi_{\mathbf{k}\mathbf{G}}^{(0)\alpha}(\mathbf{r}_{\alpha})\cdot\mathbf{Q}_{\alpha} + \mathbf{Q}_{\alpha}^{\mathrm{T}}\cdot\left[i(\mathbf{k}+\mathbf{G})-\nabla\right]\left[i(\mathbf{k}+\mathbf{G})-\nabla\right]^{\mathrm{T}}\phi_{\mathbf{k}\mathbf{G}}^{(0)\alpha}(\mathbf{r}_{\alpha})\cdot\mathbf{Q}_{\alpha}^{*}$$
(7.105a)

in the representation of the muffin-tin sphere of atom α for $2q \neq G$. Otherwise, we have to evaluate

$$\phi_{\mathbf{k}\mathbf{G}}^{(2)\alpha}(\mathbf{r})\Big|_{\mathbf{r}\in\mathrm{MT}(\alpha,\mathbf{0})} = 4\Re(\mathbf{Q}_{\alpha}^{\mathrm{T}})\cdot\left[i(\mathbf{k}+\mathbf{G})-\nabla\right]\left[i(\mathbf{k}+\mathbf{G})-\nabla\right]^{\mathrm{T}}\phi_{\mathbf{k}\mathbf{G}}^{(0)\alpha}(\mathbf{r}_{\alpha})\cdot\Re(\mathbf{Q}_{\alpha}). \tag{7.105b}$$

We identify three terms that have to be specified. The first term is

$$\underline{\phi}_{kG,1}^{(2)\alpha}(r_{\alpha}) = -(k+G)(k+G)^{\mathrm{T}}\phi_{kG}^{(0)\alpha}(r_{\alpha})$$
(7.106a)

$$= -\sum_{lm\lambda} (\mathbf{k} + \mathbf{G})(\mathbf{k} + \mathbf{G})^{\mathrm{T}} a_{lm\lambda}^{\alpha \mathbf{k} \mathbf{G}(0)} \varphi_{lm,\lambda}^{\alpha}(\mathbf{r}_{\alpha}), \tag{7.106b}$$

where we used the decomposition of the basis functions into the matching coefficients and the radial part times spherical harmonics, as introduced in Eq. (3.64).

In the second term, the sum of the reciprocal vectors and the gradient occur. Such a term appears twice, once in its transposed form. To determine its expression, we use natural coordinates and Eq. (4.17):

$$\underline{\phi}_{kG,2}^{(2)\alpha}(\boldsymbol{r}_{\alpha}) = -\sum_{lm\lambda} a_{lm\lambda}^{\alpha kG(0)} \sum_{m''=-1}^{1} (\underline{T}\hat{\boldsymbol{e}}_{m''}) \sqrt{\frac{4\pi}{3}} \sum_{l''=-1}^{1,2} G_{l+l'',l,1}^{m+m'',m,m''} Y_{l+l'',m+m''}(\hat{\boldsymbol{r}}_{\alpha}) \times \left[u_{l\lambda}^{\alpha(0)'}(r_{\alpha}) - \left(l''l - \frac{l''-1}{2} \right) \frac{u_{l\lambda}^{\alpha(0)}(r_{\alpha})}{r_{\alpha}} \right] i(\boldsymbol{k} + \boldsymbol{G})^{\mathrm{T}} \tag{7.107}$$

The Hesse matrix in the third term requires another application of Eq. (4.17). For better readability, we write out the sums over the angular momentum shifts.

$$\underline{\phi}_{kG,3}^{(2)\alpha}(r_{\alpha}) = \nabla \nabla^{T} \sum_{lm\lambda} a_{lm\lambda}^{\alpha kG(0)} u_{l\lambda}^{\alpha(0)}(r_{\alpha}) Y_{lm}(\hat{r}_{\alpha})
= \sum_{lm\lambda} a_{lm\lambda}^{\alpha kG(0)} \frac{4\pi}{3} \sum_{m',m'''=-1}^{1} (\underline{T}\hat{e}_{m'}) (\underline{T}\hat{e}_{m''})^{T}
\times \left\{ G_{l-1,l,1}^{m+m'',m,m''} G_{l-2,l-1,1}^{m+m'+m'',m+m'',m'} Y_{l-2,m+m'+m''}(\hat{r}_{\alpha}) \right.
\times \left[u_{l\lambda}^{\alpha(0)''}(r_{\alpha}) + (2l+1) \frac{u_{l\lambda}^{\alpha(0)'}(r_{\alpha})}{r_{\alpha}} + (l^{2}-1) \frac{u_{l\lambda}^{\alpha(0)}(r_{\alpha})}{r_{\alpha}^{2}} \right] \right.
+ G_{l-1,l,1}^{m+m'',m,m''} G_{l,l-1,1}^{m+m'+m'',m+m'',m'} Y_{l,m+m'+m''}(\hat{r}_{\alpha})
\times \left[u_{l\lambda}^{\alpha(0)''}(r_{\alpha}) + 2 \frac{u_{l\lambda}^{\alpha(0)'}(r_{\alpha})}{r_{\alpha}} - l(l+1) \frac{u_{l\lambda}^{\alpha(0)}(r_{\alpha})}{r_{\alpha}^{2}} \right]
+ G_{l+1,l,1}^{m+m'',m,m''} G_{l,l+1,1}^{m+m'+m'',m+m'',m'} Y_{l,m+m'+m''}(\hat{r}_{\alpha})
\times \left[u_{l\lambda}^{\alpha(0)''}(r_{\alpha}) + 2 \frac{u_{l\lambda}^{\alpha(0)'}(r_{\alpha})}{r_{\alpha}} - l(l+1) \frac{u_{l\lambda}^{\alpha(0)}(r_{\alpha})}{r_{\alpha}^{2}} \right]
+ G_{l+1,l,1}^{m+m'',m,m''} G_{l+2,l+1,1}^{m+m'',m'',m+m'',m'} Y_{l+2,m+m'+m''}(\hat{r}_{\alpha})
\times \left[u_{l\lambda}^{\alpha(0)''}(r_{\alpha}) - (2l+1) \frac{u_{l\lambda}^{\alpha(0)'}(r_{\alpha})}{r_{\alpha}} + l(l+2) \frac{u_{l\lambda}^{\alpha(0)}(r_{\alpha})}{r_{\alpha}^{2}} \right] \right\}.$$
(7.108)

The sum of the three components gives the q = 0 second-order change of the LAPW basis

in the muffin-tin sphere of atom α .

7.2.4. Evaluation of the core state change $\psi_{im{k}}^{(2)}(r)$

To completely evaluate the Pulay contribution to the second-order change in the total energy, Eq. (6.52), also knowledge of the second-order variation of the core states is required. Employing the frozen-core approximation, in which the change in the core state is only induced through the local coordinate frame $r - r_{\alpha Rw}$, $r_{\alpha Rw} = \tau_{\alpha} + R + w_{\alpha R}$, we obtain as the second-order variation of Eq. (7.25)

$$\psi_{ik}^{(2)\alpha}(\mathbf{r} - \boldsymbol{\tau}_{\alpha} - \mathbf{R}) = \delta_{\alpha\beta} \mathbf{Q}_{\beta}^{\mathrm{T}} \cdot \nabla \nabla^{\mathrm{T}} \psi_{ik+2q}^{(0)}(\mathbf{r} - \boldsymbol{\tau}_{\beta} - \mathbf{R}) \cdot \mathbf{Q}_{\beta}$$

$$+ \delta_{\alpha\beta} \mathbf{Q}_{\beta}^{\mathrm{T}} \cdot \nabla \nabla^{\mathrm{T}} \psi_{ik}^{(0)} \quad (\mathbf{r} - \boldsymbol{\tau}_{\beta} - \mathbf{R}) \cdot \mathbf{Q}_{\beta}^{*}$$

$$+ \delta_{\alpha\beta} \mathbf{Q}_{\beta}^{*\mathrm{T}} \cdot \nabla \nabla^{\mathrm{T}} \psi_{ik}^{(0)} \quad (\mathbf{r} - \boldsymbol{\tau}_{\beta} - \mathbf{R}) \cdot \mathbf{Q}_{\beta}$$

$$+ \delta_{\alpha\beta} \mathbf{Q}_{\beta}^{*\mathrm{T}} \cdot \nabla \nabla^{\mathrm{T}} \psi_{ik-2q}^{(0)}(\mathbf{r} - \boldsymbol{\tau}_{\beta} - \mathbf{R}) \cdot \mathbf{Q}_{\beta}^{*}. \tag{7.110}$$

The second-order variation $\psi_{ik}^{(2)\alpha}(r-\tau_{\alpha}-R)$ contains components that are Bloch functions of wave vector k+2q (first line), k (second and third line), and k-2q (fourth line). Seeing as $\psi_{ik}^{(2)\alpha}(r)$ only occurs in a volume integral, only the second and third line contribute if 2q is not a vector of the reciprocal lattice. If 2q is a reciprocal lattice vector, it is equivalent to 0, and all lines can be combined to

$$\psi_{i\mathbf{k}}^{(2)\alpha}(\mathbf{r} - \boldsymbol{\tau}_{\beta} - \mathbf{R}) = 4\delta_{\alpha\beta}\Re(\mathbf{Q}_{\beta}^{\mathrm{T}}) \cdot \nabla\nabla^{\mathrm{T}}\psi_{i\mathbf{k}}^{(0)}(\mathbf{r} - \boldsymbol{\tau}_{\beta} - \mathbf{R}) \cdot \Re(\mathbf{Q}_{\beta}). \tag{7.111}$$

We remind the reader that in case of the core states, $i = (\beta p l m_l)$, is a multiindex consisting of the atom which the core state belongs to and the prime, angular momentum, and magnetic quantum numbers.

7.3. The dynamical matrix

In the previous sections, every quantity required for the second-order variation of the total energy in the FLAPW formalism has been derived and discussed. We have seen that we can restrict ourselves to the representative unit cell, such that the limit $N \to \infty$ for the system size is implicitly included. We now bring the different quantities together to find an expression for the dynamical matrix.

Doing so yields the three components $\underline{\mathcal{D}}^{\text{basic}}(q)$, $\underline{\mathcal{D}}^{\text{Pulay}}(q)$, and $\underline{\mathcal{D}}^{\text{SF}}(q)$ of the dynamical matrix, consisting of the basic DFPT term, the Pulay correction and the additional terms from the muffin-tin sphere surfaces.

7.3.1. Contribution from $E_{\text{tot,basic}}^{(2),\text{simple}}$

When we introduce $\rho^{(1)}(\mathbf{r})$ from Eq. (7.30), $V_{\rm ext}^{(1)}(\mathbf{r})$ from Eq. (7.6), and $V_{\rm ext}^{(2)}(\mathbf{r})$ from Eq. (7.7) into the integrals in

$$E_{\rm tot,basic}^{(2),\rm simple} = \int_{\Omega} \rho^{(1)}({\bm r}) V_{\rm ext}^{(1)}({\bm r}) d^3r + \int_{\Omega} \rho^{(0)}({\bm r}) V_{\rm ext}^{(2)}({\bm r}) d^3r + E_{\rm ii}^{(2)}, \qquad (6.6 \text{ revisited})$$

only the combinations of the variational terms remain which have in total a vanishing Bloch vector. Hence:

$$E_{\rm tot,basic}^{(2),\rm simple} = \sum_{\alpha\beta} \boldsymbol{Q}_{\beta}^{*\rm T} \cdot \underline{\boldsymbol{D}}_{\beta\alpha}^{\rm basic}(\boldsymbol{q}) \cdot \boldsymbol{Q}_{\alpha} + \rm c.c. \tag{7.112a}$$

$$= \left[\sum_{\alpha\beta} \boldsymbol{Q}_{\beta}^{*T} \cdot \int_{\Omega} \boldsymbol{\rho}^{(1)\beta-}(\boldsymbol{r}) \boldsymbol{V}_{\text{ext}}^{(1)\alpha+T}(\boldsymbol{r}) d^{3} \boldsymbol{r} \cdot \boldsymbol{Q}_{\alpha} \right]$$
(7.112b)

$$+ \sum_{\alpha\beta} \boldsymbol{Q}_{\beta}^{*T} \cdot \int_{\Omega} \rho^{(0)}(\boldsymbol{r}) \delta_{\alpha\beta} \sum_{\boldsymbol{R}} \nabla \nabla^{T} V_{\text{ext}}^{\alpha \boldsymbol{R}}(\boldsymbol{r}) d^{3} \boldsymbol{r} \cdot \boldsymbol{Q}_{\alpha}$$
 (7.112c)

$$+ \sum_{\alpha\beta} \mathbf{Q}_{\beta}^{*T} \cdot \underline{\mathbf{E}}_{ii\beta\alpha}^{(2)} \cdot \mathbf{Q}_{\alpha} + \text{c.c.}$$
 (7.112d)

The formulas for the density variation in the interstitial region and within the muffin-tin spheres are given in Eqs. (7.33b) and (7.34a). The corresponding expressions for the first-and second-order responses in the external potential are provided by Eqs. (7.45a) and (7.47) as well as Eqs. (7.80) and (7.84). The second-order ion-ion response matrix is defined in Eqs. (7.99) and (7.103).

Any volume integrals have to be split into the contribution from the interstitial region and contributions from the muffin-tin spheres. Using the unit step function $\Theta_{IR}(r)$ of Eq. (3.74) to select the interstitial region, we have

$$\int_{\Omega} f(\boldsymbol{r})g(\boldsymbol{r})d^{3}r = \int_{\Omega} f(\boldsymbol{r})g(\boldsymbol{r})\Theta_{IR}(\boldsymbol{r})d^{3}r + \sum_{\gamma} \int_{MT(\gamma)} f(\boldsymbol{r})g(\boldsymbol{r})d^{3}r$$

$$= \Omega \sum_{\boldsymbol{G}} \hat{f}^{*}(\boldsymbol{G})\widehat{[\Theta_{IR}g]}(\boldsymbol{G}) + \sum_{\gamma} \sum_{lm} \int_{0}^{R_{\gamma}} r_{\gamma}^{2} f_{lm}^{\gamma*}(r_{\gamma})g_{lm}^{\gamma}(r_{\gamma})dr_{\gamma}, \tag{7.113}$$

which requires the folding of the Fourier components of $\Theta_{IR}(r)$ and g(r). The integrals in Eqs. (7.112b) and (7.112c) are matrices of dimension 3×3 , so the evaluation of the integrals has to be done for each of their components.

7.3.2. Contribution from $E_{ m tot,Pulay}^{(2)}$

To find the Pulay contribution to the dynamical matrix, we need to insert the first- and second-order variations of the wave functions into

$$E_{\text{tot,Pulay}}^{(2)} = \sum_{i\mathbf{k}} f_{i\mathbf{k}}^{(0)} \left(\left\langle \psi_{i\mathbf{k}}^{(2)} \middle| \hat{\mathcal{H}}_{0} - \epsilon_{i\mathbf{k}}^{(0)} \middle| \psi_{i\mathbf{k}}^{(0)} \right\rangle + \left\langle \psi_{i\mathbf{k}}^{(0)} \middle| \hat{\mathcal{H}}_{0} - \epsilon_{i\mathbf{k}}^{(0)} \middle| \psi_{i\mathbf{k}}^{(2)} \right\rangle \right)$$

$$+ 2 \sum_{i\mathbf{k}} f_{i\mathbf{k}}^{(0)} \left\langle \psi_{i\mathbf{k}}^{(1)} \middle| \hat{\mathcal{H}}_{0} - \epsilon_{i\mathbf{k}}^{(0)} \middle| \psi_{i\mathbf{k}}^{(1)} \right\rangle + \int_{\Omega} \rho^{(1)}(\mathbf{r}) V_{\text{eff}}^{(1)}(\mathbf{r}) d^{3} \mathbf{r}. \qquad (6.52 \text{ revisited})$$

The integral is treated as in the previous section:

$$\int_{\Omega} \rho^{(1)}(\boldsymbol{r}) V_{\text{eff}}^{(1)}(\boldsymbol{r}) d^3 r = \sum_{\alpha\beta} \boldsymbol{Q}_{\beta}^{*T} \cdot \int_{\Omega} \rho^{(1)\beta-}(\boldsymbol{r}) \boldsymbol{V}_{\text{eff}}^{(1)\alpha+T}(\boldsymbol{r}) d^3 r \cdot \boldsymbol{Q}_{\alpha} + \text{c.c.}$$
(7.114)

For evaluating the bra-kets, we have to distinguish between core and valence states.

The core states

The core state responses are derived in Eqs. (7.27) and (7.110). Since the core states $\psi_{i\mathbf{h}}^{(0)}(\mathbf{r})$ are pointwise solutions of the spherical Schrödinger equation with eigenvalues $\epsilon_{i\mathbf{h}}^{(0)}$,

7. Phonons in FLAPW using DFPT

the operator $\hat{\mathcal{H}}_0 - \epsilon_{i\mathbf{k}}^{(0)}$ in the bra-kets collapses to the non-spherical part of the effective potential, $V_{\text{nonsph}}^{(0)}(\mathbf{r})$. For any core state $(i\mathbf{k})$ of atom α , the bra-kets yield

$$\left\langle \psi_{ik}^{(2)} \middle| \hat{\mathcal{H}}_{0} - \epsilon_{ik}^{(0)} \middle| \psi_{ik}^{(0)} \right\rangle + \left\langle \psi_{ik}^{(0)} \middle| \hat{\mathcal{H}}_{0} - \epsilon_{ik}^{(0)} \middle| \psi_{ik}^{(2)} \right\rangle + 2 \left\langle \psi_{ik}^{(1)} \middle| \hat{\mathcal{H}}_{0} - \epsilon_{ik}^{(0)} \middle| \psi_{ik}^{(1)} \right\rangle$$

$$= \mathbf{Q}_{\alpha}^{*T} \cdot \left\{ \left\langle \nabla \nabla^{T} \psi_{ik}^{(0)} \middle| V_{\text{nonsph}}^{(0)} \middle| \psi_{ik}^{(0)} \right\rangle + \left\langle \psi_{ik}^{(0)} \middle| V_{\text{nonsph}}^{(0)} \middle| \nabla \nabla^{T} \psi_{ik}^{(0)} \right\rangle$$

$$+ \left\langle \nabla \psi_{ik}^{(0)} \middle| V_{\text{nonsph}}^{(0)} \middle| \nabla^{T} \psi_{ik}^{(0)} \right\rangle + \left\langle \nabla^{T} \psi_{ik}^{(0)} \middle| V_{\text{nonsph}}^{(0)} \middle| \nabla \psi_{ik}^{(0)} \right\rangle \right\} \cdot \mathbf{Q}_{\alpha} + \text{c.c.}$$

$$= -\mathbf{Q}_{\alpha}^{*T} \cdot \int_{\Omega} \nabla V_{\text{nonsph}}^{(0)} (\mathbf{r}) \nabla^{T} \rho_{ik}^{(0)} (\mathbf{r}) d^{3} \mathbf{r} \cdot \mathbf{Q}_{\alpha} + \text{c.c.}$$

$$(7.115)$$

We obtained this result by an integration by parts within the bra-kets containing the second-order derivative of the core state. Note that the sum in curly brackets represents a matrix. Therefore, we consider $\langle \nabla^{\rm T} \psi_{ik}^{(0)} | V_{\rm nonsph}^{(0)} | \nabla \psi \rangle$ also to be a matrix, even though the sequence of transposed and regular gradients would suggest a scalar valued quantity. We do so to provide a concise notation.

The summation $\sum_{ik} f_{ik}^{(0)}$ over the core states yields the gradient of the core density in the integral of Eq. (7.115).

The valence states

The change in the valence states is composed of the response of the expansion coefficients $z_{kG}^{ik(0)}$ and of the basis functions $\phi_{kG}^{(0)}(r)$ according to Eq. (6.24):

$$\psi_{ik}^{(1)}(\mathbf{r}) = \sum_{KG} \left[z_{KG}^{ik(1)} \phi_{KG}^{(0)}(\mathbf{r}) + z_{KG}^{ik(0)} \phi_{KG}^{(1)}(\mathbf{r}) \right]$$
(7.116)

$$\psi_{ik}^{(2)}(\mathbf{r}) = \sum_{\mathbf{KG}} \left[z_{\mathbf{KG}}^{ik(2)} \phi_{\mathbf{KG}}^{(0)}(\mathbf{r}) + 2 z_{\mathbf{KG}}^{ik(1)} \phi_{\mathbf{KG}}^{(1)}(\mathbf{r}) + z_{\mathbf{KG}}^{ik(0)} \phi_{\mathbf{KG}}^{(2)}(\mathbf{r}) \right]$$
(7.117)

The sum over K collapses to $k \pm q$ in the case of a phononic perturbation. The responses of the basis functions result from Eqs. (7.21) and (7.104), while the first-order variation of the expansion coefficients is determined by the Sternheimer equation, Eq. (7.24). The second-order variation of the expansion coefficients is not needed, because the part of $\psi_{ik}^{(2)}(\mathbf{r})$ containing $z_{KG}^{ik(2)}$ completely lies in the LAPW basis space, in which $\psi_{ik}^{(0)}(\mathbf{r})$ fulfills the Schrödinger equation variationally. Every first-order change comprises of a sum over atoms α or β , such that the product of two first-order changes results in a double sum over atoms α and β . Thus, the bra-kets in Eq. (6.52) yield for any valence state (ik)

$$\begin{split} \left\langle \psi_{ik}^{(2)} \middle| \hat{\mathcal{H}}_{0} - \epsilon_{ik}^{(0)} \middle| \psi_{ik}^{(0)} \right\rangle + \left\langle \psi_{ik}^{(0)} \middle| \hat{\mathcal{H}}_{0} - \epsilon_{ik}^{(0)} \middle| \psi_{ik}^{(2)} \right\rangle + 2 \left\langle \psi_{ik}^{(1)} \middle| \hat{\mathcal{H}}_{0} - \epsilon_{ik}^{(0)} \middle| \psi_{ik}^{(1)} \right\rangle \\ &= \sum_{\alpha\beta} Q_{\beta}^{*T} \cdot \left[\left\langle 2 \sum_{G} z_{k+q,G}^{ik(1)\beta+} \phi_{k+q,G}^{(1)\alpha-} \right.^{T} + \sum_{G} z_{kG}^{ik(0)} \underline{\phi}_{kG}^{(2)\beta} \middle| \hat{\mathcal{H}}_{0} - \epsilon_{ik}^{(0)} \middle| \sum_{G} z_{kG}^{ik(0)} \phi_{kG}^{(0)} \middle| \right. \\ &+ \left\langle \sum_{G} z_{kG}^{ik(0)} \phi_{kG}^{(0)} \middle| \hat{\mathcal{H}}_{0} - \epsilon_{ik}^{(0)} \middle| 2 \sum_{G} z_{k-q,G}^{ik(1)\beta-} \phi_{k-q,G}^{(1)\alpha+} \right.^{T} + \sum_{G} z_{kG}^{ik(0)} \underline{\phi}_{kG}^{(2)\beta} \end{split}$$

$$+2\left\langle \sum_{G} z_{k+q,G}^{ik(1)\beta+} \phi_{k+q,G}^{(0)} + \sum_{G} z_{kG}^{ik(0)} \phi_{kG}^{(1)\beta+} \middle| \hat{\mathcal{H}}_{0} - \epsilon_{ik}^{(0)} \middle| \right.$$

$$\times \left| \sum_{G} z_{k+q,G}^{ik(1)\alpha+} \phi_{k+q,G}^{(0)} + \sum_{G} z_{kG}^{ik(0)} \phi_{kG}^{(1)\alpha+} \middle| \right.$$

$$\left. \left. \left. \left| \sum_{G} z_{k+q,G}^{ik(1)\alpha+} \phi_{k+q,G}^{(0)} + \sum_{G} z_{kG}^{ik(0)} \phi_{kG}^{(1)\alpha+} \middle| \right. \right. \right. \right. \right. \right.$$

$$\left. \left. \left| \sum_{G} z_{k+q,G}^{ik(1)\alpha+} \phi_{k+q,G}^{(0)} + \sum_{G} z_{kG}^{ik(0)} \phi_{kG}^{(1)\alpha+} \middle| \right. \right. \right.$$

$$\left. \left| \sum_{G} z_{k+q,G}^{ik(1)\alpha+} \phi_{k+q,G}^{(0)} + \sum_{G} z_{kG}^{ik(0)} \phi_{kG}^{(1)\alpha+} \middle| \right. \right.$$

$$\left. \left| \sum_{G} z_{k+q,G}^{ik(1)\alpha+} \phi_{k+q,G}^{(0)} + \sum_{G} z_{kG}^{ik(0)} \phi_{kG}^{(1)\alpha+} \middle| \right. \right.$$

Since the variation $\phi_{kG}^{(n>0)\alpha}(r)$ of a basis function only contributes in the muffin-tin sphere of atom α , most of the expressions above have to be evaluated only within the corresponding muffin-tin sphere. We refer to Appendix A.4 for the technicalities of evaluating Eq. (7.118).

7.3.3. Contribution from $E_{\text{tot.SF}}^{(2)}$

By using the first-order variations calculated in section 7.1 in Eq. (6.57), we obtain as the surface correction for the DM the following expression:

$$E_{\text{tot,SF}}^{(2)} = \sum_{\alpha\beta} \boldsymbol{Q}_{\beta}^{*T} \cdot \left[2 \sum_{ik} f_{ik}^{(0)} \oint_{\partial MT(\beta)} \hat{\boldsymbol{e}} \left[\psi_{ik}^{(1)\alpha^{-}} {}^{*T} \left(\boldsymbol{r} \right) \left(\hat{\mathcal{H}}_{0} - \epsilon_{ik}^{(0)} \right) \psi_{ik}^{(0)} \left(\boldsymbol{r} \right) \right]_{SF} dS$$

$$+ 2 \sum_{ik} f_{ik}^{(0)} \oint_{\partial MT(\beta)} \hat{\boldsymbol{e}} \left[\psi_{ik}^{(0)*} \left(\boldsymbol{r} \right) \left(\hat{\mathcal{H}}_{0} - \epsilon_{ik}^{(0)} \right) \psi_{ik}^{(1)\alpha^{+}} \left(\boldsymbol{r} \right) \right]_{SF} dS$$

$$+ \delta_{\alpha\beta} \sum_{ik} f_{ik}^{(0)} \oint_{\partial MT(\beta)} \nabla \left[\psi_{ik}^{(0)*} \left(\boldsymbol{r} \right) \left(\hat{\mathcal{H}}_{0} - \epsilon_{ik}^{(0)} \right) \psi_{ik}^{(0)} \left(\boldsymbol{r} \right) \right]_{SF} \hat{\boldsymbol{e}}^{T} dS$$

$$+ \delta_{\alpha\beta} \oint_{\partial MT(\beta)} \nabla \left[\rho^{(0)} \left(\boldsymbol{r} \right) \left\{ \varepsilon_{xc}^{(0)} \left(\boldsymbol{r} \right) - \mu_{xc}^{(0)} \left(\boldsymbol{r} \right) \right\} \right]_{SF} \hat{\boldsymbol{e}}^{T} dS$$

$$+ \oint_{\partial MT(\beta)} \hat{\boldsymbol{e}} \left[\rho^{(0)} \left(\boldsymbol{r} \right) \left\{ 2 \boldsymbol{V}_{\text{ext}}^{(1)\alpha^{+}} \left(\boldsymbol{r} \right) + \boldsymbol{V}_{\text{H}}^{(1)\alpha^{+}} \left(\boldsymbol{r} \right) \right\}^{T} \right]_{SF} dS \right] \cdot \boldsymbol{Q}_{\alpha} + \text{c.c.}$$

$$(7.119)$$

We will discuss the individual contributions of Eq. (7.119) in the following and focus first on the last term. With the abbreviation $f^{(1)\alpha+}(r) = 2V_{\rm ext}^{(1)\alpha+}(r) + V_{\rm H}^{(1)\alpha+}(r)$, the last line of Eq. (7.119) is

$$\sum_{\alpha\beta} \mathbf{Q}_{\beta}^{*\mathrm{T}} \cdot \oint_{\partial \mathrm{MT}(\beta)} \hat{\mathbf{e}} \left[\rho^{(0)}(\mathbf{r}) \ \mathbf{f}^{(1)\alpha+\mathrm{T}}(\mathbf{r}) \right]_{\mathrm{SF}} dS \cdot \mathbf{Q}_{\alpha}. \tag{7.120}$$

The density and each component of $f^{(1)\alpha+}(r)$ in their IR representation are expanded according to

$$g^{\text{IR}}(\boldsymbol{r})\big|_{\boldsymbol{r}\in\partial\text{MT}(\beta)} = \sum_{lm} \left[4\pi i^l \sum_{\boldsymbol{G}} \hat{g}(\boldsymbol{G}) e^{i\boldsymbol{G}\cdot\boldsymbol{\tau}_{\beta}} Y_{lm}^*(\hat{\boldsymbol{G}}) j_l(GR_{\beta}) \right] Y_{lm}(\hat{\boldsymbol{r}}_{\beta})$$

$$=: \sum_{lm} g_{lm,\beta}^{\text{IR}}(R_{\beta}) Y_{lm}(\hat{\boldsymbol{r}}_{\beta})$$
(7.121)

The angular-momentum cutoff for this expansion can be chosen independently from the angular-momentum cutoff up to which the LAPW basis functions are constructed in the muffin-tin sphere of atom α . An analogous expansion was used for the surface term of the

7. Phonons in FLAPW using DFPT

atomic forces, Eq. (4.30). There, a cutoff of $2l_{\rm max}^{\alpha}$ produced good results. Then, the integral in Eq. (7.120) is evaluated as

$$\oint_{\partial MT(\beta)} \hat{e} \left[\rho^{(0)}(\mathbf{r}) \ \mathbf{f}^{(1)\alpha+}^{\mathrm{T}}(\mathbf{r}) \right]_{\mathrm{SF}} dS$$

$$= \sum_{i=1}^{3} \hat{e}_{i} \sum_{m''=-1}^{1} c_{i,m''}^{*} \sum_{lm} \sum_{l'm'} \left[\rho_{lm,\beta}^{(0)}(R_{\beta}) \ \mathbf{f}_{l'm',\beta}^{(1)\alpha+}^{\mathrm{T}}(R_{\beta}) \right]_{\mathrm{SF}} G_{1,l,l'}^{m'',m,m'} \tag{7.122}$$

We decomposed here the unit normal vector \hat{e} into its Cartesian components by Eq. (4.28). Effectively, the Gaunt coefficient limits the sum over the primed quantities to $|l-1|, \ldots, l+1$ and m'=m''-m.

The matrix in Eq. (7.119) containing the xc energy density and the xc potential results from the variation of a surface term (s. Eq. (6.31)) and is thus diagonal in the atom indices (it is zero for $\alpha \neq \beta$). By using the product rule of differentiation, we obtain

$$\oint_{\partial MT(\beta)} \nabla \left[\rho^{(0)}(\mathbf{r}) f^{(0)}(\mathbf{r}) \right]_{SF} \hat{\mathbf{e}}^{T} dS$$

$$= \sum_{i=1}^{3} \sum_{m''=-1}^{1} c_{i,m''}^{*} \sum_{lm} \sum_{l'm'} G_{1,l,l'}^{m'',m,m'}$$

$$\times \left[(\nabla \rho)_{lm,\beta}^{(0)}(R_{\beta}) f_{l'm',\beta}^{(0)}(R_{\beta}) + \rho_{lm,\beta}^{(0)}(R_{\beta})(\nabla f)_{l'm',\beta}^{(0)}(R_{\beta}) \right]_{SF} \hat{\mathbf{e}}_{i}^{T}, \tag{7.123}$$

where $f^{(0)}(\mathbf{r})$ stands here for $\varepsilon_{\text{xc}}^{(0)}(\mathbf{r}) - \mu_{\text{xc}}^{(0)}(\mathbf{r})$. Eq. (7.123) applies for both the MT and IR part of $\varepsilon_{\text{xc}}^{(0)}(\mathbf{r}) - \mu_{\text{xc}}^{(0)}(\mathbf{r})$, if the Rayleigh expansion, Eq. (7.121), is applied for its IR representation. However, the gradient of the IR quantities is best calculated prior to their lm expansion. Otherwise, it can be calculated analogously to the lm components of the MT functions: The gradients $\nabla \rho^{(0)}(\mathbf{r})$ and $\nabla f^{(0)}(\mathbf{r})$ are obtained by means of Eq. (4.17), the application of the gradient in natural coordinates.

The remaining surface terms of Eq. (7.119) each include the Hamiltonian $\hat{\mathcal{H}}_0$ and a sum over all states $(i\mathbf{k})$, in principle. However, since the core states are continuous at the MT sphere boundaries to any order, only the valence states actually contribute. Furthermore, the Hamiltonian is applied differently to the wave functions in the IR and the MT spheres. In the IR, the kinetic energy operator produces factors $|\mathbf{k}+\mathbf{G}|^2/2$, while in the MT spheres, the spherical part of the Hamiltonian applied to the radial basis functions yields the energy parameters E_l^{β} . Therefore, the evaluation of these terms is different for their IR and MT representation. Their calculation is discussed in Appendix A.5 in detail.

7.4. Summary

We have discussed in this chapter all necessary steps and quantities to compute phonons using density functional perturbation theory within the all-electron FLAPW method. We repeat the main steps in the following.

Starting from an electronic structure calculation for the primitive unit cell, which provides the unperturbed density $\rho^{(0)}(\mathbf{r})$, the unperturbed wave functions $\psi_{i\mathbf{k}}^{(0)}(\mathbf{r})$, and the unperturbed effective potential $V_{\text{eff}}^{(0)}(r)$, we subject the system to a phononic perturbation of an arbitrary wave vector $q \neq 0$. This gives rise to a change in the external potential. Using perturbation theory, we calculate the first-order response of the system using the Sternheimer equation, which is the linearized Schrödinger equation. This has to be done self-consistently, because the density and consequently the Hartree and xc potential adjust to the perturbation, resulting in a first-order change of the effective potential. We include Pulay terms in this step which arise from the position dependence of the LAPW basis functions in conjunction with the fact that the LAPW wave functions are not pointwise solutions of the Schrödinger equation. Also, surface corrections are considered which account for the discontinuity of the LAPW basis functions which they exhibit not only in second order, but also in zeroth and first order due to the limited l_{max} -cutoff in their MT representation in contrast to the inclusion of all angular-momentum channels in the IR representation. In literature, the former discontinuity is commonly considered, while the latter is ignored. We discussed the cancellation of the rigid part of the density and potential response in the muffin-tin sphere of the currently displaced atom when these quantities are used to find the solution of the Sternheimer equation. The numerically delicate calculation of the density and potential gradients can thus be omitted while the Sternheimer equation is solved. Furthermore, the perturbation of wave vector q results in first-order responses whose Bloch wave vector is shifted by $\pm q$. In particular, the Kohn-Sham states are shifted from k to $k \pm q$. In order to gain access to unperturbed quantities at Bloch vector $k \pm q$, the k-point grid and the perturbation vector q have to be adjusted such that $k \pm q$ is a vector of the k-point grid again. I.e., in a practical application, q should be chosen to be a vector in the k-point grid.

Afterwards, the second-order changes of the external potential, $V_{\rm ext}^{(2)}(\mathbf{r})$, of the ion-ion energy $E_{\rm ii}^{(2)}$, and of the wave functions $\psi_{ik}^{(2)}(\mathbf{r})$ are calculated. For constructing IR and MT expressions for both the first- and second-order variations in the electrostatic part of the potential, we apply the scheme introduced by Weinert, which we discussed in chapter 3.7. From these quantities we then can determine the second-order variation of the total energy.

$$E_{\text{tot}}^{(2)} = \sum_{\alpha\beta} \boldsymbol{Q}_{\beta}^{*T} \cdot \underline{\boldsymbol{D}}(\boldsymbol{q}) \cdot \boldsymbol{Q}_{\alpha} + \text{c.c.}, \qquad (7.124)$$

where $\underline{D}(q)$ denotes the dynamical matrix at wave vector q and the polarization vectors Q_{α} define the atomic displacement pattern associated with the phonon.

The dynamical matrix consists of three components: a standard perturbation theory contribution $\underline{\mathcal{D}}^{\mathrm{basic}}(q)$, a Pulay correction $\underline{\mathcal{D}}^{\mathrm{Pulay}}(q)$ compensating the incompleteness of the LAPW basis in second order, and a surface correction $\underline{\mathcal{D}}^{\mathrm{SF}}(q)$ to second order, which again deals with the slight discontinuities of the LAPW basis functions and the quantities derived from it. The phonon frequencies and polarization vectors finally result from the eigenvalues and eigenvectors of the dynamical matrix.

In order to compute a complete phonon bandstructure, the algorithm summarized above has to be repeated for different q. A backtransformation of $\underline{D}(q)$ obtained at several q to the force-constant matrix then allows to Fourier interpolate the phonon spectrum for all q of the first Brillouin zone.

8. Summary & Conclusions

The central theme of this thesis has been the intention to calculate the phonon dispersion by means of the all-electron full-potential linearized augmented-plane-wave (FLAPW) [42–45] method. The great advantage of the FLAPW method is that the method is universally applicable with high accuracy to all chemical elements of the periodic table and with no restriction on the symmetry and the dimension of the solid. This comes with one caveat: the chosen basis set is methodologically very involved. In pursuit of the theme above, we have focused on two approaches, namely the finite-displacement (FD) approach and linear response theory.

The FD method relies on the atomic force, which corresponds to the first derivative of the total energy with respect to the atomic position. From the atomic force, the forceconstant matrix (FCM), which is the second derivative of the total energy with respect to the atomic positions, is constructed. This is achieved by separately displacing each atom from its equilibrium position in each spatial direction and computing the resulting force for all atoms. By dividing the calculated forces through the amplitude of the employed atomic displacement the FCM is approximated. The procedure described here corresponds to an analytical differentiation of the total energy to obtain the atomic forces and a numerical differentiation of the forces to finally obtain the FCM. The Fourier transform of the FCM is the dynamical matrix (DM), whose eigenvalues are the phonon frequencies, squared, and whose eigenvectors are the polarization vectors defining the displacement pattern of the phonon. To calculate phonons with a nonzero wave vector \boldsymbol{q} in the FD approach, a supercell, i.e., a unit-cell which is a multiple of the minimal chemical unit-cell of the considered material, is necessary. Phonons with a wave vector \boldsymbol{q} that is commensurable with the supercell, i.e., whose periodicity fits in the supercell, are then directly available through the FD method. Phonons at an arbitrary q-vector are only accessible by Fourier interpolation. The accuracy of this interpolation substantially depends on the spatial decay of the FCM with the distance between the displaced atom and the one to which the FCM connects it.

Due to the numerical differentiation of the atomic force, phonon calculations based on the FD approach require a high precision of the calculated atomic force. In fact, typically a much higher precision than for structural optimization is necessary. Therefore, we analyzed the precision of the atomic force in the all-electron FLAPW method as realized in the FLEUR [57] code. We observed that the atomic force calculated according to the formalism of Yu et al. [54] can lead to a violation of the acoustic sum rule and the symmetry of the FCM. The acoustic sum rule states that the sum of the forces on all atoms of the unit cell adds up to zero. It is a direct consequence of the translational symmetry of the system. In practice, we found that the acoustic sum rule is fulfilled only with a precision of $m{\rm Htr}/a_{\rm B}$. Deviations of the symmetry of the FCM, i.e, discrepancies between conjugate entries of the matrix, occur at the same level of precision. The symmetry of the FCM results from Young's theorem: the second-order derivative of a quantity does not depend on the sequence of differentiation.

8. Summary & Conclusions

We have been able to trace back these issues to mainly two sources:

- (a) energetically high-lying core states whose wave functions exhibit a substantial tail outside of their muffin-tin (MT) sphere reaching into the interstitial region (IR) or even into the MT spheres of other atoms;
- (b) an improper treatment of the small discontinuities of the LAPW wave functions, density, and potential at the MT sphere boundary for finite numerical cutoff parameters.

We suggested a refined force formalism consisting of three adjustments: In comparison to the formalism of Yu et al., which we defined as Level 0, the whole unit cell is included into the calculation of the forces arising from the core states at Level 1. Thereby, the evaluation of the core-electron force is not limited to the MT sphere of the particular electron. For the force contribution of semicore states, which exhibit non-zero value outside of the artificial MT spheres, our refinement constitutes a more rigorous description. The LAPW basis functions are constructed such that they are continuous in the low angular-momentum channels at the MT sphere boundary up to first order. Level 2 correctly evaluates a surface term containing the second spatial derivative of the basis functions using its representation from the IR. At Level 0 and Level 1, this surface term uses the MT representation of the basis functions. Consequently, Level 3 takes into account the discontinuity of the LAPW basis functions, the density, and the potential in zeroth and first order, which arises because the IR representation of the basis functions contain all angular momenta in contrast to the MT representation.

We demonstrated for the systems Al, MgO, GaAs, EuTiO₃, and VO₂ that the fulfillment of the acoustic sum rule is improved by three orders of magnitude, *i.e.*, the drift force is reduced from $m{\rm Htr}/a_{\rm B}$ to $\mu{\rm Htr}/a_{\rm B}$ at Level 3. At the same time, the symmetry of the FCM is improved significantly, as we have shown for EuTiO₃. For this system, the FCM originally exhibits a deviation from symmetry of 0.1 $m{\rm Htr}/a_{\rm B}$. This is reduced to 3 $\mu{\rm Htr}/a_{\rm B}$ by our amendments. The additional computation time required for calculating the improved atomic forces is in the worst case doubled in comparison to the initial implementation. With respect to the time required for the self-consistency of the underlying DFT calculation this is still negligible.

Utilizing the improved atomic force we have calculated phonon spectra for Al, MgO, GaAs, and EuTiO₃ by combining the all-electron FLAPW program FLEUR with the PHON code of Alfe [58]. For all four systems we find a qualitatively good agreement with experiment, except for the splitting between the longitudinal (LO) and transversal optical (TO) bands at the Γ point in the polar materials MgO and GaAs, which is a consequence of a macroscopic, electrical field generated in the long-wavelength limit. The proper inclusion of the LO-TO splitting would require the construction of the static dielectric tensor and the Born-effective charges of the system. Overall, our calculations, which are based on the experimental lattice constant and use the local density approximation (LDA) for the exchange-correlation (xc) functional, have a tendency to underestimate the experimental phonon frequencies. This is in agreement with observations in the literature [129]: LDA calculations performed at the experimental lattice constant typically give rise to too soft phonons. By using the LDA predicted lattice constant, which is usually smaller than the experimental one, a better agreement with experiment can be achieved.

In the second part of the thesis we developed a formalism to compute phonons within the all-electron FLAPW method using linear response theory. In the context of DFT, this is also known as density-functional perturbation theory (DFPT). The great advantage of the linear response approach in comparison to the FD method is that it does not require the setup of supercells. Phonons of any wave vector q can be calculated starting from the wave functions, density, and potential of the minimal chemical unit cell. The system is then perturbed by a phononic displacement of the atomic nuclei from their equilibrium position with a specific q-vector. The resulting change in the external potential due to this displacement is constructed and the linear change of the occupied wave functions is calculated by solving the differential equation of first-order perturbation theory, which is also known as the Sternheimer equation. From the response of the wave functions, the change in the density is calculated. The change in the wave functions and in the density has to be found self-consistently to account for the screening of the external perturbation due to the Hartree and exchange-correlation potential. The change in the external and the Hartree potential is computed using a scheme by Weinert with which originally the unperturbed Coulomb potential is calculated. Essentially, from these quantities the dynamical matrix is then constructed directly as the second-order derivative of the total energy.

The developed linear-response formalism draws from our experience with the atomic forces and accounts for the specifics of the LAPW approach: (a) the LAPW basis functions are adjusted to the atomic positions and thus respond themselves to the applied perturbation; (b) the space is partitioned in atom-centered muffin-tin spheres and the remaining interstitial region; (c) LAPW basis functions, density and potential exhibit a small discontinuity at the sphere boundaries. These facts give rise to additional terms in the Sternheimer equation and in the dynamical matrix which are not present in a pure planewave approach. Point (a) leads to the occurrence of so-called Pulay terms. These correct for deviations of the wave functions represented in the finite LAPW basis from the exact pointwise solutions of the Hamiltonian. Point (b) and (c) give rise to additional surface terms, which account for the discontinuities at the sphere boundaries.

To put our DFPT formulation into perspective, we compare it to the linearized muffintin orbital (LMTO) realization by Savrasov [34] and the FLAPW realization by Kouba et al. [50], since also the LMTO approach [59–61] constitutes a full-potential scheme. We recognize the equivalence between our derivation and the one of Savrasov as long as no basis-set specific contributions are considered. Both the LMTO and the LAPW basis functions are dependent on the atomic position, thus both yield a rigid part $(-\nabla)$ in the change of the basis functions and later in the variation of the density and the potential. In the case of the LMTO basis functions, Savrasov comments on their discontinuity in second order at the MT sphere boundary. However, this term is neglected in calculations as it is assumed to be negligible compared to second-order contributions to the dynamical matrix. It is unclear from Ref. [34] whether or not the second-order discontinuity of the LMTO basis functions is considered during the self-consistent solution of the Sternheimer equation, since no statement is made concerning its inclusion into the Sternheimer loop. In our DFPT FLAPW formalism, surface terms arising from the discontinuity of the LAPW basis functions are included.

8. Summary & Conclusions

A comparison between our Sternheimer matrix equation (7.24) and Eq. (2.34) of Kouba *et al.* [50] corresponding to the matrix on the right-hand side of our formula yields an apparent difference in the surface terms:

$$\sum_{G} \left\langle \phi_{k\pm q,G'}^{(0)} \middle| \hat{\mathcal{H}}_{0} - \epsilon_{ik}^{(0)} \middle| \phi_{k\pm q,G}^{(0)} \right\rangle z_{k\pm q,G}^{ik(1)\alpha\pm}$$

$$= -\sum_{G} \left\{ \left\langle \phi_{k\pm q,G'}^{(0)} \middle| V_{\text{eff}}^{(1)\alpha\pm} - \delta_{q0} \epsilon_{ik}^{(1)\alpha\pm} \middle| \phi_{kG}^{(0)} \right\rangle + \left\langle \phi_{k\pm q,G'}^{(0)} \middle| \nabla V_{\text{eff}}^{(0)} \middle| \phi_{kG}^{(0)} \right\rangle_{\alpha}$$

$$- i(G' \pm q - G) \left\langle \phi_{k\pm q,G'}^{(0)} \middle| \hat{\mathcal{H}}_{0} - \epsilon_{ik}^{(0)} \middle| \phi_{kG}^{(0)} \right\rangle_{\alpha}$$

$$- \oint_{\partial \text{MT}(\alpha,0)} \hat{e} \left[\phi_{k\pm q,G'}^{\text{IR}(0)*} (\hat{\mathcal{H}}_{0} - \epsilon_{ik}^{(0)}) \phi_{kG}^{\text{IR}(0)} \right] dS \right\} z_{kG}^{ik(0)} \tag{7.24 revisited}$$

$$\begin{split} &\delta H_{\mathbf{k}+\mathbf{q}+\mathbf{G}',\mathbf{k}+\mathbf{G}} - \epsilon_{i\mathbf{k}} \delta S_{\mathbf{k}+\mathbf{q}+\mathbf{G}',\mathbf{k}+\mathbf{G}} \\ &= \sum_{\mathbf{K}} \delta^{+} V_{\text{eff}}(\mathbf{K}+\mathbf{q}) S_{\mathbf{k}+\mathbf{K},\mathbf{k}+\mathbf{G}'-\mathbf{G}}^{\text{int}} + \sum_{\alpha} \left\langle \phi_{\mathbf{k}+\mathbf{q}+\mathbf{G}'} \middle| \delta^{+} \check{\mathbf{V}}_{\text{eff}} \middle| \phi_{\mathbf{k}+\mathbf{G}} \right\rangle_{\text{MT}(\alpha)} \\ &+ \sum_{\alpha} i [(\mathbf{G} - \mathbf{G}' - \mathbf{q}) \delta^{+} \mathbf{S}_{\alpha}] [H_{\mathbf{k}+\mathbf{q}+\mathbf{G}',\mathbf{k}+\mathbf{G}}^{\alpha} - \epsilon_{i\mathbf{k}} S_{\mathbf{k}+\mathbf{q}+\mathbf{G}',\mathbf{k}+\mathbf{G}}^{\alpha}] \\ &- \sum_{\alpha} \delta^{+} \mathbf{S}_{\alpha} \oint_{\partial \text{MT}(\alpha)} \phi_{\mathbf{k}+\mathbf{q}+\mathbf{G}'}^{*}(\mathbf{r}) V_{\text{eff}}(\mathbf{r}) \phi_{\mathbf{k}+\mathbf{G}}(\mathbf{r}) \Big|_{\text{MT}(\alpha)} \hat{\mathbf{e}} dS \\ &- \epsilon_{i\mathbf{k}} \sum_{\alpha} \delta^{+} \mathbf{S}_{\alpha} \oint_{\partial \text{MT}(\alpha)} \phi_{\mathbf{k}+\mathbf{q}+\mathbf{G}'}^{*}(\mathbf{r}) \phi_{\mathbf{k}+\mathbf{G}}(\mathbf{r}) \Big|_{\text{MT}(\alpha)} \hat{\mathbf{e}} dS \\ &- \sum_{\alpha} \delta^{+} \mathbf{S}_{\alpha} \oint_{\partial \text{MT}(\alpha)} \phi_{\mathbf{k}+\mathbf{q}+\mathbf{G}'}^{*}(\mathbf{r}) \nabla^{2} \phi_{\mathbf{k}+\mathbf{G}}(\mathbf{r}) \Big|_{\text{IR}} \hat{\mathbf{e}} dS \end{aligned} \tag{2.34 in [50]}$$

In Eq. (2.34 in [50]), $\delta^+ S_\alpha$ corresponds to the polarization vector Q_α and $\check{\mathrm{V}}_{\mathrm{eff}}(r)$ corresponds to the 'soft' part of the potential variation, i.e., $\sum_{\alpha} \boldsymbol{Q}_{\alpha}^{\mathrm{T}} \cdot \{\boldsymbol{V}_{\mathrm{eff}}^{(1)\alpha+}(\boldsymbol{r}) + \nabla V_{\mathrm{eff}}^{(0)}(\boldsymbol{r})\}$ in our notation. The surface terms in Eq. (2.34 in [50]) arise from the rigid change $-\nabla \phi_{\boldsymbol{k}\boldsymbol{G}}(\boldsymbol{r})$ in the basis functions analogous to how we proceeded in obtaining Eq. (7.24). The surface term containing the kinetic energy operator is evaluated in both equations using the IR representation of the LAPW basis functions. We note that in Eq. (2.34) of Kouba et al. [50], ∇^2 must be replaced by $\hat{T} = -\nabla^2$ for consistency in their notation. However, the surface terms containing the potential and the energy eigenvalue (inconsistent sign in Ref. [50] in case of the latter) is calculated to use the MT representation of the basis functions in [50]. Our formalism rigorously acknowledges the discontinuity of the LAPW basis functions not only in second order, but also in zeroth and first order due to the finite angular-momentum cutoff applied in the MT spheres. Therefore, we obtain these two surface terms expressed in the IR representation of the basis functions in the last line of Eq. (7.24), while the MT representation cancels out. We refrain from exchanging the MT and IR representation of the basis functions in the surface terms to compute the surface terms, since a comparison between Levels 1, 2, and 3 of our force formalism implies a high sensitivity on such an exchange for low values of the l_{max} -cutoff parameter. We expect that this sensitivity also applies in the case of phonon calculations. Kouba et al. [50] report however that they perform the exchange of the MT and IR representation of the LAPW basis functions in order

to calculate the surface terms more conveniently. In terms of a practical calculation, the Sternheimer matrix equation is thus evaluated identically in [50] and in this thesis. In this light, we consider our DFPT derivation as a rigorous proof for the validity of the practical implementation of the formalism presented by Kouba *et al.* [50], while our formalism corrects their theoretical derivation.

While Kouba *et al.* concentrate in Ref. [50] on the important step of solving the Sternheimer matrix equation and omit to present a formalism for calculating the second-order variation of the external potential $V_{\rm ext}^{(2)}(r)$ and of the ion-ion energy $E_{\rm ii}^{(2)}$, we provide in this thesis a full discussion of the first- and second-order variations leading to the dynamical matrix, including the construction of the first- and second-order changes in the Coulomb potential both in the MT spheres and in the IR.

Based on this discussion, the development of a computer program enabling phonon calculations within the all-electron FLAPW approach should be straightforward. The computational cost for the calculation of phonons with a given crystal momentum \boldsymbol{q} is expected to be comparable with the cost of the underlying self-consistent electronic structure calculation. However, since the calculations of phonons at different Bloch vectors are completely independent, the workload can be efficiently distributed over many CPUs. Hence, the computational cost does not pose a fundamental problem.

A widely available all-electron FLAPW code for computing phonons in linear response will open the vista to study not only quantities directly related to phonons, like the specific heat of a material, or the temperature dependence of the lattice constant, but also intertwined effects like the scattering of electrons and phonons and magnons and phonons from first principles in the highly accurate FLAPW approach.

Finally, we want to note that the considerations concerning the leakage of the core states from their muffin-tins and the discontinuity of the LAPW basis functions at the muffin-tin sphere boundaries are valid also for other approaches where the core electrons are treated separately from the valence electrons and where a separation of space leads to surfaces at which the representation of functions is discontinuous. This is true for example for the LMTO method or for the Korringa-Kohn-Rostoker (KKR) [66–68] method.

A.1. Implementation of core states

In chapter 3.4 we introduced the core states. These states are localized at the atomic nucleus, do not participate in resonant bonding, and are either not well or not at all represented by the LAPW basis functions defined in Eq. (3.16). The choice of the muffin-tin radius R_{α} determines whether they are partially representable: If it is such that the core state is completely confined in the muffin-tin sphere of atom α , it is orthogonal to the LAPW basis functions by Eq. (3.32). Otherwise, the core state is non-vanishing outside of the muffin-tin sphere and the leaking coretail can be partially sampled by the FLAPW basis functions. The coretail density produced by all leaking core states in the interstitial and in the muffintin spheres of foreign atoms is of the same periodicity as the lattice and is usually treated via a Fourier transform for the interstitial region and a reexpansion into spherical harmonics in the other muffin-tin spheres. In this chapter, we will give details on this procedure.

We already introduced the spherical core density $\rho_{\rm core}^{\alpha}(r_{\alpha})$ of atom α and the total core density $\rho_{\text{core}}^{\text{tot}}(\boldsymbol{r})$ in chapter 3.4 as

$$\rho_{\text{core}}^{\alpha}(\mathbf{r}_{\alpha}) = \sum_{i\mathbf{k}}^{\text{core}} \delta_{\alpha\beta} f_{i\mathbf{k}} |\psi_{i\mathbf{k}}(\mathbf{r}_{\alpha})|^{2}, \qquad (3.33 \text{ revisited})$$

$$\rho_{\text{core}}^{\text{tot}}(\mathbf{r}) = \sum_{\alpha} \rho_{\text{core}}^{\alpha}(\mathbf{r} - \boldsymbol{\tau}_{\alpha}). \qquad (3.34 \text{ revisited})$$

$$\rho_{\text{core}}^{\text{tot}}(\mathbf{r}) = \sum_{\alpha} \rho_{\text{core}}^{\alpha}(\mathbf{r} - \boldsymbol{\tau}_{\alpha}).$$
(3.34 revisited)

For the core states, $i = (\beta p l m_l)$ is a multiindex consisting of the atom β to which the core state belongs, as well as the principal, angular, and magnetic quantum numbers p, l, and

To have a good representation of the local core density in the interstitial region, it is replaced inside its muffin-tin sphere by a Gaussian to allow for a fast converging Fourier expansion of this pseudo core density

$$\tilde{\rho}_{\text{core}}^{\alpha}(\boldsymbol{r}_{\alpha}) = \begin{cases} A_{\alpha}e^{-a_{\alpha}r_{\alpha}^{2}} &, r_{\alpha} \leq R_{\alpha} \\ \rho_{\text{core}}^{\alpha}(r_{\alpha}) &, r_{\alpha} > R_{\alpha} \end{cases}$$
(3.36 revisited)

with the parameters A_{α} and a_{α} given as

$$A_{\alpha} = \rho_{\text{core}}^{\alpha}(R_{\alpha})e^{a_{\alpha}R_{\alpha}^{2}}$$
 and (3.37 revisited)

$$a_{\alpha} = -\frac{1}{2R_{\alpha}} \frac{\rho_{\text{core}}^{\alpha\prime}(R_{\alpha})}{\rho_{\text{core}}^{\alpha}(R_{\alpha})}$$
 (3.38 revisited)

by a matching of the Gaussian to the coretail density at the muffin-tin sphere boundary up to first order.

Then the interstitial core density becomes

$$\begin{aligned}
&\rho_{\text{core}}^{\text{tot}}(\boldsymbol{r})\big|_{\boldsymbol{r}\in\text{IR}} = \sum_{\boldsymbol{G}} \hat{\rho}_{\text{core}}^{\text{tot}}(\boldsymbol{G})e^{i\boldsymbol{G}\cdot\boldsymbol{r}} \text{ with} \\
&\hat{\rho}_{\text{core}}^{\text{tot}}(\boldsymbol{G}) = \frac{1}{\Omega} \int \tilde{\rho}_{\text{core}}^{\text{tot}}(\boldsymbol{r})e^{-i\boldsymbol{G}\cdot\boldsymbol{r}}d^3r \\
&= \sum_{\alpha} e^{-i\boldsymbol{G}\cdot\boldsymbol{\tau}_{\alpha}} \frac{1}{\Omega} \int \tilde{\rho}_{\text{core}}^{\alpha}(\boldsymbol{r}_{\alpha})e^{-i\boldsymbol{G}\cdot\boldsymbol{r}_{\alpha}}d^3r_{\alpha} \\
&=: \sum_{\alpha} S_{\alpha}(\boldsymbol{G})F_{\alpha}(\boldsymbol{G})
\end{aligned} \tag{A.2}$$

and the structure factor $S_{\alpha}(G)$ and the form factor $F_{\alpha}(G)$ are defined by

$$S_{\alpha}(\mathbf{G}) = e^{-i\mathbf{G}\cdot\boldsymbol{\tau}_{\alpha}}$$
 and (A.3)

$$F_{\alpha}(\mathbf{G}) = \frac{1}{\Omega} \int \tilde{\rho}_{\text{core}}^{\alpha}(\mathbf{r}_{\alpha}) e^{-i\mathbf{G}\cdot\mathbf{r}_{\alpha}} d^{3}r_{\alpha}. \tag{A.4}$$

The local pseudo core density is not periodic, but the superposition with the pseudo core densities of all images of atom α is. To account for the whole coretail density of $\tilde{\rho}_{\rm core}^{\alpha}$, which might as well reach out of the unit cell, the volume of integration is not restricted to Ω but instead includes whole three-dimensional space.

In the muffin-tin sphere of atom β , the coretail of the pseudo core density of atom α has to be expanded into the spherical harmonics of the local coordinate system again:

$$\tilde{\rho}_{\text{core}}^{\alpha}(\boldsymbol{r} - \boldsymbol{\tau}_{\alpha})|_{\boldsymbol{r} \in \text{MT}(\beta)} \\
= \sum_{lm} Y_{lm}(\widehat{\boldsymbol{r} - \boldsymbol{\tau}_{\beta}}) \sum_{\boldsymbol{G}} S_{\alpha}(\boldsymbol{G}) F_{\alpha}(\boldsymbol{G}) \oint_{\partial B_{r_{\beta}}(\boldsymbol{\tau}_{\beta})} Y_{lm}^{*}(\widehat{\boldsymbol{r} - \boldsymbol{\tau}_{\beta}}) e^{i\boldsymbol{G} \cdot \boldsymbol{r}} dS \\
= \sum_{lm} Y_{lm}(\hat{\boldsymbol{r}}_{\beta}) \left[4\pi i^{l} \sum_{\boldsymbol{G}} S_{\alpha}(\boldsymbol{G}) F_{\alpha}(\boldsymbol{G}) S_{\beta}^{*}(\boldsymbol{G}) Y_{lm}^{*}(\hat{\boldsymbol{G}}) j_{l}(Gr_{\beta}) \right] \tag{A.5}$$

To be able to calculate both contributions, we still have to evaluate the form factor.

A.1.1. $F_{\alpha}(G)$ inside the muffin-tin sphere of atom α

In order to obtain the form factor inside of $MT(\alpha)$, we write for the G=0 component

$$\begin{split} F_{\alpha}^{\text{in}}(\mathbf{0}) &= \frac{A_{\alpha}}{\Omega} \int_{B_{R_{\alpha}}(\mathbf{0})} e^{-a_{\alpha}r^{2}} d^{3}r = \frac{A_{\alpha}}{\Omega} 4\pi \int_{0}^{R_{\alpha}} r^{2} e^{-a_{\alpha}r^{2}} dr \\ &= -\frac{A_{\alpha}}{\Omega} 4\pi \frac{d}{da_{\alpha}} \int_{0}^{R_{\alpha}} e^{-a_{\alpha}r^{2}} dr = -\frac{A_{\alpha}}{\Omega} 4\pi \frac{d}{da_{\alpha}} \frac{\int_{0}^{\sqrt{a_{\alpha}}R_{\alpha}} e^{-t^{2}} dt}{\sqrt{a_{\alpha}}} \\ &= -\frac{A_{\alpha}}{\Omega} \left[\frac{4\pi R_{\alpha}}{2a_{\alpha}} e^{-a_{\alpha}R_{\alpha}^{2}} - \sqrt{\frac{\pi}{a_{\alpha}}}^{3} \operatorname{erf}(\sqrt{a_{\alpha}}R_{\alpha}) \right], \end{split}$$
(A.6)

where we introduced the error function

$$\operatorname{erf}(z) = \frac{2}{\sqrt{\pi}} \int_{0}^{z} e^{-t^{2}} dt, \text{ obeying}$$
(A.7)

$$\operatorname{erf}(0) = 0 \text{ and} \tag{A.8}$$

$$\operatorname{erf}(z^*) = \operatorname{erf}^*(z). \tag{A.9}$$

For the $G \neq 0$ components, we have

$$\begin{split} F_{\alpha}^{\text{in}}(G) &= \frac{A_{\alpha}}{\Omega} \int_{B_{R_{\alpha}}(\mathbf{0})} e^{-a_{\alpha}r^{2}} e^{-i\mathbf{G}\cdot\mathbf{r}} d^{3}r = \frac{A_{\alpha}}{\Omega} 4\pi \int_{0}^{R_{\alpha}} r^{2} e^{-a_{\alpha}r^{2}} j_{0}(Gr) dr \\ &= \frac{A_{\alpha}}{\Omega} \frac{4\pi}{2iG} \int_{0}^{R_{\alpha}} r e^{-a_{\alpha}r^{2}} \left[e^{iGr} - e^{-iGr} \right] dr \end{split} \tag{A.10}$$

The last integral can be cast into a better form by an integration by parts:

$$\int_{0}^{R_{\alpha}} re^{-a_{\alpha}r^{2}} e^{\pm iGr} dr = \frac{-1}{2a_{\alpha}} \int_{0}^{R_{\alpha}} \left(e^{-a_{\alpha}r^{2}} \right)' e^{\pm iGr} dr
= \frac{-1}{2a_{\alpha}} \left\{ \left[e^{-a_{\alpha}r^{2} \pm iGr} \right]_{0}^{R_{\alpha}} - (\pm iG) \int_{0}^{R_{\alpha}} e^{-a_{\alpha}r^{2} \pm iGr} dr \right\}$$

$$\int_{0}^{R_{\alpha}} e^{-a_{\alpha}r^{2} \pm iGr} dr = e^{-\frac{G^{2}}{4a_{\alpha}}} \int_{0}^{R_{\alpha}} e^{-\left(\sqrt{a_{\alpha}}r \mp \frac{iG}{\sqrt{a_{\alpha}}}\right)^{2}} dr
= \frac{\sqrt{\pi}}{2} e^{-\frac{G^{2}}{4a_{\alpha}}} \frac{1}{\sqrt{a_{\alpha}}} \operatorname{erf} \left(\sqrt{a_{\alpha}}R_{\alpha} \mp \frac{iG}{2\sqrt{a_{\alpha}}}\right)$$
(A.12)

Using these expressions for the form factor respecting Eq. (A.9) yields

$$F_{\alpha}^{\text{in}}(G) = -\frac{A_{\alpha}}{\Omega} \frac{4\pi R_{\alpha}}{2a_{\alpha}} e^{-a_{\alpha}R_{\alpha}^{2}} j_{0}(GR_{\alpha}) + \frac{A_{\alpha}}{\Omega} \sqrt{\frac{\pi}{a_{\alpha}}}^{3} e^{-\frac{G^{2}}{4a_{\alpha}}} \Re \left[\operatorname{erf} \left(\sqrt{a_{\alpha}} R_{\alpha} - \frac{iG}{2\sqrt{a_{\alpha}}} \right) \right].$$
(A.13)

A.1.2. $F_{\alpha}(G)$ outside of the muffin-tin sphere of atom α

Since the pseudo core density $\hat{\rho}_{\text{core}}^{\alpha}$ agrees with the real one there, the remaining integral over threedimensional space without $\text{MT}(\alpha)$ is computed numerically as

$$F_{\alpha}^{\text{out}}(\mathbf{G}) = \frac{1}{\Omega} \int_{\mathbb{R}^{3} \backslash B_{R_{\alpha}}(\mathbf{0})} \tilde{\rho}_{\text{core}}^{\alpha}(\mathbf{r}_{\alpha}) e^{-i\mathbf{G} \cdot \mathbf{r}_{\alpha}} d^{3}r_{\alpha} = \frac{4\pi}{\Omega} \int_{R_{\alpha}}^{\infty} r_{\alpha}^{2} \rho_{\text{core}}^{\alpha}(r_{\alpha}) j_{0}(Gr_{\alpha}) dr_{\alpha}, \quad (A.14)$$

$$F_{\alpha}^{\text{out}}(\mathbf{0}) = \frac{4\pi}{\Omega} \int_{R_{\alpha}}^{\infty} r_{\alpha}^{2} \rho_{\text{core}}^{\alpha}(r_{\alpha}) dr_{\alpha}. \tag{A.15}$$

The total form factor of atom α is then given as the sum $F_{\alpha}(\mathbf{G}) = F_{\alpha}^{\text{in}}(\mathbf{G}) + F_{\alpha}^{\text{out}}(\mathbf{G})$.

A.2. Calculating $d\mu_{xc}/d\rho$ for the VWN-LDA functional

The exchange-correlation LDA functional as formulated by Vosko, Wilk, and Nusair [74] is presented as

$$\begin{split} \varepsilon_{\mathbf{x}}(r_s,\zeta) &= \varepsilon_{\mathbf{x}}^{\mathbf{P}}(r_s) + [\varepsilon_{\mathbf{x}}^{\mathbf{F}}(r_s) - \varepsilon_{\mathbf{x}}^{\mathbf{P}}(r_s)] f(\zeta) \\ &= \varepsilon_{\mathbf{x}}^{\mathbf{P}}(r_s) \left\{ 1 + [2^{1/3} - 1] f(\zeta) \right\} \end{split} \tag{A.16}$$

$$\varepsilon_{\mathbf{x}}^{\mathbf{P}}(r_s) = -\frac{3}{2\pi r_s} \left(\frac{9\pi}{4}\right)^{\frac{1}{3}} = \varepsilon_{\mathbf{x}}^{\mathbf{F}}(r_s) 2^{-1/3}$$
 (A.17)

$$\varepsilon_{\rm c}(r_s,\zeta) = \varepsilon_{\rm c}^{\rm P}(r_s) + \alpha_{\rm c}(r_s) \frac{f(\zeta)}{f''(0)} (1-\zeta^4) + [\varepsilon_{\rm c}^{\rm F}(r_s) - \varepsilon_{\rm c}^{\rm P}(r_s)] f(\zeta) \zeta^4$$
(A.18)

$$r_s = \left(\frac{3}{4\pi}\right)^{1/3} \rho^{-1/3} =: c_r \rho^{-1/3}$$
 (A.19)

$$\zeta = \frac{\rho_{\uparrow} - \rho_{\downarrow}}{\rho} = \frac{\rho_{\uparrow} - \rho_{\downarrow}}{\rho_{\uparrow} + \rho_{\downarrow}} \tag{A.20}$$

$$\zeta = \frac{\rho_{\uparrow} - \rho_{\downarrow}}{\rho} = \frac{\rho_{\uparrow} - \rho_{\downarrow}}{\rho_{\uparrow} + \rho_{\downarrow}}$$

$$f(\zeta) = \frac{1}{2(2^{1/3} - 1)} \left\{ (1 + \zeta)^{4/3} + (1 - \zeta)^{4/3} - 2 \right\}$$
(A.20)

$$f'(\zeta) = \frac{2}{3(2^{1/3} - 1)} \left\{ (1 + \zeta)^{1/3} - (1 - \zeta)^{1/3} \right\}$$
(A.22)

$$f''(\zeta) = \frac{2}{9(2^{1/3} - 1)} \left\{ (1 + \zeta)^{-2/3} + (1 - \zeta)^{-2/3} \right\}$$
 (A.23)

with the spin dependent exchange energy density $\varepsilon_{\rm x}$ and correlation energy density $\varepsilon_{\rm c}$, the Seitz radius r_s , the spin polarization ζ , and the function f that interpolates in the exchange case directly between the paramagnetic ($\zeta = 0$, $\varepsilon_{\mathbf{x}}(r_s, 0) = \varepsilon_{\mathbf{x}}^{\mathbf{p}}(r_s)$) and the ferromagnetic $(\zeta = \pm 1, \varepsilon_{\mathbf{x}}(r_{\mathbf{s}}, \pm 1) = \varepsilon_{\mathbf{x}}^{F}(r_{\mathbf{s}}))$ exchange energy density. The limiting cases $\varepsilon_{\mathbf{s}}^{F}$ and $\varepsilon_{\mathbf{s}}^{F}$ as well as the spin stiffness α_c are obtained from a two-point Padé approximation to the formula

$$F(x) = A \left\{ \ln \frac{x^2}{X(x)} + \frac{2b}{Q} \tan^{-1} \frac{Q}{2x+b} - \frac{bx_0}{X(x_0)} \left[\ln \frac{(x-x_0)^2}{X(x)} + \frac{2(b+2x_0)}{Q} \tan^{-1} \frac{Q}{2x+b} \right] \right\}$$
(A.24)

with fitting parameters A, b, x_0 , and c hidden within $X(x) = x^2 + bx + c$ and $Q = (4c - b^2)^{1/2}$. It is $x = \sqrt{r_s}$. A set of these parameters is given in the paper for the limiting cases and the spin stiffness each. In order to obtain the derivative of the exchange-correlation potential with respect to the density, we start by constructing the exchange component of the xc potential:

$$\mu_{\mathbf{x}\sigma} = \frac{d\rho \varepsilon_{\mathbf{x}}(r_s, \zeta)}{d\rho_{\sigma}} = \varepsilon_{\mathbf{x}}(r_s, \zeta) + \rho \frac{\partial r_s}{\partial \rho_{\sigma}} \frac{\partial \varepsilon_{\mathbf{x}}(r_s, \zeta)}{\partial r_s} + \rho \frac{\partial \zeta}{\partial \rho_{\sigma}} \frac{\partial \varepsilon_{\mathbf{x}}(r_s, \zeta)}{\partial \zeta}$$
(A.25)

 $\sigma = \uparrow / \downarrow$ or +/- denotes the spin channel. For the correlation part, we find similarly

$$\mu_{c\sigma} = \frac{d\rho \varepsilon_c(r_s, \zeta)}{d\rho_{\sigma}} = \varepsilon_c(r_s, \zeta) + \rho \frac{\partial r_s}{\partial \rho_{\sigma}} \frac{\partial \varepsilon_c(r_s, \zeta)}{\partial r_s} + \rho \frac{\partial \zeta}{\partial \rho_{\sigma}} \frac{\partial \varepsilon_c(r_s, \zeta)}{\partial \zeta}.$$
 (A.26)

The constituents of Eqs. (A.25) and (A.26) are:

$$\frac{\partial r_s}{\partial \rho_{\sigma}} = \partial_{\rho_{\sigma}} c_r \rho^{-1/3} = -\frac{1}{3\rho} r_s \tag{A.27}$$

$$\frac{\partial \zeta}{\partial \rho_{\sigma}} = \partial_{\rho_{\sigma}} \frac{\rho_{\uparrow} - \rho_{\downarrow}}{\rho} = \partial_{\rho_{\sigma}} \sigma \frac{\rho - 2\rho_{\bar{\sigma}}}{\rho} = 2\sigma \frac{\rho_{\bar{\sigma}}}{\rho^2} \tag{A.28}$$

$$\frac{\partial \varepsilon_{\mathbf{x}}(r_s,\zeta)}{\partial r_s} = \frac{d\varepsilon_{\mathbf{x}}^{\mathbf{P}}(r_s)}{dr_s} \left\{ 1 + [2^{1/3} - 1]f(\zeta) \right\} = -\frac{1}{r_s} \varepsilon_{\mathbf{x}}(r_s,\zeta) \tag{A.29}$$

$$\frac{\partial \varepsilon_{\mathbf{x}}(r_s,\zeta)}{\partial \zeta} = \varepsilon_{\mathbf{x}}^{\mathbf{P}}(r_s)[2^{1/3} - 1]f'(\zeta) \tag{A.30}$$

$$\frac{\partial \varepsilon_{\rm c}(r_s,\zeta)}{\partial r_s} = \frac{d\varepsilon_{\rm c}^{\rm P}(r_s)}{dr_s} + \frac{d\alpha_{\rm c}(r_s)}{dr_s} \frac{f(\zeta)}{f''(0)} (1-\zeta^4) + \left[\frac{d\varepsilon_{\rm c}^{\rm F}(r_s)}{dr_s} - \frac{d\varepsilon_{\rm c}^{\rm P}(r_s)}{dr_s} \right] f(\zeta) \zeta^4 \qquad (A.31)$$

$$\frac{\partial \varepsilon_{\rm c}(r_s,\zeta)}{\partial \zeta} = \alpha_{\rm c}(r_s) \frac{f'(\zeta)}{f''(0)} + \left[\varepsilon_{\rm c}^{\rm F}(r_s) - \varepsilon_{\rm c}^{\rm P}(r_s) - \frac{\alpha_{\rm c}(r_s)}{f'''(0)} \right] \left\{ f'(\zeta)\zeta^4 + 4f(\zeta)\zeta^3 \right\} \tag{A.32}$$

$$\frac{\partial F(x)}{\partial r_s} = \frac{\partial x}{\partial r_s} F'(x) = \frac{1}{2x} \frac{2A}{X(x)} \left\{ \frac{c}{x} - \frac{bx_0}{x - x_0} \right\}$$
(A.33)

We continue with the derivative of the potential μ_{σ} with respect to the density, where we omit the x or c labels for the exchange or correlation parts, since the structure of the derivative is the same in both cases:

$$\frac{d\mu_{\sigma}}{d\rho} = \frac{\partial r_{s}}{\partial \rho} \frac{\partial \varepsilon(r_{s}, \zeta)}{\partial r_{s}} + \frac{\partial \zeta}{\partial \rho} \frac{\partial \varepsilon(r_{s}, \zeta)}{\partial \zeta} + \frac{\partial r_{s}}{\partial \rho_{\sigma}} \frac{\partial \varepsilon(r_{s}, \zeta)}{\partial r_{s}} + \frac{\partial \zeta}{\partial \rho_{\sigma}} \frac{\partial \varepsilon(r_{s}, \zeta)}{\partial \zeta}
+ \rho \left\{ \frac{\partial^{2} r_{s}}{\partial \rho \partial \rho_{\sigma}} \frac{\partial \varepsilon(r_{s}, \zeta)}{\partial r_{s}} + \frac{\partial r_{s}}{\partial \rho_{\sigma}} \frac{\partial^{r_{s}}}{\partial \rho} \frac{\partial^{2} \varepsilon(r_{s}, \zeta)}{\partial r_{s}^{2}} + \frac{\partial r_{s}}{\partial \rho_{\sigma}} \frac{\partial \zeta}{\partial \rho} \frac{\partial^{2} \varepsilon(r_{s}, \zeta)}{\partial \zeta \partial r_{s}} \right\}
+ \rho \left\{ \frac{\partial^{2} \zeta}{\partial \rho \partial \rho_{\sigma}} \frac{\partial \varepsilon(r_{s}, \zeta)}{\partial \zeta} + \frac{\partial \zeta}{\partial \rho_{\sigma}} \frac{\partial r_{s}}{\partial \rho} \frac{\partial^{2} \varepsilon(r_{s}, \zeta)}{\partial r_{s} \partial \zeta} + \frac{\partial \zeta}{\partial \rho_{\sigma}} \frac{\partial \zeta}{\partial \rho} \frac{\partial^{2} \varepsilon(r_{s}, \zeta)}{\partial \zeta^{2}} \right\}$$
(A.34)

The new constituents within this equation are:

$$\frac{\partial r_s}{\partial \rho} = -\frac{1}{3\rho} r_s, \quad \frac{\partial \zeta}{\partial \rho} = -\frac{\zeta}{\rho}, \quad \frac{\partial^2 r_s}{\partial \rho \partial \rho_\sigma} = \frac{4}{9\rho^2} r_s, \quad \frac{\partial^2 \zeta}{\partial \rho \partial \rho_\sigma} = -4\sigma \frac{\rho_{\bar{\sigma}}}{\rho^3}$$
(A.35)

$$\frac{\partial^2 \varepsilon_{\mathcal{X}}(r_s,\zeta)}{\partial r_s^2} = \frac{2}{r_s} \varepsilon_{\mathcal{X}}(r_s,\zeta) \tag{A.36}$$

$$\frac{d^2\varepsilon_{\mathbf{x}}(r_s,\zeta)}{d\zeta^2} = \varepsilon_{\mathbf{x}}^{\mathbf{P}}(r_s)[2^{1/3} - 1]f''(\zeta) \tag{A.37}$$

$$\frac{d^2 \varepsilon_{\mathbf{x}}(r_s, \zeta)}{dr_s d\zeta} = -\frac{1}{r_s} \varepsilon_{\mathbf{x}}^{\mathbf{P}}(r_s) [2^{1/3} - 1] f'(\zeta) = \frac{d^2 \varepsilon_{\mathbf{x}}(r_s, \zeta)}{d\zeta dr_s}$$
(A.38)

$$\frac{\partial^2 \varepsilon_{\rm c}(r_s,\zeta)}{\partial r_s^2} = \frac{d^2 \varepsilon_{\rm c}^{\rm P}(r_s)}{dr_s^2} + \frac{d^2 \alpha_{\rm c}(r_s)}{dr_s^2} \frac{f(\zeta)}{f''(0)} (1 - \zeta^4)$$

$$+ \left[\frac{d^2 \varepsilon_c^{\mathrm{F}}(r_s)}{dr_s^2} - \frac{d^2 \varepsilon_c^{\mathrm{P}}(r_s)}{dr_s^2} \right] f(\zeta) \zeta^4$$
(A.39)

$$\frac{d^2 \varepsilon_{\rm c}(r_s, \zeta)}{d\zeta^2} = \alpha_{\rm c}(r_s) \frac{f''(\zeta)}{f''(0)} + \left[\varepsilon_{\rm c}^{\rm F}(r_s) - \varepsilon_{\rm c}^{\rm P}(r_s) - \frac{\alpha_{\rm c}(r_s)}{f''(0)} \right] \times \left\{ f''(\zeta) \zeta^4 + 8f'(\zeta) \zeta^3 + 12f(\zeta) \zeta^2 \right\} \tag{A.40}$$

$$\frac{d^2 \varepsilon_c(r_s, \zeta)}{dr_s d\zeta} = \frac{d\alpha_c(r_s)}{dr_s} \frac{f'(\zeta)}{f''(0)} + \left[\frac{d\varepsilon_c^F(r_s)}{dr_s} - \frac{d\varepsilon_c^P(r_s)}{dr_s} - \frac{d\alpha_c(r_s)}{dr_s} \frac{1}{f''(0)} \right] \\
\times \left\{ f'(\zeta)\zeta^4 + 4f(\zeta)\zeta^3 \right\} = \frac{d^2 \varepsilon_c(r_s, \zeta)}{d\zeta dr_s} \tag{A.41}$$

$$\frac{\partial^2 F(x)}{\partial r_s^2} = \frac{\partial x}{\partial r_s} \frac{\partial}{\partial x} \frac{\partial F(x)}{\partial r_s} = \frac{1}{2x} \partial_x \frac{A}{xX(x)} \left\{ \frac{c}{x} - \frac{bx_0}{x - x_0} \right\} \\
= -\frac{A}{2x^2 X(x)} \left[\left\{ \frac{1}{x} + \frac{X'(x)}{X(x)} \right\} \left\{ \frac{c}{x} - \frac{bx_0}{x - x_0} \right\} + \left\{ \frac{c}{x^2} - \frac{bx_0}{(x - x_0)^2} \right\} \right] \tag{A.42}$$

$$X'(x) = 2x + b \tag{A.43}$$

Remember that F(x) is used for $\varepsilon_c^F(r_s)$, $\varepsilon_c^P(r_s)$, and $\alpha_c(r_s)$ with a different set of parameters each

A.3. Input file for VO_2

We provide the setup for our force calculations on vanadium dioxide (see chapter 4.7) in terms of an input file for the input-file generator of FLEUR. The data is taken from the Inorganic Crystal Structure Database (ICSD) [151] hosted by the Fachinformationszentrum Karlsruhe [152]. Due to how monoclinic lattices are implemented in FLEUR, the b and c axes and the β and γ angles had to be exchanged. Namelists, which start with an ampersand & and end with a slash /, are considered to be on one line.

```
Vanadium dioxide
&input cartesian=f inistop=t oldfleur=f /
&lattice latsys='moP' a= 5.3528 b= 5.3825 c= 4.5378
        alpha= 90 beta= 90 gamma= 115.208 a0= 1.88972612457 /
12
 23
        0.2605 0.2870 0.0211
       -.2605 0.2130 0.5211
 23
       -.2605 -.2870 -.0211
 23
        0.2605 0.7870 0.4789
        0.6062 0.3976 0.2119
        -.6062 0.1024 0.7119
  8
       -.6062 -.3976 -.2119
       0.6062 0.8976 0.2881
  8
       0.0995 0.3983 0.2974
       -.0995 0.1017 0.7974
       -.0995 -.3983 -.2974
        0.0995 0.8983 0.2026
&factor 1.000 1.000 /
&atom element="v" id=23 rmt=1.90 jri=687 dx=0.017
        lmax=12 lnonsph=12 lo="3p" /
&atom element="o" id=8 rmt=1.10 jri=389 dx=0.026
        lmax=12 lnonsph=12 /
&exco xctyp='vwn' /
&comp kmax=5.5 gmax=15.3 gmaxxc=12.7 /
&end /
```

A.4. Nitty-gritties of $D^{\mathrm{Pulay}}(q)$

We want to calculate the constituents of

$$\left\langle \psi_{ik}^{(2)} \middle| \hat{\mathcal{H}}_{0} - \epsilon_{ik}^{(0)} \middle| \psi_{ik}^{(0)} \right\rangle + \left\langle \psi_{ik}^{(0)} \middle| \hat{\mathcal{H}}_{0} - \epsilon_{ik}^{(0)} \middle| \psi_{ik}^{(2)} \right\rangle + 2 \left\langle \psi_{ik}^{(1)} \middle| \hat{\mathcal{H}}_{0} - \epsilon_{ik}^{(0)} \middle| \psi_{ik}^{(1)} \right\rangle$$

$$= \sum_{\alpha\beta} \mathbf{Q}_{\beta}^{*T} \cdot \left[\left\langle 2 \sum_{\mathbf{G}} \mathbf{z}_{\mathbf{k}+\mathbf{q},\mathbf{G}}^{ik(1)\beta+} \phi_{\mathbf{k}+\mathbf{q},\mathbf{G}}^{(1)\alpha-} \right. + \sum_{\mathbf{G}} \mathbf{z}_{\mathbf{k}\mathbf{G}}^{ik(0)} \underline{\phi}_{\mathbf{k}\mathbf{G}}^{(2)\beta} \middle| \hat{\mathcal{H}}_{0} - \epsilon_{ik}^{(0)} \middle| \sum_{\mathbf{G}} \mathbf{z}_{\mathbf{k}\mathbf{G}}^{ik(0)} \phi_{\mathbf{k}\mathbf{G}}^{(0)} \right\rangle$$

$$+ \left\langle \sum_{\mathbf{G}} \mathbf{z}_{\mathbf{k}\mathbf{G}}^{ik(0)} \phi_{\mathbf{k}\mathbf{G}}^{(0)} \middle| \hat{\mathcal{H}}_{0} - \epsilon_{ik}^{(0)} \middle| 2 \sum_{\mathbf{G}} \mathbf{z}_{\mathbf{k}-\mathbf{q},\mathbf{G}}^{ik(1)\beta-} \phi_{\mathbf{k}-\mathbf{q},\mathbf{G}}^{(1)\alpha+} \right. + \sum_{\mathbf{G}} \mathbf{z}_{\mathbf{k}\mathbf{G}}^{ik(0)} \underline{\phi}_{\mathbf{k}\mathbf{G}}^{(2)\beta} \right\rangle$$

$$+ 2 \left\langle \sum_{\mathbf{G}} \mathbf{z}_{\mathbf{k}+\mathbf{q},\mathbf{G}}^{ik(1)\beta+} \phi_{\mathbf{k}+\mathbf{q},\mathbf{G}}^{(0)} + \sum_{\mathbf{G}} \mathbf{z}_{\mathbf{k}\mathbf{G}}^{ik(0)} \phi_{\mathbf{k}\mathbf{G}}^{(1)\beta+} \middle| \hat{\mathcal{H}}_{0} - \epsilon_{ik}^{(0)} \middle| \right.$$

$$\times \left. \left| \sum_{\mathbf{G}} \mathbf{z}_{\mathbf{k}+\mathbf{q},\mathbf{G}}^{ik(1)\alpha+} \nabla_{\mathbf{k}+\mathbf{q},\mathbf{G}} + \sum_{\mathbf{G}} \mathbf{z}_{\mathbf{k}\mathbf{G}}^{ik(0)} \phi_{\mathbf{k}\mathbf{G}}^{(1)\alpha+} \nabla_{\mathbf{K}}^{\top} \right. \right| \cdot \mathbf{Q}_{\alpha} + \text{c.c.},$$

$$(7.118 \text{ revisited})$$

where $\psi_{ik}^{(0)}(r)$ is a valence state. We will discuss each of the three bra-kets and refer to results already obtained when necessary.

A.4.1. First bra-ket

By using the basis function responses given in Eqs. (7.21) and (7.104), the first bra-ket transforms to

$$\left\langle 2 \sum_{\mathbf{G}} z_{\mathbf{k}\pm\mathbf{q},\mathbf{G}}^{i\mathbf{k}(1)\beta\pm} \phi_{\mathbf{k}\pm\mathbf{q},\mathbf{G}}^{(1)\alpha\mp} + \sum_{\mathbf{G}} z_{\mathbf{k}\mathbf{G}}^{i\mathbf{k}(0)} \phi_{\mathbf{k}\mathbf{G}}^{(2)\beta} \middle| \hat{\mathcal{H}}_{0} - \epsilon_{i\mathbf{k}}^{(0)} \middle| \sum_{\mathbf{G}} z_{\mathbf{k}\mathbf{G}}^{i\mathbf{k}(0)} \phi_{\mathbf{k}\mathbf{G}}^{(0)} \middle\rangle \right.$$

$$= 2 \sum_{\mathbf{G}\mathbf{G}'} \left(z_{\mathbf{k}\pm\mathbf{q},\mathbf{G}'}^{i\mathbf{k}(1)\beta\pm} \right)^{*} z_{\mathbf{k}\mathbf{G}}^{i\mathbf{k}(0)} \left\langle \phi_{\mathbf{k}\pm\mathbf{q},\mathbf{G}'}^{(1)\alpha\mp} \middle| \hat{\mathcal{H}}_{0} - \epsilon_{i\mathbf{k}}^{(0)} \middle| \phi_{\mathbf{k}\mathbf{G}}^{(0)} \middle\rangle_{\alpha} \right.$$

$$+ \sum_{\mathbf{G}\mathbf{G}'} z_{\mathbf{k}\mathbf{G}'}^{i\mathbf{k}(0)*} z_{\mathbf{k}\mathbf{G}}^{i\mathbf{k}(0)} \delta_{\alpha\beta} \left\langle \phi_{\mathbf{k}\mathbf{G}'}^{(2)\beta} \middle| \hat{\mathcal{H}}_{0} - \epsilon_{i\mathbf{k}}^{(0)} \middle| \phi_{\mathbf{k}\mathbf{G}}^{(0)} \middle\rangle_{\alpha} \right.$$

$$= 2 \sum_{\mathbf{G}\mathbf{G}'} \left(z_{\mathbf{k}\pm\mathbf{q},\mathbf{G}'}^{i\mathbf{k}(1)\beta\pm} \right)^{*} \left[i(\mathbf{k}\pm\mathbf{q}+\mathbf{G}') \right]^{*T} z_{\mathbf{k}\mathbf{G}}^{i\mathbf{k}(0)} \left\langle \phi_{\mathbf{k}\pm\mathbf{q},\mathbf{G}'}^{(0)} \middle| \hat{\mathcal{H}}_{0} - \epsilon_{i\mathbf{k}}^{(0)} \middle| \phi_{\mathbf{k}\mathbf{G}}^{(0)} \middle\rangle_{\alpha} \right.$$

$$- 2 \sum_{\mathbf{G}\mathbf{G}'} \left(z_{\mathbf{k}\pm\mathbf{q},\mathbf{G}'}^{i\mathbf{k}(1)\beta\pm} \right)^{*} z_{\mathbf{k}\mathbf{G}}^{i\mathbf{k}(0)} \left\langle \nabla^{T}\phi_{\mathbf{k}\pm\mathbf{q},\mathbf{G}'}^{(0)} \middle| \hat{\mathcal{H}}_{0} - \epsilon_{i\mathbf{k}}^{(0)} \middle| \phi_{\mathbf{k}\mathbf{G}}^{(0)} \middle\rangle_{\alpha} \right.$$

$$- \delta_{\alpha\beta} \sum_{\mathbf{G}\mathbf{G}'} z_{\mathbf{k}\mathbf{G}'}^{i\mathbf{k}(0)*} (\mathbf{k}+\mathbf{G}') (\mathbf{k}+\mathbf{G}')^{T} z_{\mathbf{k}\mathbf{G}}^{i\mathbf{k}(0)} \left\langle \phi_{\mathbf{k}\mathbf{G}'}^{(0)} \middle| \hat{\mathcal{H}}_{0} - \epsilon_{i\mathbf{k}}^{(0)} \middle| \phi_{\mathbf{k}\mathbf{G}}^{(0)} \middle\rangle_{\alpha} + (...)^{T}$$

$$+ \delta_{\alpha\beta} \sum_{\mathbf{G}\mathbf{G}'} z_{\mathbf{k}\mathbf{G}'}^{i\mathbf{k}(0)*} z_{\mathbf{k}\mathbf{G}}^{i\mathbf{k}(0)} \left\langle \nabla\nabla^{T}\phi_{\mathbf{k}\mathbf{G}'}^{(0)} \middle| \hat{\mathcal{H}}_{0} - \epsilon_{i\mathbf{k}}^{(0)} \middle| \phi_{\mathbf{k}\mathbf{G}}^{(0)} \middle\rangle_{\alpha} \right.$$
(A.44)

A.4. Nitty-gritties of
$$\mathbf{D}^{\text{Pulay}}(\mathbf{q})$$

We expand the basis functions $\phi_{kG}^{(0)}(r)$ into expansion coefficients $a_{lm\lambda}^{\alpha kG}$ and radial functions times spherical harmonics $\varphi_{lm,\lambda}^{\alpha}(r_{\alpha})$ (cf. Eqs. 3.16 and 3.64) and contract the G sums according to

$$A_{lm\lambda}^{\alpha i \boldsymbol{k}} = \sum_{\boldsymbol{G}} z_{\boldsymbol{k}\boldsymbol{G}}^{i\boldsymbol{k}(0)} a_{lm\lambda}^{\alpha \boldsymbol{k}\boldsymbol{G}}, \tag{A.45}$$

$$A_{lm\lambda}^{\alpha i \mathbf{k}} = \sum_{\mathbf{G}} \mathbf{G} z_{\mathbf{k}\mathbf{G}}^{i \mathbf{k}(0)} a_{lm\lambda}^{\alpha \mathbf{k}\mathbf{G}}, \tag{A.46}$$

$$\underline{\underline{A}}_{lm\lambda}^{\alpha i k} = \sum_{G} G G^{\mathrm{T}} z_{kG}^{ik(0)} a_{lm\lambda}^{\alpha kG}, \tag{A.47}$$

$$\mathbf{A}_{lm\lambda\beta}^{\alpha i \mathbf{k} \pm} = \sum_{\mathbf{G}} \mathbf{z}_{\mathbf{k} \pm \mathbf{q}, \mathbf{G}}^{i \mathbf{k} (1) \alpha \pm} a_{lm\lambda}^{\beta, \mathbf{k} \pm \mathbf{q}, \mathbf{G}}, \tag{A.48}$$

and

$$\underline{\underline{A}}_{lm\lambda\beta}^{\alpha ik\pm} = \sum_{G} G z_{k\pm q,G}^{ik(1)\alpha\pm} a_{lm\lambda}^{\beta,k\pm q,G}. \tag{A.49}$$

Then we obtain

$$\left\langle 2 \sum_{\boldsymbol{G}} z_{\boldsymbol{k}\pm\boldsymbol{q},\boldsymbol{G}}^{i\boldsymbol{k}(1)\beta\pm} \boldsymbol{\phi}_{\boldsymbol{k}\pm\boldsymbol{q},\boldsymbol{G}}^{(1)\alpha\mp} + \sum_{\boldsymbol{G}} z_{\boldsymbol{k}\boldsymbol{G}}^{i\boldsymbol{k}(0)} \underline{\boldsymbol{\phi}}_{\boldsymbol{k}\boldsymbol{G}}^{(2)\beta} \middle| \hat{\boldsymbol{H}}_{0} - \epsilon_{i\boldsymbol{k}}^{(0)} \middle| \sum_{\boldsymbol{G}} z_{\boldsymbol{k}\boldsymbol{G}}^{i\boldsymbol{k}(0)} \boldsymbol{\phi}_{\boldsymbol{k}\boldsymbol{G}}^{(0)} \middle\rangle \right.$$

$$= -2i \sum_{lm\lambda} \sum_{l'm'\lambda'} \left[A_{l'm'\lambda'\alpha}^{\beta i\boldsymbol{k}\pm} (\boldsymbol{k}\pm\boldsymbol{q})^{\mathrm{T}} + \underline{\boldsymbol{A}}_{l'm'\lambda'\alpha}^{\beta i\boldsymbol{k}\pm} \right]^{*} A_{lm\lambda}^{\alpha i\boldsymbol{k}} \times \left\langle \boldsymbol{\varphi}_{l'm',\lambda'}^{\alpha(0)} \middle| \hat{\boldsymbol{H}}_{0} - \epsilon_{i\boldsymbol{k}}^{(0)} \middle| \boldsymbol{\varphi}_{lm,\lambda}^{\alpha(0)} \right\rangle_{\alpha}$$

$$- 2 \sum_{lm\lambda} \sum_{l'm'\lambda'} \left(A_{l'm'\lambda'\alpha}^{\beta i\boldsymbol{k}\pm} \right)^{*} A_{lm\lambda}^{\alpha i\boldsymbol{k}} \left\langle \nabla^{\mathrm{T}} \boldsymbol{\varphi}_{l'm',\lambda'}^{\alpha(0)} \middle| \hat{\boldsymbol{H}}_{0} - \epsilon_{i\boldsymbol{k}}^{(0)} \middle| \boldsymbol{\varphi}_{lm,\lambda}^{\alpha(0)} \right\rangle_{\alpha}$$

$$- \delta_{\alpha\beta} \sum_{lm\lambda} \sum_{l'm'\lambda'} \left[A_{l'm'\lambda'}^{\alpha i\boldsymbol{k}} \boldsymbol{k} \boldsymbol{k}^{\mathrm{T}} + \boldsymbol{k} \left(A_{l'm'\lambda'}^{\alpha i\boldsymbol{k}} \right)^{\mathrm{T}} + A_{l'm'\lambda'}^{\alpha i\boldsymbol{k}} \boldsymbol{k}^{\mathrm{T}} + \underline{\boldsymbol{A}}_{l'm'\lambda'}^{\alpha i\boldsymbol{k}} \right]^{*} A_{lm\lambda}^{\alpha i\boldsymbol{k}}$$

$$\times \left\langle \boldsymbol{\varphi}_{l'm',\lambda'}^{\alpha(0)} \middle| \hat{\boldsymbol{H}}_{0} - \epsilon_{i\boldsymbol{k}}^{(0)} \middle| \boldsymbol{\varphi}_{lm,\lambda}^{\alpha(0)} \right\rangle_{\alpha}$$

$$- \delta_{\alpha\beta} i \sum_{lm\lambda} \sum_{l'm'\lambda'} \left[A_{l'm'\lambda'}^{\alpha i\boldsymbol{k}} \boldsymbol{k} + A_{l'm'\lambda'}^{\alpha i\boldsymbol{k}} \right]^{*} A_{lm\lambda}^{\alpha i\boldsymbol{k}} \left\langle \nabla^{\mathrm{T}} \boldsymbol{\varphi}_{l'm',\lambda'}^{\alpha(0)} \middle| \hat{\boldsymbol{H}}_{0} - \epsilon_{i\boldsymbol{k}}^{(0)} \middle| \boldsymbol{\varphi}_{lm,\lambda}^{\alpha(0)} \right\rangle_{\alpha} + (\ldots)^{\mathrm{T}}$$

$$+ \delta_{\alpha\beta} \sum_{lm\lambda} \sum_{l'm'\lambda'} \left(A_{l'm'\lambda'}^{\alpha i\boldsymbol{k}} \right)^{*} A_{lm\lambda}^{\alpha i\boldsymbol{k}} \left\langle \nabla\nabla^{\mathrm{T}} \boldsymbol{\varphi}_{l'm',\lambda'}^{\alpha(0)} \middle| \hat{\boldsymbol{H}}_{0} - \epsilon_{i\boldsymbol{k}}^{(0)} \middle| \boldsymbol{\varphi}_{lm,\lambda}^{\alpha(0)} \right\rangle_{\alpha}. \tag{A.50}$$

Now the muffin-tin integrals can be calculated exactly as or similarly to Eqs. (3.68)ff.

A.4.2. Second bra-ket

The second bra-ket of Eq. (7.118) can be transformed similarly to the first one:

$$\left\langle \sum_{\boldsymbol{G}} z_{\boldsymbol{k}\boldsymbol{G}}^{i\boldsymbol{k}(0)} \phi_{\boldsymbol{k}\boldsymbol{G}}^{(0)} \middle| \hat{\mathcal{H}}_{0} - \epsilon_{i\boldsymbol{k}}^{(0)} \middle| 2 \sum_{\boldsymbol{G}} z_{\boldsymbol{k}\pm\boldsymbol{q},\boldsymbol{G}}^{i\boldsymbol{k}(1)\beta\pm} \phi_{\boldsymbol{k}\pm\boldsymbol{q},\boldsymbol{G}}^{(1)\alpha\mp} + \sum_{\boldsymbol{G}} z_{\boldsymbol{k}\boldsymbol{G}}^{i\boldsymbol{k}(0)} \underline{\phi_{\boldsymbol{k}\boldsymbol{G}}^{(2)\beta}} \right\rangle \\
= 2i \sum_{lm\lambda} \sum_{l'm'\lambda'} \left(A_{l'm'\lambda'}^{\alpha i\boldsymbol{k}} \right)^{*} \left[A_{lm\lambda\alpha}^{\beta i\boldsymbol{k}\pm} (\boldsymbol{k}\pm\boldsymbol{q})^{\mathrm{T}} + \underline{A}_{lm\lambda\alpha}^{\beta i\boldsymbol{k}\pm} \right] \\
\times \left\langle \varphi_{l'm',\lambda'}^{\alpha(0)} \middle| \hat{\mathcal{H}}_{0} - \epsilon_{i\boldsymbol{k}}^{(0)} \middle| \varphi_{lm,\lambda}^{\alpha(0)} \right\rangle_{\alpha} \\
- 2 \sum_{lm\lambda} \sum_{l'm'\lambda'} \left(A_{l'm'\lambda'}^{\alpha i\boldsymbol{k}} \right)^{*} A_{lm\lambda\alpha}^{\beta i\boldsymbol{k}\pm} \left\langle \varphi_{l'm',\lambda'}^{\alpha(0)} \middle| \hat{\mathcal{H}}_{0} - \epsilon_{i\boldsymbol{k}}^{(0)} \middle| \nabla^{\mathrm{T}} \varphi_{lm,\lambda}^{\alpha(0)} \right\rangle_{\alpha} \\
- \delta_{\alpha\beta} \sum_{lm\lambda} \sum_{l'm'\lambda'} \left(A_{l'm'\lambda'}^{\alpha i\boldsymbol{k}} \right)^{*} \left[A_{lm\lambda}^{\alpha i\boldsymbol{k}} \boldsymbol{k} \boldsymbol{k}^{\mathrm{T}} + \boldsymbol{k} \left(A_{lm\lambda}^{\alpha i\boldsymbol{k}} \right)^{\mathrm{T}} + A_{lm\lambda}^{\alpha i\boldsymbol{k}} \boldsymbol{k}^{\mathrm{T}} + \underline{A}_{lm\lambda}^{\alpha i\boldsymbol{k}} \right) \\
\times \left\langle \varphi_{l'm',\lambda'}^{\alpha(0)} \middle| \hat{\mathcal{H}}_{0} - \epsilon_{i\boldsymbol{k}}^{(0)} \middle| \varphi_{lm,\lambda}^{\alpha(0)} \right\rangle_{\alpha} \\
+ \delta_{\alpha\beta} i \sum_{lm\lambda} \sum_{l'm'\lambda'} \left(A_{l'm'\lambda'}^{\alpha i\boldsymbol{k}} \right)^{*} \left[A_{lm\lambda}^{\alpha i\boldsymbol{k}} \boldsymbol{k} + A_{lm\lambda}^{\alpha i\boldsymbol{k}} \right] \left\langle \varphi_{l'm',\lambda'}^{\alpha(0)} \middle| \hat{\mathcal{H}}_{0} - \epsilon_{i\boldsymbol{k}}^{(0)} \middle| \nabla^{\mathrm{T}} \varphi_{lm,\lambda}^{\alpha(0)} \right\rangle_{\alpha} \\
+ \delta_{\alpha\beta} \sum_{lm\lambda} \sum_{l'm'\lambda'} \left(A_{l'm'\lambda'}^{\alpha i\boldsymbol{k}} \right)^{*} A_{lm\lambda}^{\alpha i\boldsymbol{k}} \left\langle \varphi_{l'm',\lambda'}^{\alpha(0)} \middle| \hat{\mathcal{H}}_{0} - \epsilon_{i\boldsymbol{k}}^{(0)} \middle| \nabla\nabla^{\mathrm{T}} \varphi_{lm,\lambda}^{\alpha(0)} \right\rangle_{\alpha}$$
(A.51)

The $\varphi_{lm,\lambda}^{\alpha(0)}(r)$ do not vanish at the muffin-tin sphere boundary. Therefore, $\hat{\mathcal{H}}_0$ is not self-adjoint in MT(α). In order to evaluate the MT integrals where the ket consists of the gradient or the Hessian of $\varphi_{lm,\lambda}^{\alpha(0)}(r)$, we have to add and subtract $\left[\frac{1}{2}\nabla^2\phi_{l'm',\lambda'}^{\alpha(0)}(r_{\alpha})\right]^*$ such that the Hamiltonian acts on the bra. With $f(r_{\alpha})$ either being a component of $\nabla^{\mathrm{T}}\varphi_{lm,\lambda}^{\alpha(0)}(r_{\alpha})$ or $\nabla\nabla^{\mathrm{T}}\varphi_{lm,\lambda}^{\alpha(0)}(r_{\alpha})$, we obtain using Gauss' theorem

$$\left\langle \varphi_{l'm',\lambda'}^{\alpha(0)} \middle| \hat{\mathcal{H}}_{0} - \epsilon_{ik}^{(0)} \middle| f \right\rangle_{\alpha}
= \left\langle f \middle| \hat{\mathcal{H}}_{0} - \epsilon_{ik}^{(0)} \middle| \varphi_{l'm',\lambda'}^{\alpha(0)} \right\rangle_{\alpha}^{*}
+ \frac{1}{2} \int_{B_{R_{\alpha}}(\mathbf{0})} \left[\nabla^{2} \varphi_{l'm',\lambda'}^{\alpha(0)} (\mathbf{r}_{\alpha}) \right]^{*} f(\mathbf{r}_{\alpha}) - \left(\varphi_{l'm',\lambda'}^{\alpha(0)} (\mathbf{r}_{\alpha}) \right)^{*} \left[\nabla^{2} f(\mathbf{r}_{\alpha}) \right] d^{3} r_{\alpha}
= \left\langle f \middle| \hat{\mathcal{H}}_{0} - \epsilon_{ik}^{(0)} \middle| \varphi_{l'm',\lambda'}^{\alpha(0)} \right\rangle_{\alpha}^{*}
+ \frac{1}{2} \oint_{\partial B_{R_{\alpha}}(\mathbf{0})} \partial_{r_{\alpha}} \left(\varphi_{l'm',\lambda'}^{\alpha(0)} (\mathbf{r}_{\alpha}) \right)^{*} f(\mathbf{r}_{\alpha}) - \left(\varphi_{l'm',\lambda'}^{\alpha(0)} (\mathbf{r}_{\alpha}) \right)^{*} \partial_{r_{\alpha}} f(\mathbf{r}_{\alpha}) dS
= \left\langle f \middle| \hat{\mathcal{H}}_{0} - \epsilon_{ik}^{(0)} \middle| \varphi_{l'm',\lambda'}^{\alpha(0)} \right\rangle_{\alpha}^{*} + \frac{1}{2} \left[u_{l'}^{\alpha'} (R_{\alpha}) f_{l'm'} (R_{\alpha}) - u_{l'}^{\alpha} (R_{\alpha}) f_{l'm'}^{\prime} (R_{\alpha}) \right]. \tag{A.52}$$

The derivatives $\partial_{r_{\alpha}}$ are radial derivatives. Using the second term of this equation as correction, the muffin-tin integrals of the second bra-ket can be evaluated as the complex conjugates of the first bra-ket.

A.4.3. Third bra-ket

The third bra-ket decomposes into four terms. The term containing the response of the expansion coefficients both in the bra and in the ket has to be evaluated over the whole unit cell. The other terms are limited again to the muffin-tin sphere of atom α or β . For these terms, we expand the basis functions into spherical harmonics as before and contract the sums over G and G'. We obtain

$$2\left\langle \sum_{G} z_{k \pm q,G}^{ik(1)\beta \pm} \phi_{k \pm q,G}^{(0)} + \sum_{G} z_{k G}^{ik(0)} \phi_{k G}^{(1)\beta \pm} \middle| \hat{\mathcal{H}}_{0} - \epsilon_{ik}^{(0)} \middle| \\ \times \middle| \sum_{G} z_{k \pm q,G}^{ik(1)\alpha \pm^{T}} \phi_{k \pm q,G}^{(0)} + \sum_{G} z_{k G}^{ik(0)} \phi_{k G}^{(1)\alpha \pm^{T}} \middle\rangle \\ = 2\sum_{GG'} \left(z_{k \pm q,G'}^{ik(1)\beta \pm^{+}} \middle| \phi_{k \pm q,G'}^{(0)} \middle| \hat{\mathcal{H}}_{0} - \epsilon_{ik}^{(0)} \middle| \phi_{k \pm q,G}^{(0)} \middle\rangle z_{k \pm q,G}^{ik(1)\alpha \pm^{T}} \right. \\ + 2\sum_{GG'} \left(z_{k G'}^{ik(1)\beta \pm^{+}} \middle| \phi_{k \pm q,G'}^{(0)} \middle| \hat{\mathcal{H}}_{0} - \epsilon_{ik}^{(0)} \middle| \left[i(k+G)^{T} - \nabla^{T} \middle| \phi_{k G}^{(0)} \middle\rangle z_{k Eq,G}^{ik(0)} \right. \\ + 2\sum_{GG'} \left(z_{k G'}^{ik(0)} \middle| f(k+G') - \nabla \middle| \phi_{k G'}^{(0)} \middle| \hat{\mathcal{H}}_{0} - \epsilon_{ik}^{(0)} \middle| \phi_{k \pm q,G}^{(0)} \middle\rangle z_{k Eq,G}^{ik(1)\alpha \pm^{T}} \right. \\ + 2\delta_{\alpha\beta} \sum_{GG'} \left(z_{k G'}^{ik(0)} \middle| f(k+G') - \nabla \middle| \phi_{k G'}^{(0)} \middle| \hat{\mathcal{H}}_{0} - \epsilon_{ik}^{(0)} \middle| \phi_{k \pm q,G}^{(0)} \middle\rangle z_{k Eq,G}^{ik(1)\alpha \pm^{T}} \right. \\ + 2i\sum_{GG'} \left(z_{k Eq,G'}^{ik(1)\beta \pm^{+}} \middle| f(H_{G'G}(k \pm q) - \epsilon_{ik}^{(0)} S_{G'G}(k \pm q) \right) z_{k \pm q,G}^{ik(1)\alpha \pm^{T}} \\ + 2i\sum_{Im\lambda} \sum_{l'm'\lambda'} \left(A_{l'm'\lambda'\alpha}^{\beta ik \pm^{+}} \middle| k A_{lm\lambda}^{\alpha ik} + A_{lm\lambda}^{\alpha ik} \middle| f^{T} \middle| \phi_{l'm'\lambda'}^{\alpha(0)} \middle| \hat{\mathcal{H}}_{0} - \epsilon_{ik}^{(0)} \middle| \phi_{lm,\lambda}^{\alpha(0)} \middle\rangle z_{k Eq,G}^{ik(1)\alpha \pm^{T}} \right. \\ - 2\sum_{Im\lambda} \sum_{l'm'\lambda'} \left\{ \left(A_{l'm'\lambda'\alpha}^{\beta ik \pm^{+}} \middle| k A_{lm\lambda}^{\alpha ik} - i \delta_{\alpha\beta} \left[k A_{l'm'\lambda'}^{\beta ik} + A_{l'm'\lambda'}^{\beta ik} \middle| \hat{\mathcal{H}}_{0} - \epsilon_{ik}^{(0)} \middle| \phi_{lm,\lambda}^{\alpha(0)} \middle\rangle z_{k Eq,G}^{\alpha(0)} \right. \\ - 2\sum_{Im\lambda} \sum_{l'm'\lambda'} \left\{ k A_{l'm'\lambda'}^{\beta ik} + A_{l'm'\lambda'}^{\beta ik} \middle| k A_{l'm\lambda}^{\beta ik} \right| A_{lm\lambda\beta}^{\alpha ik \pm^{T}} \middle| f(\mu_{l'm'\lambda'}) \left[k A_{l'm\lambda}^{\beta ik} + A_{lm\lambda}^{\beta ik} \right]^{T} \right. \\ - 2\sum_{Im\lambda} \sum_{l'm'\lambda'} \left\{ k A_{l'm'\lambda'}^{\beta ik} + A_{l'm\lambda'\lambda'}^{\alpha ik} \right| f(\mu_{l'm'\lambda'}) \left[k A_{l'm\lambda}^{\beta ik} + A_{lm\lambda}^{\beta ik} \right]^{T} \right\} \\ + 2\delta_{\alpha\beta} \sum_{Im\lambda} \sum_{l'm'\lambda'} \left[k A_{l'm'\lambda'}^{\alpha ik} + A_{l'm\lambda'\lambda'}^{\alpha ik} \middle| k A_{lm\lambda}^{\alpha ik} \middle| k A_{lm\lambda}^{\alpha ik} \right]^{T} \\ + 2\delta_{\alpha\beta} \sum_{Im\lambda} \sum_{l'm'\lambda'} \left[A_{l'm'\lambda'}^{\alpha ik} + A_{l'm\lambda'\lambda'}^{\alpha ik} \middle| k A_{lm\lambda}^{\alpha ik} \middle| k$$

We already encountered every muffin-tin integral in this equation except for the last one. For this integral, we make use of the fact that $\varphi_{lm,\lambda}^{\alpha(0)}$ solves the spherical Schrödinger equation to avoid explicit application of the kinetic energy operator. Acting with $\nabla^{\rm T}$ onto the Schrödinger equation yields

$$\hat{\mathcal{H}}_{\mathrm{sph}}^{\alpha} \nabla^{\mathrm{T}} \varphi_{lm,\lambda}^{\alpha(0)}(\boldsymbol{r}_{\alpha}) = E_{l}^{\alpha} \nabla^{\mathrm{T}} \varphi_{lm,\lambda}^{\alpha(0)}(\boldsymbol{r}_{\alpha}) + \delta_{1\lambda} \nabla^{\mathrm{T}} \varphi_{lm,0}^{\alpha(0)}(\boldsymbol{r}_{\alpha}) - [\nabla^{\mathrm{T}} V_{\mathrm{sph}}^{\alpha}(\boldsymbol{r}_{\alpha})] \varphi_{lm,\lambda}^{\alpha(0)}(\boldsymbol{r}_{\alpha}). \tag{A.54}$$

Using this result in the muffin-tin integral containing the gradient in the bra and in the ket, it can be evaluated as

$$\begin{split} & \left\langle \nabla \varphi_{l'm',\lambda'}^{\alpha(0)} \right| \hat{\mathcal{H}}_{0} - \epsilon_{i\mathbf{k}}^{(0)} \left| \nabla^{\mathrm{T}} \varphi_{lm,\lambda}^{\alpha(0)} \right\rangle_{\alpha} \\ &= \left(E_{l}^{\alpha} - \epsilon_{i\mathbf{k}}^{(0)} \right) \left\langle \nabla \varphi_{l'm',\lambda'}^{\alpha(0)} \right| \nabla^{\mathrm{T}} \varphi_{lm,\lambda}^{\alpha(0)} \right\rangle_{\alpha} + \delta_{1\lambda} \left\langle \nabla \varphi_{l'm',\lambda'}^{\alpha(0)} \right| \nabla^{\mathrm{T}} \varphi_{lm,0}^{\alpha(0)} \right\rangle_{\alpha} \\ &+ \left\langle \nabla \varphi_{l'm',\lambda'}^{\alpha(0)} \right| V_{\mathrm{nonsph}}^{\alpha} \left| \nabla^{\mathrm{T}} \varphi_{lm,\lambda}^{\alpha(0)} \right\rangle_{\alpha} - \left\langle \nabla \varphi_{l'm',\lambda'}^{\alpha(0)} \right| \nabla^{\mathrm{T}} V_{\mathrm{sph}}^{\alpha} \left| \varphi_{lm,\lambda}^{\alpha(0)} \right\rangle_{\alpha}. \end{split} \tag{A.55}$$

The expressions appearing in this equation can be easily evaluated once the expansions of $\nabla V_{\rm sph}^{\alpha}(r_{\alpha})$ and $\nabla \varphi_{lm,\lambda}^{\alpha(0)}(r_{\alpha})$ in terms of spherical harmonics are known. If not already present, they can be constructed from Eq. (4.17), the application of the gradient in natural coordinates.

A.5. Nitty-gritties of $oldsymbol{D}^{\mathrm{SF}}(oldsymbol{q})$

We want to evaluate the integrals

$$\underline{\boldsymbol{I}}_{1} = \oint_{\partial \mathrm{MT}(\beta)} \hat{\boldsymbol{e}} \left[\psi_{i\boldsymbol{k}}^{(1)\alpha \mp *T} \left(\boldsymbol{r} \right) \left(\hat{\mathcal{H}}_{0} - \epsilon_{i\boldsymbol{k}}^{(0)} \right) \psi_{i\boldsymbol{k}}^{(0)} \left(\boldsymbol{r} \right) \right]_{\mathrm{SF}} dS, \tag{A.56}$$

$$\underline{\boldsymbol{I}}_{2} = \oint_{\partial \mathbf{MT}(\beta)} \hat{\boldsymbol{e}} \left[\psi_{i\boldsymbol{k}}^{(0)*}(\boldsymbol{r}) \left(\hat{\mathcal{H}}_{0} - \epsilon_{i\boldsymbol{k}}^{(0)} \right) \psi_{i\boldsymbol{k}}^{(1)\alpha \pm \mathrm{T}} (\boldsymbol{r}) \right]_{\mathrm{SF}} dS, \tag{A.57}$$

$$\underline{\boldsymbol{I}}_{3} = \oint_{\partial \mathbf{MT}(\beta)} \nabla \left[\psi_{ik}^{(0)*}(\boldsymbol{r}) \left(\hat{\mathcal{H}}_{0} - \epsilon_{ik}^{(0)} \right) \psi_{ik}^{(0)}(\boldsymbol{r}) \right]_{SF} \hat{\boldsymbol{e}}^{\mathrm{T}} dS. \tag{A.58}$$

The last integral occurred from the variation of a surface integral and is thus zero for $\beta \neq \alpha$. In chapter 7.3.3, we established that each IR quantity is processed as far as possible and is then Rayleigh expanded such that the IR and MT quantities can be treated in one formula (s. Eqs. (4.30) and (7.121)). Due to the differences in how the Hamiltonian acts on the LAPW basis functions in the IR and the MT spheres, the terms discussed in this section need to be evaluated separately in the IR and MT spheres.

Interstitial region

In the IR, the wave function variation decomposes to

$$\psi_{ik}^{(1)\alpha\pm}(r) = \sum_{\boldsymbol{G}} z_{k\pm\boldsymbol{q},\boldsymbol{G}}^{ik(1)\alpha\pm} \phi_{k\pm\boldsymbol{q},\boldsymbol{G}}^{(0)}(r). \tag{A.59}$$

Thus, In each of \underline{I}_1 , \underline{I}_2 , and \underline{I}_3 , the kinetic energy operator is applied either to the plane wave $\phi_{kG}^{(0)}(r)$ or $\phi_{k\pm q,G}^{(0)}(r)$ and produces factors $|k+G|^2/2$ or $|k\pm q+G|^2/2$ which have to be included in the G-contraction in the Rayleigh expansion. In \underline{I}_3 , the gradient acts once more on the basis function after the product rule is applied. Therefore, the factor to be included in the G-contraction is here $|k+G|^2(k+G)/2$. The potential (or the gradient thereof) also need to be Rayleigh expanded. Then the interstitial part of the integrals are

$$\underline{I}_{1}^{\text{IR}} = -\sum_{i=1}^{3} \hat{e}_{i} \sum_{t=-1}^{1} c_{i,t}
\times \left\{ \sum_{l'm'} \left[\psi_{ik}^{(1)\alpha\mp} \right]_{l'm',\beta}^{\text{IR}*} (R_{\beta}) \sum_{lm} \left[\left(-\frac{1}{2} \nabla^{2} - \epsilon_{ik}^{(0)} \right) \psi_{ik}^{(0)} \right]_{lm,\beta}^{\text{IR}} (R_{\beta}) G_{l',1,l}^{m',t,m}
+ \sum_{l'm'} \left[\psi_{ik}^{(1)\alpha\mp} \right]_{l'm',\beta}^{\text{IR}*} (R_{\beta}) \sum_{lm} \left[\left(-\frac{1}{2} \nabla^{2} - \epsilon_{ik}^{(0)} \right) \psi_{ik}^{(0)} \right]_{lm,\beta}^{\text{IR}} (R_{\beta})
\times \sum_{l'm''} \left[V_{\text{eff}}^{(0)} \right]_{l'm'',\beta}^{\text{IR}} (R_{\beta}) \sum_{s=|l''-1|} G_{s,1,l''}^{t+m'',t,m''} G_{l',s,l}^{m',t+m'',m} \right\}^{\text{T}}, \quad (A.60)$$

$$\underline{I}_{2}^{\text{IR}} = -\sum_{i=1}^{3} \hat{e}_{i} \sum_{t=-1}^{1} c_{i,t}
\times \left\{ \sum_{l'm'} \left[\psi_{ik}^{(0)} \right]_{l'm',\beta}^{\text{IR}*} (R_{\beta}) \sum_{lm} \left[\left(-\frac{1}{2} \nabla^{2} - \epsilon_{ik}^{(0)} \right) \psi_{ik}^{(1)\alpha\pm} \right]_{lm,\beta}^{\text{IR}} (R_{\beta}) G_{l',1,l}^{m',t,m} + \dots \right\} \right\}$$

$$\begin{split} \dots & + \sum_{l'm'} \left[\psi_{ik}^{(0)} \right]_{l'm',\beta}^{\text{IR*}} \left(R_{\beta} \right) \sum_{lm} \left[\left(-\frac{1}{2} \nabla^{2} - \epsilon_{ik}^{(0)} \right) \psi_{ik}^{(1)\alpha\pm} \right]_{lm,\beta}^{\text{IR}} \left(R_{\beta} \right) \\ & \times \sum_{l''m''} \left[V_{\text{eff}}^{(0)} \right]_{l''m'',\beta}^{\text{IR}} \left(R_{\beta} \right) \sum_{s=|l''-1|}^{l''+1,2} G_{s,1,l''}^{l+m'',t,m''} G_{l',s,l}^{m',t,t+m'',m} \right]^{\text{T}}, \quad \text{(A.61)} \\ & \times \left\{ \sum_{l'm'} \left[\nabla \psi_{ik}^{(0)} \right]_{l'm',\beta}^{\text{IR*}} \left(R_{\beta} \right) \sum_{lm} \left[\left(-\frac{1}{2} \nabla^{2} - \epsilon_{ik}^{(0)} \right) \psi_{ik}^{(0)} \right]_{lm,\beta}^{\text{IR}} \left(R_{\beta} \right) G_{l',1,l}^{m',t,m} \\ & + \sum_{l'm'} \left[\nabla \psi_{ik}^{(0)} \right]_{l'm',\beta}^{\text{IR*}} \left(R_{\beta} \right) \sum_{lm} \left[\left(-\frac{1}{2} \nabla^{2} - \epsilon_{ik}^{(0)} \right) \psi_{ik}^{(0)} \right]_{lm,\beta}^{\text{IR}} \left(R_{\beta} \right) \\ & \times \sum_{l''m''} \left[V_{\text{eff}}^{(0)} \right]_{l'm'',\beta}^{\text{IR*}} \left(R_{\beta} \right) \sum_{s=|l''-1|}^{l''+1,2} G_{s,1,l''}^{t+m'',t,m''} G_{l',s,l}^{m',t,t+m'',m} \\ & + \sum_{l'm'} \left[\psi_{ik}^{(0)} \right]_{l'm',\beta}^{\text{IR*}} \left(R_{\beta} \right) \sum_{lm} \left[\left(-\frac{1}{2} \nabla^{2} - \epsilon_{ik}^{(0)} \right) \nabla \psi_{ik}^{(0)} \right]_{lm,\beta}^{\text{IR}} \left(R_{\beta} \right) G_{l',1,l}^{m',t,m} \\ & + \sum_{l'm''} \left[\psi_{ik}^{(0)} \right]_{l'm',\beta}^{\text{IR*}} \left(R_{\beta} \right) \sum_{lm} \left[\left(-\frac{1}{2} \nabla^{2} - \epsilon_{ik}^{(0)} \right) \nabla \psi_{ik}^{(0)} \right]_{lm,\beta}^{\text{IR}} \left(R_{\beta} \right) \\ & \times \sum_{l''m''} \left[V_{\text{eff}}^{(0)} \right]_{l''m'',\beta}^{\text{IR*}} \left(R_{\beta} \right) \sum_{s=|l''-1|}^{l''+1,2} G_{s,1,l''}^{t+m'',t,m''} G_{l',s,l}^{m',t,t+m'',m} \\ & + \sum_{l'm''} \left[\psi_{ik}^{(0)} \right]_{l'm',\beta}^{\text{IR*}} \left(R_{\beta} \right) \sum_{lm} \left[\psi_{ik}^{(0)} \right]_{lm,\beta}^{\text{IR}} \left(R_{\beta} \right) \\ & \times \sum_{l''m''} \left[\nabla V_{\text{eff}}^{(0)} \right]_{l''m'',\beta}^{\text{IR}} \left(R_{\beta} \right) \sum_{s=|l''-1|}^{l''+1,2} G_{s,1,l''}^{t+m'',t,m''} G_{l',s,l}^{m',t,t+m'',m} \right\} \hat{e}_{l}^{\text{T}} \end{aligned}$$

Whenever the potential is involved, we first evaluated the product of its spherical harmonic $Y_{l''m''}(r_{\beta})$ with the spherical harmonic of the unit vector $\hat{\boldsymbol{e}}$, $Y_{1t}(r_{\beta})$.

Muffin-tins

Only in the case $\beta = \alpha$, the MT representation of the wave function response is complemented by the variation of the basis function,

$$\psi_{ik}^{(1)\alpha\pm}(\mathbf{r}) = \sum_{\mathbf{C}} z_{k\pm\mathbf{q},\mathbf{G}}^{ik(1)\alpha\pm} \phi_{k\pm\mathbf{q},\mathbf{G}}^{(0)}(\mathbf{r}) + \Theta(\mathbf{r} \in \mathrm{MT}(\alpha)) \sum_{\mathbf{C}} z_{k\mathbf{G}}^{ik(0)} \phi_{k\mathbf{G}}^{(1)\alpha\pm}(\mathbf{r}). \tag{A.63}$$

A.5. Nitty-gritties of
$$\mathbf{D}^{SF}(\mathbf{q})$$

Therefore, we will evaluate the MT components of \underline{I}_1 , \underline{I}_2 , and \underline{I}_3 for $\beta \neq \alpha$ first and complement the result in the case $\beta = \alpha$ afterwards. However, \underline{I}_3 is zero for $\beta \neq \alpha$, so we only need to find expressions for the first two integrals for now. They are given by

$$\underline{I}_{1}^{\text{MT}} = \sum_{i=1}^{3} \hat{e}_{i} \sum_{t=-1}^{1} c_{i,t} \sum_{lm\lambda \, l'm'\lambda'} \\
\times \left\{ A_{l'm'\lambda'\beta}^{\alpha ik \mp *} A_{lm\lambda}^{\beta ik} (E_{l}^{\beta} - \epsilon_{ik}^{(0)}) u_{l\lambda'}^{\beta} (R_{\beta}) u_{l\lambda}^{\beta} (R_{\beta}) G_{l',1,l}^{m',t,m} \\
+ \delta_{\lambda 1} A_{l'm'\lambda'\beta}^{\alpha ik \mp *} A_{lm1}^{\beta ik} u_{l'\lambda'}^{\beta} (R_{\beta}) u_{l0}^{\beta} (R_{\beta}) G_{l',1,l}^{m',t,m} \\
+ A_{l'm'\lambda'\beta}^{\alpha ik \mp *} A_{lm\lambda}^{\beta ik} u_{l'\lambda'}^{\beta} (R_{\beta}) u_{l\lambda}^{\beta} (R_{\beta}) \\
\times \sum_{l'' > 0,m''} V_{\text{eff},l''m''}^{\beta(0)} (R_{\beta}) \sum_{s=|l''-1|}^{l''+1,2} G_{s,1,l''}^{t+m'',t,m''} G_{l',s,l}^{m',t+m'',m} \right\}^{T}, \quad (A.64)$$

$$\underline{I}_{2}^{\text{MT}} = \sum_{i=1}^{3} \hat{e}_{i} \sum_{t=-1}^{1} c_{i,t} \sum_{lm\lambda \, l'm'\lambda'} \\
\times \left\{ A_{l'm'\lambda'}^{\beta ik *} A_{lm\lambda\beta}^{\alpha ik \pm} (E_{l}^{\beta} - \epsilon_{ik}^{(0)}) u_{l\lambda'}^{\beta} (R_{\beta}) u_{l\lambda}^{\beta} (R_{\beta}) G_{l',1,l}^{m',t,m} \\
+ \delta_{\lambda 1} A_{l'm'\lambda'}^{\beta ik *} A_{lm\lambda\beta}^{\alpha ik \pm} u_{l'\lambda'}^{\beta} (R_{\beta}) u_{l\lambda}^{\beta} (R_{\beta}) G_{l',1,l}^{m',t,m} \\
+ A_{l'm'\lambda'}^{\beta ik *} A_{lm\lambda\beta}^{\alpha ik \pm} u_{l'\lambda'}^{\beta} (R_{\beta}) u_{l\lambda}^{\beta} (R_{\beta}) \\
\times \sum_{l'' > 0,m''} V_{\text{eff},l''m''}^{\beta(0)} (R_{\beta}) \sum_{s=|l''-1|}^{l''+1,2} G_{s,1,l''}^{t+m'',t,m''} G_{l',s,l}^{m',t+m'',m} \right\}^{T}. \quad (A.65)$$

Both integrals can be combined easily, since they only deviate in the order of perturbed and unperturbed expansion coefficients.

We continue by considering the special case $\beta=\alpha$, where the variation of the wave function also involves the change in the basis functions. In the MT sphere of atom α of the representative unit cell, the variation of the basis functions is given by

$$\phi_{\mathbf{k}\mathbf{G}}^{(1)\alpha\pm}(\mathbf{r}) = [i(\mathbf{k} + \mathbf{G}) - \nabla]\phi_{\mathbf{k}\mathbf{G}}^{(0)}(\mathbf{r}). \tag{A.66}$$

In the MT representation, the first part is simple to evaluate, since the $i(\pmb{k} + \pmb{G})$ factor can be combined with the matching coefficients and only the radial basis functions remain to be considered. For this component of the basis function response, the integrals $\underline{\pmb{I}}_1$ and $\underline{\pmb{I}}_2$ become

$$\begin{split} \underline{\boldsymbol{I}}_{1,\boldsymbol{k}+\boldsymbol{G}}^{\mathrm{MT}(\alpha)} &= -i\sum_{i=1}^{3} \hat{\boldsymbol{e}}_{i} \sum_{t=-1}^{1} c_{i,t} \sum_{lm\lambda\; l'm'\lambda'} \\ &\times \left\{ \left[\boldsymbol{k} A_{l'm'\lambda'}^{\alpha i \boldsymbol{k}} + \boldsymbol{A}_{l'm'\lambda'}^{\alpha i \boldsymbol{k}} \right]^{*} A_{lm\lambda}^{\alpha i \boldsymbol{k}} (E_{l}^{\alpha} - \epsilon_{i \boldsymbol{k}}^{(0)}) u_{l'\lambda'}^{\alpha} (R_{\alpha}) u_{l\lambda}^{\alpha} (R_{\alpha}) G_{l',1,l}^{m',t,m} \right. \\ &+ \delta_{\lambda 1} \left[\boldsymbol{k} A_{l'm'\lambda'}^{\alpha i \boldsymbol{k}} + \boldsymbol{A}_{l'm'\lambda'}^{\alpha i \boldsymbol{k}} \right]^{*} A_{lm1}^{\alpha i \boldsymbol{k}} u_{l'\lambda'}^{\alpha} (R_{\alpha}) u_{l0}^{\alpha} (R_{\alpha}) G_{l',1,l}^{m',t,m} + \dots \end{split}$$

$$\dots + \left[k A_{l'm'\lambda'}^{\alpha i k} + A_{l'm'\lambda'}^{\alpha i k} \right]^{*} A_{lm\lambda}^{\alpha i k} u_{l'\lambda'}^{\alpha}(R_{\alpha}) u_{l\lambda}^{\alpha}(R_{\alpha}) \\
\times \sum_{l''>0,m''} V_{\text{eff},l''m''}^{\alpha(0)}(R_{\alpha}) \sum_{s=|l''-1|}^{l''+1,2} G_{s,1,l''}^{t+m'',t,m''} G_{l',s,l}^{m',t+m'',m} \right]^{T}, (A.67)$$

$$\underline{I}_{2,k+G}^{\text{MT}(\alpha)} = i \sum_{i=1}^{3} \hat{e}_{i} \sum_{t=-1}^{1} c_{i,t} \sum_{lm\lambda} \sum_{l'm'\lambda'} \\
\times \left\{ A_{l'm'\lambda'}^{\alpha i k} \left[k A_{lm\lambda}^{\alpha i k} + A_{lm\lambda}^{\alpha i k} \right] (E_{l}^{\alpha} - \epsilon_{ik}^{(0)}) u_{l'\lambda'}^{\alpha}(R_{\alpha}) u_{l\lambda}^{\alpha}(R_{\alpha}) G_{l',1,l}^{m',t,m} \\
+ \delta_{\lambda 1} A_{l'm'\lambda'}^{\alpha i k} \left[k A_{lm\lambda}^{\alpha i k} + A_{lm\lambda}^{\alpha i k} \right] u_{l'\lambda'}^{\alpha}(R_{\alpha}) u_{l0}^{\alpha}(R_{\alpha}) G_{l',1,l}^{m',t,m} \\
+ A_{l'm'\lambda'}^{\alpha i k} \left[k A_{lm\lambda}^{\alpha i k} + A_{lm\lambda}^{\alpha i k} \right] u_{l'\lambda'}^{\alpha}(R_{\alpha}) u_{l\lambda}^{\alpha}(R_{\alpha}) \\
\times \sum_{l''>0,m''} V_{\text{eff},l''m''}^{\alpha(0)}(R_{\alpha}) \sum_{s=|l''-1|}^{l''+1,2} G_{s,1,l''}^{t+m'',t,m''} G_{l',s,l}^{m',t+m'',m} \right]^{T}. (A.68)$$

For \underline{I}_1 and \underline{I}_2 , only the MT contributions containing the gradient of the basis functions remain to be calculated. By the product rule of differentiation, such terms also appear for \underline{I}_3 . Application of the gradient in natural coordinates (Eq. (4.17)) to $\varphi_{lm\lambda}^{\beta(0)}(r_\beta)$, shifts the angular momentum l by one and the magnetic momentum m by at most one. We will denote the shift in l by p and the shift in m by q in the following. Then, the last component of the MT part of \underline{I}_1 can be expressed by

$$\underline{I}_{1,\nabla}^{MT(\alpha)} = -\sum_{i=1}^{3} \hat{e}_{i} \sum_{t=-1}^{1} c_{i,t} \sum_{lm\lambda} \sum_{l'm'\lambda'} \sum_{p=-1}^{1,2} \sum_{q=-1}^{1} \times \left\{ A_{l'm'\lambda'}^{\alpha ik*} A_{lm\lambda}^{\alpha ik} (E_{l}^{\alpha} - \epsilon_{ik}^{(0)}) \left[\nabla \varphi_{l'm'\lambda'}^{\alpha(0)} \right]_{l'+p,m'+q}^{*} (R_{\alpha}) u_{l\lambda}^{\alpha} (R_{\alpha}) G_{l'+p,1,l}^{m'+q,t,m} + \delta_{\lambda 1} A_{l'm'\lambda'}^{\alpha ik*} A_{lm1}^{\alpha ik} \left[\nabla \varphi_{l'm'\lambda'}^{\alpha(0)} \right]_{l'+p,m'+q}^{*} (R_{\alpha}) u_{l0}^{\alpha} (R_{\alpha}) G_{l'+p,1,l}^{m'+q,t,m} + A_{l'm'\lambda'}^{\alpha ik*} A_{lm\lambda}^{\alpha ik} \left[\nabla \varphi_{l'm'\lambda'}^{\alpha(0)} \right]_{l'+p,m'+q}^{*} (R_{\alpha}) u_{l\lambda}^{\alpha} (R_{\alpha}) \times \sum_{l''>0,m''} V_{\text{eff},l''m''}^{\alpha(0)} (R_{\alpha}) \sum_{s=ll''-1}^{l''+1,2} C_{s,1,l''}^{t+m'',t,m''} C_{l'+p,s,l}^{m'+q,t+m'',m} \right\}^{T}. (A.69)$$

The evaluation of the equivalent expression in \underline{I}_2 contains the application of the spherical Hamiltonian $\hat{\mathcal{H}}_{\rm sph}^{\alpha}$ to the gradient of the basis function $\nabla \varphi_{lm\lambda}^{\alpha(0)}(\boldsymbol{r})$. Eq. (A.54) supplies the corresponding result. We obtain

$$\underline{\boldsymbol{I}}_{2,\nabla}^{\mathrm{MT}(\alpha)} = -\sum_{i=1}^{3} \hat{\boldsymbol{e}}_{i} \sum_{t=-1}^{1} c_{i,t} \sum_{lm\lambda} \sum_{l'm'\lambda'} \sum_{p=-1}^{1,2} \sum_{q=-1}^{1} \times \left\{ A_{l'm'\lambda'}^{\alpha i \boldsymbol{k}*} A_{lm\lambda}^{\alpha i \boldsymbol{k}} (E_{l}^{\alpha} - \epsilon_{i \boldsymbol{k}}^{(0)}) u_{l'\lambda'}^{\alpha} (R_{\alpha}) \left[\nabla \varphi_{lm\lambda}^{\alpha(0)} \right]_{l+p,m+q} (R_{\alpha}) G_{l',1,l+p}^{m',t,m+q} \right\}$$

A.5. Nitty-gritties of
$$\mathbf{D}^{\mathrm{SF}}(\mathbf{q})$$

$$+ \delta_{\lambda 1} A_{l'm'\lambda'}^{\alpha i k *} A_{lm1}^{\alpha i k} u_{l'\lambda'}^{\alpha}(R_{\alpha}) \left[\nabla \varphi_{lm0}^{\alpha(0)} \right]_{l+p,m+q} (R_{\alpha}) G_{l',1,l+p}^{m',t,m+q}$$

$$+ A_{l'm'\lambda'}^{\alpha i k *} A_{lm\lambda}^{\alpha i k} u_{l'\lambda'}^{\alpha}(R_{\alpha}) \left[\nabla \varphi_{lm\lambda}^{\alpha(0)} \right]_{l+p,m+q} (R_{\alpha})$$

$$\times \sum_{l''>0,m''} V_{\text{eff},l''m''}^{\alpha(0)}(R_{\alpha}) \sum_{s=|l''-1|}^{l''+1,2} G_{s,1,l''}^{t+m'',t,m''} G_{l',s,l+p}^{m',t+m'',m+q}$$

$$- A_{l'm'\lambda'}^{\alpha i k *} A_{lm\lambda}^{\alpha i k} u_{l'\lambda'}^{\alpha}(R_{\alpha}) u_{l\lambda}^{\alpha}(R_{\alpha})$$

$$\times \delta_{p1} \left[\nabla V_{\text{eff},00}^{\alpha(0)} \right]_{pq} (R_{\alpha}) \sum_{s=0}^{2,2} G_{s,1,p}^{t+q,t,q} G_{l',s,l}^{m',t+q,m} \right]^{T}. \tag{A.70}$$

In \underline{I}_3 , the gradients of the basis functions appear transposed and with a different sign. In addition, the product rule of differentiation generates a term involving the gradient of the potential, which also has to be added:

$$\underline{I}_{3}^{\text{MT}(\alpha)} = -\underline{I}_{1,\nabla}^{\text{MT}(\alpha)}{}^{\text{T}} - \underline{I}_{2,\nabla}^{\text{MT}(\alpha)}{}^{\text{T}} + \sum_{i=1}^{3} \sum_{t=-1}^{1} c_{i,t} \sum_{lm\lambda} \sum_{l'm'\lambda'} u_{l'\lambda'}^{\alpha}(R_{\alpha}) u_{l\lambda}^{\alpha}(R_{\alpha})$$

$$\times \sum_{l''>0,m''} \sum_{p=-1}^{1,2} \sum_{q=-1}^{1} \left[\nabla V_{\text{eff},l''m''}^{\alpha(0)} \right]_{l''+p,m''+q} (R_{\alpha}) \hat{e}_{i}^{\text{T}}$$

$$\times \sum_{s=|l''+p-1|} G_{s,1,l''+p}^{m''+q+t,t,m''+q} G_{l',s,l}^{m',m''+q+t,m} \qquad (A.71)$$

We note that \underline{I}_1 and \underline{I}_2 appear with a factor of 2 in Eq. (7.119). Therefore, there is no complete cancellation between the gradient terms in them and in \underline{I}_3 .

Now, all terms for the evaluation of the surface integrals $\underline{I}_1, \underline{I}_2$, and \underline{I}_3 are known. They are composed of

$$\underline{\boldsymbol{I}}_{1} = \underline{\boldsymbol{I}}_{1}^{\mathrm{IR}} + \underline{\boldsymbol{I}}_{1}^{\mathrm{MT}} + \underline{\boldsymbol{I}}_{1,\boldsymbol{k}+\boldsymbol{G}}^{\mathrm{MT}(\alpha)} + \underline{\boldsymbol{I}}_{1,\nabla}^{\mathrm{MT}(\alpha)}, \tag{A.72}$$

$$\underline{I}_{2} = \underline{I}_{2}^{\text{IR}} + \underline{I}_{2}^{\text{MT}} + \underline{I}_{2,k+G}^{\text{MT}(\alpha)} + \underline{I}_{2,\nabla}^{\text{MT}(\alpha)}, \tag{A.73}$$

and

$$\underline{I}_{3} = \underline{I}_{3}^{IR} + \underline{I}_{3}^{MT(\alpha)}. \tag{A.74}$$

Bibliography

- Y. Yamada and G. Shirane. Neutron Scattering and Nature of the Soft Optical Phonon in SrTiO₃. Journal of the Physical Society of Japan, 26(2):396–403, 1969.
- [2] J. D. Axe and G. Shirane. Inelastic-Neutron-Scattering Study of Acoustic Phonons in Nb₃Sn. Phys. Rev. B, 8:1965–1977, Sep 1973.
- [3] N. Pyka, W. Reichardt, L. Pintschovius, G. Engel, J. Rossat-Mignod, and J. Y. Henry. Superconductivity-induced phonon softening in YBa₂Cu₃O₇ observed by inelastic neutron scattering. *Phys. Rev. Lett.*, 70:1457–1460, Mar 1993.
- [4] J. A. Kash, J. C. Tsang, and J. M. Hvam. Subpicosecond Time-Resolved Raman Spectroscopy of LO Phonons in GaAs. Phys. Rev. Lett., 54:2151–2154, May 1985.
- [5] D. S. Knight and W. B. White. Characterization of diamond films by Raman spectroscopy. *Journal of Materials Research*, 4:385–393, 1989.
- [6] L.M. Malard, M.A. Pimenta, G. Dresselhaus, and M.S. Dresselhaus. Raman spectroscopy in graphene. *Physics Reports*, 473(5-6):51 87, 2009.
- [7] E. S. Koteles, W. R. Datars, and G. Dolling. Far-infrared phonon absorption in InSb. Phys. Rev. B, 9:572–582, Jan 1974.
- [8] C. D. Clark and S. T. Davey. One-phonon infrared absorption in diamond. *Journal of Physics C: Solid State Physics*, 17(6):1127, 1984.
- [9] M. M. Pradhan, R. K. Garg, and M. Arora. Multiphonon infrared absorption in silicon. *Infrared Physics*, 27(1):25 – 30, 1987.
- [10] B. Dorner, E. Burkel, Th. Illini, and J. Peisl. First measurement of a phonon dispersion curve by inelastic X-ray scattering. Zeitschrift für Physik B Condensed Matter, 69(2-3):179–183, 1987.
- [11] J. Serrano, A. Bosak, R. Arenal, M. Krisch, K. Watanabe, T. Taniguchi, H. Kanda, A. Rubio, and L. Wirtz. Vibrational Properties of Hexagonal Boron Nitride: Inelastic X-Ray Scattering and Ab Initio Calculations. Phys. Rev. Lett., 98:095503, Mar 2007.
- [12] M. Mohr, J. Maultzsch, E. Dobardžić, S. Reich, I. Milošević, M. Damnjanović, A. Bosak, M. Krisch, and C. Thomsen. Phonon dispersion of graphite by inelastic x-ray scattering. *Phys. Rev. B*, 76:035439, Jul 2007.
- [13] P. A. Thiry, A. Degbomont, J. J. Pireaux, R. Caudano, J. R. Naegele, J. Rebizant, and J. C. Spirlet. The surface phonon structure of UO₂ single crystals investigated by high resolution electron energy loss spectroscopy. *Journal of the Less Common Metals*, 122:31 33, 1986. Proceedings of Actinides 85 Part 2.

- [14] W. Gao, Y. Fujikawa, K. Saiki, and A. Koma. Surface phonons of LiBr/Si(100) epitaxial layers by high resolution electron energy loss spectroscopy. Solid State Communications, 87(11):1013 1015, 1993.
- [15] K. L. Kostov, S. Polzin, S. K. Saha, O. Brovko, V. Stepanyuk, and W. Widdra. Surface-phonon dispersion of a NiO(100) thin film. *Phys. Rev. B*, 87:235416, Jun 2013.
- [16] M. Born and K. Huang. Dynamical Theory of Crystal Lattices. Clarendon press, Oxford, 1954.
- [17] M. Born and R. Oppenheimer. Zur Quantentheorie der Molekeln. Annalen der Physik, 389(20):457–484, 1927.
- [18] V. Fock. Näherungsmethode zur Lösung des quantenmechanischen Mehrkörperproblems. Zeitschrift für Physik, 61(1-2):126–148, 1930.
- [19] I. Shavitt. The history and evolution of configuration interaction. Molecular Physics, 94(1):3–17, 1998.
- [20] J. Čížek. On the Correlation Problem in Atomic and Molecular Systems. Calculation of Wavefunction Components in Ursell-Type Expansion Using Quantum-Field Theoretical Methods. The Journal of Chemical Physics, 45(11):4256–4266, 1966.
- [21] P. Hohenberg and W. Kohn. Inhomogeneous Electron Gas. Phys. Rev., 136:B864–B871, Nov 1964.
- [22] W. Kohn and L. J. Sham. Self-Consistent Equations Including Exchange and Correlation Effects. Phys. Rev., 140:A1133–A1138, Nov 1965.
- [23] L. H. Thomas. The calculation of atomic fields. Proceedings of the Cambridge Philosophical Society, 23:542, 1927.
- [24] E. Fermi. Un metodo statistico per la determinazione di alcune priorieta dell'atome. Rend. Accad. Naz. Lincei, 6(602-607):32, 1927.
- [25] H. Wendel and R. M. Martin. Theory of structural properties of covalent semiconductors. Phys. Rev. B, 19:5251–5264, May 1979.
- [26] M. T. Yin and M. L. Cohen. Microscopic Theory of the Phase Transformation and Lattice Dynamics of Si. Phys. Rev. Lett., 45:1004–1007, Sep 1980.
- [27] M. T. Yin and M. L. Cohen. Theory of lattice-dynamical properties of solids: Application to Si and Ge. Phys. Rev. B, 26:3259–3272, Sep 1982.
- [28] K. Kunc and R. M. Martin. Density-functional calculation of static and dynamic properties of GaAs. Phys. Rev. B, 24:2311–2314, Aug 1981.
- [29] R. Biswas, R. M. Martin, R. J. Needs, and O. H. Nielsen. Stability and electronic properties of complex structures of silicon and carbon under pressure: Density-functional calculations. *Phys. Rev. B*, 35:9559–9568, Jun 1987.
- [30] X. Zhao and D. Vanderbilt. Phonons and lattice dielectric properties of zirconia. Phys. Rev. B, 65:075105, Jan 2002.

- [31] K. Parlinski, Z. Q. Li, and Y. Kawazoe. First-Principles Determination of the Soft Mode in Cubic ZrO₂. Phys. Rev. Lett., 78:4063–4066, May 1997.
- [32] X. Gonze, J.-M. Beuken, R. Caracas, F. Detraux, M. Fuchs, G.-M. Rignanese, L. Sindic, M. Verstraete, G. Zerah, F. Jollet, M. Torrent, A. Roy, M. Mikami, Ph. Ghosez, J.-Y. Raty, and D.C. Allan. First-principles computation of material properties: the ABINIT software project. *Computational Materials Science*, 25(3):478 – 492, 2002.
- [33] M. Verstraete. DFPT tutorial. In 45th IFF Spring School, 2014.
- [34] S. Y. Savrasov. Linear-response theory and lattice dynamics: A muffin-tin-orbital approach. Phys. Rev. B, 54:16470–16486, Dec 1996.
- [35] S. Baroni, P. Giannozzi, and A. Testa. Green's-function approach to linear response in solids. Phys. Rev. Lett., 58:1861–1864, May 1987.
- [36] S. Baroni, S. de Gironcoli, A. Dal Corso, and P. Giannozzi. Phonons and related crystal properties from density-functional perturbation theory. Rev. Mod. Phys., 73:515–562, Jul 2001.
- [37] R. M. Sternheimer. Electronic Polarizabilities of Ions from the Hartree-Fock Wave Functions. Phys. Rev., 96:951–968, Nov 1954.
- [38] R. M. Sternheimer. Electronic Polarizabilities of Ions. Phys. Rev., 107:1565–1569, Sep 1957
- [39] R. M. Sternheimer. Electronic Polarizabilities of Ions. Phys. Rev., 115:1198–1206, Sep 1959
- [40] R. M. Sternheimer. Electronic Polarizabilities of the Alkali Atoms. II. Phys. Rev., 183:112–122, Jul 1969.
- [41] P. Giannozzi, S. Baroni, N. Bonini, M. Calandra, R. Car, C. Cavazzoni, D. Ceresoli, G. L. Chiarotti, M. Cococcioni, I. Dabo, A. Dal Corso, S. de Gironcoli, S. Fabris, G. Fratesi, R. Gebauer, U. Gerstmann, C. Gougoussis, A. Kokalj, M. Lazzeri, L. Martin-Samos, N. Marzari, F. Mauri, R. Mazzarello, S. Paolini, A. Pasquarello, L. Paulatto, C. Sbraccia, S. Scandolo, G. Sclauzero, A. P. Seitsonen, A. Smogunov, P. Umari, and R. M. Wentzcovitch. QUANTUM ESPRESSO: a modular and open-source software project for quantum simulations of materials. Journal of Physics Condensed Matter, 21:5502, September 2009.
- [42] E. Wimmer, H. Krakauer, M. Weinert, and A. J. Freeman. Full-potential self-consistent linearized-augmented-plane-wave method for calculating the electronic structure of molecules and surfaces: O₂ molecule. *Phys. Rev. B*, 24:864–875, Jul 1981.
- [43] M. Weinert, E. Wimmer, and A. J. Freeman. Total-energy all-electron density functional method for bulk solids and surfaces. Phys. Rev. B, 26(8):4571–4578, Oct 1982.
- [44] H. J. F. Jansen and A. J. Freeman. Total-energy full-potential linearized augmentedplane-wave method for bulk solids: Electronic and structural properties of tungsten. *Phys. Rev. B*, 30:561–569, Jul 1984.

Bibliography

- [45] D. J. Singh and L. Nordström. Planewaves, Pseudopotentials, and the LAPW Method. Springer, 2nd edition edition, 2005.
- [46] R. Yu and H. Krakauer. Linear-response calculations within the linearized augmented plane-wave method. Phys. Rev. B, 49:4467–4477, Feb 1994.
- [47] C.-Z. Wang, R. Yu, and H. Krakauer. First principles linear response calculations of lattice dynamics for CuCl. Phys. Rev. Lett., 72:368–371, Jan 1994.
- [48] R. Yu and H. Krakauer. First-Principles Determination of Chain-Structure Instability in KNbO₃. Phys. Rev. Lett., 74:4067–4070, May 1995.
- [49] C.-Z. Wang, R. Yu, and H. Krakauer. Pressure dependence of Born effective charges, dielectric constant, and lattice dynamics in SiC. Phys. Rev. B, 53:5430–5437, Mar 1996
- [50] R. Kouba, A. Taga, C. Ambrosch-Draxl, L. Nordström, and B. Johansson. Phonons and electron-phonon interaction by linear-response theory within the LAPW method. *Phys. Rev. B*, 64:184306, Oct 2001.
- [51] J. H. Lee. First-principles Linear Response All-electron FLAPW Study of Lattice Dynamics/phonons and the Effect of Magnetism. Northwesterns University, 2005.
- [52] J. M. Soler and A. R. Williams. Simple formula for the atomic forces in the augmented-plane-wave method. *Phys. Rev. B*, 40(3):1560–1564, Jul 1989.
- [53] J. M. Soler and A. R. Williams. Augmented-plane-wave forces. Phys. Rev. B, 42:9728–9731. Nov 1990.
- [54] R. Yu, D. Singh, and H. Krakauer. All-electron and pseudopotential force calculations using the linearized-augmented-plane-wave method. *Phys. Rev. B*, 43:6411–6422, Mar 1991.
- [55] P. Pulay. Ab initio calculation of force constants and equilibrium geometries in polyatomic molecules. *Molecular Physics*, 17(2):197–204, 1969.
- [56] B. Kohler, S. Wilke, M. Scheffler, R. Kouba, and C. Ambrosch-Draxl. Force calculation and atomic-structure optimization for the full-potential linearized augmented planewave code WIEN. Computer Physics Communications, 94(1):31 – 48, 1996.
- [57] http://www.flapw.de, Jul 2015.
- [58] D. Alfè. Phon: A program to calculate phonons using the small displacement method. Computer Physics Communications, 180(12):2622 – 2633, 2009.
- [59] O. K. Andersen. Linear methods in band theory. Phys. Rev. B, 12(8):3060–3083, Oct 1975.
- [60] H. L. Skriver. The LMTO method. Springer, 1983.
- [61] M. Methfessel, M. van Schilfgaarde, and R.A. Casali. Electronic Structure and Physical Properties of Solids: The Uses of the LMTO Method, chapter A Full-Potential LMTO Method Based on Smooth Hankel Functions, pages 114–147. Springer, 2000.

- [62] M. Weinert. Solution of Poisson's equation: Beyond Ewald-type methods. *Journal of Mathematical Physics*, 22:2433–2439, 1981.
- [63] D. A. Klüppelberg, M. Betzinger, and S. Blügel. Atomic force calculations within the all-electron FLAPW method: Treatment of core states and discontinuities at the muffin-tin sphere boundary. *Phys. Rev. B*, 91:035105, Jan 2015.
- [64] P. A. M. Dirac. Quantum Mechanics of Many-Electron Systems. Proc. R. Soc. Lond. A, 123:714–733, 1929.
- [65] T. Kato. On the eigenfunctions of many-particle systems in quantum mechanics. Communications on Pure and Applied Mathematics, 10(2):151–177, 1957.
- [66] J. Korringa. On the calculation of the energy of a Bloch wave in a metal. Physica, 13(6-7):392-400, 1947.
- [67] W. Kohn and N. Rostoker. Solution of the Schrödinger Equation in Periodic Lattices with an Application to Metallic Lithium. Phys. Rev., 94:1111–1120, Jun 1954.
- [68] N. Papanikolaou, R. Zeller, and P. H. Dederichs. Conceptual improvements of the KKR method. *Journal of Physics: Condensed Matter*, 14(11):2799, 2002.
- [69] D. Hsieh, Y. Xia, L. Wray, D. Qian, A. Pal, J. H. Dil, J. Osterwalder, F. Meier, G. Bihlmayer, C. L. Kane, Y. S. Hor, R. J. Cava, and M. Z. Hasan. Observation of unconventional quantum spin textures in topological insulators. *Science*, 323(5916):919–922, 2009.
- [70] H. Zhang and S.-C. Zhang. Topological insulators from the perspective of first-principles calculations. physica status solidi (RRL) Rapid Research Letters, 7(1-2):72-81, 2013.
- [71] R. Q. Hood, M. Y. Chou, A. J. Williamson, G. Rajagopal, and R. J. Needs. Exchange and correlation in silicon. *Phys. Rev. B*, 57:8972–8982, Apr 1998.
- [72] U. von Barth and L. Hedin. A local exchange-correlation potential for the spin polarized case. J. Phys. C: Solid State Phys., 5:1629–1642, 1972.
- [73] D. M. Ceperley and B. J. Alder. Ground State of the Electron Gas by a Stochastic Method. Phys. Rev. Lett., 45:566–569, Aug 1980.
- [74] S. H. Vosko, L. Wilk, and M. Nusair. Accurate spin-dependent electron liquid correlation energies for local spin density calculations: a critical analysis. *Canadian Journal of Physics*, 58(8):1200–1211, 1980.
- [75] J. P. Perdew and A. Zunger. Self-interaction correction to density-functional approximations for many-electron systems. *Phys. Rev. B*, 23:5048–5079, May 1981.
- [76] L. A. Cole and J. P. Perdew. Calculated electron affinities of the elements. Phys. Rev. A, 25:1265–1271, 1982.
- [77] J. P. Perdew and Y. Wang. Accurate and simple analytic representation of the electrongas correlation energy. *Phys. Rev. B*, 45:13244–13249, 1992.

- [78] J. P. Perdew and K. Schmidt. Jacob's ladder of density functional approximations for the exchange-correlation energy. AIP Conference Proceedings, 577(1):1–20, 2001.
- [79] J. P. Perdew and Y. Wang. Accurate and simple density functional for the electronic exchange energy: Generalized gradient approximation. *Phys. Rev. B*, 33:8800–8802, 1986.
- [80] Y. Wang and J. P. Perdew. Spin scaling of the electron-gas correlation energy in the high-density limit. Phys. Rev. B, 43:8911–8916, 1991.
- [81] J. P. Perdew, K. Burke, and M. Ernzerhof. Generalized Gradient Approximation Made Simple. Phys. Rev. Lett., 77(18):3865–3868, Oct 1996.
- [82] J. P. Perdew. Accurate Density Functional for the Energy: Real-Space Cutoff of the Gradient Expansion for the Exchange Hole. Phys. Rev. Lett., 55:1665–1668, Oct 1985.
- [83] S. K. Ghosh and R. G. Parr. Phase-space approach to the exchange-energy functional of density-functional theory. *Phys. Rev. A*, 34:785–791, Aug 1986.
- [84] J. P. Perdew, S. Kurth, A. Zupan, and P. Blaha. Accurate Density Functional with Correct Formal Properties: A Step Beyond the Generalized Gradient Approximation. *Phys. Rev. Lett.*, 82:2544–2547, Mar 1999.
- [85] M. Ernzerhof. Construction of the adiabatic connection. Chemical Physics Letters, 263(3-4):499 – 506, 1996.
- [86] J. P. Perdew, M. Ernzerhof, and K. Burke. Rationale for mixing exact exchange with density functional approximations. The Journal of Chemical Physics, 105(22):9982– 9985, 1996.
- [87] K. Burke, M. Ernzerhof, and J. P. Perdew. The adiabatic connection method: a non-empirical hybrid. Chemical Physics Letters, 265(1-2):115 – 120, 1997.
- [88] T. Grabo and E. K. U. Gross. The optimized effective potential method of density functional theory: Applications to atomic and molecular systems. *International Jour*nal of Quantum Chemistry, 64(1):95–110, 1997.
- [89] S. Ivanov, S. Hirata, and R. J. Bartlett. Exact Exchange Treatment for Molecules in Finite-Basis-Set Kohn-Sham Theory. Phys. Rev. Lett., 83:5455–5458, Dec 1999.
- [90] A. Görling. New KS Method for Molecules Based on an Exchange Charge Density Generating the Exact Local KS Exchange Potential. *Phys. Rev. Lett.*, 83:5459–5462, Dec 1999.
- [91] V. I. Anisimov, J. Zaanen, and O. K. Andersen. Band theory and Mott insulators: Hubbard U instead of Stoner I. Phys. Rev. B, 44:943–954, Jul 1991.
- [92] V. I. Anisimov, F. Aryasetiawan, and A. I. Lichtenstein. First-principles calculations of the electronic structure and spectra of strongly correlated systems: the LDA + U method. *Journal of Physics: Condensed Matter*, 9(4):767, 1997.
- [93] A. B. Shick, A. I. Liechtenstein, and W. E. Pickett. Implementation of the LDA+U method using the full-potential linearized augmented plane-wave basis. *Phys. Rev. B*, 60:10763–10769, Oct 1999.

- [94] B. Himmetoglu, V. M. Katukuri, and M. Cococcioni. Origin of magnetic interactions and their influence on the structural properties of Ni 2 MnGa and related compounds. *Journal of Physics: Condensed Matter*, 24(18):185501, 2012.
- [95] V. I. Anisimov and O. Gunnarsson. Density-functional calculation of effective Coulomb interactions in metals. *Phys. Rev. B*, 43:7570–7574, Apr 1991.
- [96] M. Springer and F. Aryasetiawan. Frequency-dependent screened interaction in Ni within the random-phase approximation. Phys. Rev. B, 57:4364–4368, Feb 1998.
- [97] F. Aryasetiawan, M. Imada, A. Georges, G. Kotliar, S. Biermann, and A. I. Lichtenstein. Frequency-dependent local interactions and low-energy effective models from electronic structure calculations. *Phys. Rev. B*, 70:195104, Nov 2004.
- [98] F. Aryasetiawan, K. Karlsson, O. Jepsen, and U. Schönberger. Calculations of Hubbard U from first-principles. Phys. Rev. B, 74:125106, Sep 2006.
- [99] Ersoy Şaşıoğlu, Christoph Friedrich, and Stefan Blügel. Strength of the Effective Coulomb Interaction at Metal and Insulator Surfaces. *Phys. Rev. Lett.*, 109:146401, Oct 2012.
- [100] L. Vaugier, H. Jiang, and S. Biermann. Hubbard U and Hund exchange J in transition metal oxides: Screening versus localization trends from constrained random phase approximation. *Phys. Rev. B*, 86:165105, Oct 2012.
- [101] V. I. Anisimov, I. V. Solovyev, M. A. Korotin, M. T. Czyżyk, and G. A. Sawatzky. Density-functional theory and NiO photoemission spectra. *Phys. Rev. B*, 48:16929–16934, Dec 1993.
- [102] B. Himmetoglu, A. Floris, S. de Gironcoli, and M. Cococcioni. Hubbard-corrected DFT energy functionals: The LDA+U description of correlated systems. *International Journal of Quantum Chemistry*, 114(1):14–49, 2014.
- [103] V. I. Anisimov, A. V. Kozhevnikov, M. A. Korotin, A. V. Lukoyanov, and D. A. Khafizullin. Orbital density functional as a means to restore the discontinuities in the total-energy derivative and the exchange-correlation potential. *Journal of Physics: Condensed Matter*, 19(10):106206, 2007.
- [104] F. Lechermann, A. Georges, A. Poteryaev, S. Biermann, M. Posternak, A. Yamasaki, and O. K. Andersen. Dynamical mean-field theory using Wannier functions: A flexible route to electronic structure calculations of strongly correlated materials. *Phys. Rev. B*, 74:125120, Sep 2006.
- [105] O. Bengone, M. Alouani, P. Blöchl, and J. Hugel. Implementation of the projector augmented-wave LDA+U method: Application to the electronic structure of NiO. Phys. Rev. B, 62:16392–16401, Dec 2000.
- [106] U. von Barth and L. Hedin. A local exchange-correlation potential for the spin polarized case: I. Journal of Physics C: Solid State Physics, 5(13):1629, 1972.
- [107] G. Michalicek. Extending the precision and efficiency of the all-electron full-potential linearized augmented plane-wave density-functional theory method. PhD thesis, RWTH Aachen University, Jülich, 2015.

- [108] P. Kurz. Non-Collinear Magnetism at Surfaces and in Ultrathin Films. PhD thesis, RWTH Aachen, 2000.
- [109] D. D. Koelling and B. N. Harmon. A technique for relativistic spin-polarised calculations. *Journal of Physics C: Solid State Physics*, 10(16):3107, 1977.
- [110] F. Bloch. Über die Quantenmechanik der Elektronen in Kristallgittern. Z. Physik, 52:555–600, 1928.
- [111] J. R. Chelikowsky. The pseudopotential-density functional method applied to nanostructures. *Journal of Physics D: Applied Physics*, 33(8):R33, 2000.
- [112] P. E. Blöchl, C. J. Först, and J. Schimpl. The Projector Augmented Wave Method: abinitio molecular dynamics with full wave functions. eprint arXiv:cond-mat/0201015, January 2002.
- [113] M. Weinert and J. W. Davenport. Fractional occupations and density-functional energies and forces. Phys. Rev. B, 45:13709–13712, 1992.
- [114] J. C. Slater. Wave functions in a periodic potential. Phys. Rev., 51:846–851, May 1937.
- [115] G. Michalicek, M. Betzinger, C. Friedrich, and S. Blügel. Elimination of the linearization error and improved basis-set convergence within the FLAPW method. Computer Physics Communications, 184(12):2670 – 2679, 2013.
- [116] D. Singh. Ground-state properties of lanthanum: Treatment of extended-core states. Phys. Rev. B, 43:6388–6392, Mar 1991.
- [117] E. E. Krasovskii, A. N. Yaresko, and V. N. Antonov. Theoretical study of ultraviolet photoemission spectra of noble metals. *Journal of Electron Spectroscopy and Related Phenomena*, 68(0):157 – 166, 1994.
- [118] E. E. Krasovskii. Accuracy and convergence properties of the extended linear augmented-plane-wave method. Phys. Rev. B, 56(20):12866–12873, Nov 1997.
- [119] C. Friedrich, A. Schindlmayr, S. Blügel, and T. Kotani. Elimination of the linearization error in GW calculations based on the linearized augmented-plane-wave method. Phys. Rev. B, 74(4):045104, Jul 2006.
- [120] M. Betzinger, C. Friedrich, S. Blügel, and A. Görling. Local exact exchange potentials within the all-electron FLAPW method and a comparison with pseudopotential results. *Phys. Rev. B*, 83:045105, Jan 2011.
- [121] R. Fletcher. Practical Methods of Optimization; (2nd Ed.). Wiley-Interscience, New York, NY, USA, 1987.
- [122] F. Tran, J. Kuneš, P. Novák, P. Blaha, L. D. Marks, and K. Schwarz. Force calculation for orbital-dependent potentials with FP-(L)APW + lo basis sets. *Computer Physics Communications*, 179(11):784 – 790, 2008.
- [123] J. H. Park, J. M. Coy, T. S. Kasirga, C. Huang, Z. Fei, S. Hunter, and D. H. Cobden. Measurement of a solid-state triple point at the metal-insulator transition in VO₂. Nature, 500:431–434, Aug 2013.

- [124] S. Klotz, J. M. Besson, M. Braden, K. Karch, P. Pavone, D. Strauch, and W. G. Marshall. Pressure Induced Frequency Shifts of Transverse Acoustic Phonons in Germanium to 9.7 GPa. Phys. Rev. Lett., 79:1313–1316, Aug 1997.
- [125] F. Decremps, J. Zhang, B. Li, and R. C. Liebermann. Pressure-induced softening of shear modes in ZnO. Phys. Rev. B, 63:224105, May 2001.
- [126] G. Kresse, J. Furthmüller, and J. Hafner. Ab initio force constant approach to phonon dispersion relations of diamond and graphite. EPL (Europhysics Letters), 32(9):729, 1995.
- [127] R. M. Pick, M. H. Cohen, and R. M. Martin. Microscopic Theory of Force Constants in the Adiabatic Approximation. Phys. Rev. B, 1:910–920, Jan 1970.
- [128] R. Stedman and G. Nilsson. Dispersion Relations for Phonons in Aluminum at 80 and 300K. Phys. Rev., 145:492–500, May 1966.
- [129] A. van de Walle and G. Ceder. Correcting overbinding in local-density-approximation calculations. Phys. Rev. B, 59:14992–15001, Jun 1999.
- [130] J. R. Jasperse, A. Kahan, J. N. Plendl, and S. S. Mitra. Temperature Dependence of Infrared Dispersion in Ionic Crystals LiF and MgO. Phys. Rev., 146:526–542, Jun 1966
- [131] G. Peckham. The phonon dispersion relation for magnesium oxide. Proceedings of the Physical Society, 90(3):657, 1967.
- [132] M. J. L. Sangster, G. Peckham, and D. H. Saunderson. Lattice dynamics of magnesium oxide. *Journal of Physics C: Solid State Physics*, 3(5):1026, 1970.
- [133] D. Strauch and B. Dorner. Phonon dispersion in GaAs. Journal of Physics: Condensed Matter, 2(6):1457, 1990.
- [134] K. Z. Rushchanskii, N. A. Spaldin, and M. Ležaić. First-principles prediction of oxygen octahedral rotations in perovskite-structure EuTiO₃. Phys. Rev. B, 85:104109, Mar 2012.
- [135] G. Kresse and J. Hafner. Ab initio molecular dynamics for liquid metals. Phys. Rev. B, 47:558–561, Jan 1993.
- [136] G. Kresse and J. Furthmüller. Efficient iterative schemes for ab initio total-energy calculations using a plane-wave basis set. Phys. Rev. B, 54:11169–11186, Oct 1996.
- [137] P. E. Blöchl. Projector augmented-wave method. Phys. Rev. B, 50:17953–17979, Dec 1994.
- [138] G. Kresse and D. Joubert. From ultrasoft pseudopotentials to the projector augmented-wave method. Phys. Rev. B, 59:1758–1775, Jan 1999.
- [139] X. Gonze. First-principles responses of solids to atomic displacements and homogeneous electric fields: Implementation of a conjugate-gradient algorithm. *Phys. Rev. B*, 55:10337–10354, Apr 1997.

Bibliography

- [140] W. H. Press, S. A. Teukolsky, W. T. Vetterling, and B. P. Flannery. Numerical Recipes: The Art of Scientific Computing. Cambridge University Press, Cambridge, U.K., 1989.
- [141] I. Štich, R. Car, M. Parrinello, and S. Baroni. Conjugate gradient minimization of the energy functional: A new method for electronic structure calculation. *Phys. Rev. B*, 39:4997–5004, Mar 1989.
- [142] M. C. Payne, M. P. Teter, D. C. Allan, T. A. Arias, and J. D. Joannopoulos. Iterative minimization techniques for ab initio total-energy calculations: molecular dynamics and conjugate gradients. Rev. Mod. Phys., 64:1045–1097, Oct 1992.
- [143] Y. Saad and Martin H. Schultz. Gmres: A generalized minimal residual algorithm for solving nonsymmetric linear systems. SIAM Journal on Scientific and Statistical Computing, 7(3):856–869, 1986.
- [144] X. Gonze and J.-P. Vigneron. Density-functional approach to nonlinear-response coefficients of solids. Phys. Rev. B, 39:13120–13128, Jun 1989.
- [145] X. Gonze. Perturbation expansion of variational principles at arbitrary order. Phys. Rev. A, 52:1086–1095, Aug 1995.
- [146] X. Gonze. Adiabatic density-functional perturbation theory. Phys. Rev. A, 52:1096– 1114, Aug 1995.
- [147] X. Gonze. Erratum: Adiabatic density-functional perturbation theory. Phys. Rev. A, 54:4591–4591, Nov 1996.
- [148] J. O. Hirschfelder, W. Byers Brown, and S. T. Epstein. Advances in Quantum Chemistry, volume 1. Academic, New York, 1964.
- [149] M. Betzinger, C. Friedrich, A. Görling, and S. Blügel. Precise response functions in all-electron methods: Application to the optimized-effective-potential approach. *Phys. Rev. B*, 85:245124, Jun 2012.
- [150] M. Betzinger, C. Friedrich, and S. Blügel. Precise response functions in all-electron methods: Generalization to nonspherical perturbations and application to NiO. *Phys. Rev. B*, 88:075130, Aug 2013.
- [151] http://www.fiz-karlsruhe.de/icsd_home.html, Jul 2015.
- [152] http://www.fiz-karlsruhe.de/, Jul 2015.

Publikationen

Teile dieser Arbeit, insbesondere die Kraft-Analyse der Materialien MgO und Eu TiO_3 aus den Kapiteln 4.7 und 5.5.1 wurden bereits im Journal *Physical Review* $\mathbf B$ veröffentlicht:

D. A. Klüppelberg, M. Betzinger, and S. Blügel. Atomic force calculations within the all-electron FLAPW method: Treatment of core states and discontinuities at the muffin-tin sphere boundary. *Phys. Rev. B*, 91:035105, Jan 2015

Acknowledgments

The creation of a PhD thesis and the studies involved with it take a significant amount of time. It is therefore mandatory to be able to rely on the people with whom this time is spent. Here, I wish to thank these people.

First and foremost, I would like to express my gratitude to my supervisor Prof. Dr. Stefan Blügel, who allowed me to perform my doctoral studies at his institute PGI 1 at Forschungszentrum Jülich. His ambitious enthusiasm and scientific curiosity created at every time an environment in which thoughts and ideas could prosper.

I am grateful to Prof. Dr. Carsten Honerkamp for agreeing in the blink of an eye to take the time and effort to act as my second referee.

Furthermore, I thank my direct supervisor Dr. Markus Betzinger for his counsel and advise. His expertise, broad scope of view, and patience helped me greatly in my work. More than once, when I was stuck, a discussion with Markus would allow for a new point of view from which the current problem could be solved.

I wish to thank my long time office mates, too. Dr. Gregor Michalicek, Dr. Martin Schlipf, and Kaustubh Bhat were always willing to exchange thoughts, to answer questions, and to provide help. They facilitated an enjoyable work atmosphere in the office.

I thank Dr. Konstantin Ruchshanskii for discussing with me his experiences with phonon spectra, Dr. Gustav Bihlmayer for explaining to me the inner working mechanism of FLEUR and the FLAPW method, and Dr. Christoph Friedrich for sharing his opinion on several approaches that went through my mind.

Specifically for their careful proofreading of this manuscript, I am indebted to Dr. Markus Betzinger, Dr. Gregor Michalicek, and Mathias Müller.

Frankly, I am grateful to everyone in the *Peter Grünberg Institut* I / *Institute for Advanced Simulations* I. In many ways and at many times, pleasant, really unforgettable moments were forged academically and socially, be it during meetings, during lunch time, at boardgame events, movie nights, etc. In particular, I thank Kerstin Dörr, Marta Gibertini, Markus Hoffmann, and Dr. Timo Schena for the enjoyable time spent in and out of office and for their friendship.

Also, I would like to explicitly thank Ute Winkler for her organizational miracle work.

Last but not least, I express my gratitude towards my parents Edgar and Marthina Klüppelberg. They were constantly encouraging me and helping me out in case of unexpected events. Their unbreakable faith in me and their loving support I would not want to miss.

Schriften des Forschungszentrums Jülich Reihe Schlüsseltechnologien / Key Technologies

Band / Volume 106

Neutron Scattering

Lectures of the JCNS Laboratory Course held at Forschungszentrum Jülich and at the Heinz-Maier-Leibnitz Zentrum Garching edited by Th. Brückel, D. Richter, G. Roth, A. Wischnewski and R. Zorn (2015), ca 300 pp

ISBN: 978-3-95806-055-5

Band / Volume 107

Neutron Scattering

Experimental Manuals of the JCNS Laboratory Course held at Forschungszentrum Jülich and at the Heinz-Maier-Leibnitz Zentrum Garching edited by Th. Brückel, D. Richter, G. Roth, A. Wischnewski and R. Zorn (2015), ca 150 pp

ISBN: 978-3-95806-056-2

Band / Volume 108

STM-based quantum transport through molecular wires

N. Fournier (2015), ix, 295 pp ISBN: 978-3-95806-059-3

Band / Volume 109

Study on the electroforming and resistive switching behaviour of nickel oxide thin fims for non-volatile memory applications

R. Weng (2015), xxi, 159 pp ISBN: 978-3-95806-062-3

Band / Volume 110

Microswimmers - From Single Particle Motion to Collective Behaviour

Lecture Notes of the DFG SPP Summer School 2015 edited by G. Gompper, C. Bechinger, S. Herminghaus, R. E. Isele-Holder, U.B. Kaupp, H. Löwen, H. Stark, R. G. Winkler (2015) ISBN: 978-3-95806-083-8

Band / Volume 111

Long range order in 3D nanoparticle assemblies

E. Josten (2015), 238 pp ISBN: 978-3-95806-087-6

Band / Volume 112

Silicon nanowire structures for neuronal cell interfacing

S. Pud (2015), 153 pp ISBN: 978-3-95806-089-0

Schriften des Forschungszentrums Jülich Reihe Schlüsseltechnologien / Key Technologies

Band / Volume 113

Memristive Phenomena -

From Fundamental Physics to Neuromorphic Computing

Lecture Notes of the 47th IFF Spring School 2016 22 February – 04 March 2016, Jülich, Germany ed. by R. Waser and M. Wuttig (2016), ca 1000 pp

ISBN: 978-3-95806-091-3

Band / Volume 114

Single-Cell Analysis of Microbial Production Strains in Microfluidic Bioreactors

A. M. Grünberger (2015), XIX, 225 pp

ISBN: 978-3-95806-092-0

Band / Volume 115

Magnetic order and spin dynamics in the extended kagome system CaBaCo₂Fe₂O₇

J. Reim (2015), viii, 144 pp ISBN: 978-3-95806-097-5

Band / Volume 116

Structural and electronic investigations on homo- and hetero-organic layers involving CuPc on silver single crystal surfaces

K. M. Schönauer (2015), x, 148 pp

ISBN: 978-3-95806-112-5

Band / Volume 117

First-principles investigation of inelastic magnetic excitations in nanostructures deposited on surfaces

B. J. Schweflinghaus (2016), v. 204 pp

ISBN: 978-3-95806-115-6

Band / Volume 118

Magnetic, structural, and electronic properties of NiFe₂O₄ ultrathin films

M. Hoppe (2016), vii, 118 pp ISBN: 978-3-95806-122-4

Band / Volume 119

First-principle investigation of displacive response in complex solids

D. A. Klüppelberg (2016), xi, 179 pp

ISBN: 978-3-95806-123-1

Weitere Schriften des Verlags im Forschungszentrum Jülich unter

http://wwwzb1.fz-juelich.de/verlagextern1/index.asp



Schlüsseltechnologien/ Key Technologies Band/Volume 119 ISBN 978-3-95806-123-1

